THE QUASI-BICIRCULAR PROBLEM

M.A. Andreu

Departament de Matemàtica Aplicada i Anàlisi
Universitat de Barcelona

Programa de doctorat de Matemàtica Aplicada i Anàlisi. Bienni 89-91.
Memòria presentada per aspirar al grau de Doctor en Ciències Matemàtiques per la Universitat de Barcelona.

Certifiquem que la present memòria ha estat realitzada per Miquel Àngel Andreu i Barrieras, i dirigida per nosaltres.

Barcelona, 30 d'octubre de 1.998.

Gerard Gómez i Muntané   Carles Simó i Torres

A la Sílvia i al nostre fill David.

When Neil Armstrong arrived at the Moon the 21st of July 1.969, before stepping on it, he said: *This is a small step for a man, a big step for the Humanity.* Now, after finishing my thesis, I thought: *This is a big step for a man, a small step for the Humanity.*

Acknowledgements

First of all, I want to thank Dr. G.Gómez and Dr. C.Simó for the time that they have spent discussing with me several topics of this thesis. Their knowledge and teaching have been fundamental to carry out this research.

I thank the Departament de Matemàtica Aplicada i Anàlisi (MAiA) for providing me all the equipment necessary for my work. I also want to thank all the authors of reports [8], [9], [10] and [11] for allowing me to use all their software and papers. Certainly, I have learnt a lot from them. I also want to express my gratitude to all the companions of Departament de MAiA who have helped me in many different ways. I would like to mention Jaume Timoneda because of his work as system manager which allows that other people uses the computers of our Department as simple users. I also want to mention Àlex Haro who has followed closely the progress of my research. I acknowledge the enthusiasm about the Quasi-bicircular Problem shown by Enric Castellà and Josep Maria Mondelo. I am also in debt with the last one because he advised me about the frequency analysis done in chapters 4 and 5. He also provided me a C code implementation of the algorithm used by him for that task. I am also in debt with Gerard Albà for substituting me in my teaching obligations at the latter part of my thesis. I also want to thank Dr. Josep Masdemont (Universitat Politècnica de Catalunya) for fruitful discussions about the reduction of the Hamiltonian to the central manifold shown in chapter 4. He also provided me software which help me to implement the algorithm in the case of the Quasi-bicircular Problem. I want to thank all the people who has encouraged me to write this thesis. In this sense, I want to make reference to Samuel L. Buxton and Dr. Teresa Stuchi (Universidade Federal do Rio de Janeiro). I also want to thank my parents and my parents in law for all what they have done for me.

Finally, I want to say that there is a person who, without her, I would not have been able to do this thesis: my wife Sílvia. She always has been on my side, specially in bad moments. She is the only person who really knows the effort that this thesis has represented for me.

Preface

The objective of this thesis is the study of the neighbourhood of the collinear libration points of the Earth-Moon system. The motivation for this study is that translunar Halo orbits have been proposed by R.Farquhar in 1971 as a means to establish a continuous communications link between the Earth and the far side of the Moon. However, it was difficult to compute this kind of orbits for a long time interval (say, for instance, 20 years, so that it covers a full Saros period). Till now, as far as we know, nobody was able to produce such kind of orbits. We have succeeded and the results can be found in chapter 5.

Our research started studying the Restricted Three Body Problem (RTBP) and the Bicircular Problem (BCP). After several computations, it seemed that both models do not fit well the real problem in the vicinity of L_2. It was necessary to find another intermediate model. This is the Quasi-bicircular Problem (QBCP). A model similar to the BCP, but in such a way that the three primaries move in orbits coherent with the gravitational Newton's law. The first chapter is devoted to derive the equations of motion of this new model, the Quasi-bicircular Problem. Most of the other chapters are devoted to study several issues of this Problem.

The QBCP is a Hamiltonian system with three degrees of freedom and depending periodically on time. Let T be this period and $\omega_s = 2\pi/T$ the frequency. Chapter 2 deals with the computation of T-periodic orbits. It is not easy to find these orbits directly. For this reason, we start with periodic orbits of the RTBP which have as period a fraction of T. Most of them can be continued up to orbits of the QBCP. To do this, several numerical techniques are applied: study of bifurcation of periodic orbits from an autonomous to a non-autonomous system; a continuation method using arc parameter; computation of stability parameters of orbits; study of bifurcations of periodic orbits and so on. Among all the orbits computed, there are some that, later on, become very important. They are the orbits around L_2 coming from the orbits with period $T/2$ in the RTBP.

Chapter 3 is devoted to study quasi-periodic orbits of the QBCP around L_1 and L_2. Firstly, using the Lindstedt-Poincaré method, we find analytical approximation of quasi-periodic orbits in a neighbourhood of these libration points. In this way, Lyapunov and Lissajous type orbits are computed. They lie on 2D and 3D tori, respectively. But, in the QBCP, the Lindstedt-Poincaré method does not give good approximation of Halo orbits. For this reason, to find quasi-periodic Halo orbits, we have used the method that we have called analytical refinement. Basically, it consists in looking for the Fourier coefficients of a solution of the differential equations of motion. To solve the problem a Newton's method is applied to the infinite dimensional nonlinear system of equations satisfied by the coefficients. We stress that a lot of algebraic manipulation must be carried out to achieve good analytical approximations of Halo orbits. Our main contribution, to improve the analytical refinement method, has been the introduction of a relative threshold in the selection of the frequencies involved in Newton's method. With the computation of the Halo orbits, we have shown the important role played by the resonance $\omega_p = 2\omega_s$, where ω_p denotes the proper frequency of the Halo orbit. We also have studied the stability of the planar Lyapunov quasi-periodic orbits, pointing out that the change of stability in the z direction is related with the bifurcation where the Halo quasi-periodic orbits start.

The objective of chapter 4 is to give a full description of the different types of orbits in a big neighbourhood around L_2. This is accomplished by means of the reduction of the Hamiltonian to the central manifold. Several symplectic change of variables must be performed, but the process can be summarized in three steps. The first one is to perform a translation to the small periodic orbit around L_2. The second one is a Floquet change of variables to diagonalize the quadratic terms of the Hamiltonian. The third step is to cancel terms of order bigger than two. We want to remark that, in our case, it is possible to remove the dependence on time up to high order without introducing small divisors.

In chapter 4, we compute the Hamiltonian reduced to the central manifold up to order sixteen. This is a Hamiltonian with two degrees of freedom. It is studied by means of Poincaré maps for different levels of energy. All the objects studied (say fixed points, periodic orbits, invariant manifolds, 2D tori, ...) are interpreted in terms of the initial coordinates of the QBCP.

Chapter 5 is devoted to Halo orbits of the Solar System. JPL ephemeris has been used as model of the Solar System. As we have said before, we have been able to obtain Halo orbits for a long time interval. These orbits have been computed from Halo orbits of the QBCP of chapter 3. An important key in the success of the computation of Halo orbits has been the improvement of the parallel shooting method (also called multiple shooting method). In our case, a new minimizing condition reduces the size of the system to be solved and improves the convergence towards the desired solution.

Finally, the section of *Conclusions and outlook* gives several points to continue our line of research.

Contents

List of Figures

List of Tables

Chapter 1

The Quasi-bicircular Problem: equations of the motion.

1.1 Introduction

Everybody knows the Moon rotates around the Earth and its movement, as a first approximation, can be considered as circular. If we are interested in the behaviour of a spacecraft in the Earth-Moon system, we can use, as a first approximation, the well known model called Restricted Three Body Problem (RTBP). But, these bodies are not alone in the Solar System. The main perturbation is originated by the gravity pull of the Sun. A more realistic model should include, in some way, the effect of the Sun. Except for chapter 5, gravity attraction of the planets, eccentricity of the orbits of the Earth and the Moon, inclination of the Moon's orbit or some other factors are not considered.

We are interested in the dynamics of the movement of a spacecraft in the Earth-Moon-Sun system and specially interested in the dynamics around the Lagrange points. The study of this dynamical system can be useful for future space missions. For instance, some orbits around the translunar libration point have been proposed as a mean for establishing a continuous communications link between the Earth and the hidden side of the Moon [6].

One of the models that has been widely used in Celestial Mechanics is the Bicircular Problem. This model is a restricted four body problem. It considers the Earth and the Moon moving in circular orbits around their barycenter which is also moving in circular orbit around the Sun. For instance, the Bicircular Problem was used in [29] and [9] to study the motion near the triangular libration points of the Earth-Moon system. Nevertheless this model is not coherent because the movement of the three primaries is not solution of the Three Body Problem. The existence of the Sun modifies the Earth-Moon distance and therefore it can not be constant. This is specially important if we are interested in the motion near the collinear libration points. We also want to mention that some models more realistic were developed by several authors like [20] and [16], but those models have not been considered.

Another model was introduced by D.Scheeres *et al.* in [24]. That model is called Restricted Hill Four Body Problem (RHFBP). Starting from the Four Body Problem they derive a nice generalization of Hill's and RTB Problems. The influence of the biggest mass (the Sun) to the other masses is considered as in Hill's Problem. However, for our point of view, that model is also not sufficiently accurate. Due to the Hill approximation, the RHFBP is half-month time periodic (for Earth-Moon parameters). As we will see later on, the model that we are going to derive is one month periodic. This is the main difference between both models.

Our first objective is to derive a coherent model close to the Bicircular Problem. This means that we should find a quasi-bicircular solution of the Three Body Problem Earth-Moon-Sun, and then we would be able to write the equations of the motion of a spacecraft subjected to the gravity attraction of these bodies.

Before that, we are going to remind something about the RTBP and the Bicircular Problem.

1.2 Restricted Three Body Problem

Let m_1 and m_2 be two point masses, subjected to their mutual attraction, moving in circular orbits about their center of mass. If we consider these masses in a rotating reference frame, centered in the center of mass, then the two masses are located at fixed points. Figure 1.1 shows how xyz axes have been chosen and the position of the primaries. This coordinate system is called synodical.

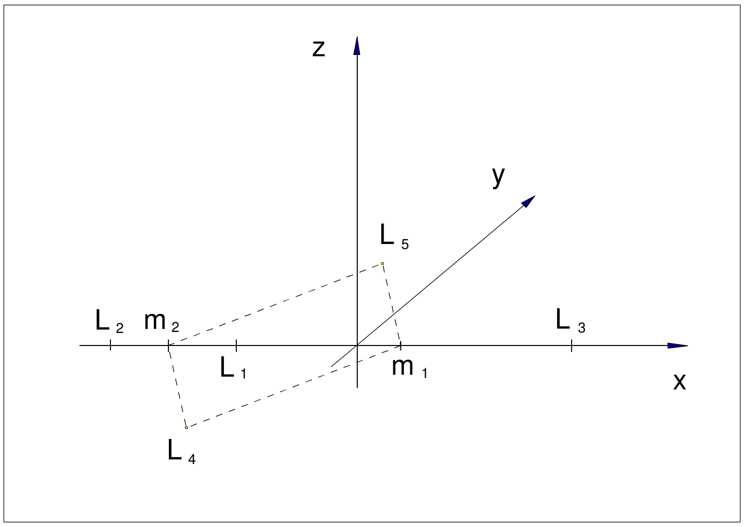

Figure 1.1: Synodical coordinates.

In this system of reference the masses m_1 and m_2 are located, respectively, at the points $(\mu, 0, 0)$ and $(\mu - 1, 0, 0)$, where $\mu = m_2/(m_1 + m_2)$. The unit of length is the distance between the two masses and the unit of time is chosen in order that the period of revolution of the primaries is 2π time units. The unit of mass is $m_1 + m_2 = 1$. Using these units, the gravitational constant is $G = 1$.

The third body has an infinitesimal mass, so it does not influence the motion of the other bodies. The second order differential equations of the movement of the third mass are

$$\begin{aligned} \ddot{x} - 2\dot{y} &= \Omega_x \ , \\ \ddot{y} + 2\dot{x} &= \Omega_y \ , \\ \ddot{z} &= \Omega_z \ , \end{aligned}$$

where

$$\Omega = \frac{1}{2}\,(x^2 + y^2) + \frac{1-\mu}{r_1} + \frac{\mu}{r_2} + \frac{1}{2}\,\mu\,(1-\mu) \ ,$$

and r_1, r_2 are the distances to the masses:

$$\begin{aligned} r_1^2 &= (x-\mu)^2 + y^2 + z^2 \ , \\ r_2^2 &= (x-\mu+1)^2 + y^2 + z^2 \ . \end{aligned}$$

It is well known that this system of equations has five equilibrium points. Two of them, L_4 and L_5, form an equilateral triangle with the primaries. The location on the x-axis of the other three, L_1, L_2 and L_3, can be computed easily solving the Euler's quintic equations. In case that the first body is the Earth and the second one is the Moon, we have used the value of the mass parameter

$$\mu = 0.0121505816$$

The coordinates of the Lagrange points, using this value of μ, are shown in table 1.1.

L_i	x	y
1	–0.8369151455	0.0000000000
2	–1.1556821500	0.0000000000
3	1.0050626441	0.0000000000
4	–0.4878494184	–0.8660254038
5	–0.4878494184	0.8660254038

Table 1.1: Coordinates of the Lagrange points. All of them are at the $z = 0$ plane.

The Hamiltonian of the problem is

$$H = \frac{1}{2}\,(p_x^2 + p_y^2 + p_z^2) - xp_y + yp_x - \frac{1-\mu}{r_1} - \frac{\mu}{r_2} \ ,$$

and the Hamiltonian equations of the motion are

$$
\begin{aligned}
\dot{x} &= p_x + y \ , \\
\dot{y} &= p_y - x \ , \\
\dot{z} &= p_z \ , \\
\dot{p}_x &= p_y - \frac{1-\mu}{r_1^3}(x-\mu) - \frac{\mu}{r_2^3}(x-\mu+1) \ , \\
\dot{p}_y &= -p_x - \frac{1-\mu}{r_1^3}\, y - \frac{\mu}{r_2^3}\, y \ , \\
\dot{p}_z &= -\frac{1-\mu}{r_1^3}\, z - \frac{\mu}{r_2^3}\, z \ .
\end{aligned}
$$

1.3 Bicircular Problem

The Bicircular Problem (BCP) considers two primaries (the Earth and the Moon) revolving in circular orbits around their barycenter B_{EM}. At the same time, B_{EM} and the third body (the Sun) are moving in circular orbits around the center of masses of the Earth-Moon-Sun system B. The three primaries move in the same plane. Beginning with an inertial reference frame, we can perform a change of variables to write the equations in synodical Earth-Moon coordinates. In this way, we obtain a set of equations, similar to the equations of the RTBP, and so we can consider the BCP as a perturbation (not too small) of the RTBP. To see more details about the derivation of these equations see [29], [9] or [11]. Figure 1.2 shows the position of the Earth, Moon and Sun in synodical coordinates.

Here, we continue using the same units of the previous section, but we are going to introduce some new quantities: m_s, the Sun mass, a_s, the distance between the Earth-Moon barycenter and the Sun, n_s and ω_s the mean angular velocity of the Sun in inertial and synodical coordinates, respectively. All these quantities are not independent. The following equalities hold:

$$
\begin{gathered}
\omega_s = 1 - n_s \ , \\
a_s^3\, n_s^2 = 1 + m_s \ , \\
\theta = \omega_s\, t \ .
\end{gathered}
$$

The first one is easy to understand if we remind of the mean angular velocity of the Moon, in inertial coordinates, is 1. The second one is consequence of the third Kepler's law. θ is the angle between the Earth-Moon line and the Sun, clockwise measured. Notice that, in inertial coordinates, the Moon and the Sun rotate counterclockwise, but the angular velocity of the Moon is greater than the velocity of the Sun. For this reason, in synodical coordinates, the Sun rotates in reverse sense.

The values used for these quantities have been

$$
\begin{aligned}
a_s &= 388.81114 \ , \\
\omega_s &= 0.925195985520347 \ , \\
m_s &= n_s^2\, a_s^3 - 1 \simeq 328900.54 \ .
\end{aligned}
$$

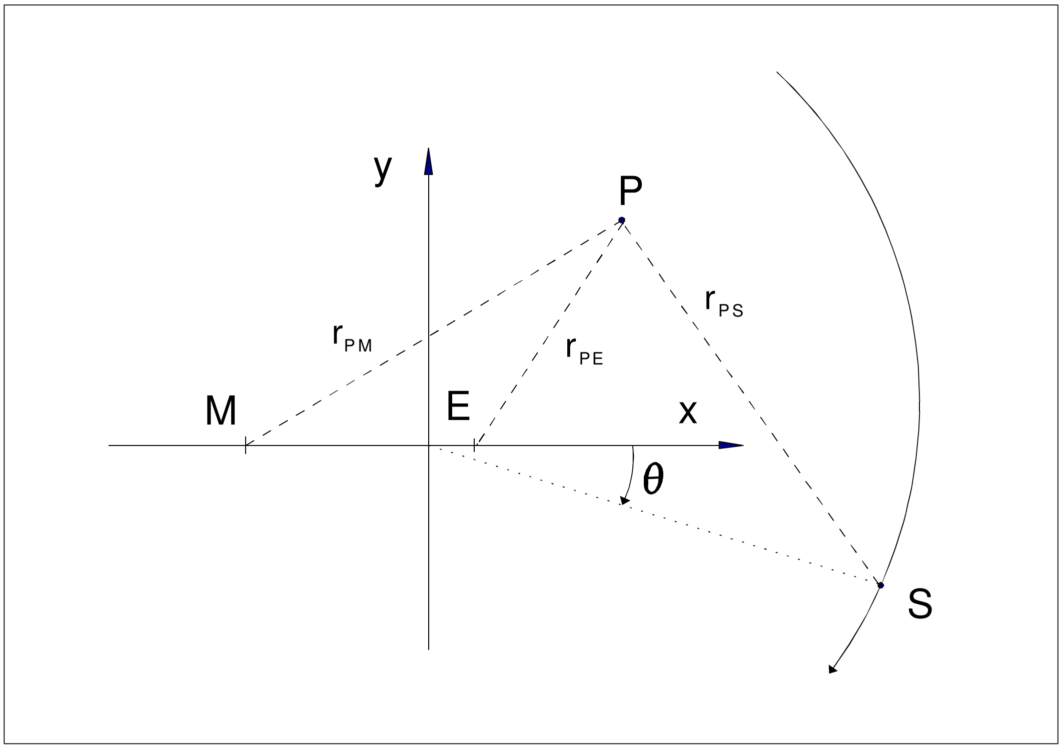

Figure 1.2: Bicircular Problem in synodical coordinates.

The Hamiltonian of this problem is

$$H = \frac{1}{2}(p_x^2 + p_y^2 + p_z^2) - xp_y + yp_x + \frac{m_s}{a_s^2}(x\cos\theta - y\sin\theta) - \frac{1-\mu}{r_{pe}} - \frac{\mu}{r_{pm}} - \frac{m_s}{r_{ps}} ,$$

where r_{pe}, r_{pm} and r_{ps} are the distances from the particle to the Earth, Moon and Sun, respectively, and so

$$\begin{aligned} r_{pe}^2 &= (x-\mu)^2 + y^2 + z^2 , \\ r_{pm}^2 &= (x-\mu+1)^2 + y^2 + z^2 , \\ r_{ps}^2 &= (x-x_s)^2 + (y-y_s)^2 + z^2 , \end{aligned}$$

where x_s and y_s are the coordinates of the Sun:

$$x_s = a_s\cos\theta , \qquad y_s = -a_s\sin\theta .$$

This Hamiltonian is non autonomous. It depends periodically on time through the angle θ and the distance r_{ps}. The Hamiltonian equations are

$$\begin{aligned} \dot{x} &= p_x + y , \\ \dot{y} &= p_y - x , \\ \dot{z} &= p_z , \end{aligned}$$

$$\begin{aligned}
\dot{p}_x &= p_y - \frac{1-\mu}{r_{pe}^3}(x-\mu) - \frac{\mu}{r_{pm}^3}(x-\mu+1) - \frac{m_s}{r_{ps}^3}(x-x_s) - \frac{m_s}{a_s^2}\cos\theta \ , \\
\dot{p}_y &= -p_x - \frac{1-\mu}{r_{pe}^3}y - \frac{\mu}{r_{pm}^3}y - \frac{m_s}{r_{ps}^3}(y-y_s) + \frac{m_s}{a_s^2}\sin\theta \ , \\
\dot{p}_z &= -\frac{1-\mu}{r_{pe}^3}z - \frac{\mu}{r_{pm}^3}z - \frac{m_s}{r_{ps}^3}z \ .
\end{aligned}$$

1.4 Quasi-bicircular solution of the Three Body Problem

This section deals with the derivation of a quasi-bicircular solution of the general Three Body Problem. We want to apply this to the Earth-Moon-Sun system. For this purpose, it is convenient to use the Jacobi formulation of the Three Body Problem. It uses two vectors: $\vec{r}$ from the mass m_1 to m_2 and $\vec{R}$ from B_{12}, the center of mass of m_1 and m_2, to the mass m_3. Figure 1.3 helps to understand this decomposition.

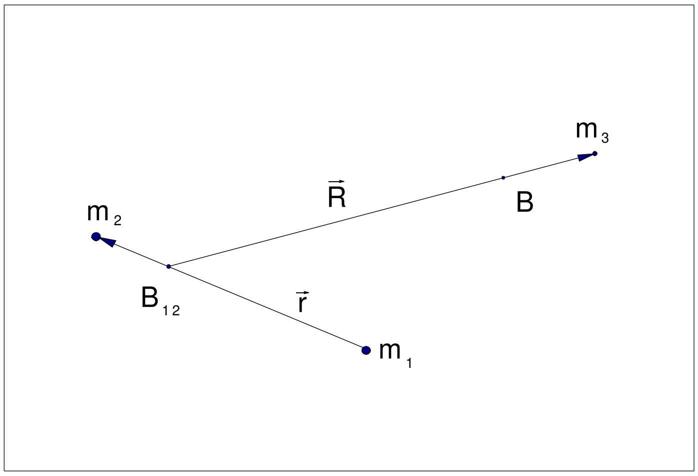

Figure 1.3: Jacobi decomposition of the Three Body Problem.

Let $\alpha = m_1/(m_1+m_2)$, $\beta = m_2/(m_1+m_2) = 1-\alpha$ and $M = m_1+m_2+m_3$. The following equalities hold:

$$\begin{aligned}
\vec{r}_{13} &= \vec{R} + \beta\vec{r} \ , \\
\vec{r}_{23} &= \vec{R} - \alpha\vec{r} \ , \\
\vec{R} &= \alpha\vec{r}_{13} + \beta\vec{r}_{23} \ .
\end{aligned}$$

The Jacobi equations for the Three Body Problem are

$$\ddot{\vec{r}} = -G(m_1+m_2)\frac{\vec{r}}{r^3} + Gm_3\left(\frac{\vec{r}_{23}}{r_{23}^3} - \frac{\vec{r}_{13}}{r_{13}^3}\right) \ , \tag{1.1}$$

$$\ddot{\vec{R}} = -GM\left(\alpha\frac{\vec{r}_{13}}{r_{13}^3} + \beta\frac{\vec{r}_{23}}{r_{23}^3}\right) . \tag{1.2}$$

The derivation of these equations can be found in [18]. G is the universal constant of gravitation.

Now, consider two fixed values a_i and a_e. We want to look for a quasi-bicircular solution of equations (1.1) and (1.2) with radius a_i and a_e. This means a solution with $r \simeq a_i$ and $R \simeq a_e$. Related to these radius, we have the mean angular motions which are

$$\begin{aligned} n_i^2 &= \frac{G(m_1+m_2)}{a_i^3} , \\ n_e^2 &= \frac{GM}{a_e^3} , \end{aligned}$$

according to the third Kepler's law.

Now, we are going to suppose that the movement of the three bodies stands on a plane and then $\vec{r}$ and $\vec{R}$ are two dimensional vectors. At this moment, it is more convenient to introduce the complex notation. Let z and Z be complex variables corresponding to the real vectors $\vec{r}$ and $\vec{R}$, respectively. The equations of the motion (1.1) and (1.2) become

$$\ddot{z} = -G(m_1+m_2)\frac{z}{r^3} + Gm_3\left(\frac{Z-\alpha z}{r_{23}^3} - \frac{Z+\beta z}{r_{13}^3}\right) , \tag{1.3}$$

$$\ddot{Z} = -GM\left(\alpha\,\frac{Z+\beta z}{r_{13}^3} + \beta\,\frac{Z-\alpha z}{r_{23}^3}\right) , \tag{1.4}$$

where

$$\begin{aligned} r &= |z| , \\ r_{13} &= |Z+\beta z| , \\ r_{23} &= |Z-\alpha z| . \end{aligned}$$

Using complex notation, the problem of finding a quasi-bicircular solution can be stated saying that we want to look for a solution of (1.3) and (1.4) with

$$\begin{aligned} z &\simeq a_i e^{i(n_i t+\theta_i)} , \\ Z &\simeq a_e e^{i(n_e t+\theta_e)} . \end{aligned}$$

We assume that the three bodies are on the real axis at $t=0$ and, in particular, the initial phases θ_i and θ_e can be taken as zero.

It is possible to find a solution of this kind as a Fourier series of the form

$$z = a_i e^{in_i t}\sum_{j=-\infty}^{+\infty} b_j e^{ijnt} , \tag{1.5}$$

$$Z = a_e e^{in_e t}\sum_{j=-\infty}^{+\infty} c_j e^{ijnt} , \tag{1.6}$$

being $n = n_i - n_e$ the relative angular velocity of inner to outer motion. The basic idea is to substitute the expressions (1.5) and (1.6) into the equations of the motion (1.3) and (1.4), obtaining the coefficients b_j and c_j by identification. For this purpose, it is useful to introduce a small parameter. In the Earth-Moon-Sun case this parameter can be

$$\epsilon = \frac{a_i}{a_e} ,$$

which has an approximate value of 1/389. Furthermore, use will be made of the fact that, in this case,

$$\frac{m_3}{m_1 + m_2} \simeq 2.1756\, \epsilon^{-2} = O(\epsilon^{-2}) .$$

Hence, we are going to look for a solution of the form

$$\begin{aligned} z &= a_i e^{i n_i t} \sum_{k=0}^{+\infty} \epsilon^k u_k , \\ Z &= a_e e^{i n_e t} \sum_{k=0}^{+\infty} \epsilon^k v_k , \end{aligned}$$

where u_k and v_k are complex periodic functions with basic frequency n.

First of all, we should verify that $u_0 = v_0 = 1$ gives a zero order solution. This is indispensable to get a solution close to a bicircular movement with zero initial phases, as prescribed before. Then, we substitute

$$\begin{aligned} z &= a_i e^{i n_i t}(1 + O(\epsilon)) , \\ Z &= a_e e^{i n_e t}(1 + O(\epsilon)) , \end{aligned}$$

in the equations (1.3) and (1.4). Using $a_i = a_e \epsilon$, we get

$$Z - \alpha z = a_e e^{i n_e t}(1 + O(\epsilon) - \alpha \epsilon e^{i n t}(1 + O(\epsilon))) = a_e e^{i n_e t}(1 + O(\epsilon)) ,$$

and also

$$Z + \beta z = a_e e^{i n_e t}(1 + O(\epsilon)) .$$

Taking into account these expressions, it is easy to confirm that we obtain, at zero order, the same in both sides of the equalities (1.3) and (1.4).

Now, we are going to see that u_k and v_k can be determined recursively. Suppose that $u_0, v_0, u_1, v_1, \ldots, u_{m-1}, v_{m-1}$ are known. Substituting

$$\begin{aligned} z &= a_i e^{i n_i t} \sum_{k=0}^{m} \epsilon^k u_k , \\ Z &= a_e e^{i n_e t} \sum_{k=0}^{m} \epsilon^k v_k , \end{aligned} \tag{1.7}$$

into the equations of the motion and identifying the terms of the order ϵ^m, we arrive at a linear differential equation for u_m and v_m. Before doing this, it is better to simplify a little bit the expressions, using the units introduced in section 1.2. Henceforth the masses m_1, m_2 and m_3 will be those of the Moon, the Earth and the Sun, respectively. Therefore,

$$G = 1 \,, \qquad m_1 + m_2 = 1 \,, \qquad a_i = 1 \,, \qquad n_i = 1 \,,$$

$$\alpha = \mu \,, \qquad \beta = 1 - \mu \,, \qquad n = 1 - n_s \,.$$

In fact, this does not mean a loss of generality, it is only a change of units. Then, the equations of the motion are

$$\ddot{z} \;=\; -\frac{z}{r^3} + m_s \left(\frac{Z - \mu z}{r_{23}^3} - \frac{Z + (1-\mu) z}{r_{13}^3} \right) \,, \tag{1.8}$$

$$\ddot{Z} \;=\; -(1 + m_s) \left(\mu \, \frac{Z + (1-\mu) z}{r_{13}^3} + (1-\mu) \, \frac{Z - \mu z}{r_{23}^3} \right) \,, \tag{1.9}$$

and the expressions (1.7) become

$$\begin{aligned} z \;&=\; e^{it} \left(1 + \sum_{k=1}^{m} \epsilon^k u_k \right) \,, \\ Z \;&=\; a_s e^{i n_s t} \left(1 + \sum_{k=1}^{m} \epsilon^k v_k \right) \,. \end{aligned} \tag{1.10}$$

The left hand side of (1.8) is

$$\ddot{z} = e^{it} \left(-1 + \sum_{k=1}^{m} \epsilon^k (\ddot{u}_k + 2i\dot{u}_k - u_k) \right) \,,$$

and then

$$\ddot{z}\big|_m = e^{it} (\ddot{u}_m + 2i\dot{u}_m - u_m) \,,$$

where $|_m$ means terms of order ϵ^m. In the same way, from the left hand side of the equation (1.9) we get

$$\ddot{Z}\Big|_m = a_s e^{i n_s t} (\ddot{v}_m + 2 i n_s \dot{v}_m - n_s^2 v_m) \,.$$

On the right part of the equations (1.8) and (1.9), we have several terms:

$$\begin{aligned} \frac{z}{r^3} \;&=\; \frac{z}{(z\overline{z})^{3/2}} = z^{-1/2} \overline{z}^{-3/2} = e^{it} \left(1 + \sum_{k=1}^{m} \epsilon^k u_k \right)^{-1/2} \left(1 + \sum_{k=1}^{m} \epsilon^k \overline{u}_k \right)^{-3/2} = \\ &= e^{it} \left(1 - \frac{1}{2} \left(\sum_{k=1}^{m} \epsilon^k u_k \right) - \frac{1}{8} \left(\sum_{k=1}^{m} \epsilon^k u_k \right)^2 + \ldots \right) \\ &\qquad \left(1 - \frac{3}{2} \left(\sum_{k=1}^{m} \epsilon^k \overline{u}_k \right) + \frac{15}{8} \left(\sum_{k=1}^{m} \epsilon^k \overline{u}_k \right)^2 + \ldots \right) \,, \end{aligned} \tag{1.11}$$

$$\frac{z}{r^3}\bigg|_m \;=\; e^{it} \left(-\frac{1}{2} u_m - \frac{3}{2} \overline{u}_m + \text{ k. t.} \right) \,,$$

where k.t. means "known terms" which can be computed from the previous u_k's. On the right hand side of the equality we also have

$$
\begin{aligned}
Z-\mu z &= a_s e^{in_s t}\left(\left(1+\sum_{k=1}^{m}\epsilon^k v_k\right)-\mu\epsilon e^{int}\left(1+\sum_{k=1}^{m}\epsilon^k u_k\right)\right)= \\
&= a_s e^{in_s t}\left(1+\sum_{k=1}^{m}\epsilon^k(v_k-\mu e^{int}u_{k-1})+O(\epsilon^{m+1})\right) , \\
\frac{Z-\mu z}{r_{23}^3} &= \frac{e^{it}}{a_s^2}e^{-int}\left(1+\sum_{k=1}^{m}\epsilon^k(v_k-\mu e^{int}u_{k-1})+O(\epsilon^{m+1})\right)^{-1/2} \\
&\quad\left(1+\sum_{k=1}^{m}\epsilon^k(\overline{v}_k-\mu e^{int}\overline{u}_{k-1})+O(\epsilon^{m+1})\right)^{-3/2} , \qquad (1.12)
\end{aligned}
$$

and then, the terms of order ϵ^m are

$$
\left.\frac{Z-\mu z}{r_{23}^3}\right|_m = \frac{e^{it}}{a_s^2}e^{-int}(-\frac{1}{2}v_k-\frac{3}{2}\overline{v}_k+\text{ k. t.}) .
$$

Following the same way, we also arrive at

$$
\left.\frac{Z-(1-\mu)z}{r_{13}^3}\right|_m = \frac{e^{it}}{a_s^2}e^{-int}(-\frac{1}{2}v_k-\frac{3}{2}\overline{v}_k+\text{ k. t.}) .
$$

Note that in (1.8) the terms containing Z have a factor m_s in front of them, but as they also have the factor $1/a_s^2$, the total contribution, m_s/a_s^2, is $O(1)$. Consequently, we only should solve the linear differential equations:

$$
\begin{aligned}
\ddot{u}_m+2i\dot{u}_m-\frac{3}{2}u_m-\frac{3}{2}\overline{u}_m &= P_m(e^{int}) , &(1.13)\\
\ddot{v}_m+2in_s\dot{v}_m-\frac{3}{2}n_s^2v_m-\frac{3}{2}n_s^2\overline{v}_m &= Q_m(e^{int}) , &(1.14)
\end{aligned}
$$

where P_m and Q_m are polynomials depending on the precedent u_k and v_k for $k=0,\ldots,m-1$. These polynomials have real coefficients and integer exponents as will be proved later on.

1.4.1 Solving the differential equation

In this section, we are going to make some comments about the resolution of the differential equations (1.13) and (1.14). In order to make more clear the exposition, we are going to skip the subscript m. Then, the question is to find a solution of the equation:

$$
\ddot{u}+2i\dot{u}-\frac{3}{2}u-\frac{3}{2}\overline{u}=P(e^{int}) , \qquad (1.15)
$$

where

$$P(e^{int}) = \sum_{|j|\leq J} p_j e^{ijnt} ,$$

where J is finite. Later on we will say something about the degree of the polynomials P and Q.

A particular solution of the (1.15) is of the form:

$$u = \sum_{|j|\leq J} u_j e^{ijnt} .$$

Therefore, we only should derivate twice this expression, substitute into (1.15), identify similar terms and find the coefficients u_j. To compute this coefficients is only necessary to solve some 2×2 systems of linear equations. But, we are going to distinguish two different cases:

- $j = 0$, the constant case. Corresponding to the independent term of the polynomial P we have the constant solution:

$$u_0 = -\frac{1}{3} p_0 .$$

- if $j \neq 0$, for each couple of terms of the type $p_{-j}e^{-ijnt} + p_j e^{ijnt}$, we look for a solution of the same type.

$$\begin{aligned} u &= u_{-j}e^{-ijnt} + u_j e^{ijnt} , \\ \dot{u} &= -ijnu_{-j}e^{-ijnt} + ijnu_j e^{ijnt} , \\ \ddot{u} &= -(jn)^2 u_{-j}e^{-ijnt} - (jn)^2 u_j e^{ijnt} , \\ \overline{u} &= u_j e^{-ijnt} + u_{-j}e^{ijnt} . \end{aligned}$$

Substituting into (1.15) and equating to terms of the same degree of P, we obtain the following system of linear equations:

$$\left. \begin{aligned} \left(-(jn)^2 + 2jn - \frac{3}{2}\right) u_{-j} - \frac{3}{2} u_j &= p_{-j} \\ -\frac{3}{2} u_{-j} + \left(-(jn)^2 - 2jn - \frac{3}{2}\right) u_j &= p_j \end{aligned} \right\} \qquad (1.16)$$

Notice that all the coefficients u_j are real because P and Q also have real coefficients.

For the differential equation (1.14) we proceed in the same way and obtain

- if $j = 0$,

$$v_0 = -\frac{1}{3n_s^2} q_0 .$$

- if $j \neq 0$,

$$\left.\begin{aligned} \left(-(jn)^2 + 2jnn_s - \frac{3}{2}n_s^2\right) v_{-j} - \frac{3}{2}n_s^2 v_j &= q_{-j} \\ -\frac{3}{2}n_s^2 v_{-j} + (-(jn)^2 - 2jnn_s - \frac{3}{2}n_s^2) v_j &= q_j \end{aligned}\right\} \tag{1.17}$$

The systems of linear equations are solved easily. In all the possible cases the determinant is different from zero. The determinant of system (1.16) is

$$(jn)^2((jn)^2 - 1) ,$$

and the one of (1.17) is

$$(jn)^2((jn)^2 - n_s^2) .$$

Taking into account that $n \simeq 0.9252$ and $n_s \simeq 0.0748$ we see that no problems of small divisors occur. The smallest value of the first determinant is reached for $j = 1$.

Proposition 1.1 *The polynomials P_m and Q_m of the equations (1.13) and (1.14) have real coefficients, integer exponents and their degrees satisfy*

$$\begin{array}{l} deg(P_m) \leq 2\,m , \\ deg(Q_m) \leq 2\,m - 2 , \end{array} \qquad \forall m \geq 1 .$$

Proof: We remind that we know the functions $u_0 = 1$ and $v_0 = 1$. First of all we are going to compute u_1 and v_1. By straightforward calculation we find

$$\begin{aligned} P_1 &= \left(\frac{1}{2} + \frac{3}{2}e^{-2int}\right)\frac{m_s}{a_s^2} , \\ Q_1 &= 0 . \end{aligned}$$

Solving the corresponding system of linear equations we get

$$\begin{aligned} u_1 &= \left(-\frac{1}{6} - \frac{24n^2 + 24n + 9}{64n^4 - 16n^2}e^{-2int} + \frac{9}{64n^4 - 16n^2}e^{2int}\right)\frac{m_s}{a_s^2} , \\ v_1 &= 0 . \end{aligned}$$

We have seen that $deg(P_1) = 2$ and $deg(Q_1) = 0$. Now, we proceed by induction. Suppose that $deg(P_k) \leq 2\,k$ and $deg(Q_k) \leq 2\,k - 2$ for all $k = 1, \ldots, m-1$. We want to see that this hypothesis is also true for $k = m$. It is clear that u_k and v_k are trigonometric polynomials of the same degree than P_k and Q_k. Looking attentively at the equations (1.8) and (1.9) and the formulas (1.11) and (1.12), it is easy to see that $deg(P_m) \leq 2\,m$ and $deg(Q_m) \leq 2\,m - 2$. We only want to remark that in (1.12) some terms of degree $2m - 1$ are involved. When calculating $\dfrac{Z - (1-\mu)z}{r_{13}^3}$ and $\dfrac{Z - \mu z}{r_{23}^3}$ some terms of that degree appear, but when adding both in (1.9), those terms of degree $2m - 1$ cancel, and so $deg(Q_m) \leq 2\,m - 2$. ■

1.4.2 The algebraic manipulator

To compute a quasi-bicircular solution of the Three Body Problem, one can begin calculating some terms by hand, following the steps that we have explained in the previous sections. Even in the case that one wants a solution up to low order, the computational effort is very high. The task is very tedious and the probability of making some mistakes increases at the same time than the computational time. For all these reasons it is better to build an specific algebraic manipulator. As this is the first time an algebraic manipulator appears in this work, we are going to explain a few things in detail. We will skip this task for all the subsequent manipulators that have been used.

We have implemented C code to compute the quasi-bicircular solution for the Earth-Moon-Sun case. Obviously, if a quasi-bicircular motion of another three bodies is wanted, it is only necessary to change the parameters of the problem: μ, m_s and a_s. The program is able to compute the solution up to high order in few seconds. Table 1.2 shows the CPU time using an HP-9000/715 computer, up to different orders.

m	10	15	20	25	30
CPU (sec.)	0.5	4.3	21.8	76.1	215.5

Table 1.2: CPU time with an HP-9000/715 computer up to different orders.

The C language is very adequate to make programs which manipulate different types of series. One of the advantages is the possibility of using structures. The coefficients of a polynomial are usually stored in a one-dimensional array. Sometimes the coefficients of a polynomial are not real numbers. Imagine, for instance, that they are sparse trigonometric polynomials. Then, an one-dimensional array of structures can be used. Each component of the array is a structure storing a trigonometric polynomial and the number of terms of it. In turn, the trigonometric polynomial can be stored in an array of structures, where each component has the coefficient and the exponent. Of course, it is possible to program all of this without structures, but then several arrays of different types are needed. Programming with structures is easier for the programmer and sometimes it is more efficient.

Our program is able to make operations with polynomials in one variable, ϵ, whose coefficients are trigonometric polynomials. In fact, they can be managed as polynomials in two variables. We have routines to add, multiply and copy different kind of polynomials. Using these routines, the program computes recursively the functions u_1, v_1, u_2, v_2, $\ldots$, up to the desired order. Finally, it adds all the functions with their corresponding power of ϵ to obtain the solution in the way

$$z = e^{it}\sum_{k=0}^{m}\epsilon^k u_k = e^{it}\sum_{|j|\le 2m} b_j e^{ijnt} ,$$

$$Z = a_s e^{in_s t} \sum_{k=0}^{m} \epsilon^k v_k = a_s e^{in_s t} \sum_{|j| \le 2m-2} c_j e^{ijnt} .$$

In order to study the convergence of the solution, the program gives the maximum coefficient of each term $\epsilon^k u_k$ and $\epsilon^k v_k$. This maximum is denoted by $\|\cdot\|_m$. Table 1.3 shows this maximum for some degrees. We see that $\|\epsilon^k u_k\|_m$ and $\|\epsilon^k v_k\|_m$ show

k	$\|\epsilon^k u_k\|_m$	$\|\epsilon^k v_k\|_m$
5	1.39189e–05	2.43716e–13
10	1.15466e–07	2.02341e–15
15	9.58163e–10	1.67902e–17
20	7.95281e–12	1.39358e–19
25	6.60176e–14	1.37143e–21
30	5.48047e–16	1.38933e–23

Table 1.3: Maximum coefficient of $\epsilon^k u_k$ and $\epsilon^k v_k$ for some values of k.

a very regular behaviour. The quotient between each term and the next one is approximately 2.6. We decided to compute the solution up to order 30. At this point the round-off errors are certainly bigger than the truncation errors. Table 1.4 shows the coefficients b_j and c_j of the solution.

The results obtained have been tested in two different ways:

1. Analytical test: the analytical solution computed, as a polynomial in ϵ and e^{int}, can be substituted into the differential equations (1.8) and (1.9). If everything is correct, both sides of each equality lead to the same result. It is easy to make a program to do this using the same routines that we have made for the main program. We have verified the perfect agreement between both sides of the equalities.

2. Numerical test: this test is a comparison between the analytical solution and the numerical integration of the differential equations (1.8) and (1.9), during a time span of 2π. The initial condition was obtained from the analytical solution doing $t = 0$. The maximum difference between the analytical and the numerical solution in each component of z, $\dot{z}$, Z and $\dot{Z}$ is about 10^{-12}, which is a very good result.

1.5 Quasi-bicircular Problem

The Quasi-bicircular Problem (QBCP) is a four body problem, where the first three masses are moving in a quasi-bicircular movement and the fourth is an infinitesimal mass. In this section we are going to derive the Hamiltonian and the equations of the motion of the fourth particle under the gravitational influence of the other three.

j	b_j	c_j
−10	6.405746745897675e−14	
−9	8.611551796434800e−15	
−8	1.224069117472013e−11	
−7	6.666645777704854e−12	
−6	2.444541403181094e−09	
−5	4.604798391613412e−09	
−4	1.545864413695503e−07	1.919314137136288e−13
−3	7.360514539804505e−06	−2.956886640606096e−13
−2	−8.688592707298765e−03	2.626400997925652e−10
−1	−4.483846462932090e−04	−2.481941620308044e−12
0	9.990930211448791e−01	1.000000018781437e+00
1	1.607506070429252e−04	−8.027647529367435e−13
2	1.514503555873263e−03	4.361396994236632e−11
3	1.474833975440193e−07	−3.524688857655007e−14
4	5.874877029010216e−06	3.512396554007162e−14
5	−1.212071450975000e−09	
6	3.001784387420479e−08	
7	−1.788769852254027e−11	
8	1.752254234365158e−10	
9	−1.796209196976786e−13	
10	1.106557279892681e−12	
11	−1.632934201917820e−15	
12	7.360649029213635e−15	

Table 1.4: Coefficients of the quasi-bicircular motion of the Earth-Moon-Sun system. The coefficients less than 10^{-15} have not been printed.

Consider an inertial reference frame centered at the center of masses B. Let $\vec{r}$ and $\vec{R}$ be the vectors introduced in section 1.4 in the Jacobi decomposition (see figure 1.4). We suppose that the motion of the three primaries stands on a plane. This plane can be considered the xy plane, without loss of generality. In this reference frame, the position vectors of the Earth, Moon and Sun are the following:

$$\begin{aligned}
\vec{\rho}_e &= -\frac{m_s}{M}\vec{R} + \frac{m_m}{m_m+m_e}\vec{r} &&= -\frac{m_s}{1+m_s}\vec{R} + \mu\,\vec{r}\,, \\
\vec{\rho}_m &= -\frac{m_s}{M}\vec{R} - \frac{m_e}{m_m+m_e}\vec{r} &&= -\frac{m_s}{1+m_s}\vec{R} - (1-\mu)\,\vec{r}\,, \\
\vec{\rho}_s &= \frac{m_m+m_e}{M}\vec{R} &&= \frac{1}{1+m_s}\vec{R}\,,
\end{aligned}$$

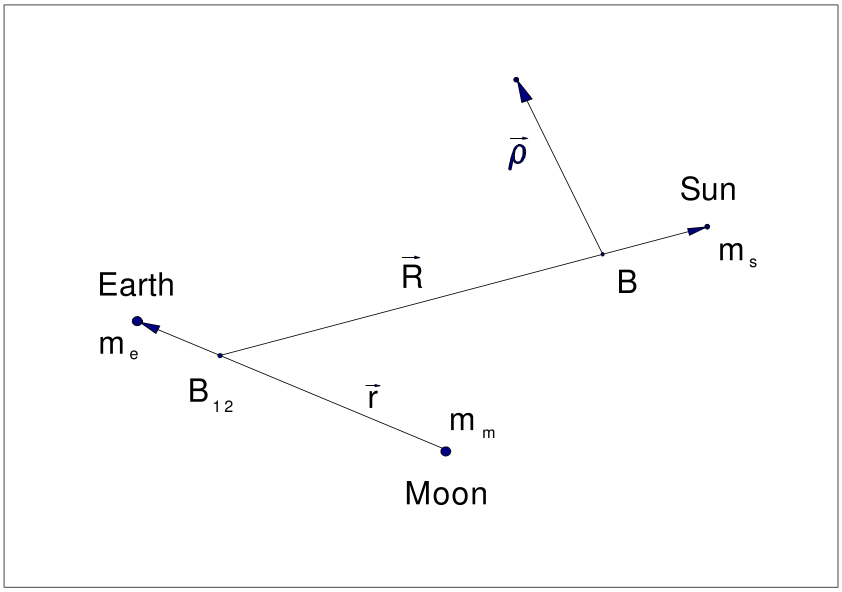

Figure 1.4: Quasi-bicircular Problem in an inertial reference frame.

being $M = m_e + m_m + m_s$ and

$$\vec{r}(t) = (r_1(t), r_2(t), 0)^T \,, \qquad \vec{R}\,(t) = (R_1(t), R_2(t), 0)^T \,.$$

Now, we are going to perform a change of coordinates. The change consists in a translation followed by a rotation and followed by an homothetic transformation. The translation sends the origin of coordinates to the Earth-Moon barycenter. The rotation puts the Earth and the Moon on the x axis. Finally, the homothetic transformation makes constant the Earth-Moon distance. This is a rotating pulsating reference frame. The new coordinates are related to the old ones by the formula

$$\vec{q} = \frac{1}{r}\, C^T \left(\vec{\rho} + \frac{m_s}{1+m_s}\, \vec{R}\right) \,,$$

where

$$C = \begin{pmatrix} \frac{r_1}{r} & -\frac{r_2}{r} & 0 \\ \frac{r_2}{r} & \frac{r_1}{r} & 0 \\ 0 & 0 & 1 \end{pmatrix} \,.$$

Notice that $C\,C^T = I$, because $r^2 = r_1^2 + r_2^2$. Using this reference frame, the coordinates of the Earth, Moon and Sun become

$$\begin{aligned} \vec{q}_e &= (\mu, 0, 0)^T \,, \\ \vec{q}_m &= (\mu - 1, 0, 0)^T \,, \\ \vec{q}_s &= \frac{1}{r}\, C^T\, \vec{R} \,. \end{aligned}$$

In this way, the Earth and the Moon are located at the same place as in the RTBP and the BCP. This is useful to make comparisons and also we can think about the QBCP as a perturbation of the RTBP. If we write the old coordinates of the particle as a function of the new ones, we have

$$\vec{\rho} = -\frac{m_s}{1+m_s}\vec{R} + B\vec{q} \ ,$$

where

$$B = r\,C = \begin{pmatrix} r_1 & -r_2 & 0 \\ r_2 & r_1 & 0 \\ 0 & 0 & r \end{pmatrix} .$$

In this case, the following equalities hold:

$$B\,B^T = r^2 I \ , \qquad\qquad B^{-1} = \frac{1}{r^2} B^T \ .$$

It is easy to see that the distances from the particle to the primaries have changed in the following way:

$$\|\vec{\rho}_e - \vec{\rho}\| = r\,\|\vec{q}_e - \vec{q}\| \ , \qquad \|\vec{\rho}_m - \vec{\rho}\| = r\,\|\vec{q}_m - \vec{q}\| \ , \qquad \|\vec{\rho}_s - \vec{\rho}\| = r\,\|\vec{q}_s - \vec{q}\| \ .$$

Therefore, the potential energy is

$$U = -\frac{1-\mu}{r\,\|\vec{q}_e - \vec{q}\|} - \frac{\mu}{r\,\|\vec{q}_m - \vec{q}\|} - \frac{m_s}{r\,\|\vec{q}_s - \vec{q}\|} \ .$$

The next step is to transform the kinetic energy

$$T = \frac{1}{2} < \dot{\vec{\rho}}, \dot{\vec{\rho}} > \ .$$

Taking into account that

$$\dot{\vec{\rho}} = -\frac{m_s}{1+m_s}\dot{\vec{R}} + \dot{B}\vec{q} + B\dot{\vec{q}} \ ,$$

substituting into the previous expression we have

$$T = \frac{1}{2} r^2 \dot{\vec{q}}^{\,2} + \vec{q}^{\,T} \dot{B}^T B \dot{\vec{q}} + \frac{1}{2} \vec{q}^{\,T} \dot{B}^T \dot{B} \vec{q} -$$

$$- \frac{m_s}{1+m_s} \dot{\vec{R}}^T \dot{B} \vec{q} - \frac{m_s}{1+m_s} \dot{\vec{R}}^T B \dot{\vec{q}} + \frac{m_s^2}{2(1+m_s)^2} \dot{\vec{R}}^2 \ .$$

We define the momentum

$$\vec{p} = \frac{\partial T}{\partial \dot{\vec{q}}} = r^2 \dot{\vec{q}} + B^T \dot{B} \vec{q} - \frac{m_s}{1+m_s} B^T \dot{\vec{R}} \ ,$$

and so

$$\dot{\vec{q}} = \frac{1}{r^2}\left(\vec{p} - B^T\dot{B}\vec{q} + \frac{m_s}{1+m_s}B^T\dot{\vec{R}}\right) .$$

Substituting this expression in the kinetic energy, by a straightforward calculation, we arrive at

$$T = \frac{1}{2r^2}\,\vec{p}^{\,2} .$$

Then, we define the Hamiltonian

$$\begin{aligned} H &= \vec{p}\dot{\vec{q}} - T + U = \\ &= \frac{1}{2r^2}\vec{p}^{\,2} - \frac{1}{r^2}\vec{p}B^T\dot{B}\vec{q} + \frac{m_s}{1+m_s}\frac{1}{r^2}\dot{\vec{R}}^T B\vec{p} + U , \end{aligned}$$

and then the Hamiltonian equations are

$$\dot{\vec{q}} = \frac{\partial H}{\partial \vec{p}} = \frac{1}{r^2}\vec{p} - \frac{1}{r^2}B^T\dot{B}\vec{q} + \frac{m_s}{1+m_s}\frac{1}{r^2}B^T\dot{\vec{R}} , \tag{1.18}$$

$$\dot{\vec{p}} = -\frac{\partial H}{\partial \vec{q}} = \frac{1}{r^2}\dot{B}^T B\vec{p} - \frac{\partial U}{\partial \vec{q}} . \tag{1.19}$$

However, we are going to modify the Hamiltonian slightly. The system of first order differential equations (1.18) and (1.19) is equivalent to the second order equation

$$\frac{d}{dt}(r^2\dot{\vec{q}} + B^T\dot{B}\vec{q}) = \frac{1}{r^2}\dot{B}^T B(r^2\dot{\vec{q}} + B^T\dot{B}\vec{q}) + \frac{m_s}{1+m_s}B^T\ddot{\vec{R}} - \frac{\partial U}{\partial \vec{q}} .$$

Therefore, we can redefine the momentum as

$$\vec{p} = r^2\dot{\vec{q}} + B^T\dot{B}\vec{q} ,$$

and then the first order differential equations are

$$\begin{aligned} \dot{\vec{q}} &= \frac{1}{r^2}\left(\vec{p} - B^T\dot{B}\vec{q}\right) , \\ \dot{\vec{p}} &= \frac{1}{r^2}\dot{B}^T B\vec{p} + \frac{m_s}{1+m_s}B^T\ddot{\vec{R}} - \frac{\partial U}{\partial \vec{q}} . \end{aligned}$$

Finally, the Hamiltonian corresponding to these equations is

$$H = \frac{1}{2r^2}\,\vec{p}^{\,2} - \frac{1}{r^2}\vec{p}B^T\dot{B}\vec{q} - \frac{m_s}{1+m_s}\ddot{\vec{R}}^T B\vec{q} + U . \tag{1.20}$$

We want to remark that the Hamiltonian of the BCP is a particular case of the (1.20). Using

$$\vec{r} = (\cos t, \sin t, 0)^T , \qquad \vec{R} = a_s(\cos n_s t, \sin n_s t, 0)^T ,$$

$$B = \begin{pmatrix} \cos t & -\sin t & 0 \\ \sin t & \cos t & 0 \\ 0 & 0 & 1 \end{pmatrix} ,$$

the Hamiltonian of section 1.3 is easily obtained.

1.5.1 The Hamiltonian and the equations of motion

At this moment we have all the ingredients to display the Hamiltonian of the QBCP. The formula (1.20) expresses the general form of the Hamiltonian and a solution of the quasi-bicircular movement of the Earth-Moon-Sun system was given in section 1.4.2. Then, we only should take that solution, put it into the Hamiltonian (1.20) and arrange it to have a pretty look.

Remind that in section 1.4.2 we got the expression of the quasi-bicircular motion in the complex form:

$$\begin{aligned} z &= e^{it}\sum_j b_j e^{ijnt} , \\ Z &= a_s e^{in_s t}\sum_j c_j e^{ijnt} . \end{aligned}$$

The complex variables z and Z correspond to the real vectors $\vec{r}$ and $\vec{R}$, respectively. This means that

$$z = r_1 + r_2 i , \qquad Z = R_1 + R_2 i ,$$

and

$$r^2 = z\overline{z} .$$

On the other hand, it is easy to obtain

$$B^T\dot{B} = \begin{pmatrix} \beta_1 & -\beta_2 & 0 \\ \beta_2 & \beta_1 & 0 \\ 0 & 0 & \beta_1 \end{pmatrix} ,$$

where

$$\begin{aligned} \beta_1 &= r_1\dot{r_1} + r_2\dot{r_2} = Re(\dot{z}\overline{z}) , \\ \beta_2 &= r_1\dot{r_2} - r_2\dot{r_1} = Im(\dot{z}\overline{z}) . \end{aligned}$$

In the same way, we calculate

$$\ddot{\vec{R}}^T B = (\beta_3, \beta_4, 0) ,$$

being

$$\begin{aligned} \beta_3 &= r_1\ddot{R}_1 + r_2\ddot{R}_2 = Re(\ddot{Z}\overline{z}) , \\ \beta_4 &= r_1\ddot{R}_2 - r_2\ddot{R}_1 = Im(\ddot{Z}\overline{z}) . \end{aligned}$$

The potential energy is also depending on time through the position vector of the Sun which is

$$\vec{q}_s = \frac{1}{r^2} B^T\vec{R} = \frac{1}{r^2}\begin{pmatrix} \beta_5 \\ \beta_6 \\ 0 \end{pmatrix} ,$$

where

$$\begin{aligned}\beta_5 &= r_1R_1 + r_2R_2 = Re(Z\overline{z}) \ ,\\ \beta_6 &= r_1R_2 - r_2R_1 = Im(Z\overline{z}) \ .\end{aligned}$$

Now, we perform all the products of Fourier series which appeared above to obtain

$$\begin{aligned}
z\overline{z} &= \left(\sum_j b_j e^{ijnt}\right)\left(\sum_j b_j e^{-ijnt}\right) \ ,\\
\dot{z}\overline{z} &= i\left(\sum_j (1+jn) b_j e^{ijnt}\right)\left(\sum_j b_j e^{-ijnt}\right) \ ,\\
Z\overline{z} &= a_s e^{-int}\left(\sum_j c_j e^{ijnt}\right)\left(\sum_j b_j e^{-ijnt}\right) \ ,\\
\ddot{Z}\overline{z} &= -a_s e^{-int}\left(\sum_j (n_s+jn)^2 c_j e^{ijnt}\right)\left(\sum_j b_j e^{-ijnt}\right) \ ,
\end{aligned}$$

and we see that all the products depend only on one frequency. This is $n = 1 - n_s$, the difference between the mean angular velocity of the Moon and the Sun.

We introduce the following periodic functions $\alpha_k(t)$:

$$\alpha_1 = \frac{1}{r^2} \ , \qquad \alpha_2 = -\frac{Re(\dot{z}\overline{z})}{r^2} \ , \qquad \alpha_3 = \frac{Im(\dot{z}\overline{z})}{r^2} \ ,$$

$$\alpha_4 = -\frac{m_s}{1+m_s} Re(\ddot{Z}\overline{z}) \ , \qquad \alpha_5 = -\frac{m_s}{1+m_s} Im(\ddot{Z}\overline{z}) \ , \qquad \alpha_6 = \frac{1}{r} \ ,$$

$$\alpha_7 = \frac{1}{r^2} Re(Z\overline{z}) \ , \qquad \alpha_8 = \frac{1}{r^2} Im(Z\overline{z}) \ .$$

We realize that all the α_k functions are even or odd. The Fourier series of the even functions have only terms with cosines and the odd functions only terms with sinus. The functions α_1, α_3, α_4, α_6, α_7 are even. The other ones, α_2, α_5, α_8 are odd. In other words, the α_k functions are of the following types:

$$\alpha_k(t) = \alpha_{k0} + \sum_{j\geq 1} \alpha_{kj} \cos(jnt) \ , \qquad \text{for } k = 1,3,4,6,7, \tag{1.21}$$

$$\alpha_k(t) = \sum_{j\geq 1} \alpha_{kj} \sin(jnt) \ , \qquad \text{for } k = 2,5,8, \tag{1.22}$$

being α_{kj} real numbers.

We can compute the Fourier coefficients of the α_k functions using the coefficients of z and Z given in section 1.4.2. It is easy to make a small program to perform these calculations. We only want to make a remark. Since $r \simeq 1$, in order to compute $1/r$, we write $r = (1+\Delta)^{1/2}$ and we use the Taylor expansion

$$\frac{1}{r} = (1+\Delta)^{-1/2} = 1 - \frac{1}{2}\Delta + \frac{3}{8}\Delta^2 - \frac{5}{16}\Delta^3 + \dots \ .$$

j	α_1 c	α_2 s	α_3 c
0	1.00184160892484e+00		9.99999999999998e-01
1	5.76751772619840e-04	-2.64437602849994e-04	5.63412599755369e-04
2	1.43877702550763e-02	-1.32868690340017e-02	1.88968744017288e-02
3	-2.63036297497202e-06	9.38609320808975e-06	-9.91175880256713e-06
4	1.17627835611893e-04	-1.21850905751741e-04	1.56870813603113e-04
5	-8.06858139100555e-08	1.52212759855701e-07	-1.70776257617348e-07
6	9.84324976650129e-07	-1.07210266427800e-06	1.31961367970744e-06
7	-1.17205439441820e-09	1.88937126137405e-09	-2.13655004198565e-09
8	8.31190597087959e-09	-9.32498503892749e-09	1.11716891667389e-08
9	-1.40858423869539e-11	2.11449098128026e-11	-2.38725363103111e-11
10	7.05071378646684e-11	-8.07111174314435e-11	9.49087962209590e-11
11	-1.49425963491046e-13	2.21811805042017e-13	-2.46273258155843e-13
12	5.98241897945123e-13	-7.03615516188201e-13	8.10106770800974e-13
14		-3.96722989612218e-15	1.35423199846983e-15

j	α_4 c	α_5 s	α_6 c
0	-9.75524232748489e-04		1.00090745770816e+00
1	2.15476436270711e+00	-2.19257075104007e+00	2.87092175005313e-04
2	3.65748446896870e-04	-3.33721048547287e-04	7.18717799861288e-03
3	3.29567337616659e-03	-3.29500143020097e-03	-2.35118314721325e-06
4	3.30103140081243e-07	-3.10063505305263e-07	4.58575897112206e-05
5	1.27884068737632e-05	-1.27777733685413e-05	-3.84868362010704e-08
6	-2.62379795212793e-09	2.65280640549811e-09	3.27067750493567e-07
7	6.53380551456151e-08	-6.52847924508507e-08	-4.40696648104188e-10
8	-3.89172070778351e-11	3.89172070778351e-11	2.45260066257026e-09
9	3.81227583894443e-10	-3.81227583894443e-10	-4.54293880067344e-12
10	-3.90790604983488e-13	3.90790604983488e-13	1.89234885511262e-11
11	2.40747118757644e-12	-2.40747118757644e-12	-4.17842010148012e-14
12			1.48004894696158e-13

j	α_7 c	α_8 s
0	-6.31406956800623e-02	
1	3.88563862309805e+02	-3.89743725623765e+02
2	1.73691020334556e-01	-1.73427916632252e-01
3	3.38290807166970e+00	-3.38569648664212e+00
4	1.57483756538049e-04	-1.55588663241340e-04
5	2.93636048900444e-02	-2.93758267196753e-02
6	-1.22443455011601e-05	1.22585121310793e-05
7	2.53893543426244e-04	-2.53959688769264e-04
8	-2.27892904000757e-07	2.28002922020236e-07
9	2.19043270618166e-06	-2.19083462442904e-06
10	-3.03331196123435e-09	3.03610903512086e-09
11	1.88697154529022e-08	-1.88745764757932e-08
12	-3.43237510689845e-11	3.43237510689845e-11
13	1.61151370399910e-10	-1.63172364150645e-10

Table 1.5: Fourier coefficients of α_k functions. In the top right corner of each table we have put c or s to indicate if the series is of the type 1.21 or 1.22, respectively.

The Fourier coefficients of the α_k functions are shown in table 1.5. Here, the criterion to truncate the series is based on the relative value of the coefficient with respect to the one with maximal absolute value, inside each series.

Let $\vec{q} = (x, y, z)^T$ be the position vector and $\vec{p} = (p_x, p_y, p_z)^T$ the momentum. We hope that there is no confusion between the coordinate z and the previous use of z. The Hamiltonian of the QBCP is

$$\begin{aligned} H &= \frac{1}{2}\alpha_1(p_x^2 + p_y^2 + p_z^2) + \alpha_2(p_x x + p_y y + p_z z) + \alpha_3(p_x y - p_y x) + \\ &\quad + \alpha_4 x + \alpha_5 y - \alpha_6 \left(\frac{1-\mu}{q_{pe}} + \frac{\mu}{q_{pm}} + \frac{m_s}{q_{ps}}\right) , \end{aligned} \tag{1.23}$$

where

$$\begin{aligned} q_{pe}^2 &= (x-\mu)^2 + y^2 + z^2 , \\ q_{pm}^2 &= (x-\mu+1)^2 + y^2 + z^2 , \\ q_{ps}^2 &= (x-\alpha_7)^2 + (y-\alpha_8)^2 + z^2 . \end{aligned}$$

Therefore, the Hamiltonian equations are the following:

$$\begin{aligned} \dot{x} &= \alpha_1 p_x + \alpha_2 x + \alpha_3 y , \\ \dot{y} &= \alpha_1 p_y + \alpha_2 y - \alpha_3 x , \\ \dot{z} &= \alpha_1 p_z + \alpha_2 z , \\ \dot{p}_x &= -\alpha_2 p_x + \alpha_3 p_y - \alpha_4 - \alpha_6 \left(\frac{1-\mu}{q_{pe}^3}(x-\mu) + \frac{\mu}{q_{pm}^3}(x-\mu+1) + \frac{m_s}{q_{ps}^3}(x-\alpha_7)\right) , \\ \dot{p}_y &= -\alpha_2 p_y - \alpha_3 p_x - \alpha_5 - \alpha_6 \left(\frac{1-\mu}{q_{pe}^3}y + \frac{\mu}{q_{pm}^3}y + \frac{m_s}{q_{ps}^3}(y-\alpha_8)\right) , \\ \dot{p}_z &= -\alpha_2 p_z - \alpha_6 \left(\frac{1-\mu}{q_{pe}^3}z + \frac{\mu}{q_{pm}^3}z + \frac{m_s}{q_{ps}^3}z\right) . \end{aligned} \tag{1.24}$$

These equations present two trivial symmetries:

$$\begin{aligned} S_1 : (x, y, z, \dot{x}, \dot{y}, \dot{z}, t) &\longleftrightarrow (x, y, -z, \dot{x}, \dot{y}, -\dot{z}, t) , \\ S_2 : (x, y, z, \dot{x}, \dot{y}, \dot{z}, t) &\longleftrightarrow (x, -y, z, -\dot{x}, \dot{y}, -\dot{z}, -t) . \end{aligned}$$

To check the second one it is necessary to take into account the parity properties of the α_k functions. The equations of the RTBP and the BCP present also the same symmetries S_1 and S_2. They will be useful in subsequent chapters when looking for periodic and quasi-periodic orbits.

Once we have the Hamiltonian of the QBCP, it is interesting to go back to section 1.3 and compare it with the one of the BCP. Indeed, in the BCP the values of the

α coefficients are as follows:

$$\alpha_1 = \alpha_3 = \alpha_6 = 1 \ , \qquad \alpha_2 = 0 \ ,$$

$$\alpha_4 = \frac{m_s}{a_s^2} \cos\theta \ , \qquad \alpha_5 = -\frac{m_s}{a_s^2} \sin\theta \ ,$$

$$\alpha_7 = a_s \cos\theta \ , \qquad \alpha_8 = -a_s \sin\theta \ .$$

We recall that $\dfrac{m_s}{a_s^2} \simeq 2.1756$ and $a_s \simeq 388.81$.

Chapter 2

Periodic orbits around Lagrange points

2.1 Introduction

We have seen in the previous chapter that the QBCP is a time periodic three degrees of freedom Hamiltonian system. It can be considered as a time periodic perturbation of the RTBP. The main difference between both models is that the RTBP is autonomous while the QBCP is non-autonomous. Let T be the period of the perturbation. Then, in the QBCP all the periodic orbits have period T or multiples of T. Furthermore, the RTBP has five equilibrium points. The QBCP does not have equilibrium points, but we expect the existence of some periodic orbits substituting, in some sense, the equilibrium points of the RTBP.

In this chapter, we are going to compute T-periodic orbits of the QBCP. Most of them come from periodic orbits of RTBP and they will be obtained using continuation techniques. In particular, it will be useful to consider the family of Hamiltonians

$$H = H_{RTBP} + \epsilon \left(H_{QBCP} - H_{RTBP} \right) , \tag{2.1}$$

depending on the parameter ϵ and compute families of T-periodic orbits of this Hamiltonian when varying ϵ. For $\epsilon = 0$ we have the Hamiltonian of the RTBP and for $\epsilon = 1$ the Hamiltonian of the QBCP.

Before showing the results, we are going to summarize the numerical methods used.

2.2 Numerical tools

This section is devoted to explain the numerical tools used to compute periodic orbits, study their stability, compute families of periodic orbits using continuation methods and analyze the bifurcations along the families. Most of these topics are discussed in [25].

2.2.1 T-periodic orbits

Consider an autonomous system $\dot{x} = f(x)$, with $x \in U \subset \mathbb{R}^n$. Let $\phi(t, x_0)$ (or $\phi_t(x_0)$) be the solution of that system with the initial condition $\phi(0, x_0) = x_0$. The problem of computing a T-periodic orbit could be stated as finding a zero of the function $G(x_0) = \phi(T, x_0) - x_0$. But, if x_0 is a solution then for all $t \in \mathbb{R}$, $\phi(t, x_0)$ is also a solution, because of the autonomous character of the system. As a consequence of that, $DG(x_0) = D\phi(T, x_0) - I$ is singular, where I means the n-dimensional identity matrix. In other words, the monodromy matrix $D\phi(T, x_0)$ has an eigenvalue equal to 1 and the corresponding eigenvector is $f(x_0)$.

For that reason, it is better not to fix the period. Instead of that approach, the Poincaré map can be used with a certain section Σ transversal to the flow. Then, the problem is to find fixed points of the Poincaré map. Once we have a fixed point, the corresponding periodic orbit will not probably have the wanted period, but if it is not isolated then it is possible to use a continuation method to compute the orbits of the family in which it is embedded, in order to look for a T-periodic orbit of the system. For instance, in the Hamiltonian case, periodic orbits are not isolated.

Now, consider a system of the form

$$\dot{x} = f(t, x) \ , \tag{2.2}$$

where $x \in U \subset \mathbb{R}^n$ and f is T-periodic in t. The periodic orbits should have period T or multiples of T. If we want a T-periodic orbit, we can look for a zero of the function $G(x_0) = \phi(T, x_0) - x_0$. In the non autonomous case, generally, $DG(x_0)$ is nonsingular and so, we do not have the troubles of the autonomous case (unless the system is a too small perturbation of an autonomous one). Furthermore, we notice that not all the points of a periodic orbit can be taken as initial condition at $t = 0$. Another point which is interesting to comment is the fact that, in the non autonomous case, generically, periodic orbits are isolated.

If the system has some symmetries, we can take advantage of that to restrict the search of periodic orbits to a subset of the phase space of lower dimension. Moreover, sometimes, it is only necessary to integrate the differential equations during a fraction of the period. For instance, in the RTBP and the QBCP, many orbits that we are going to compute have initial conditions at $y = \dot{x} = \dot{z} = 0$. Due to the symmetry S_2 of section 1.5.1, those orbits are symmetric with respect to the $y = 0$ plane, and it is enough to integrate up to $T/2$.

2.2.2 Variational equations and monodromy matrix

We continue considering a system of the form (2.2) and suppose that a T-periodic orbit, $x_0(t)$, is known. In order to study the linear stability of that orbit, the first variational equations are considered:

$$\frac{d}{dt}\frac{d\phi_t(x)}{dx} = D_x f(t, x_0(t)) \frac{d\phi_t(x)}{dx} \ , \qquad \left.\frac{d\phi_t(x)}{dx}\right|_{t=0} = I \ .$$

That is a linear matrix differential equation of the form

$$\dot{A} = B(t)\, A\ , \qquad A(0) = I\ , \tag{2.3}$$

where $B(t)$ is a T-periodic $n \times n$ matrix. The solution $A(t)$ verifies

$$A(t+T) = A(t)\, A(T)\ ,$$

by the uniqueness of the solutions of differential equations, because both sides of this equality satisfy (2.3) and coincide at $t = 0$. The solution after a period of time, $A(T)$, is called the monodromy matrix and its eigenvalues are the characteristic multipliers of the periodic orbit.

The matrix equation (2.3) is said reversible (or G-reversible, to be more accurate) if there exists a nonsingular constant matrix G such that (2.3) is invariant under the change of variables

$$t = -\tau\ , \quad A = G\,\tilde{A}\ ,$$

and $G^2 = I$. In such case, the matrix $B(t)$ satisfies identically

$$B(t) = -G^{-1} B(-t)\, G\ , \tag{2.4}$$

and the solution

$$A(-t) = G^{-1} A(t)\, G\ .$$

Hence, knowing the solution $A(t)$ for all $t \in [0, T/2]$, it is possible to compute $A(t)$ for all $t \in \mathbb{R}$. As a particular case, the monodromy matrix can be obtained from

$$A(T) = G^{-1}\, A(T/2)^{-1} G\, A(T/2)\ .$$

This is specially useful for highly unstable solutions because it allows to compute the monodromy matrix and its eigenvalues with more accuracy. Further properties about linear differential equations with periodic coefficients can be found in [30].

In the QBCP, from (1.24), the matrix of the variational equations is

$$B = \begin{pmatrix} \alpha_2 & \alpha_3 & 0 & \alpha_1 & 0 & 0 \\ -\alpha_3 & \alpha_2 & 0 & 0 & \alpha_1 & 0 \\ 0 & 0 & \alpha_2 & 0 & 0 & \alpha_1 \\ b_1 & b_2 & b_4 & -\alpha_2 & \alpha_3 & 0 \\ b_2 & b_3 & b_5 & -\alpha_3 & -\alpha_2 & 0 \\ b_4 & b_5 & b_6 & 0 & 0 & -\alpha_2 \end{pmatrix} ,$$

where

$$b_1 = \alpha_6 \left(\frac{3\bar{\mu}}{q_{pe}^5}(x-\mu)^2 - \frac{\bar{\mu}}{q_{pe}^3} + \frac{3\mu}{q_{pm}^5}(x+\bar{\mu})^2 - \frac{\mu}{q_{pm}^3} + \frac{3m_s}{q_{ps}^5}(x-\alpha_7)^2 - \frac{ms}{q_{ps}^3} \right) ,$$

$$b_2 = \alpha_6 \left(\frac{3\bar{\mu}}{q_{pe}^5}(x-\mu)y + \frac{3\mu}{q_{pm}^5}(x+\bar{\mu})y + \frac{3m_s}{q_{ps}^5}(x-\alpha_7)(y-\alpha_8) \right) ,$$

$$
\begin{aligned}
b_3 &= \alpha_6 \left(\frac{3\bar{\mu}}{q_{pe}^5} y^2 - \frac{\bar{\mu}}{q_{pe}^3} + \frac{3\mu}{q_{pm}^5} y^2 - \frac{\mu}{q_{pm}^3} + \frac{3m_s}{q_{ps}^5} (y-\alpha_8)^2 - \frac{ms}{q_{ps}^3} \right) , \\
b_4 &= \alpha_6 \left(\frac{3\bar{\mu}}{q_{pe}^5} (x-\mu) z + \frac{3\mu}{q_{pm}^5} (x+\bar{\mu}) z + \frac{3m_s}{q_{ps}^5} (x-\alpha_7) z \right) , \\
b_5 &= \alpha_6 \left(\frac{3\bar{\mu}}{q_{pe}^5} yz + \frac{3\mu}{q_{pm}^5} yz + \frac{3m_s}{q_{ps}^5} (y-\alpha_8) z \right) , \\
b_6 &= \alpha_6 \left(\frac{3\bar{\mu}}{q_{pe}^5} z^2 - \frac{\bar{\mu}}{q_{pe}^3} + \frac{3\mu}{q_{pm}^5} z^2 - \frac{\mu}{q_{pm}^3} + \frac{3m_s}{q_{ps}^5} z^2 - \frac{ms}{q_{ps}^3} \right) ,
\end{aligned}
$$

being $\bar{\mu} = 1 - \mu$. For symmetric periodic orbits ($y(0) = \dot{x}(0) = \dot{z}(0) = 0$), the variational equations are reversible. It is easy to check the symmetry condition (2.4) with the diagonal matrix

$$
G = \begin{pmatrix} 1 & & & & & \\ & -1 & & & & \\ & & 1 & & & \\ & & & -1 & & \\ & & & & 1 & \\ & & & & & -1 \end{pmatrix} .
$$

We notice that $G^2 = I$ and so $G^{-1} = G$.

2.2.3 Eigenvalues of the monodromy matrix

To study the linear stability of a periodic orbit it is necessary to compute the eigenvalues of the monodromy matrix. The QBCP is a three degrees of freedom Hamiltonian system and so, the monodromy matrix, M, is a 6×6 symplectic matrix. In such case, we know that if $\lambda \in \mathrm{Spec}(M)$ then $\lambda^{-1} \in \mathrm{Spec}(M)$. Therefore, the eigenvalues are

$$
\lambda_1, \;\; 1/\lambda_1, \;\; \lambda_2, \;\; 1/\lambda_2, \;\; \lambda_3, \;\; 1/\lambda_3 \; ,
$$

and they can be real or complex. The characteristic polynomial is

$$
\begin{aligned}
p(\lambda) &= \det(M - \lambda I) = \\
&= (\lambda^2 - s_1\lambda + 1)(\lambda^2 - s_2\lambda + 1)(\lambda^2 - s_3\lambda + 1) \, ,
\end{aligned} \tag{2.5}
$$

where

$$
s_k = \lambda_k + 1/\lambda_k \; , \quad \text{for } \; k = 1, 2, 3 \; ,
$$

and they are called stability parameters. Notice that for autonomous systems, at least one of the eigenvalues is equal to 1 with multiplicity 2. But, the QBCP is non autonomous and then all the eigenvalues can be different from 1. An orbit is lineary stable if its stability parameters are real and their absolute values are less than 2.

To compute the stability parameters we can evaluate $p(1)$ and $p(-1)$. These values can be obtained through the determinant, using Gaussian elimination. Now, we define

$$a = s_1 + s_2 + s_3\ ,\quad b = s_1 s_2 + s_1 s_3 + s_2 s_3\ ,\quad c = s_1 s_2 s_3\ .$$

Notice that $a = Tr(M)$ and it is trivially computed. Taking into account (2.5) we find the following relationships

$$\begin{aligned} 16 + 4b &= p(1) + p(-1)\ , \\ 8a + 2c &= -p(1) + p(-1)\ , \end{aligned}$$

which allow to determine b and c. Then, the problem of computing the stability parameters is reduced to find the roots of the polynomial

$$q(x) = x^3 - ax^2 + bx - c\ .$$

It is clear that at least one of the stability parameters is real. This one can be found with Newton's method. After that, using backward deflation, we arrive at a second degree equation which gives the other two stability parameters. We want to remark that, in our case, one of the stability parameters is often very large ($> 10^6$). For this reason, it is better to use backward instead of forward deflation (see [28]).

2.2.4 Bifurcation of periodic orbits from an autonomous system to a non autonomous system

In this section, we are going to deal with a non-autonomous system which is a perturbation of an autonomous system. Consider

$$\dot{x} = f(x) + \epsilon\, g(x, t)\ , \tag{2.6}$$

where $x \in U \subset \mathbb{R}^n$ and g is T-periodic with respect to t. Suppose that we have a T-periodic orbit, $x_0(t)$, of the autonomous system $\dot{x} = f(x)$. In this system, any point of that orbit, for example $x_0(0)$, can be taken as initial point for any initial epoch, t, and we get the same periodic orbit. We are interested in knowing what points (or equivalently, for which values of t the point $x_0(0)$) can be continued leading to periodic orbits for small values of the parameter ϵ. For this purpose, we introduce an unknown time shift s into the equation (2.6). Then, we look for a solution of (2.6) of the form

$$x(t) = x_0(t) + \epsilon x_1(t) + \epsilon^2 x_2(t) + \dots\ . \tag{2.7}$$

We substitute (2.7) into (2.6) and expand f and g around the periodic orbit. Equating terms of first order in ϵ, we obtain

$$\dot{x}_1 = Df(x_0)x_1 + g(x_0, t+s)\ , \qquad x_1(0) = a\ ,$$

where the time shift s and the initial condition a are unknowns which are wanted to be determined. The differential equation for x_2 is obtained from the terms of second order in ϵ and it is

$$\dot{x}_2 = Df(x_0)x_2 + \frac{1}{2}D^2 f(x_0)(x_1)^2 + D_x g(x_0, t+s)x_1 \ ,$$

and the initial condition can be chosen $x_2(0) = 0$. In fact, $x_k(0)$ can be taken equal to zero for all $k \geq 2$.

Let $A(t)$ be the solution of the variational equations along the periodic orbit of the autonomous system

$$\dot{A}(t) = Df(x_0)A(t) \ , \qquad A(0) = I \ .$$

Then, x_1 and x_2 can be expressed in the following way:

$$\begin{aligned} x_1(t) &= A(t)\,(a + y_1(t,s)) \ , \\ x_2(t) &= A(t)\,y_2(t,s) \ , \end{aligned}$$

where

$$\begin{aligned} \dot{y}_1 &= A^{-1}(t)\,g(x_0(t), t+s) \ , \\ \dot{y}_2 &= A^{-1}(t)\left(\frac{1}{2}D^2 f(x_0(t))(x_1(t))^2 + D_x g(x_0(t), t+s)x_1(t)\right) \ , \end{aligned}$$

with $y_1(t=0) = y_2(t=0) = 0$. The periodicity condition for $x(t)$ is

$$x_0(0) + \epsilon a = x_0(T) + \epsilon x_1(T) + \epsilon^2 x_2(T) + \dots \ ,$$

which should be taken into account to determine a and s. Then, for x_1 we have

$$(A(T) - I)\,a = -A(T)\,y_1(T,s) \ . \tag{2.8}$$

From now on, in order to make easier the explanation, we are going to particularize to the case which we are interested in. That is the case where the autonomous system is the RTBP and the non autonomous is the QBCP. Then, due to the Hamiltonian character of the system, we know that the monodromy matrix $A(T)$ has an eigenvalue equal to 1 with multiplicity two, at least. Moreover, we will discuss only the case where the other eigenvalues are $\alpha \pm \beta i$, λ and λ^{-1}, $\lambda \in \mathbb{R}$. It is possible to change the basis and express the matrix $A(T)$ in Jordan form

$$A(T) = \begin{pmatrix} 1 & 0 & 0 & \gamma & 0 & 0 \\ 0 & \alpha & 0 & 0 & \beta & 0 \\ 0 & 0 & \lambda & 0 & 0 & 0 \\ 0 & 0 & 0 & 1 & 0 & 0 \\ 0 & -\beta & 0 & 0 & \alpha & 0 \\ 0 & 0 & 0 & 0 & 0 & \lambda^{-1} \end{pmatrix} . \tag{2.9}$$

The fact that the Jordan block associated to the eigenvalue 1 is non diagonal ($\gamma \neq 0$) is generic. This is related to variation of the period with the energy in the autonomous system. Let $b_1, \ldots, b_6$ the components of the vector $-A(T)\, y_1(T, s)$ in such basis. The periodicity condition (2.8) brings to the one dimensional equation $b_4(s) = 0$. The solutions of this equation give the possible time shifts leading to bifurcated orbits. Notice that $b_4(s)$ is a T-periodic function of s, and then, generically, it has an even number of zeroes.

If s^* is a zero of the function $b_4(s)$, then the equation (2.8) allows to determine all the components of a except a_1. To find a first approximation of a_1, it is necessary to look at the terms of second order in ϵ. Knowing $a_2, \ldots, a_6$, the fourth component of $A(T)\, y_2(T, s^*)$ gives a second degree equation in a_1. We notice that y_2 depends on a through x_1. The solutions of that second degree equation complete the vector a. In fact, in all the cases studied, there was only one useful solution. The other was zero. The reason is that, generically, there is only one branch for $\epsilon > 0$. The other branch is on $\epsilon = 0$ and it corresponds to the periodic orbit of the autonomous system.

2.2.5 Continuation method using the arc parameter

We are interested in finding T-periodic orbits in the QBCP. This task is difficult to perform directly because such orbits are isolated and frequently are unstable. In the previous section, we have seen that some points of a T-periodic orbit of an autonomous system can be continued under a T-periodic perturbation. So, firstly, we look for T-periodic orbits in the RTBP. This is done following some family of periodic orbits using a continuation method. Then, we consider the family of Hamiltonians (2.1). We study the bifurcating points as we have explained in the previous section. The continuation method using the arc parameter has been used to continue T-periodic orbits from RTBP to QBCP along the family of Hamiltonians (2.1). This method allows to continue periodic orbits while a bifurcation does not occur. Such case will be studied in the next section.

Taking into account that looking for a periodic orbit is equivalent to look for a fixed point of a map (see section 2.2.1), we are going to explain the continuation method with arc parameter in the case of maps. For that purpose, consider a map $P : U \times I \longrightarrow \mathbb{R}^n$, where $U \in \mathbb{R}^n$, $I \in \mathbb{R}^n$ and P is, at least, of class $\mathcal{C}^1$. Imagine that we have the equation $P(x, \epsilon) = 0$ and we know a solution $x(\epsilon_0)$. Our objective is to follow the solution curve, $x(\epsilon)$, up to a certain value of the parameter ϵ_1. While the rank of $DP(x, \epsilon)$ is maximal, the implicit function theorem ensures the existence of the solution curve.

The parameter ϵ can be considered as an additional coordinate, so $x_{n+1} \equiv \epsilon$. From $P(x) = 0$, we have $DP(x)\Delta x = 0$, where $DP(x)$ is the matrix of a linear map from $\mathbb{R}^{n+1}$ to $\mathbb{R}^n$. Let A_j the determinant of the matrix obtained from $DP(x)$ erasing the j-th column times $(-1)^{j+1}$. Then, we have

$$\frac{\Delta x_1}{A_1} = \frac{\Delta x_2}{A_2} = \ldots = \frac{\Delta x_n}{A_n} = \frac{\Delta x_{n+1}}{A_{n+1}} \, .$$

Now, we introduce the arc length in $\mathbb{R}^{n+1}$ as $\Delta s = \left(\sum_{j=1}^{n+1} (\Delta x_j)^2\right)^{1/2}$. Using this definition and the previous equation, passing to the limit, we obtain the differential equation for the solution curve

$$\frac{dx_j}{ds} = \frac{\pm A_j}{\sqrt{\sum_{k=1}^{n+1} A_k^2}} , \quad j = 1, \ldots, n+1 . \tag{2.10}$$

The sign $\pm$ depends on the sense taken along the curve. If the rank of $DP(x)$ is maximum then there is some determinant A_k different from zero and the denominator does not vanish.

The differential equations (2.10) can be integrated using, for instance, Euler's method. After every step in the integration method, it is convenient to refine the obtained point in order to satisfy $P(x) = 0$. This is a nonlinear system of n equations with $n+1$ unknowns. To look for a solution close to the point given by the integration method, one can use a modified Newton's method. The linearized equation around $x^{(k)}$ is

$$P(x^{(k)}) + DP(x^{(k)}) \Delta x^{(k)} = 0 .$$

This is an infradetermined linear system. Demanding $\Delta x^{(k)}$ to be minimum with respect to the Euclidean norm, we obtain the iterative method given by

$$x^{(k+1)} = x^{(k)} - DP(x^{(k)})^T (DP(x^{(k)}) DP(x^{(k)})^T)^{-1} P(x^{(k)}) .$$

The step of the integration method can be controlled depending on the number of iterations needed for the refinement method to achieve a certain threshold. Finally, we want to note that the continuation method using arc parameter works also in the case that a turning point in the parameter ϵ occurs.

2.2.6 Bifurcation analysis

In the previous section, we have seen how the continuation of periodic orbits can be performed in a system of the form

$$\dot{x} = f(t, x, \epsilon) ,$$

with $x \in U \subset \mathbb{R}^n$, $\epsilon \in I \subset \mathbb{R}$ and f T-periodic with respect to t. When we are following a family of periodic orbits, if we arrive at an orbit which has a characteristic multiplier equal to 1, then a bifurcation can appear [19]. In the Hamiltonian case, a characteristic multiplier equal to 1 means that one of the stability parameters is equal to 2.

Let $x_0(t)$ be a possible bifurcating T-periodic orbit of the system for a certain value of the parameter ϵ_0. We want to know what corrections can be added to $x_0(0)$

and ϵ_0 in order to continue having a periodic orbit. These corrections are denoted by Δx and $\Delta\epsilon$, respectively. Expanding around the periodic orbit we have

$$\begin{aligned}\phi_T(x_0+\Delta x,\epsilon_0+\Delta\epsilon) &= \phi_T(x_0,\epsilon_0)+\frac{\partial\phi_T(x_0,\epsilon_0)}{\partial x}\Delta x+\frac{\partial\phi_T(x_0,\epsilon_0)}{\partial\epsilon}\Delta\epsilon+ \\ &+\frac{1}{2}\frac{\partial^2\phi_T(x_0,\epsilon_0)}{\partial x^2}(\Delta x)^2+\frac{\partial^2\phi_T(x_0,\epsilon_0)}{\partial x\,\partial\epsilon}\Delta x\Delta\epsilon+\frac{1}{2}\frac{\partial^2\phi_T(x_0,\epsilon_0)}{\partial\epsilon^2}(\Delta\epsilon)^2+\dots\ ,\end{aligned}$$

which should be equal to $x_0+\Delta x$. We recall that x_0 is a periodic orbit and so $\phi_T(x_0,\epsilon_0)=x_0$.

Now, it is convenient to perform a linear change of variables with the purpose of express the monodromy matrix in Jordan form. Let R be the matrix of that linear change. Then, we have $\Delta x = R\,z$, where z are the new coordinates. Aside from the eigenvalue 1 (double), we are going to suppose that the other eigenvalues are of the form $\alpha\pm\beta i$, λ and λ^{-1}, $\lambda\in\mathbb{R}$. In such case, the monodromy matrix is of the form (2.9). The preceding equations are of the form

$$0=(A-I)z+b\Delta\epsilon+\begin{pmatrix} z^TQ_1z \\ \vdots \\ z^TQ_6z\end{pmatrix}+Cz\Delta\epsilon+d(\Delta\epsilon)^2+\dots\ ,$$

where $b,d\in\mathbb{R}^6$ and A, Q_1, …, Q_6 and C are symmetric 6×6 real matrices. In those equations, many different cases of bifurcation can be studied. Here, we are going to consider only the case in which $b_4=0$ and $b_j\neq 0$, for all $j\neq 4$ (this is the situation for the bifurcations which will be shown later). In this case, the dominant terms of the previous equations are

$$\begin{aligned} 0 &= \gamma z_4+b_1\Delta\epsilon\ , \\ 0 &= (\alpha-1)z_2+\beta z_5+b_2\Delta\epsilon\ , \\ 0 &= (\lambda-1)z_3+b_3\Delta\epsilon\ , \\ 0 &= \sum_{i,j,=1}^{6} q_{4ij}z_iz_j+\sum_{j=1}^{6}c_{4j}\Delta\epsilon z_j+d_4(\Delta\epsilon)^2\ , \\ 0 &= -\beta z_2+(\alpha-1)z_5+b_5\Delta\epsilon\ , \\ 0 &= (\lambda^{-1}-1)z_6+b_6\Delta\epsilon\ .\end{aligned}$$

Hence, we get z_2, z_3, z_4, z_5 and z_6, which are $O(\Delta\epsilon)$. Substituting them into the fourth equation, we have a second degree equation for z_1, which is also $O(\Delta\epsilon)$. In this case, generically, we obtain two bifurcating directions.

2.3 Periodic orbits in the QBCP

To look for T-periodic orbits of the QCBP we begin looking for periodic orbits of the RTBP with period a fraction of T. If an orbit has period T/q with $q\in\mathbb{N}$, it

Label RTBP	N	Labels QBCP
012	2	12, 13
014	4	14, 15, 16, 17
018	4	18, 19, 1A, 1B
01C	2	1C, 1D
01E	2	1E, 1F
022	4	22, 23, 24, 25
026	4	26, 27, 28, 29
02A	4	2A, 2C
02E	2	2E, 2F
02G	2	2G, 2H

Table 2.1: Labels of periodic orbits in RTBP and QBCP. N is the number of bifurcating points of each orbit of the RTBP. The labels in the RTBP are of the form $0jk$, where $j = 1$ or 2 refers to the vicinity of $\mathrm{L_j}$. The index k is different for each orbit around $\mathrm{L_j}$. The labels in the QBCP are simply of the form jk.

can be considered as T-periodic orbit turning q times. We are interested in periodic orbits around the collinear equilibrium points $\mathrm{L_i}$, $i = 1, 2, 3$. Then, following the Lyapunov and Halo families around these points, we have found some periodic orbits with periods T, $T/2$, $T/3$ and $T/4$. Table 2.2 shows the initial conditions for those orbits. All of them are symmetric with respect to the hyperplane $y = 0$. Table 2.2 also shows the stability parameters of those orbits. We remind that the RTBP is autonomous and therefore one of the eigenvalues of the monodromy matrix is equal to 1 with multiplicity 2. This means that one of the stability parameters is equal to 2.

Table 2.1 shows the labels of the periodic orbits of the RTBP given in table 2.2. Second column of table 2.1 shows the number of bifurcating points of each orbit. That is the number of zeroes of the function $b_4(s)$ of section 2.2.4 over the minimal period of the orbit. Figure 2.1 shows the function $b_4(s)$ for all those orbits of table 2.2. The third column of table 2.1 shows the labels of the orbits of QBCP coming from each orbit of the RTBP. All the bifurcating points of the orbits of table 2.2 can be continued up to periodic orbits of the QBCP, except the ones of the orbit $02A$. Later one, we will explain how two branches of periodic orbits coming from orbit $02A$ disappear at a bifurcation.

We notice that it is equivalent to have one point of an orbit of the RTBP with n bifurcating times or n points bifurcating at $t = 0$. We are going to use this second approach for the next tables and figures.

The equilibrium points of the RTBP can also be continued leading to small T-periodic orbits in the QBCP which substitute, in some sense, the equilibrium points of the RTBP. Tables 2.3, 2.4 and 2.5 show the initial conditions for $t = 0$ of the computed periodic orbits. In table 2.4, there are also three orbits around $\mathrm{L_5}$, but we are going to talk about them in the next section.

Figures 2.2–2.14 show the periodic orbits around the collinear points of tables 2.3, 2.4 and 2.5. The initial point of each orbit has been marked with $\times$. In each figure, the corresponding periodic orbit of the RTBP has been drawn with a dotted line (unless they replace a fixed point). The bifurcating points of these orbits have also been marked.

Figures 2.2, 2.3 and 2.4 show, respectively, the orbits labelled as 11, 21 and 31, which are the substitutes of the points L_1, L_2 and L_3. In many figures, we see that the initial point of an orbit is close to the bifurcating point in the RTBP which generates it. That does not happen in the case of the orbits 23 and 25 of figure 2.10. For example, in case of the orbit 25, when the continuation parameter is increased, the initial point follows a long path starting at the point marked as A and ending at the point with the label 25. The case of the orbit 23 is symmetric with respect to the x axis, starting at B.

Figure 2.12 shows the orbits 2A and 2C. We notice that the orbit 02A of the RTBP has four points of bifurcation. Increasing the continuation parameter, the points B and D go towards the point C, following a path similar to the plotted orbits. For the value $\epsilon \simeq 0.99833$ the branches from B and D disappear in a pitchfork bifurcation joining with the branch of the orbit 2C. For this reason, only two orbits remain in the QBCP (see figure 2.15).

When the orbit 01C is continued we also find pitchfork bifurcations. Initially, there are two points, C and D, of the orbit 01C which can be continued. For the value $\epsilon \simeq 0.39682$ a bifurcation occurs in the branch of D and two new symmetric branches appear. Figure 2.16 shows one of them. The other one is symmetric with respect to the (x, ϵ)-plane. For the value $\epsilon \simeq 0.86646$, those branches disappear in another bifurcation, joining with the branch coming from the point C.

L	x	z	$\dot{y}$	P	s_1	s_2
012	$-9.10086877684124e{-}01$	$0.00000000000000e{+}00$	$4.65532893422856e{-}01$	T/2	$5.527114e{+}05$	$2.960912e{+}00$
014	$-9.72236476972442e{-}01$	$0.00000000000000e{+}00$	$1.27054247773702e{+}00$	T	$1.102145e{+}02$	$-7.445751e{+}00$
018	$-9.83496241614730e{-}01$	$0.00000000000000e{+}00$	$2.55866139745726e{+}00$	T	$7.376828e{+}02$	$-1.429794e{+}02$
01C	$-9.87162249854154e{-}01$	$-5.21310697447108e{-}02$	$6.45800936855262e{-}01$	T/3	$1.229670e{+}01$	$1.700884e{+}00$
01E	$-9.87982557457513e{-}01$	$-2.48226957833054e{-}03$	$3.13139586195729e{+}00$	T/3	$-1.337491e{+}02$	$1.358855e{+}02^{(c)}$
022	$-1.17538861012898e{+}00$	$0.00000000000000e{+}00$	$1.17400836641063e{-}01$	T/2	$1.730934e{+}06$	$1.880679e{+}00$
026	$-1.33372677155106e{+}00$	$0.00000000000000e{+}00$	$6.25647720207331e{-}01$	T	$9.920759e{+}01$	$-5.939062e{+}00$
02A	$-1.17834365491694e{+}00$	$4.91020357768158e{-}02$	$1.68413790344365e{-}01$	T/2	$1.020898e{+}06$	$1.645466e{+}00$
02E	$-1.07503686925031e{+}00$	$2.02129888541409e{-}01$	$1.92190554338587e{-}01$	T/3	$1.598952e{+}00$	$-2.066665e{-}01$
02G	$-1.03604076821928e{+}00$	$1.90329439977321e{-}01$	$1.31839932435425e{-}01$	T/4	$7.105471e{+}01$	$-1.051794e{+}00$

Table 2.2: Periodic orbits in the RTBP. All the initial conditions are in $y = \dot{x} = \dot{z} = 0$. The stability parameters are s_1 and s_2. Note that the stability parameters are given, in all cases, after a period T (not the minimal period). They are real in all the cases except the one marked with $^{(c)}$. In that case, they are complex conjugated $s_1 \pm s_2 i$. L = Label. P = Period.

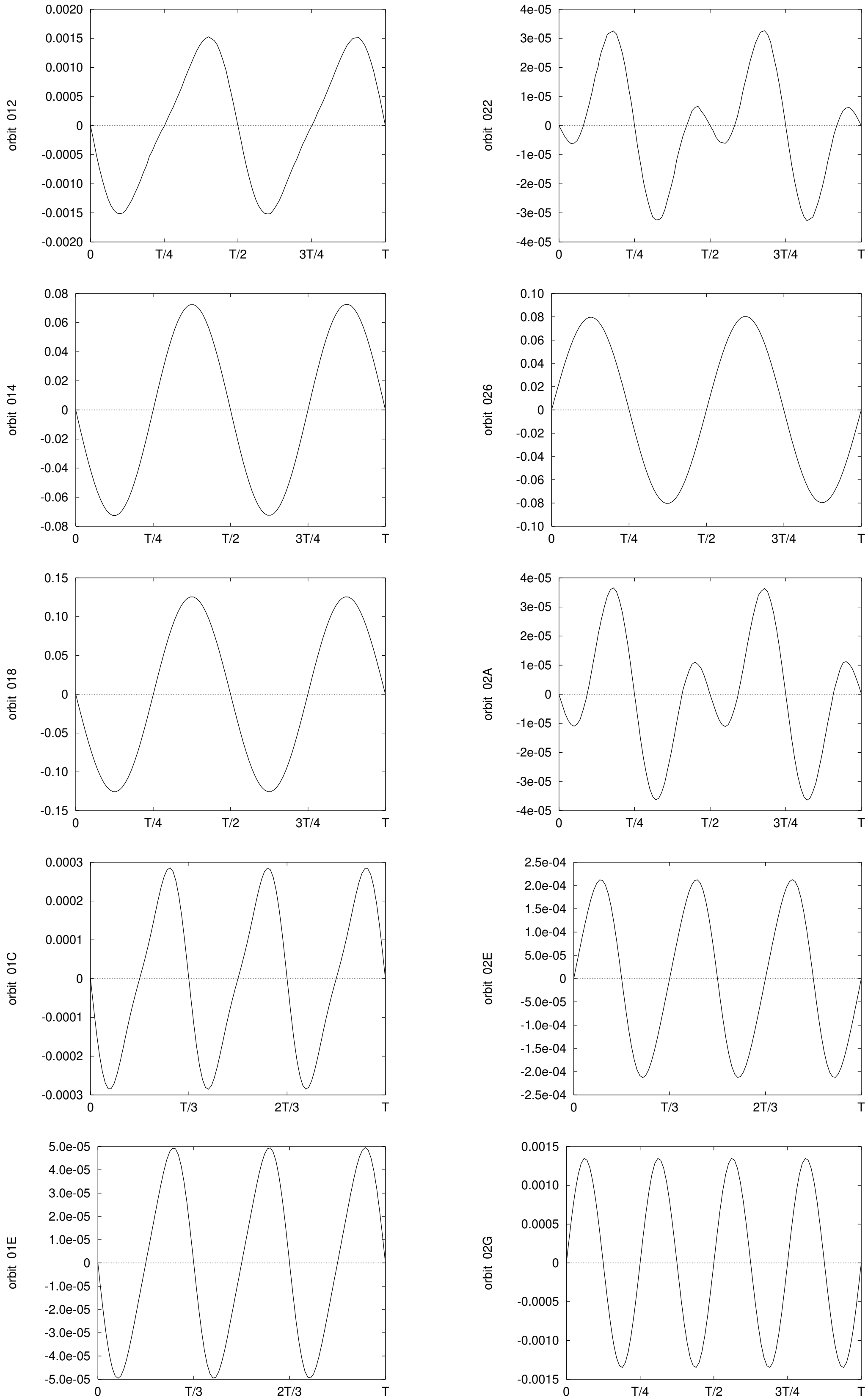

Figure 2.1: Function $b_4(s)$ for the periodic orbits of the RTBP of the table 2.2.

Label	x	$\dot{y}$	s_1	s_2	s_3
11	−8.369141677649319e−01	−6.247467360366576e−06	4.6018213e+08	−1.9272794e+00	−1.9743038e+00
12	−9.104743857262562e−01	4.739377810674471e−01	5.6020544e+05	2.8751711e+00	2.0119296e+00
13	−7.974817205388040e−01	−3.777122446326863e−01	5.5630422e+05	2.8781160e+00	1.9829068e+00
14	−9.707903423961295e−01	1.227264255095907e+00	1.0707448e+02	2.7941893e+00	−6.5466158e+00
16	−6.319707096253444e−01	−8.048438775487632e−01	1.0679946e+02	2.7925586e+00	−6.5445020e+00
18	−9.833707656190477e−01	2.567074732637316e+00	7.8273624e+02	1.6616046e+00	−1.4382884e+02
1A	−3.157060844894300e−02	−6.660529956098080e+00	7.7978210e+02	1.6593058e+00	−1.4341804e+02
21	−1.155683607833265e+00	6.017986175277379e−06	2.3971968e+06	1.9916366e+00	1.8350556e+00
22	−1.176464998903008e+00	1.258366678951874e−01	1.7294557e+06	1.9998183e+00	1.9089728e+00
24	−1.129103186619580e+00	−1.360498544279923e−01	1.7347233e+06	1.9999987e+00	1.9068600e+00
26	−1.327907131342701e+00	6.273575150937974e−01	1.0307752e+02	3.1475696e+00	−5.4535842e+00
28	−9.968163858146143e−01	−1.672727233760071e+00	1.0332779e+02	3.1657009e+00	−5.4509608e+00
31	1.005496271917929e+00	−8.535429112775904e−04	3.6675160e+00	1.7276817e+00	1.6822970e+00

Table 2.3: Planar symmetric T-periodic orbits in the QBCP. All these initial conditions are in $y = z = \dot{x} = \dot{z} = 0$. The stability parameters are s_1, s_2 and s_3.

Label	x $\dot{x}$	y $\dot{y}$	s_1	s_2	s_3	Label sym.
15	$-8.649123493272060\mathrm{e}{-01}$	$-6.850629712613727\mathrm{e}{-01}$				17
	$-3.697831323993490\mathrm{e}{-01}$	$1.290830775689127\mathrm{e}{-01}$	$1.1477163\mathrm{e}{+02}$	$1.3569325\mathrm{e}{+00}$	$-8.3828806\mathrm{e}{+00}$	
19	$-2.576393485112625\mathrm{e}{-01}$	$-1.407550442675300\mathrm{e}{+00}$				1B
	$-1.217367338258969\mathrm{e}{+00}$	$5.810429565427219\mathrm{e}{-02}$	$6.9678676\mathrm{e}{+02}$	$2.3116538\mathrm{e}{+00}$	$-1.3452167\mathrm{e}{+02}$	
25	$-1.129233449272826\mathrm{e}{+00}$	$1.201546108418750\mathrm{e}{-02}$				23
	$2.989676786515735\mathrm{e}{-03}$	$-1.336123538307202\mathrm{e}{-01}$	$1.7347639\mathrm{e}{+06}$	$2.0000025\mathrm{e}{+00}$	$1.9068636\mathrm{e}{+00}$	
27	$-8.691641240246463\mathrm{e}{-01}$	$-5.773037128316959\mathrm{e}{-01}$				29
	$-2.838886062403770\mathrm{e}{-01}$	$-9.286856718375611\mathrm{e}{-02}$	$9.3697253\mathrm{e}{+01}$	$5.8579532\mathrm{e}{-01}$	$-6.3651867\mathrm{e}{+00}$	
51	$-4.884778524279210\mathrm{e}{-01}$	$8.796344947241680\mathrm{e}{-01}$				41
	$3.214223507115407\mathrm{e}{-02}$	$6.346913101441202\mathrm{e}{-03}$	$2.0108291\mathrm{e}{+00}$	$1.7202821\mathrm{e}{+00}$	$-9.0254614\mathrm{e}{-01}$	
52	$-7.399674262482810\mathrm{e}{-01}$	$8.212142002592290\mathrm{e}{-01}$				42
	$9.218638691492127\mathrm{e}{-02}$	$2.362732084445861\mathrm{e}{-01}$	$1.9784855\mathrm{e}{+00}$	$1.7075337\mathrm{e}{+00}$	$-1.1813687\mathrm{e}{+00}$	
53	$-5.300056011342860\mathrm{e}{-02}$	$9.601745154388760\mathrm{e}{-01}$				43
	$-3.376978922406530\mathrm{e}{-02}$	$-1.829081424042000\mathrm{e}{-01}$	$1.9775597\mathrm{e}{+00}$	$1.7068247\mathrm{e}{+00}$	$-1.1905931\mathrm{e}{+00}$	

Table 2.4: Planar non symmetric (initial condition $y \neq 0$) T-periodic orbits in the QBCP. The stability parameters, s_1, s_2 and s_3, are real for all these orbits. Each orbit has a corresponding one through the symmetry S_2 (see section 1.5.1). The last column of the table shows the label of those orbits.

Label	x	z	$\dot{y}$
	s_1	s_2	s_3
1C	−9.879629720523710e−01	−5.108383968268400e−02	6.622660818240399e−01
	1.2803741e+01	1.9903252e+00	1.7249097e+00
1D	−8.681380897120420e−01	1.888325357210310e−01	−2.473565712365180e−01
	1.3166157e+01	2.0132409e+00	1.7009442e+00
1E	−9.879722904635280e−01	−2.462095060502300e−03	3.184909363998671e+00
	1.9997894e+00	−1.7026881e+02	1.7152336e+02$^{(c)}$
1F	−9.236861280052134e−01	3.180943609744754e−01	−8.454341835457363e−02
	2.0001990e+00	−1.7039714e+02	1.7169089e+02$^{(c)}$
2A	−1.178881928424990e+00	4.366399706256980e−02	1.671602937502402e−01
	1.1381097e+06	2.0002929e+00	1.7358171e+00
2C	−1.113829762948268e+00	−3.103557789878931e−02	−1.962023688188478e−01
	1.1308529e+06	1.9999994e+00	1.7292282e+00
2E	−1.077049895739677e+00	2.015253011952958e−01	1.997859497018916e−01
	1.9952806e+00	1.6996526e+00	−2.9529774e−01
2F	−9.904316673796599e−01	−3.844291276661444e−02	−7.619049294735286e−01
	2.0043536e+00	1.6966419e+00	−3.1912692e−01
2G	−1.036008068335600e+00	1.910211094926160e−01	1.350819667635190e−01
	7.1163118e+01	1.9905110e+00	−1.0259725e+00
2H	−9.871245890063380e−01	−1.536478051466330e−02	−1.239507689039360e+00
	7.1092698e+01	2.0095035e+00	−1.0244564e+00

Table 2.5: Symmetric non planar T-periodic orbits in the QBCP. The initial conditions are in $y = \dot{x} = \dot{z} = 0$. The stability parameters, s_1, s_2 and s_3, are real for all these orbits, except for the ones marked with $^{(c)}$. In those cases, they are s_1, $s_2 \pm s_3 i$. Each orbit has a corresponding symmetric orbit with respect to the plane $z = 0$.

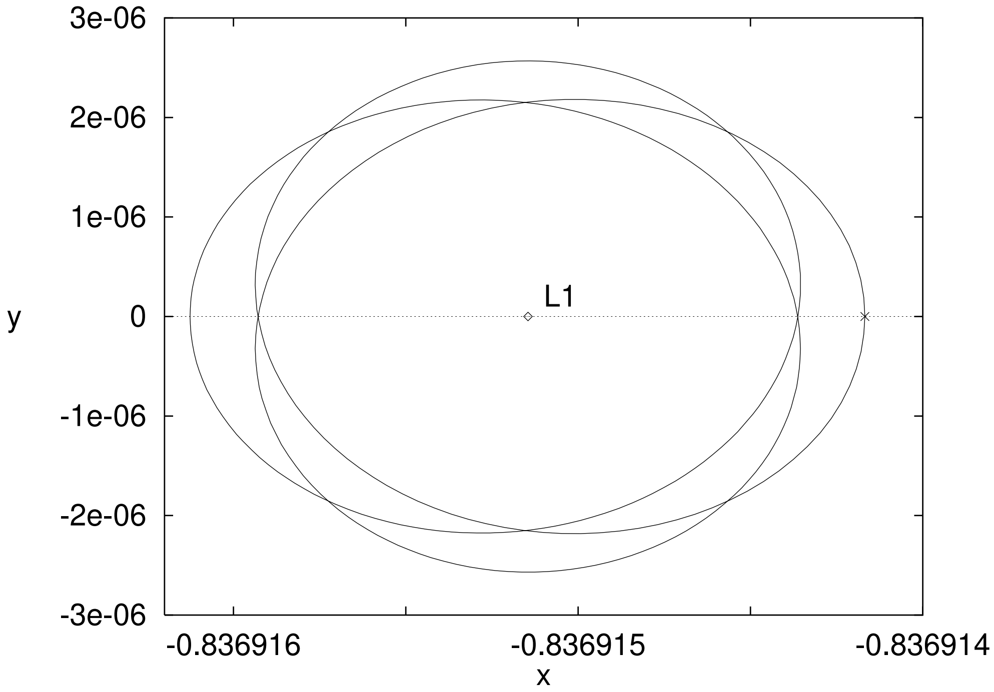

Figure 2.2: Periodic orbit 11 around L_1.

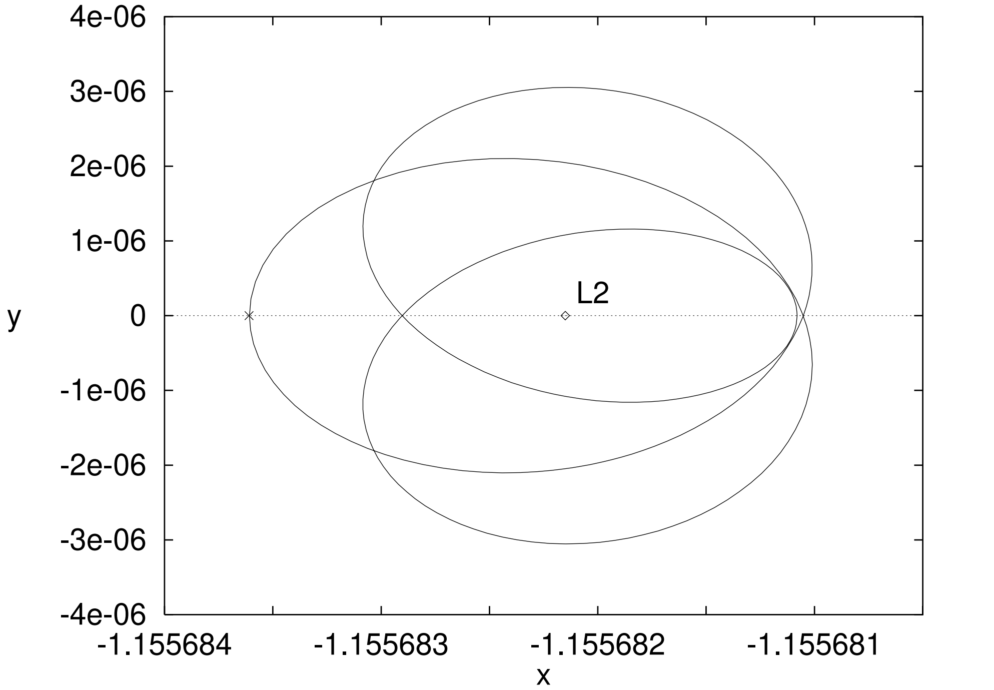

Figure 2.3: Periodic orbit 21 around L_2.

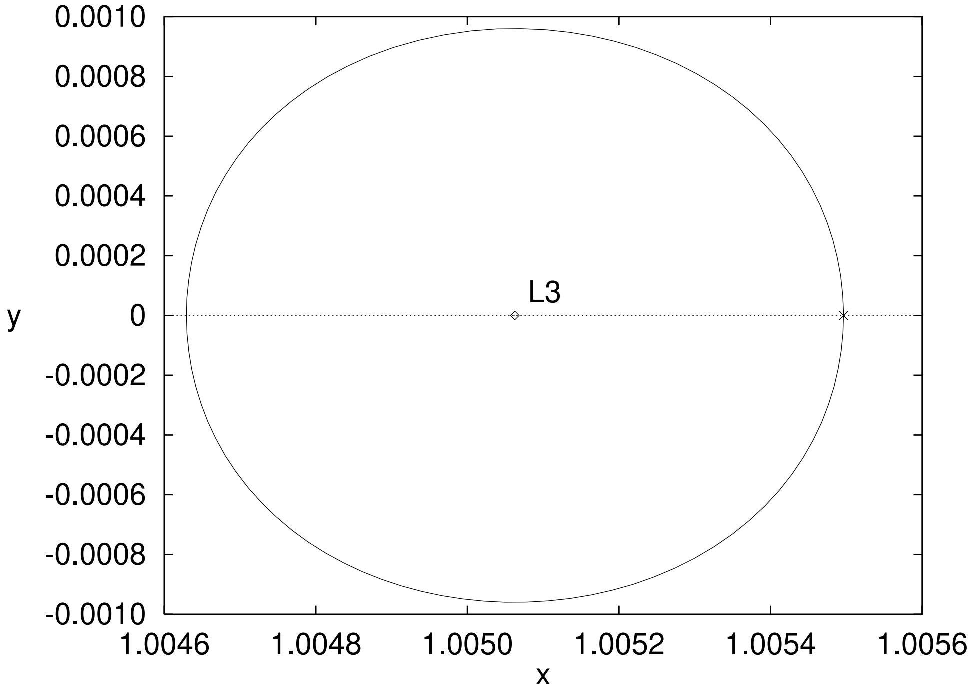

Figure 2.4: Periodic orbit 31 around L_3.

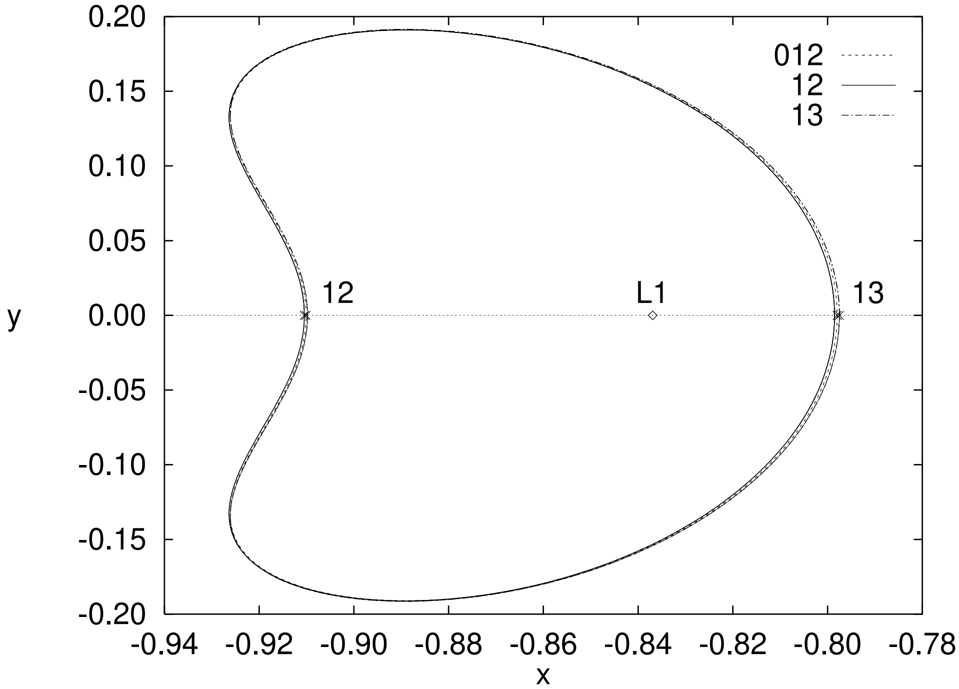

Figure 2.5: Periodic orbits 12 and 13. The orbit 012 of the RTBP is also displayed. Each orbit turns twice around L_1.

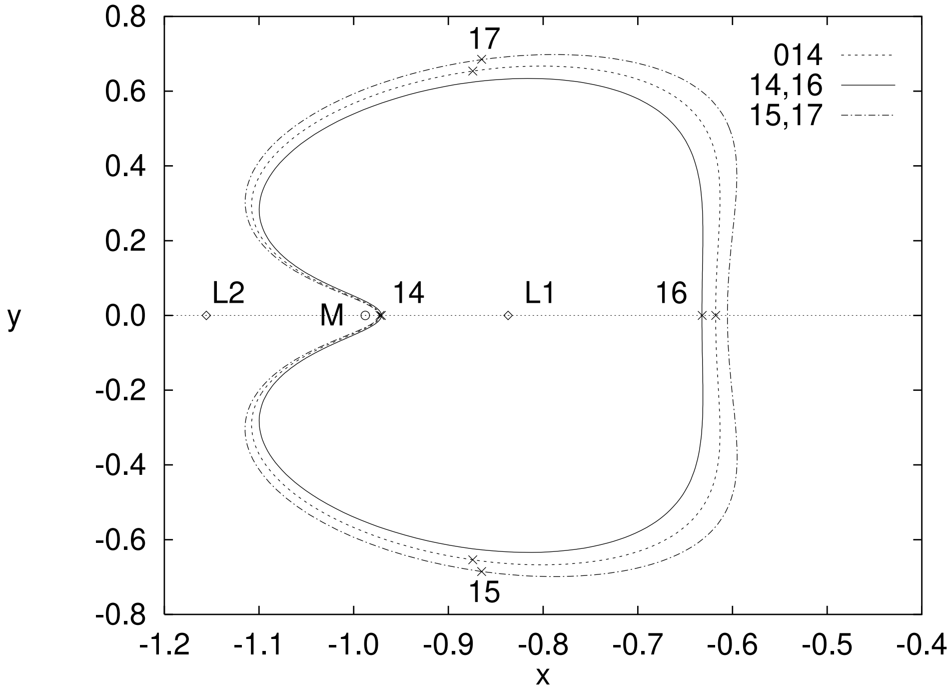

Figure 2.6: Periodic orbits 14, 15, 16 and 17. The orbit 014 of the RTBP is also shown.

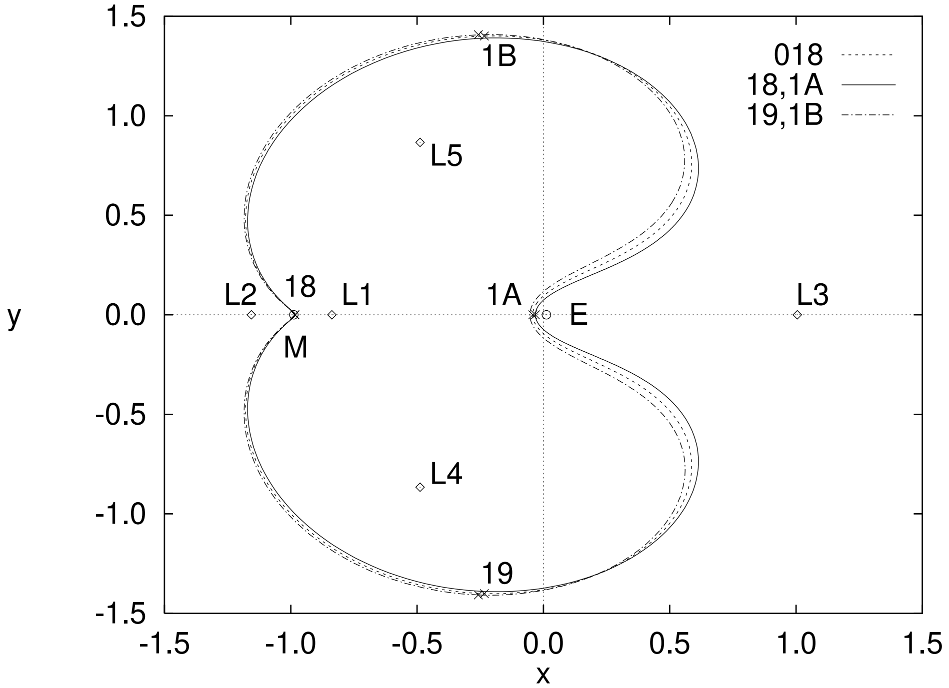

Figure 2.7: Periodic orbits 18, 19, 1A and 1B. The orbit 018 of the RTBP also has been printed.

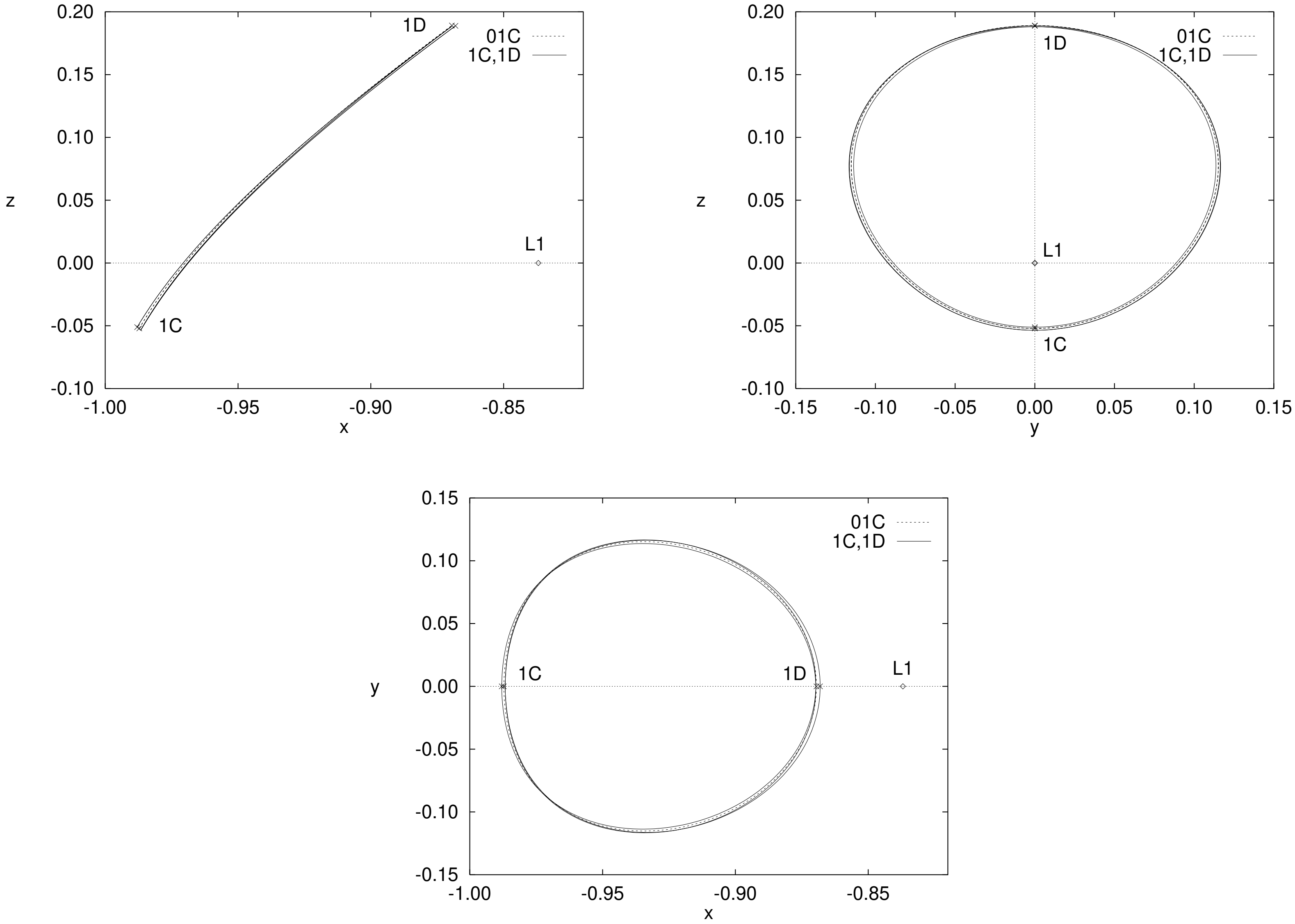

Figure 2.8: Periodic orbits 1C and 1D of the QBCP and orbit 01C of the RTBP. Each orbit turns three times.

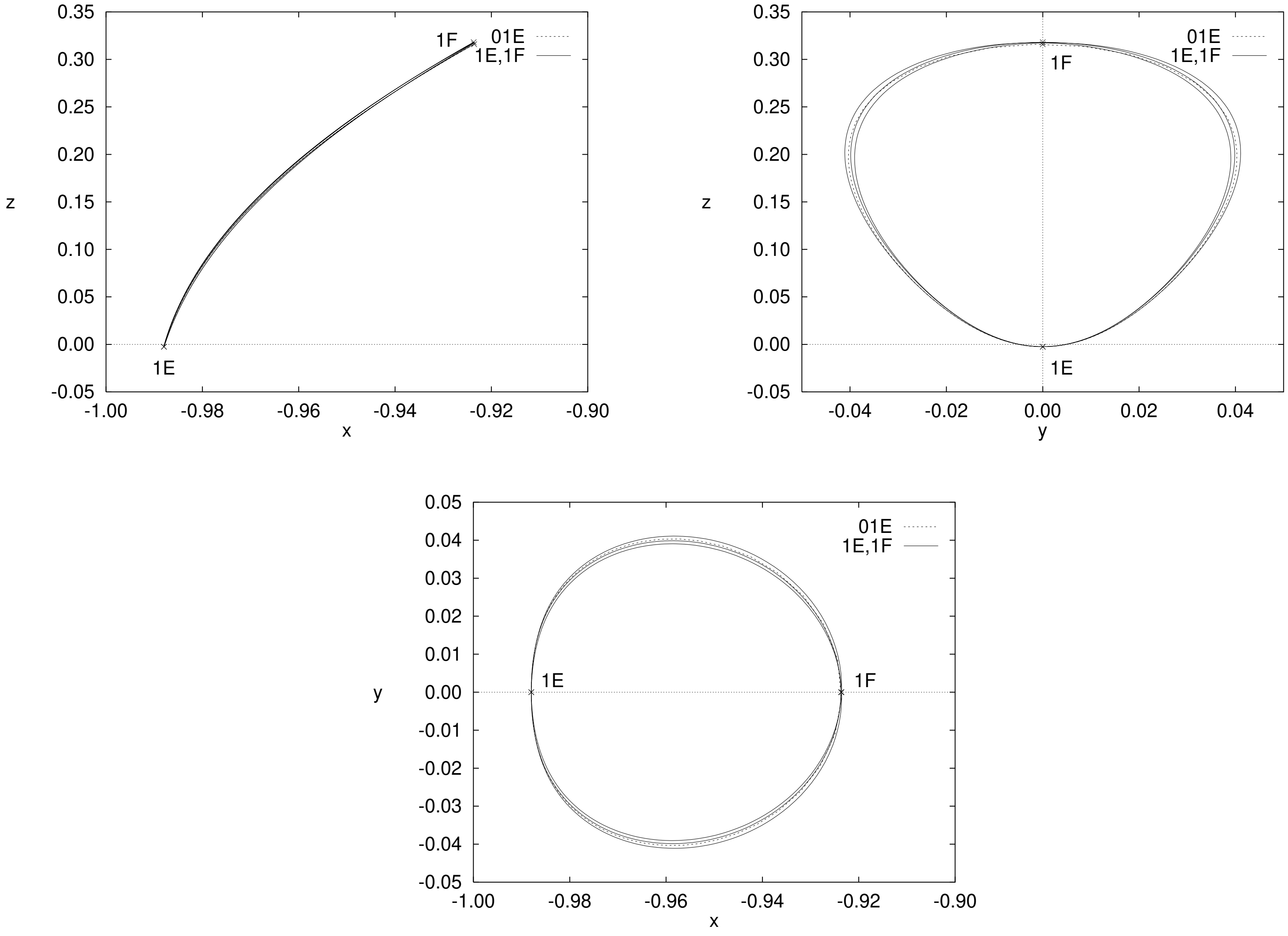

Figure 2.9: Periodic orbits 1E and 1F. The orbit 01E of the RTBP is also shown. Each orbit turns three times.

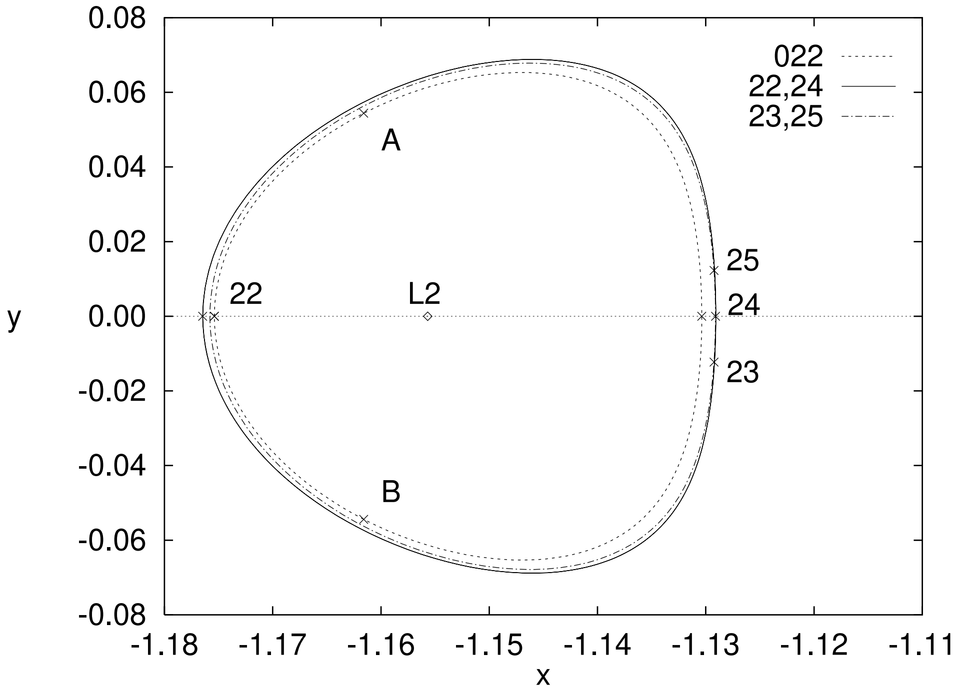

Figure 2.10: Periodic orbits 22, 23, 24 and 25 around L_2. The orbit 022 of the RTBP is also displayed. Each orbit turns twice around L_2. The points labelled as A and B are bifurcating points of 022 which generate the orbits 23 and 25, respectively.

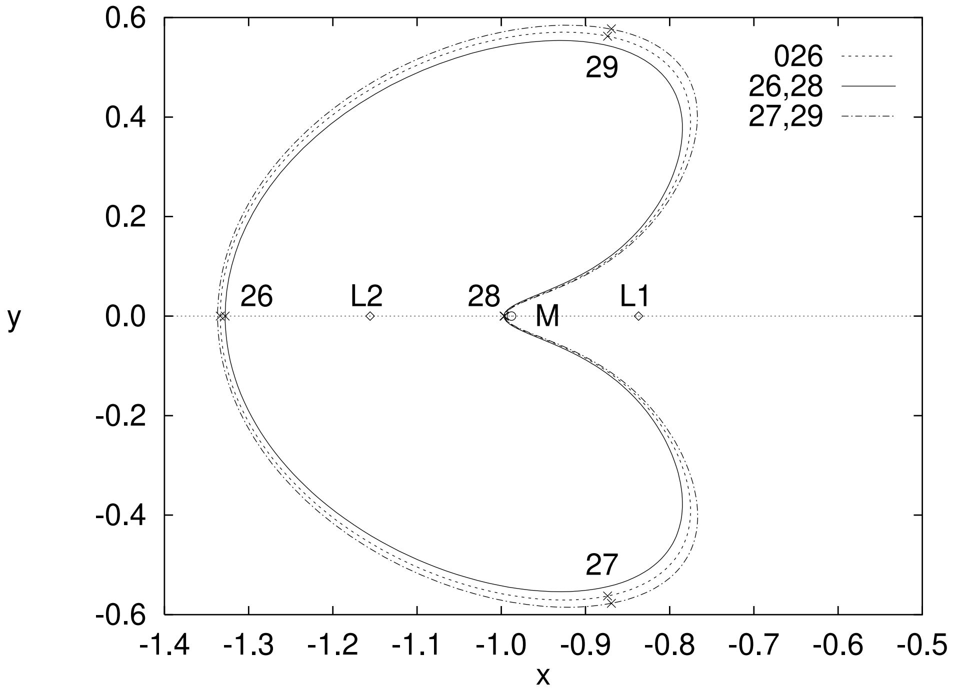

Figure 2.11: Periodic orbits 26, 27, 28 and 29. The orbit 026 of the RTBP is also shown.

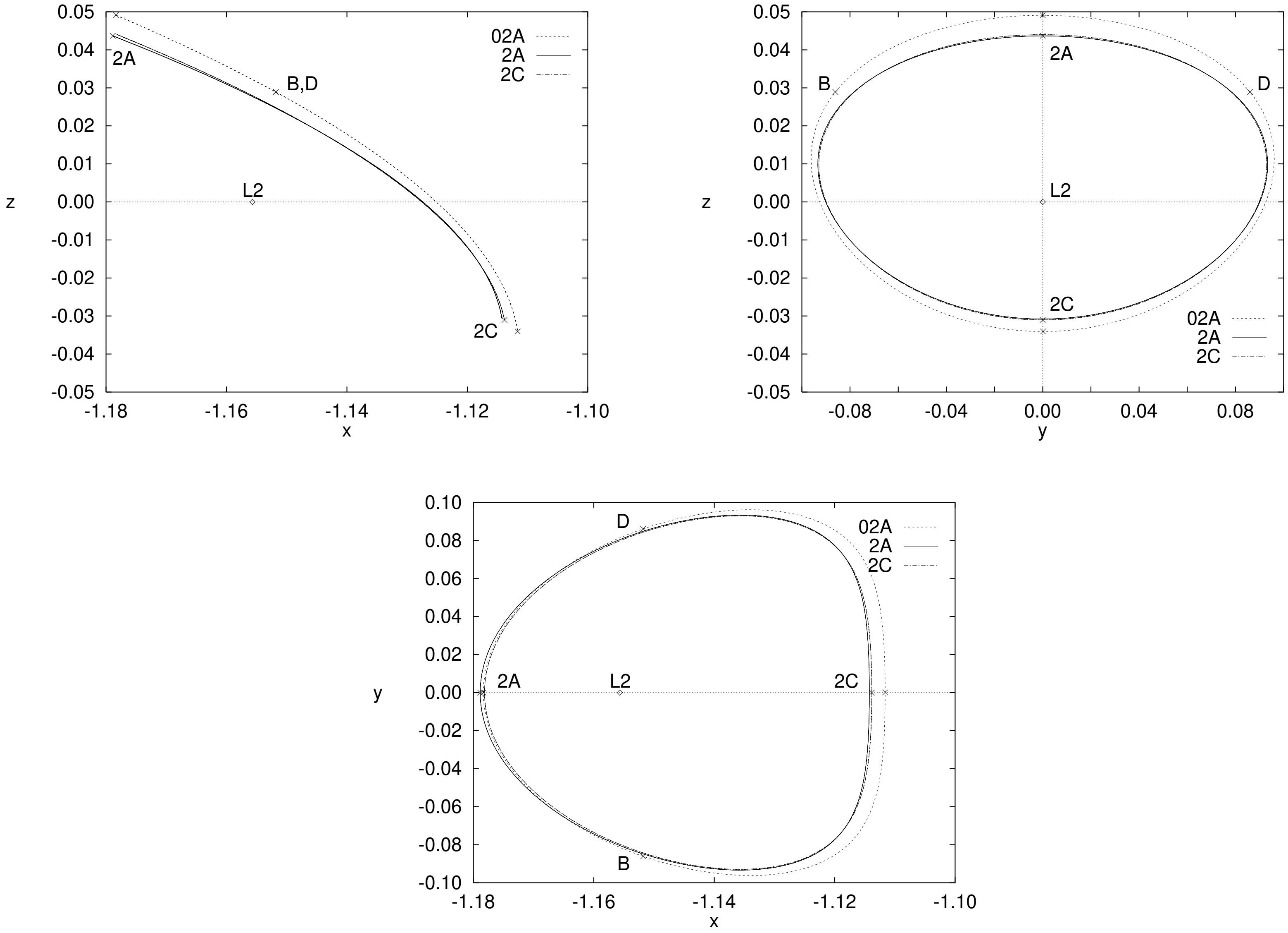

Figure 2.12: Periodic orbits 2A and 2C of the QBCP and orbit 02A of the RTBP. Each orbit turns twice around L_2. The orbits starting at the points B and D join before arriving at the QBCP with the branch of 2C (see also figure 2.15).

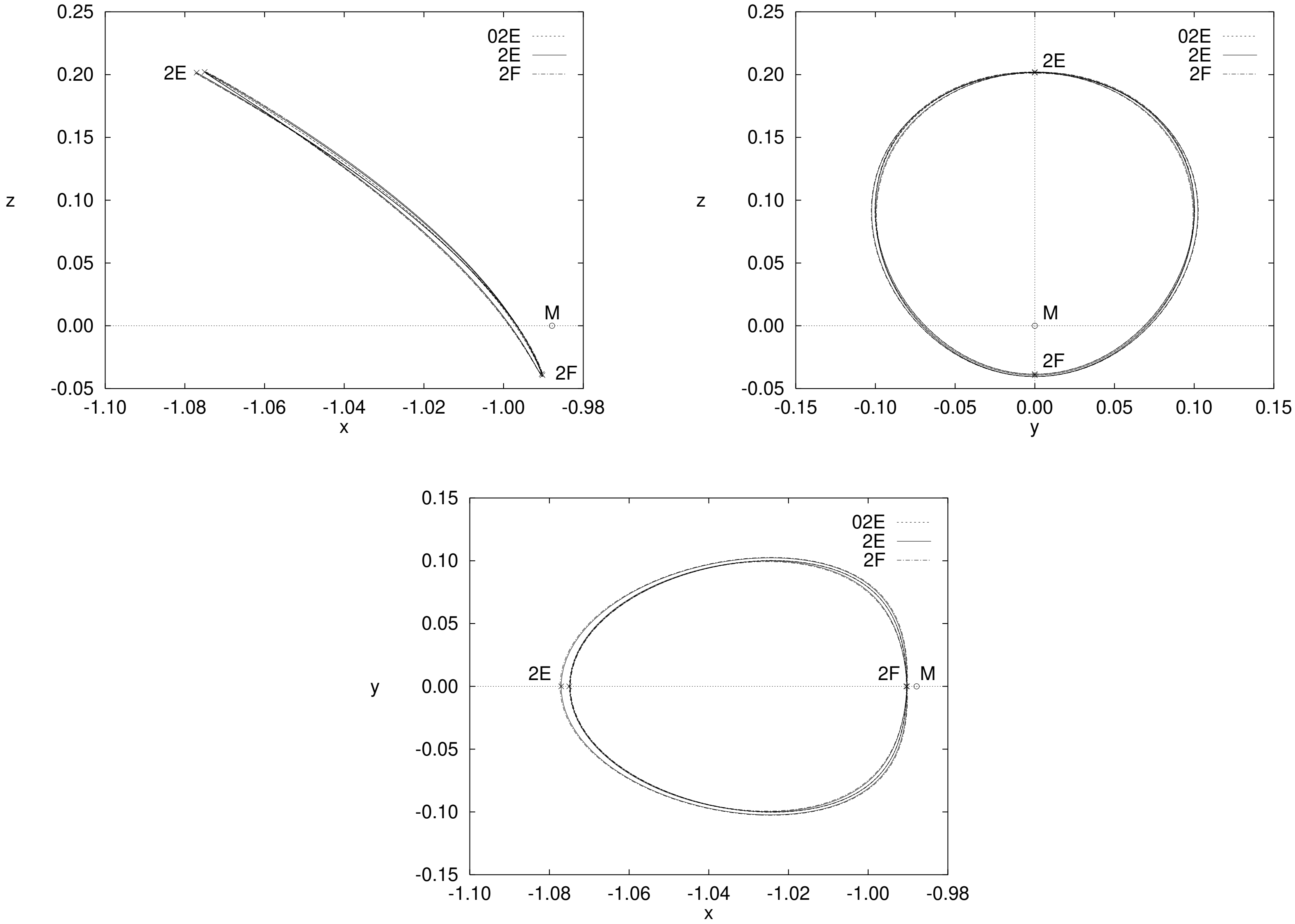

Figure 2.13: Periodic orbits 2E and 2F. The orbit 02E of the RTBP is also shown. Each orbit turns three times.

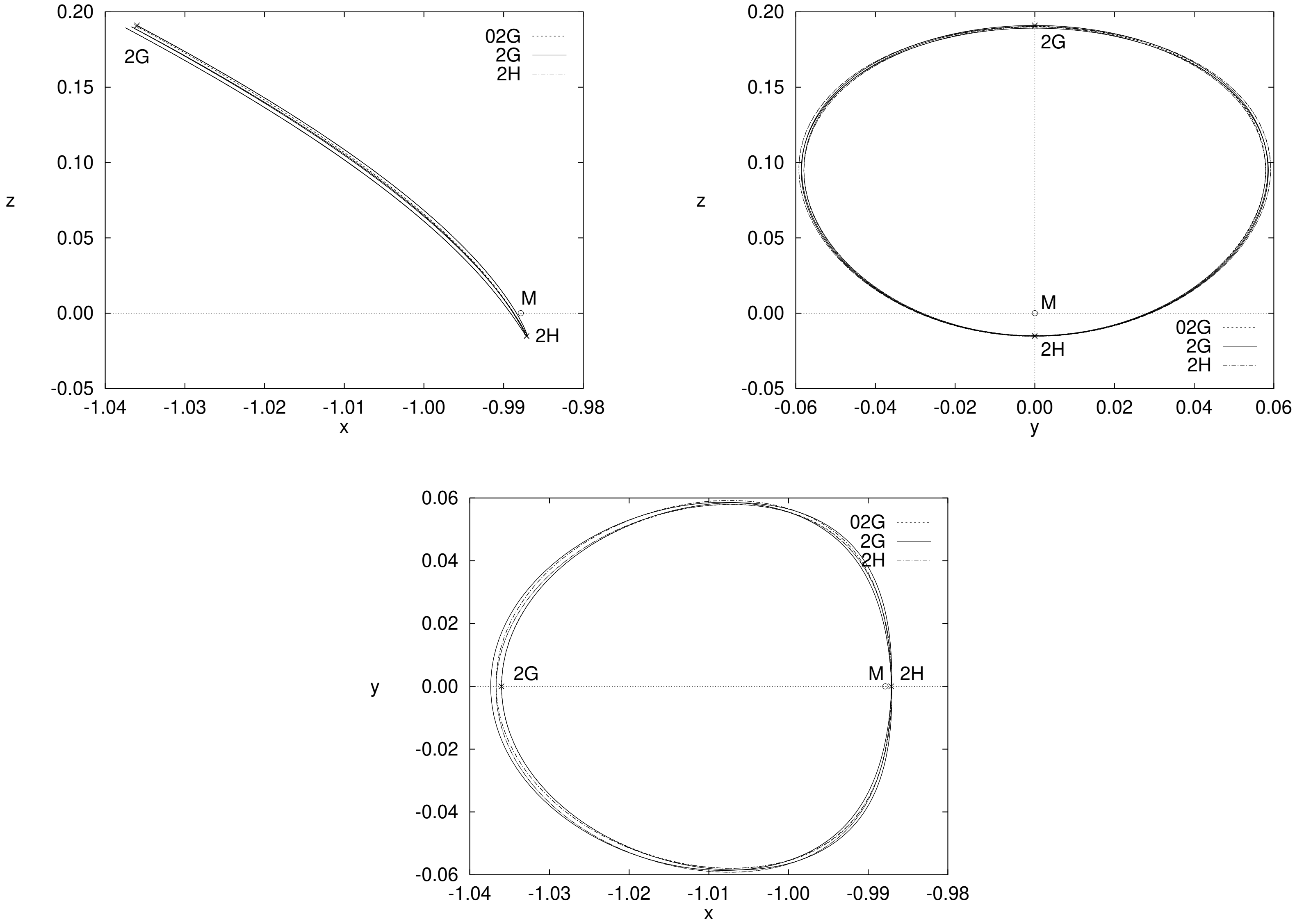

Figure 2.14: Periodic orbits 2G and 2H. The orbit 02G of the RTBP has also been drawn. Each orbit turns four times.

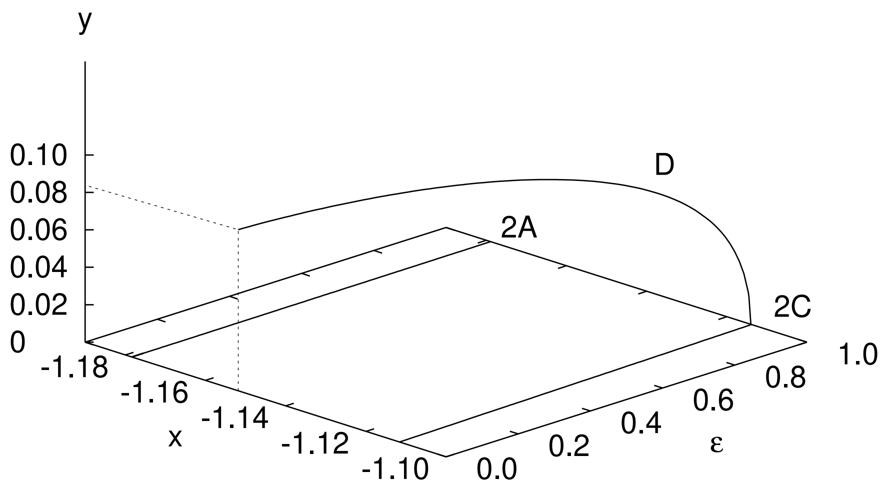

Figure 2.15: Continuation from orbit 02A. The branch of periodic orbits labelled as D and its symmetric B (not drawn in the figure) join at a pitchfork bifurcation with the branch 2C (see also figure 2.12).

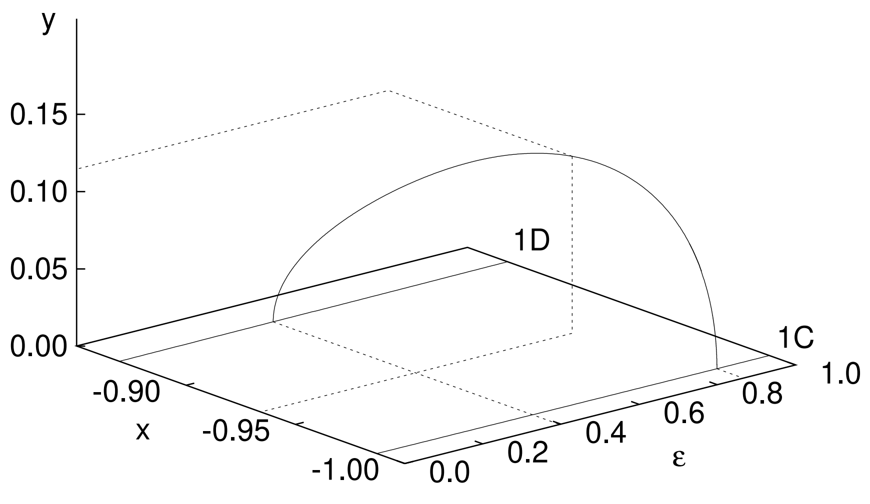

Figure 2.16: Continuation from orbit 01C. Branch of periodic orbits which starts at a bifurcation in the branch of D and disappears in another bifurcation in the branch of C.

2.4 Comparison between QBCP and BCP

In the previous section, we have studied the continuation of T-periodic orbits from the RTBP to the QBCP. It is clear that the QBCP should fit the real problem better than the BCP, but the point is whether the differences between the BCP and the QBCP are only quantitative or if there are qualitative differences between both models. Here, we are going to compare the periodic orbits around L_5 and L_2 in both models. The conclusion will be that the differences are very important around L_2.

In the same way as (2.1), we can write a family of Hamiltonians

$$\tilde{H} = H_{RTBP} + \epsilon \left(H_{BCP} - H_{RTBP} \right) ,$$

in order to use the continuation method. Figure 2.17 shows the curves of planar periodic orbits emanating from L_5 for the QBCP and the BCP. In both cases, there are small periodic orbits around the point L_5. However, the size of these orbits is quite different (see figure 2.18). The periodic orbits of the QBCP labelled as 52 and 53 have been drawn in figure 2.19.

The situation is quite different around L_2. In the BCP, there is no periodic orbit substituting the equilibrium point. The periodic orbit emanating from L_2 disappears in a turning point for the value $\epsilon \simeq 0.070156$. Figure 2.20 shows the branches starting at L_2 and three bifurcating points of the RTBP, two of the orbit 022 (labelled here as a and b) and another of a Halo orbit symmetric from the orbit 02A (the point labelled as c). We see that the branch starting at L_2 joins in a turning point with the one coming from the point a. On the other hand, the branch starting at c also disappears. In this case, it occurs by means of a bifurcation for the value $\epsilon \simeq 0.28647$, where it meets the symmetric branch (with $z < 0$) along a point of the branch starting at b. This last one continues up to $\epsilon = 1$.

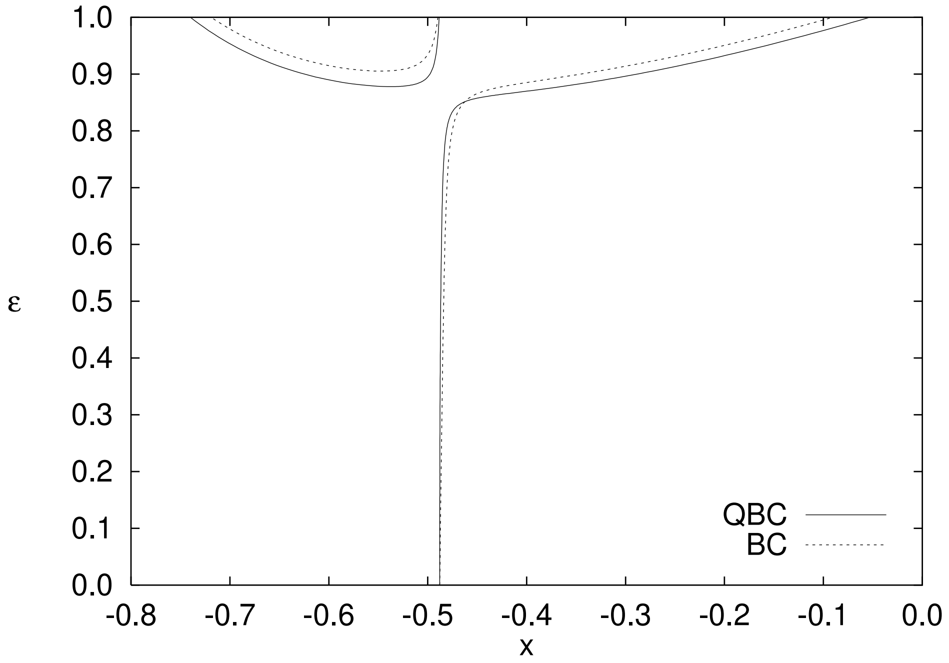

Figure 2.17: Continuation of the periodic orbit substituting the point L_5, in the QBC and the BC cases.

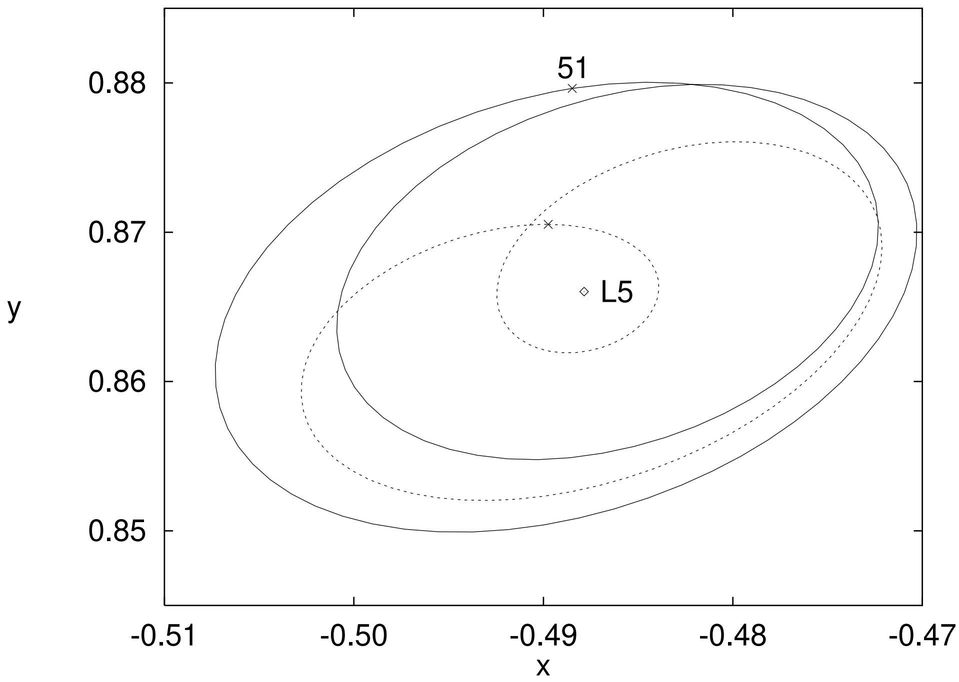

Figure 2.18: Small periodic orbit of the QBCP labelled as 51. The corresponding orbit in the BCP has been drawn with a dotted line.

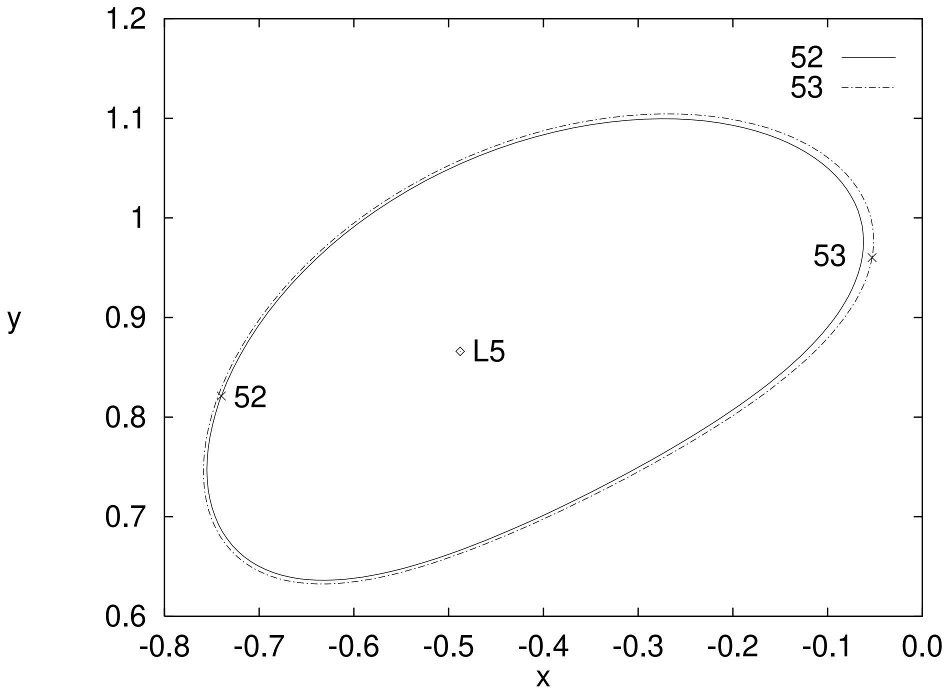

Figure 2.19: Periodic orbits 52 and 53 of the QBCP.

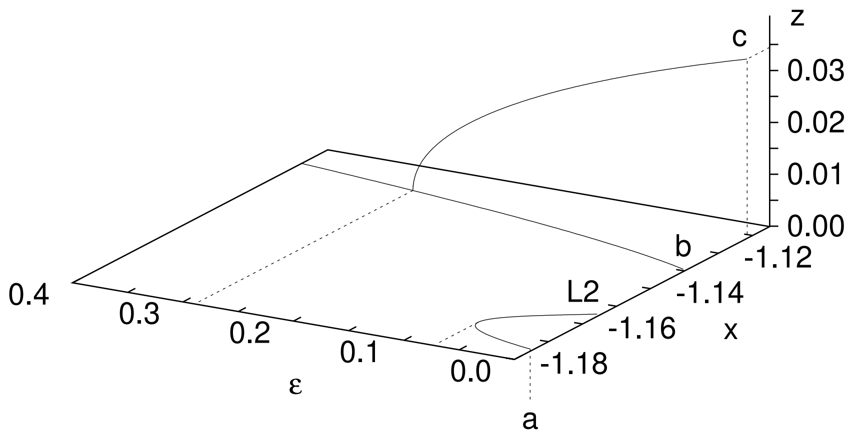

Figure 2.20: Continuation of periodic orbits from the RTBP to the BCP. The points a and b are bifurcating points of the orbit 022 of the RTBP. The point c corresponds to a symmetric orbit of the orbit 02A.

Chapter 3

Quasi-periodic orbits around L_1 and L_2 points

3.1 Introduction

It is well known that the equilibrium points L_1 and L_2 of the RTBP are of the type saddle $\times$ center $\times$ center. Around each point, there is a family of planar Lyapunov periodic orbits and another of vertical orbits, called the eight-shaped family. Let ω_1 and ω_2 be the frequencies of the orbits of the two families, respectively. These frequencies are very similar near the libration points and they change slightly along the families. Around the equilibrium points there are also Lissajous orbits. This means orbits with two basic frequencies. If the quotient of the two basic frequencies is irrational then we have a quasi-periodic orbit lying on a 2D torus. In the case that the quotient is rational then we have a periodic orbit, eventually of long period. Following the planar Lyapunov family, increasing the amplitude, we arrive at a point where a bifurcation occurs. At this point, the frequency of the Lyapunov family becomes equal to the frequency in the vertical direction and the Halo family of periodic orbits starts. In fact, there are two symmetric Halo families with respect to the xy plane. All these orbits has been exhaustively studied. In [3] Breakwell and Brown showed numerically that Halo orbits originating in the vicinities of both L_1 and L_2 grow larger, but shorter in period, as they shift towards the Moon. They also found a narrow band of stable orbits roughly half-way to the Moon. Numerical computations by Howell [13] extended the results to different values of the mass ratio. Halo orbits were computed numerically and analytically in [8], in the Earth-Moon case as well as the Earth-Sun case. The analytical computation of the Lissajous orbits can be found in [10].

In this chapter, we are going to compute the corresponding Lyapunov, Lissajous and Halo orbits in the QBCP. We point out that this is a Hamiltonian system with three degrees of freedom which depends periodically on time. For this reason we have an extra frequency in each of these orbits, and therefore, all of them are quasi-periodic. The main tools used for the computation of the quasi-periodic orbits have been Lindstedt-Poincaré method and what we call the method of analytical refinement. In the next sections, we are going to explain how to perform these calculations, which difficulties appear and how to overcome them.

3.2 Equations of the motion in a suitable way

In order to use the Lindstedt-Poincaré method, it is convenient to transform the Hamilton equations (1.24) into second order differential equations. For this purpose, isolating the momenta from the first equations we get:

$$
\begin{aligned}
P_X &= \frac{1}{\alpha_1}\,\dot{X} - \frac{\alpha_2}{\alpha_1}\,X - \frac{\alpha_3}{\alpha_1}\,Y\ ,\\
P_Y &= \frac{1}{\alpha_1}\,\dot{Y} - \frac{\alpha_2}{\alpha_1}\,Y + \frac{\alpha_3}{\alpha_1}\,X\ ,\\
P_Z &= \frac{1}{\alpha_1}\,\dot{Z} - \frac{\alpha_2}{\alpha_1}\,Z\ .
\end{aligned}
$$

We also need the derivatives of the momenta with respect to time,

$$
\begin{aligned}
\dot{P_X} &= \left(\frac{1}{\alpha_1}\right)^{\cdot}\dot{X} + \frac{1}{\alpha_1}\,\ddot{X} - \left(\frac{\alpha_2}{\alpha_1}\right)^{\cdot} X - \frac{\alpha_2}{\alpha_1}\,\dot{X} - \left(\frac{\alpha_3}{\alpha_1}\right)^{\cdot} Y - \frac{\alpha_3}{\alpha_1}\,\dot{Y}\ ,\\
\dot{P_Y} &= \left(\frac{1}{\alpha_1}\right)^{\cdot}\dot{Y} + \frac{1}{\alpha_1}\,\ddot{Y} - \left(\frac{\alpha_2}{\alpha_1}\right)^{\cdot} Y - \frac{\alpha_2}{\alpha_1}\,\dot{Y} + \left(\frac{\alpha_3}{\alpha_1}\right)^{\cdot} X + \frac{\alpha_3}{\alpha_1}\,\dot{X}\ ,\\
\dot{P_Z} &= \left(\frac{1}{\alpha_1}\right)^{\cdot}\dot{Z} + \frac{1}{\alpha_1}\,\ddot{Z} - \left(\frac{\alpha_2}{\alpha_1}\right)^{\cdot} Z - \frac{\alpha_2}{\alpha_1}\,\dot{Z}\ .
\end{aligned}
$$

Then, substituting these expressions into the fourth, fifth and sixth equations of (1.24) we can write them as:

$$
\begin{aligned}
\ddot{X} - 2\dot{Y} - X &= \left(1 - \frac{1}{\alpha_1}\right)\ddot{X} - \left(\frac{1}{\alpha_1}\right)^{\cdot}\dot{X} + 2\left(\frac{\alpha_3}{\alpha_1} - 1\right)\dot{Y} + \left(\frac{\alpha_3}{\alpha_1}\right)^{\cdot} Y + \\
&\quad + \left[\left(\frac{\alpha_2}{\alpha_1}\right)^{\cdot} + \frac{\alpha_2^2 + \alpha_3^2}{\alpha_1} - 1\right] X - \alpha_4 + \alpha_6\,\frac{\partial}{\partial X}\left(\frac{1-\mu}{q_{pe}} + \frac{\mu}{q_{pm}} + \frac{m_s}{q_{ps}}\right)\ ,\\[2ex]
\ddot{Y} + 2\dot{X} - Y &= \left(1 - \frac{1}{\alpha_1}\right)\ddot{Y} - 2\left(\frac{\alpha_3}{\alpha_1} - 1\right)\dot{X} - \left(\frac{1}{\alpha_1}\right)^{\cdot}\dot{Y} - \left(\frac{\alpha_3}{\alpha_1}\right)^{\cdot} X + \\
&\quad + \left[\left(\frac{\alpha_2}{\alpha_1}\right)^{\cdot} + \frac{\alpha_2^2 + \alpha_3^2}{\alpha_1} - 1\right] Y - \alpha_5 + \alpha_6\,\frac{\partial}{\partial Y}\left(\frac{1-\mu}{q_{pe}} + \frac{\mu}{q_{pm}} + \frac{m_s}{q_{ps}}\right)\ ,\\[2ex]
\ddot{Z} &= \left(1 - \frac{1}{\alpha_1}\right)\ddot{Z} - \left(\frac{1}{\alpha_1}\right)^{\cdot}\dot{Z} + \left[\left(\frac{\alpha_2}{\alpha_1}\right)^{\cdot} + \frac{\alpha_2^2}{\alpha_1}\right] Z +
\end{aligned}
$$

$$+\alpha_6 \frac{\partial}{\partial Z}\left(\frac{1-\mu}{q_{pe}}+\frac{\mu}{q_{pm}}+\frac{m_s}{q_{ps}}\right) ,$$

where the expressions of α_j, $j=1,\dots,8$ where given in the first chapter (table 1.5). We have kept some terms on the left hand side of the equations because we want to express the QBCP as a perturbation of the RTBP.

3.2.1 Normalized coordinates

To study the orbits about the point $\mathrm{L_i}$ (for $i = 1,\ 2$) it is suitable to change the system of reference [22]. We take the point $\mathrm{L_i}$ as origin of coordinates. The unit of distance, γ, is the distance between $\mathrm{L_i}$ and the smaller primary. Finally, we take the positive x and y axes opposite to the synodical ones. Therefore, the equations of the change of coordinates are

$$\begin{aligned} x &= -\frac{1}{\gamma}X + c_1 ,\\ y &= -\frac{1}{\gamma}Y ,\\ z &= \frac{1}{\gamma}Z , \end{aligned}$$

where

$$c_1 = \frac{\mu - 1 \pm \gamma}{\gamma} ,$$

with the upper sign for $\mathrm{L_1}$ and the lower sign for $\mathrm{L_2}$. With the Earth-Moon mass parameter given in chapter 1, the values of γ are

$$\gamma = \begin{cases} 0.1509342729 & \text{for } \mathrm{L_1} ,\\ 0.1678327316 & \text{for } \mathrm{L_2} . \end{cases}$$

Figure 3.1 shows the relationship between synodical and normalized coordinates, in the case of $\mathrm{L_2}$.

Performing that change of variables, the equations of motion become

$$\begin{aligned} \ddot{x} - 2\dot{y} - x + c_1 &= \left(1-\frac{1}{\alpha_1}\right)\ddot{x} - \left(\frac{1}{\alpha_1}\right)^{\cdot}\dot{x} + 2\left(\frac{\alpha_3}{\alpha_1}-1\right)\dot{y} + \left(\frac{\alpha_3}{\alpha_1}\right)^{\cdot} y + \frac{\alpha_4}{\gamma} + \\ &+\left[\left(\frac{\alpha_2}{\alpha_1}\right)^{\cdot} + \frac{\alpha_2^2+\alpha_3^2}{\alpha_1} - 1\right](x-c_1) + \frac{\alpha_6}{\gamma^2}\frac{\partial}{\partial x}\left(\frac{1-\mu}{q_{pe}}+\frac{\mu}{q_{pm}}+\frac{m_s}{q_{ps}}\right) ,\\ \ddot{y} + 2\dot{x} - y &= \left(1-\frac{1}{\alpha_1}\right)\ddot{y} - 2\left(\frac{\alpha_3}{\alpha_1}-1\right)\dot{x} - \left(\frac{1}{\alpha_1}\right)^{\cdot}\dot{y} - \left(\frac{\alpha_3}{\alpha_1}\right)^{\cdot}(x-c_1) + \\ &+\left[\left(\frac{\alpha_2}{\alpha_1}\right)^{\cdot} + \frac{\alpha_2^2+\alpha_3^2}{\alpha_1} - 1\right] y + \frac{\alpha_5}{\gamma} + \frac{\alpha_6}{\gamma^2}\frac{\partial}{\partial y}\left(\frac{1-\mu}{q_{pe}}+\frac{\mu}{q_{pm}}+\frac{m_s}{q_{ps}}\right) , \end{aligned}$$

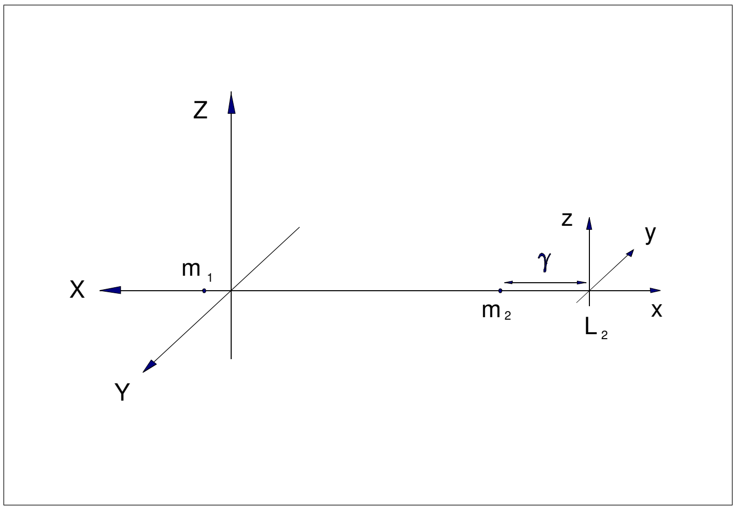

Figure 3.1: Synodical (X, Y, Z) and normalized (x, y, z) coordinates in the case of L_2.

$$\begin{aligned} \ddot{z} &= \left(1-\frac{1}{\alpha_1}\right)\ddot{z} - \left(\frac{1}{\alpha_1}\right)^{\cdot}\dot{z} + \left[\left(\frac{\alpha_2}{\alpha_1}\right)^{\cdot} + \frac{\alpha_2^2}{\alpha_1}\right] z + \\ &+ \frac{\alpha_6}{\gamma^2}\frac{\partial}{\partial z}\left(\frac{1-\mu}{q_{pe}} + \frac{\mu}{q_{pm}} + \frac{m_s}{q_{ps}}\right) . \end{aligned}$$

3.2.2 Expanding the potential

The next task is to expand the potential

$$\frac{1-\mu}{q_{pe}} + \frac{\mu}{q_{pm}} + \frac{m_s}{q_{ps}}$$

in Legendre polynomials. This is useful to make algebraic manipulation. This kind of expansion was already used by D.L. Richardson in [22] for the RTBP. The main tool is the generating function:

$$\frac{1}{\sqrt{1-2\alpha u+\alpha^2}} = \sum_{n=0}^{\infty} \alpha^n P_n(u) , \tag{3.1}$$

where P_n are the Legendre polynomials. This series is convergent for $-1 \leq u \leq 1$ and $|\alpha| < 1$.

First of all, we are going to expand the potential corresponding to the Earth and the Moon. Using (3.1), it is easy to derive

$$q_{pe}^{-1} = ((X-\mu)^2 + Y^2 + Z^2)^{-1/2} = (1\mp\gamma)^{-1} \sum_{n=0}^{\infty} \left(\frac{-\gamma\rho}{1\mp\gamma}\right)^n P_n\left(\frac{x}{\rho}\right) ,$$

$$q_{pm}^{-1} = ((X-\mu+1)^2+Y^2+Z^2)^{-1/2} = \gamma^{-1}\sum_{n=0}^{\infty}(\pm\rho)^n P_n\left(\frac{x}{\rho}\right) ,$$

using, as before, the upper sign for L_1 and the lower sign for L_2 and being

$$\rho^2 = x^2+y^2+z^2 .$$

So, the gravitational potential from the Earth and the Moon is

$$U_{em} = \frac{1}{\gamma^2}\left(\frac{1-\mu}{q_{pe}}+\frac{\mu}{q_{pm}}\right) = \sum_{n=0}^{\infty} c_n \rho^n P_n\left(\frac{x}{\rho}\right) ,$$

where

$$c_n = \frac{1}{\gamma^3}\left((\pm 1)^n\mu + (-1)^n(1-\mu)\left(\frac{\gamma}{1\mp\gamma}\right)^{n+1}\right) .$$

The Legendre polynomials satisfy the following recurrent relationship:

$$P_n(u) = \frac{2n-1}{n}\, u\, P_{n-1}(u) - \frac{n-1}{n}\, P_{n-2}(u) ,$$

starting with $P_0(u)=1$ and $P_1(u)=u$. This can be found, for instance, in [1]. In [10], Gómez *et al.* introduced the functions

$$\begin{aligned} T_n(x,y,z) &= \rho^n P_n(x/\rho) , \\ R_n(x,y,z) &= y^{-1}\frac{\partial T_{n+2}}{\partial y} = z^{-1}\frac{\partial T_{n+2}}{\partial z} , \end{aligned}$$

for $n \geq 0$. These functions are homogeneous polynomials of degree n. Recursive formulas for them can be deduced from the recurrence of the Legendre polynomials. They are

$$\begin{aligned} T_n &= \frac{2n-1}{n}\, x\, T_{n-1} - \frac{n-1}{n}\,\rho^2 T_{n-2} , \\ R_n &= \frac{2n+3}{n+2}\, x R_{n-1} - \frac{2n+2}{n+2}\, T_n - \frac{n+1}{n+2}\,\rho^2 R_{n-2} , \end{aligned}$$

with the initial terms $T_0=1$, $T_1=x$, $R_0=-1$ and $R_1=-3x$. By straightforward calculation, it is also possible to see that

$$\frac{\partial T_n}{\partial x} = n\, T_{n-1} .$$

Then, we can rewrite the potential U_{em} and its derivatives in terms of these functions:

$$\begin{aligned} U_{em} &= \sum_{n=0}^{\infty} c_n T_n , \\ \frac{\partial U_{em}}{\partial x} &= c_1 + 2c_2 x + \sum_{n=2}^{\infty} c_{n+1}(n+1)\, T_n , \\ \frac{\partial U_{em}}{\partial y} &= -c_2 y + y\sum_{n=2}^{\infty} c_{n+1} R_{n-1} , \qquad (3.2) \\ \frac{\partial U_{em}}{\partial z} &= -c_2 z + z\sum_{n=2}^{\infty} c_{n+1} R_{n-1} . \end{aligned}$$

The recurrences of T_n and R_n allow us to perform the expansion of the derivatives of the potential in a very fast way.

Now, we are going to make a similar expansion of the potential corresponding to the Sun. Here, the expressions are a little bit longer, but few terms are enough to achieve very small errors. Firstly, we expand the inverse of the distance from the particle to the Sun in terms of Legendre polynomials. So, we have

$$\begin{aligned} q_{ps}^{-1} &= ((X-\alpha_7)^2 + (Y-\alpha_8)^2 + Z^2)^{-1/2} = \\ &= \frac{1}{\sqrt{\alpha_7^2+\alpha_8^2}} \sum_{n=0}^{\infty} \left(\frac{-\gamma\,\hat\rho}{\sqrt{\alpha_7^2+\alpha_8^2}} \right)^n P_n \left(\frac{(x-c_1)\alpha_7 + y\alpha_8}{\hat\rho\sqrt{\alpha_7^2+\alpha_8^2}} \right) , \end{aligned}$$

where

$$\hat\rho^2 = (x-c_1)^2 + y^2 + z^2 \ .$$

Instead of using α_7 and α_8, we introduce

$$\tilde\alpha_7 = a_s^{-1}\,\alpha_7 \ , \qquad \tilde\alpha_8 = a_s^{-1}\,\alpha_8 \ ,$$

with the purpose of knowing the order of magnitude of each term. With the same goal, we are going to use again the small parameter introduced in chapter 1,

$$\epsilon = \frac{1}{a_s} \ .$$

We also define some new functions

$$\alpha_{20} = \frac{\alpha_6\, m_s}{a_s^2\sqrt{\tilde\alpha_7^2+\tilde\alpha_8^2}} \ , \qquad \alpha_{21} = \frac{1}{\tilde\alpha_7^2+\tilde\alpha_8^2} \ ,$$

$$\alpha_{22} = \frac{\tilde\alpha_7}{\tilde\alpha_7^2+\tilde\alpha_8^2} \ , \qquad \alpha_{23} = \frac{\tilde\alpha_8}{\tilde\alpha_7^2+\tilde\alpha_8^2} \ ,$$

which will often appear in the next expressions. Right after that, we can consider the term corresponding to the gravitational potential of the Sun,

$$\frac{\alpha_6\, m_s}{\gamma^2 q_{ps}} = \alpha_{20} \sum_{n=0}^{\infty} G_n \ ,$$

defining

$$G_n = \frac{a_s}{\gamma^2} \left(\frac{-\gamma\,\hat\rho}{\sqrt{\tilde\alpha_7^2+\tilde\alpha_8^2}}\,\epsilon \right)^n P_n \left(\frac{(x-c_1)\tilde\alpha_7 + y\tilde\alpha_8}{\hat\rho\sqrt{\tilde\alpha_7^2+\tilde\alpha_8^2}} \right) \ .$$

These functions and its derivatives can be computed by recurrence, which can also be derived from the recursive relationship of the Legendre polynomials. The first terms and the recurrence are

$$
\begin{aligned}
G_0 &= \frac{a_s}{\gamma^2} \, , \\
G_1 &= -\frac{1}{\gamma} \left((x - c_1)\alpha_{22} + y\alpha_{23} \right) , \\
G_n &= -\frac{2n-1}{n} \left((x - c_1)\alpha_{22} + y\alpha_{23} \right) \gamma\epsilon \, G_{n-1} - \frac{n-1}{n} \, \alpha_{21}\hat{\rho}^2\gamma^2\epsilon^2 \, G_{n-2} \, .
\end{aligned}
$$

We notice that $G_n = O(\epsilon^{n-1}\gamma^{n-2})$. By derivation of the previous expressions, we get immediately the recurrence for the derivatives of the G_n functions. The first terms are

$$
\frac{\partial G_0}{\partial x} = \frac{\partial G_0}{\partial y} = \frac{\partial G_0}{\partial z} = \frac{\partial G_1}{\partial z} = 0 \, ,
$$

$$
\frac{\partial G_1}{\partial x} = -\frac{\alpha_{22}}{\gamma} \, , \qquad \frac{\partial G_1}{\partial y} = -\frac{\alpha_{23}}{\gamma} \, ,
$$

and the recurrences

$$
\begin{aligned}
\frac{\partial G_n}{\partial x} &= -\frac{2n-1}{n} \gamma\epsilon \left(\alpha_{22} G_{n-1} + \left((x - c_1)\alpha_{22} + y\alpha_{23} \right) \frac{\partial G_{n-1}}{\partial x} \right) - \\
&\quad -\frac{n-1}{n} \gamma^2\epsilon^2\alpha_{21} \left(2(x - c_1) G_{n-2} + \hat{\rho}^2 \frac{\partial G_{n-2}}{\partial x} \right) , \\
\frac{\partial G_n}{\partial y} &= -\frac{2n-1}{n} \gamma\epsilon \left(\alpha_{23} G_{n-1} + \left((x - c_1)\alpha_{22} + y\alpha_{23} \right) \frac{\partial G_{n-1}}{\partial y} \right) - \\
&\quad -\frac{n-1}{n} \gamma^2\epsilon^2\alpha_{21} \left(2y G_{n-2} + \hat{\rho}^2 \frac{\partial G_{n-2}}{\partial y} \right) , \\
\frac{\partial G_n}{\partial z} &= -\frac{2n-1}{n} \gamma\epsilon \left((x - c_1)\alpha_{22} + y\alpha_{23} \right) \frac{\partial G_{n-1}}{\partial z} - \\
&\quad -\frac{n-1}{n} \gamma^2\epsilon^2\alpha_{21} \left(2z G_{n-2} + \hat{\rho}^2 \frac{\partial G_{n-2}}{\partial z} \right) .
\end{aligned}
$$

3.2.3 Normalized equations of the motion

After performing the change of coordinates and the expansions of the potential, we are ready to write the equations of the motion in a suitable way to use algebraic manipulation. The equations have the same form for L_1 and L_2. The only difference are the values of the constants γ and c_n. The equations are

$$
\ddot{x} - 2\dot{y} - (1 + 2c_2)x = \sum_{n=2}^{\infty} c_{n+1}(n+1) \, T_n +
$$

$$
\begin{aligned}
& +\alpha_{10}\ddot{x} + \alpha_{11}\dot{x} + \alpha_{12}\dot{y} + \alpha_{13}x + \alpha_{14}y + \alpha_{15} + \\
& +\alpha_{16}\sum_{n=2}^{\infty} c_{n+1}(n+1)\,T_n + \alpha_{20}\sum_{n=2}^{\infty}\frac{\partial G_n}{\partial x}\,, \qquad (3.3)\\
\ddot{y} + 2\dot{x} + (c_2-1)y &= y\sum_{n=2}^{\infty} c_{n+1}R_{n-1} + \\
& +\alpha_{10}\ddot{y} - \alpha_{12}\dot{x} + \alpha_{11}\dot{y} - \alpha_{14}x + \alpha_{17}y + \alpha_{18} + \\
& +\alpha_{16}y\sum_{n=2}^{\infty} c_{n+1}R_{n-1} + \alpha_{20}\sum_{n=2}^{\infty}\frac{\partial G_n}{\partial y}\,, \qquad (3.4)\\
\ddot{z} + c_2 z &= z\sum_{n=2}^{\infty} c_{n+1}R_{n-1} + \\
& +\alpha_{10}\ddot{z} + \alpha_{11}\dot{z} + \alpha_{19}z + \\
& +\alpha_{16}z\sum_{n=2}^{\infty} c_{n+1}R_{n-1} + \alpha_{20}\sum_{n=2}^{\infty}\frac{\partial G_n}{\partial z}\,, \qquad (3.5)
\end{aligned}
$$

where

$$
\alpha_{10} = 1 - \frac{1}{\alpha_1}\,, \qquad \alpha_{11} = -\left(\frac{1}{\alpha_1}\right)^{\cdot}\,, \qquad \alpha_{12} = 2\left(\frac{\alpha_3}{\alpha_1} - 1\right)\,,
$$

$$
\alpha_{13} = \left(\frac{\alpha_2}{\alpha_1}\right)^{\cdot} + \frac{\alpha_2^2+\alpha_3^2}{\alpha_1} - 1 + 2c_2(\alpha_6 - 1)\,,
$$

$$
\alpha_{14} = \left(\frac{\alpha_3}{\alpha_1}\right)^{\cdot}\,, \qquad \alpha_{16} = \alpha_6 - 1\,,
$$

$$
\alpha_{15} = c_1\left(\alpha_6 - \left(\frac{\alpha_2}{\alpha_1}\right)^{\cdot} - \frac{\alpha_2^2+\alpha_3^2}{\alpha_1}\right) + \frac{\alpha_4}{\gamma} - \frac{m_s\alpha_6\tilde{\alpha}_7}{a_s^2(\tilde{\alpha}_7^2+\tilde{\alpha}_8^2)^{3/2}}\,,
$$

$$
\alpha_{17} = \left(\frac{\alpha_2}{\alpha_1}\right)^{\cdot} + \frac{\alpha_2^2+\alpha_3^2}{\alpha_1} - 1 - c_2(\alpha_6 - 1)\,,
$$

$$
\alpha_{18} = c_1\left(\frac{\alpha_3}{\alpha_1}\right)^{\cdot} + \frac{\alpha_5}{\gamma} - \frac{m_s\alpha_6\tilde{\alpha}_8}{a_s^2(\tilde{\alpha}_7^2+\tilde{\alpha}_8^2)^{3/2}}\,,
$$

$$
\alpha_{19} = \left(\frac{\alpha_2}{\alpha_1}\right)^{\cdot} + \frac{\alpha_2^2}{\alpha_1} - c_2(\alpha_6 - 1)\,.
$$

The functions α_k, $k = 10, \ldots, 23$, are real periodic functions, but we are going to work with them using complex notation and keeping the small parameter ϵ. Therefore, the functions can be written in this way

$$
\begin{aligned}
\alpha_k(t) &= \sum_{m\geq 0}\epsilon^m\sum_j \alpha_{kmj}e^{\sqrt{-1}j\omega_s t}\,, \qquad \text{for } k = 10, 12, 13, 15, 16, 17, 19, 20, 21, 22,\\
\alpha_k(t) &= \sqrt{-1}\sum_{m\geq 0}\epsilon^m\sum_j \alpha_{kmj}e^{\sqrt{-1}j\omega_s t}\,, \qquad \text{for } k = 11, 14, 18, 23,
\end{aligned}
$$

with $\alpha_{kmj} \in \mathbb{R}$. The first type of functions are even and they satisfy $\alpha_{kmj} = \alpha_{km,-j}$. On the other hand, the second type of functions are odd and they verify $\alpha_{kmj} = -\alpha_{km,-j}$.

We note that the equations (3.3), (3.4) and (3.5) have been written in such a way that the first line corresponds to the equations of the RTBP and all the terms on the second and third lines are $O(\epsilon)$. This is true because all the functions from α_{10} to α_{19} are $O(\epsilon)$. Furthermore, the derivatives $\frac{\partial G_n}{\partial x}$, $\frac{\partial G_n}{\partial y}$ and $\frac{\partial G_n}{\partial z}$ are of the same order as G_n.

3.3 Quasi-periodic planar Lyapunov orbits

We start dealing with the quasi-periodic planar orbits because they are the simplest ones. We have said before that in the RTBP there are families of planar Lyapunov periodic orbits around the L_1 and L_2 points. In the RTBP the orbits can be computed numerically, using the Poincaré map and some continuation method, or analytically, using the Lindstedt-Poincaré method, which in the periodic case is convergent in some domain around the collinear points. In our case, the orbits are quasi-periodic and then we are going to use the Lindstedt-Poincaré technique to get a solution as a formal series.

In the planar RTBP, the solution of the linearized problem, restricted to the central manifold, is

$$\begin{aligned} x &= -A\cos(\lambda t + \varphi) , \\ y &= KA\sin(\lambda t + \varphi) , \end{aligned} \tag{3.6}$$

where the frequency

$$\lambda = \sqrt{\frac{2 - c_2 + \sqrt{9c_2^2 - 8c_2}}{2}} = \begin{cases} 2.3343858538 & \text{for } L_1 , \\ 1.8626458835 & \text{for } L_2 , \end{cases} \tag{3.7}$$

and

$$K = \frac{\lambda^2 + 2c_2 + 1}{2\lambda} . \tag{3.8}$$

The amplitude of the orbit, A, and the phase, φ, are arbitrary.

We look for a solution of the form

$$\begin{aligned} x &= \sum x_{ik_1k_2m} A^i \gamma_1^{k_1} \gamma_2^{k_2} \epsilon^m , \\ y &= \sqrt{-1} \sum y_{ik_1k_2m} A^i \gamma_1^{k_1} \gamma_2^{k_2} \epsilon^m , \end{aligned} \tag{3.9}$$

where $x_{ik_1k_2m}$, $y_{ik_1k_2m} \in \mathbb{R}$, i, k_1, k_2, $m \in \mathbb{Z}$, $i, m \geq 0$, and

$$\begin{aligned} \gamma_1 &= \exp(\sqrt{-1}(\lambda\omega t + \varphi)) , \\ \gamma_2 &= \exp(\sqrt{-1}\omega_s t) , \end{aligned}$$

with ω depending on the amplitude and the solar perturbation parameter, ϵ, in the following form:

$$\omega = 1 + \sum d_{im} A^i \epsilon^m , \tag{3.10}$$

and the frequency of the Sun in the synodical system of reference is taken as

$$\omega_s = 0.925195985520347 \;, \tag{3.11}$$

the value that we took in section 1.3. After obtaining a solution as (3.9), we should take into account that ϵ is a fictitious parameter, in the sense that it has a value perfectly known. Then, we should add all the terms of the different powers of ϵ to get

$$\begin{aligned} x &= \sum \left(\sum_m x_{ik_1k_2m} \epsilon^m \right) A^i \gamma_1^{k_1} \gamma_2^{k_2} = \sum \overline{x}_{ik_1k_2} A^i \gamma_1^{k_1} \gamma_2^{k_2} \;, \\ y &= \sqrt{-1} \sum \left(\sum_m y_{ik_1k_2m} \epsilon^m \right) A^i \gamma_1^{k_1} \gamma_2^{k_2} = \sqrt{-1} \sum \overline{y}_{ik_1k_2} A^i \gamma_1^{k_1} \gamma_2^{k_2} \;, \end{aligned} \tag{3.12}$$

and also

$$\omega = \sum_i \left(\sum_m d_{im} \epsilon^m \right) A^i = \sum \overline{d}_i A^i \;. \tag{3.13}$$

If we want to insert the expressions (3.9) into the equations (3.3) and (3.4), we also need the derivatives

$$\begin{aligned} \dot{x} &= \sqrt{-1} \left(\omega \sum x_{ik_1k_2m} \lambda k_1 A^i \gamma_1^{k_1} \gamma_2^{k_2} \epsilon^m + \sum x_{ik_1k_2m} \omega_s k_2 A^i \gamma_1^{k_1} \gamma_2^{k_2} \epsilon^m \right) \;, \\ \ddot{x} &= - \Big(\omega^2 \sum x_{ik_1k_2m} \lambda^2 k_1^2 A^i \gamma_1^{k_1} \gamma_2^{k_2} \epsilon^m + 2\omega \sum x_{ik_1k_2m} \lambda k_1 \omega_s k_2 A^i \gamma_1^{k_1} \gamma_2^{k_2} \epsilon^m + \\ &\quad + \sum x_{ik_1k_2m} \omega_s^2 k_2^2 A^i \gamma_1^{k_1} \gamma_2^{k_2} \epsilon^m \Big) \;, \end{aligned}$$

and the derivatives $\dot{y}$, $\ddot{y}$, which are similar to the above ones. The only difference is that, in the case of y, one should multiply by $\sqrt{-1}$.

Let $n_i, n_e \in \mathbb{N}$ be two fixed values. We say that we compute the solution up to order (n_i, n_e) if we compute all the terms with $0 \leq i \leq n_i$, $0 \leq m \leq n_e$. It is important to note that we can obtain a formal solution up to order (n_i, n_e) recursively, beginning with (3.6). Writing them in complex notation

$$\begin{aligned} x &= -\frac{1}{2} A(\gamma_1 + \gamma_1^{-1}) \;, \\ y &= -\sqrt{-1} \frac{K}{2} A(\gamma_1 - \gamma_1^{-1}) \;, \end{aligned}$$

we get the first coefficients

$$x_{0000} = y_{0000} = 0 \;, \qquad x_{1100} = -\frac{1}{2} \;, \qquad y_{1100} = -\frac{K}{2} \;.$$

Here, the main point is that we can compute the terms of a given order (i_0, m_0) if we know all the terms of order (i, m), for $i \le i_0$, $m \le m_0$, except, of course, (i_0, m_0) which are what we want to compute. For this reason, if we wish the solution up to order (n_i, n_e), we can proceed by "rows" or by "columns" (see figure 3.2). This means that for every value of m we can compute all the terms from $i = 0$ to $i = n_i$, or reversely, for every value of i we can compute the terms from $m = 0$ to $m = n_e$.

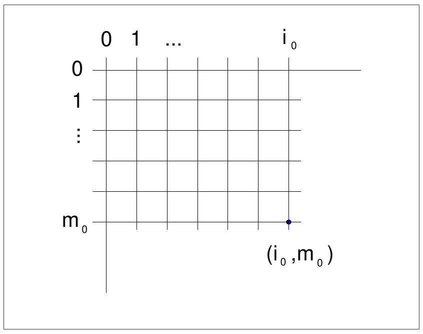

Figure 3.2.

If we insert the expressions (3.9) into the equations (3.3) and (3.4), to obtain the coefficients of the terms of order (i, m), we need to solve some 2×2 linear system of equations. There are two possible cases:

- if $(k_1, k_2) \neq (1, 0)$ the system is

$$\begin{aligned} -\Big((k_1\lambda + k_2\omega_s)^2 + 1 + 2c_2\Big)\, x_I + 2(k_1\lambda + k_2\omega_s)\, y_I &= M_I\,, \\ 2(k_1\lambda + k_2\omega_s)\, x_I + \Big(-(k_1\lambda + k_2\omega_s)^2 + c_2 - 1\Big)\, y_I &= N_I\,, \end{aligned} \tag{3.14}$$

  where I means the multiindex $(i\, k_1\, k_2\, m)$ and M_I, N_I are known. The determinant is always different from zero, provided that λ/ω_s is irrational. Later on, we will see that some difficulties with small divisors can appear.

- if $(k_1, k_2) = (1, 0)$ the previous system has determinant equal to zero. Then, we set $x_{i10m} = 0$, and we take advantage of this to compute the coefficients of the frequency ω, solving the system

$$\begin{aligned} 2\lambda\, y_{i10m} + (\lambda^2 - \lambda K)\, d_{i-1,m} &= M_{i10m}\,, \\ (-\lambda^2 + c_2 - 1)\, y_{i10m} + (\lambda^2 K - \lambda)\, d_{i-1,m} &= N_{i10m}\,, \end{aligned}$$

  where M_{i10m} and N_{i10m} are known. We notice that the terms of ω determined here are of order $(i-1, m)$. We want to emphasize that should we not allow that ω depends on the amplitude A, then we would not be able to determine the coefficients of x and y, as it is usual in the Lindstedt-Poincaré method. On the other hand the choice $x_{i10m} = 0$ can be seen as a normalization of the parameter A.

In both cases, the terms of the right hand side of the equations are known. They can be computed from the terms of lower order of x, y and ω.

Now, looking at the method used to compute recursively the coefficients and the symmetries of the equations (3.3) and (3.4), we can conclude that the coefficients of x and y satisfy the following relationships:

(a) $i, m \geq 0, \ |k_1| \leq i, \ i - k_1 \equiv 0 \,(\mathrm{mod}\, 2)$.

(b) $x_{ik_1k_2m} = x_{i,-k_1,-k_2m}$ and $y_{ik_1k_2m} = -y_{i,-k_1,-k_2m}$. For this reason, when making computations, there is only need to keep the coefficients with $k_1 > 0$ or if $k_1 = 0$ with $k_2 \geq 0$.

(c) $x_{i10m} = 0, \forall (i, m) \neq (1, 0)$.

(d) $d_{im} = 0$, if i is odd.

3.3.1 Results

We have implemented C code to compute formally the family of Lyapunov quasi-periodic orbits, up to a certain order (n_i, n_e), following the method described before. The program is able to manipulate series of the type (3.9) with four variables, series of the type (3.10) with two variables and series of the type of the α functions also with two variables. This means that we have developed routines to carry out basic operations, as sums or products, between two series of the same or different type.

A particular case of the Lyapunov quasi-periodic orbits are the orbits with amplitude $A = 0$. They are the periodic orbits which substitute the equilibrium points of the RTBP. We had already computed these orbits in chapter 2, numerically, using a continuation method from the libration points L_1 and L_2. Now, we check, that the orbits computed numerically and analytically agree very well. The initial condition computed numerically and analytically differs about 10^{-11} in position and 10^{-10} in velocity (normalized coordinates). In figures 3.3 and 3.4, we have drawn these periodic orbits labelled as 11 and 21, respectively, using their analytical expressions. Table 3.1 shows the coefficients of their developments, which are, in this case, the Fourier coefficients of the orbits.

We note that the orbit turns three times around the point $\mathrm{L_i}$, for $i = 1, 2$. This is due to the fact that the largest amplitude corresponds to the frequency $3\,\omega_s$ (look at table 3.1). But, the point is why this amplitude is the largest one? If one looks at the equation (3.3), it is checked that the terms purely depending on time come from α_{15} and the derivatives $\frac{\partial G_n}{\partial x}$, for $n \geq 2$. There are not terms of order ϵ because the terms coming from α_{15} cancel the ones from $\frac{\partial G_2}{\partial x}$. At order ϵ^2, α_{15} certainly has terms with frequencies $j\,\omega_s$, for $j = 0$ to 4, but when adding the corresponding terms of $\frac{\partial G_2}{\partial x}$ and $\frac{\partial G_3}{\partial x}$ only the terms with frequencies ω_s and $3\,\omega_s$ remain. All the other ones are cancelled again. Then, the largest coefficients correspond to the frequency $3\,\omega_s$. The frequency $2\,\omega_s$ begins to appear at order ϵ^3. Something similar happens with the equation (3.4), in the terms α_{18}, $\frac{\partial G_2}{\partial y}$ and $\frac{\partial G_3}{\partial y}$. Finally, we want to say that all what is true in the case of L_1 is also true for L_2.

For the computation of the Lyapunov quasi-periodic orbits we have said that we have to solve 2×2 linear systems of the kind (3.14). The determinant of those

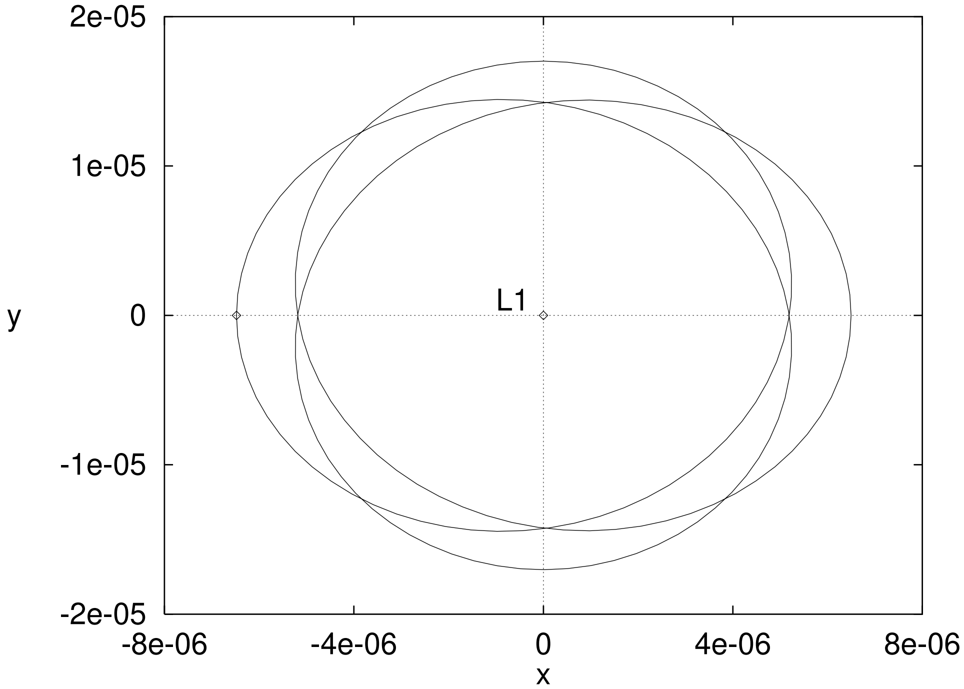

Figure 3.3: Periodic orbit 11 around L_1, analytically computed up to order 20 in ϵ. Normalized coordinates are used.

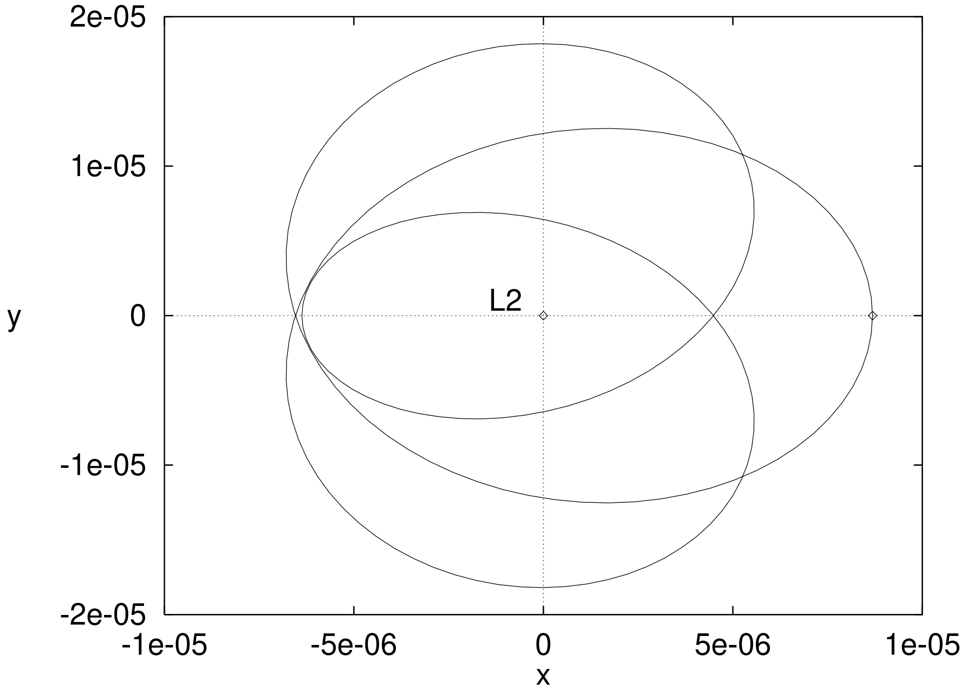

Figure 3.4: Periodic orbit 21 around L_2, analytically computed up to order 20 in ϵ. Normalized coordinates are used.

	L_1		L_2	
k_2	x_{00k_2}	y_{00k_2}	x_{00k_2}	y_{00k_2}
0	3.60193404e−09		−1.25986765e−08	
1	−3.84066830e−07	9.39784581e−07	4.29967846e−07	−2.88369732e−06
2	−1.13971127e−09	−1.80670921e−08	5.85478457e−07	1.73273102e−06
3	−2.82750008e−06	−7.64214318e−06	3.30191815e−06	6.16578500e−06
4	3.87771725e−09	5.96718702e−09	−9.21556459e−10	3.37981350e−09
5	−3.16586413e−08	−7.32803251e−08	3.26355339e−08	5.64374598e−08
6	4.85489480e−11	9.60629993e−11	−2.54798954e−11	−2.07697094e−11
7	−3.04832815e−10	−6.43255594e−10	2.96445700e−10	4.85395656e−10
8	5.87423786e−13	1.23310649e−12	−3.36549331e−13	−5.15257984e−13
9	−2.78471160e−12	−5.55398590e−12	2.62789929e−12	4.13113423e−12
10	4.37406891e−14	6.21919237e−14	−1.18077226e−15	−3.42390985e−15
11	−2.68370650e−14	−5.98929554e−14	2.23676470e−14	3.46655660e−14
12	4.61522418e−15	5.06026955e−15		

Table 3.1: Coefficients of the periodic orbits 11 and 21, about L_1 and L_2 respectively.

systems vanishes if $(k_1, k_2) = (1, 0)$. It is straightforward to see that

$$\begin{vmatrix} -\lambda^2 - 1 - 2c_2 & 2\lambda \\ 2\lambda & -\lambda^2 + c_2 - 1 \end{vmatrix} = 0 \,,$$

using the relationship between λ and c_2 (see (3.7), or simply, the fact that λ is an eigenvalue of the differential of the vector field).

Unfortunately, there are values of (k_1, k_2) that, although they do not make the determinant zero, they make it small. When solving the linear system of equations, the small determinant becomes a small divisor. As a consequence of that, some coefficients of the analytical expression of the orbits grow when increasing the order of the solution. Of course, this fact has influence on the convergence of the series. The small divisors appear when

$$k_1\lambda + k_2\omega_s \simeq \pm\lambda \,,$$

this is

$$(k_1 \pm 1)\lambda + k_2\omega_s \simeq 0 \,.$$

In the L_1 case, developing in continued fraction the quotient between ω_s and λ, with their present numerical values, we find the first approximants:

$$\frac{\omega_s}{\lambda} = \frac{1}{2}, \frac{1}{3}, \frac{2}{5}, \frac{21}{53}, \dots$$

The resonance $2/5$ is the most important. We note that $2\lambda - 5\omega_s \simeq 0.043$, and related with this resonance we have the values of the indexes $(k_1, k_2) = (1, -5)$ and $(3, -5)$.

In the L_2 case, following the same way of the previous case, we have the first approximants:

$$\frac{\omega_s}{\lambda} = \frac{1}{2}, \frac{75}{151}, \ldots$$

Here, the most important resonance is 1/2. We notice that $\lambda - 2\omega_s \simeq 0.012$. It produces the main small divisors, from $(k_1, k_2) = (0, 2)$ and $(2, -2)$. But, there are many others like $(1, -4)$ and $(3, -4)$.

In spite of the appearance of low order resonances, we have computed the analytical expression up to order $(n_i, n_e) = (15, 20)$. An HP-9000/819 spends about 13h for this computation. At the beginning, one might think that there is not need to go very far in the order n_e, because the parameter ϵ is small, roughly 1/389. But, this is not true because of the growth of some coefficients. If one wants to keep bounded the relative error of the coefficients, it is realized that one must increase the order n_e, more less, in the same way that n_i.

Looking at the solution series, we see that, indeed, the coefficients which grow faster are related with the resonances mentioned above. If we pay attention to these coefficients we can estimate the "radius" of convergence, through the quotient of consecutive terms and using Aitken extrapolation to improve the results. We have said "radius" because, in fact, we know that the series are not convergent in any open domain, due to the accumulation of the high order resonances. But, when computing the solution up to a certain order, it seems to be convergent in a certain zone, and there, an approximate analytical solution can be useful.

In the L_1 case, the series seems to be convergent up to an amplitude of $A \simeq 0.073$. In the QBCP, there are a couple of $2T$-periodic orbits with amplitude $A \simeq 0.069$, where T is the period of the Sun in the synodical system of reference. Those orbits come from the continuation of a periodic orbit of the RTBP with period $2T/5$.

In the L_2 case, the estimation of the radius of convergence gives the value $A \simeq 0.137$. In chapter 2, we got the T-periodic orbits 22, 23, 24 and 25, from an orbit of the RTBP with a period of $T/2$. Those orbits have approximately the amplitude $A \simeq 0.14$. We see that the existence of periodic orbits corresponding to resonances of low order is an obstruction for the existence of a good analytical approximation in a big area, as is quite natural.

We have just talked about the zone where the analytical expression of the Lyapunov quasi-periodic orbit seems to be convergent (or, rather, provides a good approximation), but we also are interested in knowing where there is a good agreement between analytical and numerical computations. For this purpose, we have done the following test. Imagine that we have certain values of the amplitude A, phase φ and initial time t_0. For these values, the analytical expression (3.12) gives a point in the phase space. We can integrate the Hamilton equations (1.24) with these initial conditions during a time span of π, for instance. The final point is then compared with the point calculated using the analytical expression for the final time of the integration span. There will be a certain difference, say d, which comes from the amplification of the error in the initial conditions. We then define a function ϕ such

i	d_i for L_1	d_i for L_2
0	1.0009568283e+00	1.0006533877e+00
2	−1.7581979004e+00	−3.4945744853e−01
4	4.8502273612e+00	−5.0038409145e−01
6	−1.2212106965e+01	2.1915123821e−01
8	1.4577904928e+01	−4.4323514570e+01
10	8.7423988699e+01	−3.8530661403e+03
12	−8.4681711425e+02	−3.0224527024e+05
14	−2.9017857403e+04	−2.2332915751e+07

Table 3.2: Coefficients of ω.

that for each value of A:

$$\phi(A) = \max\{d(A,\varphi,t_0) \mid \varphi \in [0,2\pi],\ t_0 \in [0,T]\} .$$

We point out that A is measured in normalized units while d is measured in synodical units. We have used a grid of values of φ and t_0, of 8×8 equally spaced points. Taking into account the symmetries we only need to integrate 32 initial conditions. This is an increasing function of the amplitude because if it rises then the analytical solution have poorer accuracy leading to big errors. Finally, a certain δ threshold has been fixed and the corresponding amplitude A_δ such that $\phi(A_\delta) = \delta$ is determined, through an iterative process. Then, we can assure that the difference in the phase space between the analytical and numerical solution after the integration during π time units is less than δ, for all $A < A_\delta$. This test was done taking the value $\delta = 10^{-5}$ ($\simeq$ 3.8 km in the positions, $\simeq$ 10 mm/s in velocities). For L_1 the result was $A_\delta = 0.056$ and for L_2 was $A_\delta = 0.073$.

The Lyapunov quasi-periodic orbits have two basic frequencies: $\lambda\omega$ and ω_s. The first one depends on the amplitude as given by (3.13). Table 3.2 shows the computed coefficients of that expression. We have said before that the most important frequency in the periodic orbits substituting the libration points is $3\omega_s$. Here, increasing a little the amplitude of the Lyapunov quasi-periodic orbit, the main frequency becomes $\lambda\omega$. Figures 3.5a-d show the analytical orbits about L_1 for $A = 10^{-5}$, $4{\cdot}10^{-5}$, 10^{-4} and 0.05, respectively. Figures 3.6a-d show the analytical orbits about L_2 for $A = 10^{-5}$, $4{\cdot}10^{-5}$, 10^{-4} and 0.07, respectively. For all of them, we have taken phase $\varphi = 0$ and initial time $t_0 = 0$. The final time is indicated in each figure. The figures of the orbits help to understand the evolution of the families of quasi-periodic orbits. Figures 3.5d and 3.6d seem to show "thick" periodic orbits. The point is that by increasing the amplitude of the orbit, the terms with frequencies multiples of ω_s become small compared with the size of the orbit.

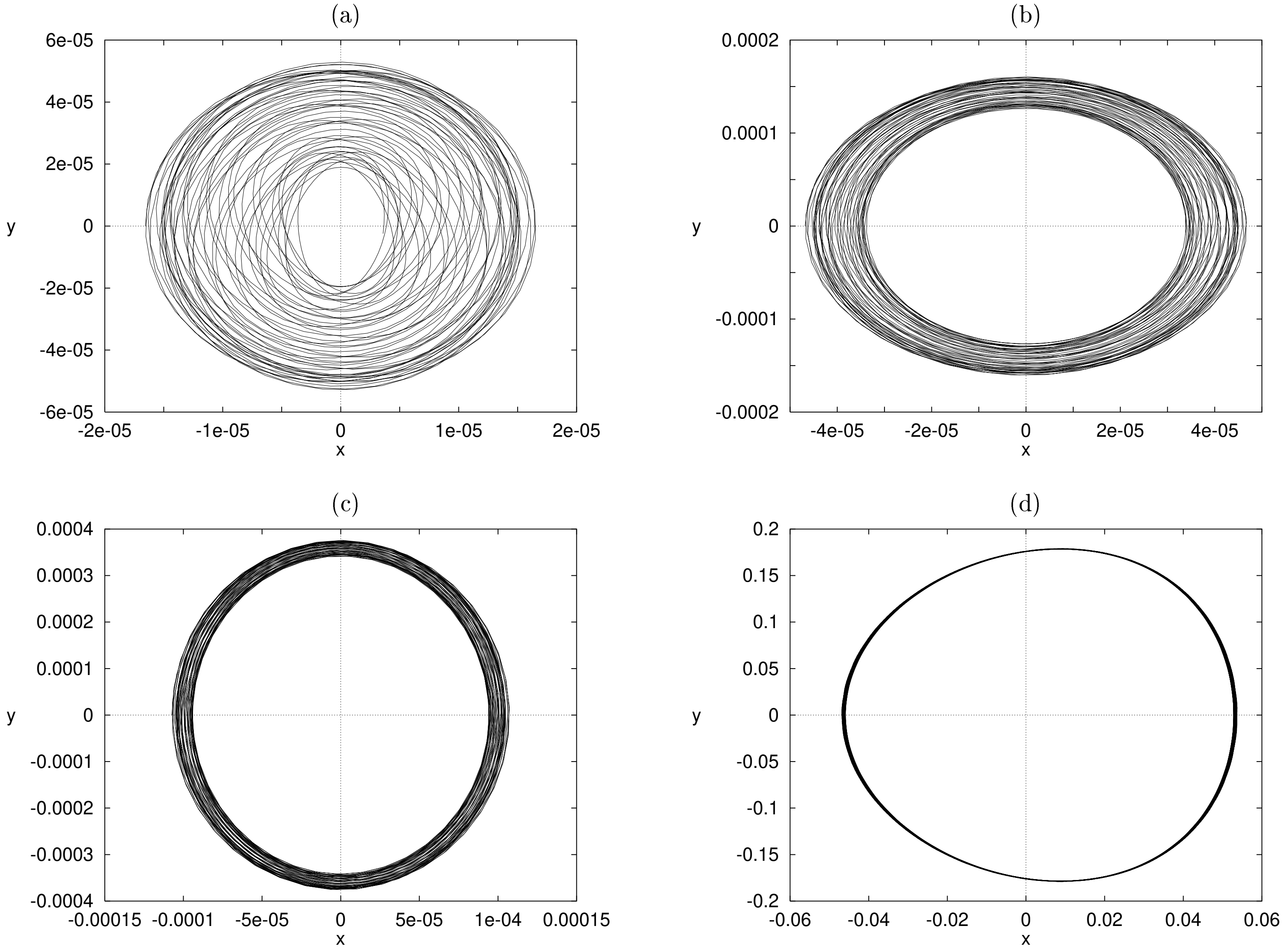

Figure 3.5: Evolution of the Lyapunov planar quasi-periodic orbits around L_1 (normalized units). (a) $A = 10^{-5}$, $t_f = 20\mathrm{T}$, $\lambda\omega = 2.3366194598$. (b) $A = 4{\cdot}10^{-5}$, $t_f = 20\mathrm{T}$. $\lambda\omega = 2.3366194536$. (c) $A = 10^{-4}$, $t_f = 20\mathrm{T}$, $\lambda\omega = 2.3366194191$. (d) $A = 0.05$, $t_f = 20\mathrm{T}$, $\lambda\omega = 2.3264289997$.

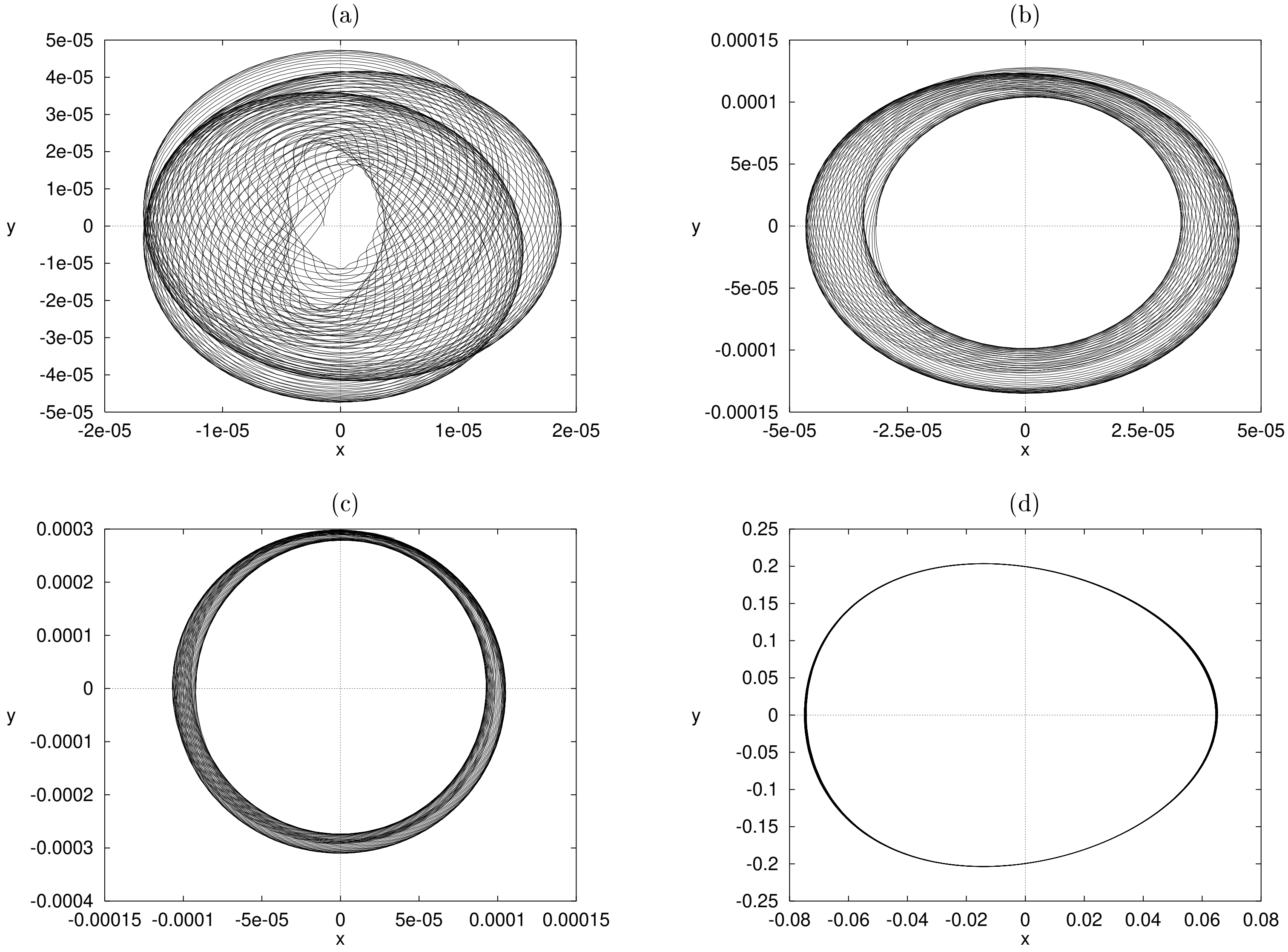

Figure 3.6: Evolution of the Lyapunov planar quasi-periodic orbits around L_2 (normalized units). (a) $A = 10^{-5}$, $t_f = 50\text{T}$, $\lambda\omega = 1.8638629134$. (b) $A = 4 \cdot 10^{-5}$, $t_f = 25\text{T}$. $\lambda\omega = 1.8638629125$. (c) $A = 10^{-4}$, $t_f = 25\text{T}$, $\lambda\omega = 1.8638629070$. (d) $A = 0.07$, $t_f = 25\text{T}$, $\lambda\omega = 1.8606510190$.

3.4 Lissajous orbits

In this section we are going to talk about the Lissajous orbits. In the spatial RTBP, it is well known the existence of this kind of orbits around the collinear equilibrium points. Gómez *et al.* studied the Lissajous orbits about L_1 in the case of Earth-Sun (see [10]). In our case, the task is a little bit more laborious because our system is non autonomous and it depends on one small parameter. To carry out the computations, we are going to follow the Lindstedt-Poincaré method in the same way than it was presented in the previous section.

First of all, we consider the spatial RTBP. The solution of the linearized equations, restricted to the central manifold is

$$\begin{aligned} x &= -A\cos(\lambda_1 t + \varphi_1) , \\ y &= KA\sin(\lambda_1 t + \varphi_1) , \\ z &= B\cos(\lambda_2 t + \varphi_2) , \end{aligned} \tag{3.15}$$

where the frequency λ_1 of the motion in the xy-plane and the constant K are the same which were given in (3.7) and (3.8). On the other hand, the values of the frequency are

$$\lambda_2 = \sqrt{c_2} = \begin{cases} 2.2688310630 \ \text{ for } L_1 , \\ 1.7861761647 \ \text{ for } L_2 . \end{cases} \tag{3.16}$$

The amplitudes in the x direction, A, and the vertical direction, B, as well as the phases φ_1 and φ_2 are arbitrary.

We are going to look for a formal solution of the equations (3.3), (3.4) and (3.5) of the form

$$\begin{aligned} x &= \sum x_{ijk_1k_2k_3m} A^i B^j \gamma_1^{k_1} \gamma_2^{k_2} \gamma_3^{k_3} \epsilon^m , \\ y &= \sqrt{-1} \sum y_{ijk_1k_2k_3m} A^i B^j \gamma_1^{k_1} \gamma_2^{k_2} \gamma_3^{k_3} \epsilon^m , \\ z &= \sum z_{ijk_1k_2k_3m} A^i B^j \gamma_1^{k_1} \gamma_2^{k_2} \gamma_3^{k_3} \epsilon^m , \end{aligned} \tag{3.17}$$

where $x_{ijk_1k_2k_3m}$, $y_{ijk_1k_2k_3m}$, $z_{ijk_1k_2k_3m} \in \mathbb{R}$, i, j, k_1, k_2, k_3, $m \in \mathbb{Z}$, $i, j, m \geq 0$, and

$$\begin{aligned} \gamma_1 &= \exp(\sqrt{-1}(\lambda_1 \omega_1 t + \varphi_1)) , \\ \gamma_2 &= \exp(\sqrt{-1}(\lambda_2 \omega_2 t + \varphi_2)) , \\ \gamma_3 &= \exp(\sqrt{-1}\omega_s t) , \end{aligned}$$

with ω_1 and ω_2 depending on the amplitudes in the following form:

$$\begin{aligned} \omega_1 &= 1 + \sum d_{ijm} A^i B^j \epsilon^m , \\ \omega_2 &= 1 + \sum f_{ijm} A^i B^j \epsilon^m , \end{aligned}$$

and the frequency ω_s as usual.

After computing a solution of the type (3.17), we add all the terms with different powers of ϵ to get

$$\begin{aligned}
x &= \sum \overline{x}_{ijk_1k_2k_3} A^i B^j \gamma_1^{k_1} \gamma_2^{k_2} \gamma_3^{k_3} \ , \\
y &= \sqrt{-1} \sum \overline{y}_{ijk_1k_2k_3} A^i B^j \gamma_1^{k_1} \gamma_2^{k_2} \gamma_3^{k_3} \ , \\
z &= \sum \overline{z}_{ijk_1k_2k_3} A^i B^j \gamma_1^{k_1} \gamma_2^{k_2} \gamma_3^{k_3} \ ,
\end{aligned} \tag{3.18}$$

and

$$\begin{aligned}
\omega_1 &= \sum \overline{d}_{ij} A^i B^j \ , \\
\omega_2 &= \sum \overline{f}_{ij} A^i B^j \ .
\end{aligned} \tag{3.19}$$

In order to insert the expressions (3.17) into the differential equations (3.3), (3.4) and (3.5), it is suitable to write the derivatives

$$\begin{aligned}
\dot{x} &= \sqrt{-1} \sum_{r=1,2} \left(\omega_r \sum x_{ijk_1k_2k_3m} \lambda_r k_r A^i B^j \gamma_1^{k_1} \gamma_2^{k_2} \gamma_3^{k_3} \epsilon^m \right) + \\
&\quad + \sqrt{-1} \sum x_{ijk_1k_2k_3m} \omega_s k_3 A^i B^j \gamma_1^{k_1} \gamma_2^{k_2} \gamma_3^{k_3} \epsilon^m \ , \\
\ddot{x} &= - \sum_{r=1,2} \left(\omega_r^2 \sum x_{ijk_1k_2k_3m} \lambda_r^2 k_r^2 A^i B^j \gamma_1^{k_1} \gamma_2^{k_2} \gamma_3^{k_3} \epsilon^m \right) - \\
&\quad - 2\omega_1 \omega_2 \sum x_{ijk_1k_2k_3m} \lambda_1 k_1 \lambda_2 k_2 A^i B^j \gamma_1^{k_1} \gamma_2^{k_2} \gamma_3^{k_3} \epsilon^m - \\
&\quad - 2 \sum_{r=1,2} \left(\omega_r \sum x_{ijk_1k_2k_3m} \lambda_r k_r \omega_s k_3 A^i B^j \gamma_1^{k_1} \gamma_2^{k_2} \gamma_3^{k_3} \epsilon^m \right) - \\
&\quad - \sum x_{ijk_1k_2k_3m} \omega_s^2 k_3^2 A^i B^j \gamma_1^{k_1} \gamma_2^{k_2} \gamma_3^{k_3} \epsilon^m \ .
\end{aligned}$$

Similar expansions appear for $\dot{y}$, $\ddot{y}$, $\dot{z}$ and $\ddot{z}$, except that $\dot{y}$ and $\ddot{y}$ are multiplied by $\sqrt{-1}$.

Here, in the same way than in section 3.3, it is possible to compute recursively the coefficients of the series x, y, z, ω_1 and ω_2. We say that we compute the solution up to a order (n_{ij}, n_e) if we compute all the terms with $0 \le i+j \le n_{ij}$, $0 \le m \le n_e$. We begin the recurrence with (3.15), which written in complex notation gives

$$\begin{aligned}
x &= -\frac{1}{2} A(\gamma_1 + \gamma_1^{-1}) \ , \\
y &= -\sqrt{-1} \frac{K}{2} A(\gamma_1 - \gamma_1^{-1}) \ , \\
z &= \frac{1}{2} B(\gamma_2 + \gamma_2^{-1}) \ .
\end{aligned}$$

Therefore, the first coefficients are

$$x_{000000} = y_{000000} = z_{000000} = 0 \ ,$$

$$x_{101000} = -\frac{1}{2} \ , \qquad y_{101000} = -\frac{K}{2} \ , \qquad z_{010100} = \frac{1}{2} \ .$$

To obtain the terms of a certain order we have to solve several 3×3 linear systems. In these systems, the two first equations are independent of the third one.

We also want to point out that the terms of the right hand side of the equations are known in all the cases. They depend on the terms of lower order of x, y, z, ω_1 and ω_2. The linear systems can be of the following types:

- if $(k_1, k_2, k_3) \neq (1,0,0), (0,1,0)$ the system is

$$\begin{aligned} -(W^2+1+2c_2)\, x_I + 2W\, y_I &= M_I\,, \\ 2W\, x_I + (-W^2+c_2-1)\, y_I &= N_I\,, \\ (-W^2+c_2)\, z_I &= P_I\,, \end{aligned} \tag{3.20}$$

  where $W = k_1\lambda_1 + k_2\lambda_2 + k_3\omega_s$ and I means the multiindex $(i\, j\, k_1\, k_2\, k_3\, m)$. In this case, the determinant is different from zero if we assume that the triple $(\lambda_1, \lambda_2, \omega_s)$ satisfies some Diophantine condition, but later on, we will discuss about the possibility of having small divisors.

- if $(k_1, k_2, k_3) = (1,0,0)$ the two first equations of (3.20) have determinant equal to zero. Then, we set $x_{ij100m} = 0$ and determine the coefficient of y and the correcting term, $d_{i-1,j,m}$ of the first frequency by solving

$$\begin{aligned} 2\lambda_1\, y_{ij100m} + (\lambda_1^2 - \lambda_1 K)\, d_{i-1,j,m} &= M_{ij100m}\,, \\ (-\lambda_1^2 + c_2 - 1)\, y_{ij100m} + (\lambda_1^2 K - \lambda_1)\, d_{i-1,j,m} &= N_{ij100m}\,. \end{aligned}$$

  We note that the terms of ω_1 involved in this system are of order $(i+j-1, m)$. Here, the third equation of (3.20) does not bring any problem.

- if $(k_1, k_2, k_3) = (0,1,0)$, in the third equation of (3.20), the coefficient of z_I vanishes. Then, we can set $z_{ij010m} = 0$ and determine the corresponding terms of ω_2 through the equation

$$-\lambda_2^2\, f_{i,j-1,m} = P_{ij100m}\,.$$

Again note that taking $x_{ij100m} = 0$ and $z_{ij010m} = 0$ is just a normalization of the A and B amplitudes.

As a consequence of the form of the equations (3.3), (3.4) and (3.5), and taking into account the recursive algorithm used to determine the coefficients of the series, it is possible to see that they verify the following relationships:

(a) $i, j, m \geq 0$, $|k_1| \leq i$, $|k_2| \leq j$, $i - k_1 = 0 \,(\mathrm{mod}\ 2)$, $j - k_2 = 0 \,(\mathrm{mod}\ 2)$, for all the series.

(b) $x_{ik_1k_2k_3m} = x_{i,-k_1,-k_2,-k_3m}$, $y_{ik_1k_2k_3m} = -y_{i,-k_1,-k_2,-k_3m}$ and $z_{ik_1k_2k_3m} = z_{i,-k_1,-k_2,-k_3m}$. Due to these symmetries, in performing computations it is only necessary to keep the coefficients with $k_1 > 0$ or if $k_1 = 0$ with $k_2 > 0$ or if $k_1, k_2 = 0$ with $k_3 \geq 0$.

(c) For x and y we only have terms with $j \equiv 0 \,(\mathrm{mod}\ 2)$. For z there are only terms with $j \equiv 1 \,(\mathrm{mod}\ 2)$.

(d) $x_{ij100m} = 0$, $\forall (i,j,m) \neq (1,0,0)$ and $z_{ij010m} = 0$, $\forall (i,j,m) \neq (0,1,0)$.

(e) If i or j are odd then $d_{ijm} = f_{ijm} = 0$.

3.4.1 The algebraic manipulator and the results

With the purpose of computing an analytical expression of the Lissajous quasi-periodic orbits up to a certain order, the algorithm described above has been implemented in a C code. The computational task is not so simple. The required quantity of memory and time of CPU grow sharply with the order. For this reason we have different codes for the Lyapunov and the Lissajous orbits, although the first ones are a particular case of the second ones.

There are basically two different approaches to make algebraic computations with series. If the series are full or have some special structure (for example, if all the terms have even exponents) it is sufficient to keep the coefficients in an array. The exponents associated with a component of the array can be recovered in a more or less easy way, depending on the number of variables and the structure of the series. On the other hand, if the series is sparse it is better to keep only the non zero coefficients, but in this case also the exponents corresponding to each coefficient should be kept. In our case, we decided to use a mixed approach.

Our work involves series on six variables of the type (3.17). It is true that these series have a certain structure derived from the properties (a)-(e) exposed before, but it is also true that it is difficult to know a priori how many values of k_3 should be kept. On the other hand, it is necessary to locate easily the terms of each order (n, m), where $n = i + j$. Then, we decide to work with the series using the sparse approach, but keeping only four of the six exponents of each monomial. To store them, we define an structure composed by one *double* and four *signed char*. The *char* variables can be used to store small integers of one byte. The structure is as follows:

$$x_{ijk_1k_2k_3m} A^i B^j \gamma_1^{k_1} \gamma_2^{k_2} \gamma_3^{k_3} \epsilon^m \longrightarrow \boxed{\; j \;|\; k_1 \;|\; k_2 \;|\; k_3 \;|\; x_{ijk_1k_2k_3m} \;}$$

Then, we use an one dimensional array of structures for every series and an auxiliary table of integers to locate the beginning and the end of the terms of order (n, m).

With our program, we have computed the analytical expression of the Lissajous orbits up to order (9,11) and (11,9). For these computations, in the second case, the program spends 3h. 43min. 42s. of CPU time (in an HP 9000/819) and about 100 Mb of memory. At this order, we notice that we need to store about 64000 terms of the series x. If we compute the solution up to order (n_i, n_e) then the quantity of monomials of the series x is proportional to $n_i^4 n_e^2$. Moreover, it is necessary to take into account that the series T_n, R_n, G_n, $\frac{\partial G_n}{\partial x}$, $\frac{\partial G_n}{\partial y}$ and $\frac{\partial G_n}{\partial z}$ must also be kept, besides many other auxiliary series. With respect to the CPU time, after some tests, it seems to be proportional to $n_i^7 n_e^5$. Due to this growth of memory and CPU time, it is not easy to go to higher orders.

Another difficulty to obtain a good analytical approximation of the Lissajous orbits is the existence of resonances. As mentioned before, the linear system (3.20) is non singular for all $(k_1, k_2, k_3) \neq (1, 0, 0), (0, 1, 0)$. But, for some values of these indexes the determinant of the two first equations becomes small. There are also values of the indexes which produce small divisors in the third equation of (3.20).

Now, we should be aware that small divisors can appear by solving the linear system. To the end, it is convenient to introduce a definition. Let M be a real (or complex) matrix $n \times n$. We define the *inner spectral radius* as

$$\nu(M) = \min\{|\lambda| \,:\, \lambda \in Spec(M)\} \,.$$

If the matrix M is singular then $\nu(M) = 0$, otherwise,

$$\nu(M) = \frac{1}{\rho(M^{-1})} \,,$$

where $\rho(M^{-1})$ is the spectral radius of the inverse of M.

Proposition 3.1 *Let M be an $n \times n$ real symmetric matrix and $Mx = y$ a linear system of equations. The following inequality holds*

$$\nu(M)\|x\|_2 \leq \|y\|_2 \,.$$

When solving the linear system (3.20), there are two quantities related with the growth of the solution of the system and so, with the growth of the coefficients of the solution series. Those quantities are

$$D_1(W) = \nu \begin{pmatrix} -W^2 - 1 - 2c_2 & 2W \\ 2W & -W^2 + c_2 - 1 \end{pmatrix} \,,$$

the inner spectral radius of the two first equations of the linear system (3.20), where $W = k_1\lambda_1 + k_2\lambda_2 + k_3\omega_s$, and

$$D_2(W) = |-W^2 + c_2| \,,$$

the divisor of the third equation of (3.20). If one of those quantities is small then the associated coefficient becomes large.

We know that $D_1(\lambda_1) = D_2(\lambda_2) = 0$. The point is that for some values of (k_1, k_2, k_3) we can have $W \simeq \pm\lambda_1$ or $W \simeq \pm\lambda_2$. A test was done with the purpose of knowing what low order combination of the frequencies can give small divisors. We look for values of (k_1, k_2, k_3) which satisfy $|W \pm \lambda_i| < 0.15$ for $i = 1$ or 2 among all $|k_1|, |k_2|, |k_3| \leq 5$. Tables 3.3 and 3.4 show the values which pass the test in the L_1 and L_2 case, respectively. The divisors D_1 and D_2 have also been printed in those tables.

At this point, it is suitable to remind of the series x and y only have terms with k_2 even and z only with k_2 odd. Taking into account that, in the L_1 case, for the series x and y, the smallest (non zero) divisors are associated with $(1, 0, -5)$ and $(3, 0, -5)$. For the series z the smallest divisor comes from $(2, \pm 1, -5)$. Nevertheless, looking at the solution series up to order 11, the biggest coefficients are related with $(1, -2, 0)$ and $(3, -2, 0)$ for x and y. In the case of z, the biggest coefficients correspond to the indexes $(2, -1, 0)$, $(2, -3, 0)$ and $(4, -3, 0)$.

k_1	k_2	k_3	$W+\lambda_1$	$W-\lambda_1$	$D_1(W)$	$W+\lambda_2$	$W-\lambda_2$	$D_2(W)$
0	1	−5	−0.023		0.083	−0.088		0.409
0	1	0		−0.066	0.235		0.000	0.000
0	3	−5					−0.088	0.393
1	−2	0	0.131		0.462	0.066		0.293
1	−2	5		0.088	0.327			
1	0	−5	0.043		0.154	−0.023		0.104
1	0	0		0.000	0.000		0.066	0.302
1	2	−5		−0.088	0.314		−0.023	0.103
2	−3	0				0.131		0.578
2	−1	−5	0.108		0.384	0.043		0.192
2	−1	0		0.066	0.242		0.131	0.612
2	1	−5		−0.023	0.082		0.043	0.196
3	−2	−5				0.108		0.480
3	−2	0		0.131	0.491			
3	0	−5		0.043	0.157		0.108	0.503
4	−1	−5		0.108	0.404			
5	−5	−3	−0.113		0.423			
5	−5	2					−0.091	0.403

Table 3.3: Low order resonances in L_1 case.

In the L_2 case, looking at table 3.4, we see that the smallest values of D_1 correspond to $(0,0,2)$, $(2,0,-2)$, $(1,0,-4)$ and $(3,0,-4)$. Besides these indexes, we have that some coefficients of x and y with $(1,0,2)$ and $(3,0,-2)$ are also big. With respect to D_2, the smallest values are obtained from the indexes $(1,\pm1,-2)$ and $(2,\pm1,-4)$. In the solution series of z, we also find large coefficients related with the indexes $(0,1,-2)$ and $(2,-1,-2)$.

In order to know the zone with good agreement between analytical and numerical orbits, we are going to do a test like the one we did in section 3.3.1 for the Lyapunov orbits. If we fix the amplitudes A and B, the phases φ_1 and φ_2 and the initial time t_0, the computed analytical solution of the form (3.18) gives us a point in the phase space. The Hamilton equations of the motion (1.24) can be integrated with these initial conditions during a certain time interval (for instance, π time units). The final point of the integration can be compared with the point given by the analytical solution for the final time. Let d be the distance between these two points in the phase space. For each value of A and B, we can define the function

$$\phi(A,B) = \max\{d(A,B,\varphi_1,\varphi_2,t_0) \mid \varphi_1,\varphi_2 \in [0,2\pi],\ t_0 \in [0,T]\}\ .$$

In figures 3.7 and 3.8, we have drawn the zones where the function ϕ is less than 10^{-5} for the L_1 and L_2 cases respectively. Notice that those zones are short in the direction of the amplitude A. The reason of that is the existence of low order

k_1	k_2	k_3	$W+\lambda_1$	$W-\lambda_1$	$D_1(W)$	$W+\lambda_2$	$W-\lambda_2$	$D_2(W)$
0	0	2		−0.012	0.030		0.064	0.234
0	1	−4	−0.052		0.132	−0.128		0.475
0	1	0		−0.076	0.186		0.000	0.000
0	2	−2		−0.141	0.336		−0.064	0.225
0	3	−4					−0.128	0.442
1	−3	2				0.141		0.483
1	−2	0				0.076		0.267
1	−2	4		0.128	0.334			
1	−1	−2	0.089		0.215	0.012		0.044
1	−1	2		0.064	0.164		0.141	0.522
1	0	−4	0.025		0.061	−0.052		0.188
1	0	0		0.000	0.000		0.076	0.279
1	1	−2		−0.064	0.157		0.012	0.044
1	2	−4		−0.128	0.308		−0.052	0.183
2	−2	−2				0.089		0.309
2	−2	2		0.141	0.367			
2	−1	−4	0.101		0.244	0.025		0.087
2	−1	0		0.076	0.196			
2	0	−2		0.012	0.031		0.089	0.325
2	1	−4		−0.052	0.128		0.025	0.088
3	−2	−4				0.101		0.351
3	−1	−2		0.089	0.228			
3	0	−4		0.025	0.062		0.101	0.371
4	−1	−4		0.101	0.260			

Table 3.4: Low order resonances in L_2 case.

resonant periodic orbits, which was explained in the section dedicated to the planar orbits (see 3.3.1). On the other hand, in the vertical direction there are not low order resonant periodic orbits. For this reason, the zone of good agreement between the analytical and the numerical solution is much bigger in the B direction.

The Lissajous quasi-periodic orbits depend on three basic frequencies: $\lambda_1\omega_1$, $\lambda_2\omega_2$ and ω_s. In turn, ω_1 and ω_2 depend on the amplitudes A and B as given by (3.19). Figure 3.9 shows a typical Lissajous orbit. Planar Lyapunov orbits of section 3.3 are a particular case of Lissajous orbits setting $B = 0$. These orbits depend only on the frequencies $\lambda_1\omega_1$ and ω_s. Another particular case is gotten setting $A = 0$. These orbits correspond to the eight-shaped family of periodic orbits of the RTBP. But, in this case, they depend on two frequencies $\lambda_2\omega_2$ and ω_s. As a consequence of that, for small values of B, they lose their characteristic shape. Figures 3.10 and 3.11 show two of these orbits. We notice that the orbits of those figures are almost vertical (check the scales). They are very narrow in the x and y directions.

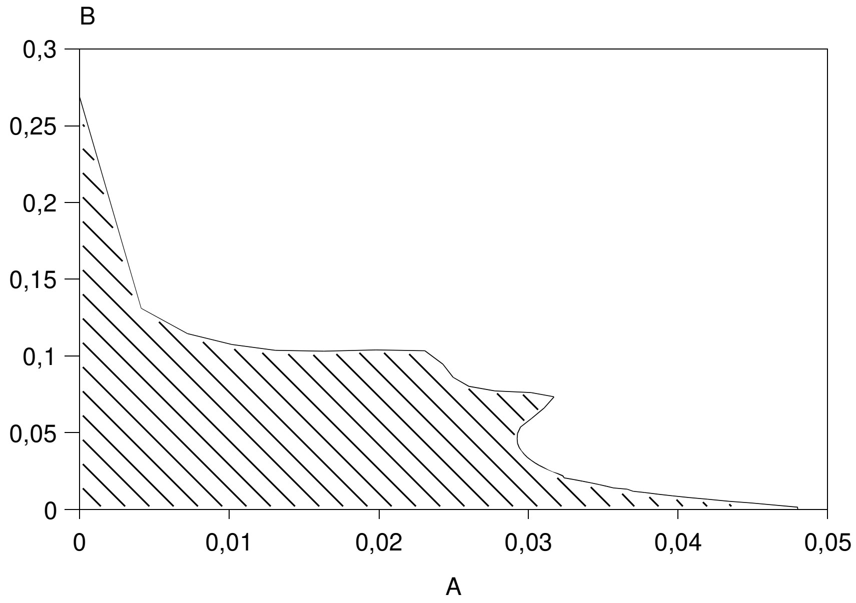

Figure 3.7: Zone with good agreement between analytical and numerical orbits. Analytical solution up to order (9,11) about L_1.

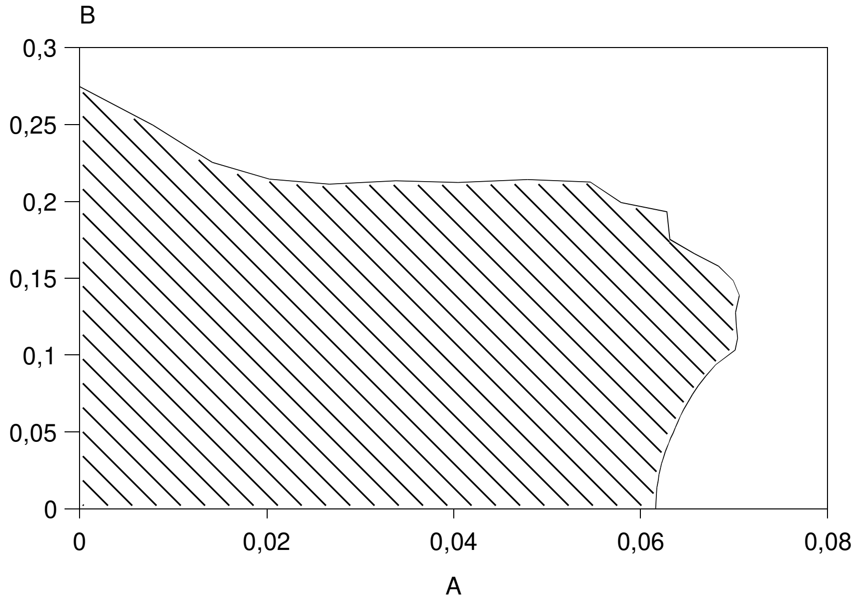

Figure 3.8: Zone with good agreement between analytical and numerical orbits. Analytical solution up to order (11,9) about L_2.

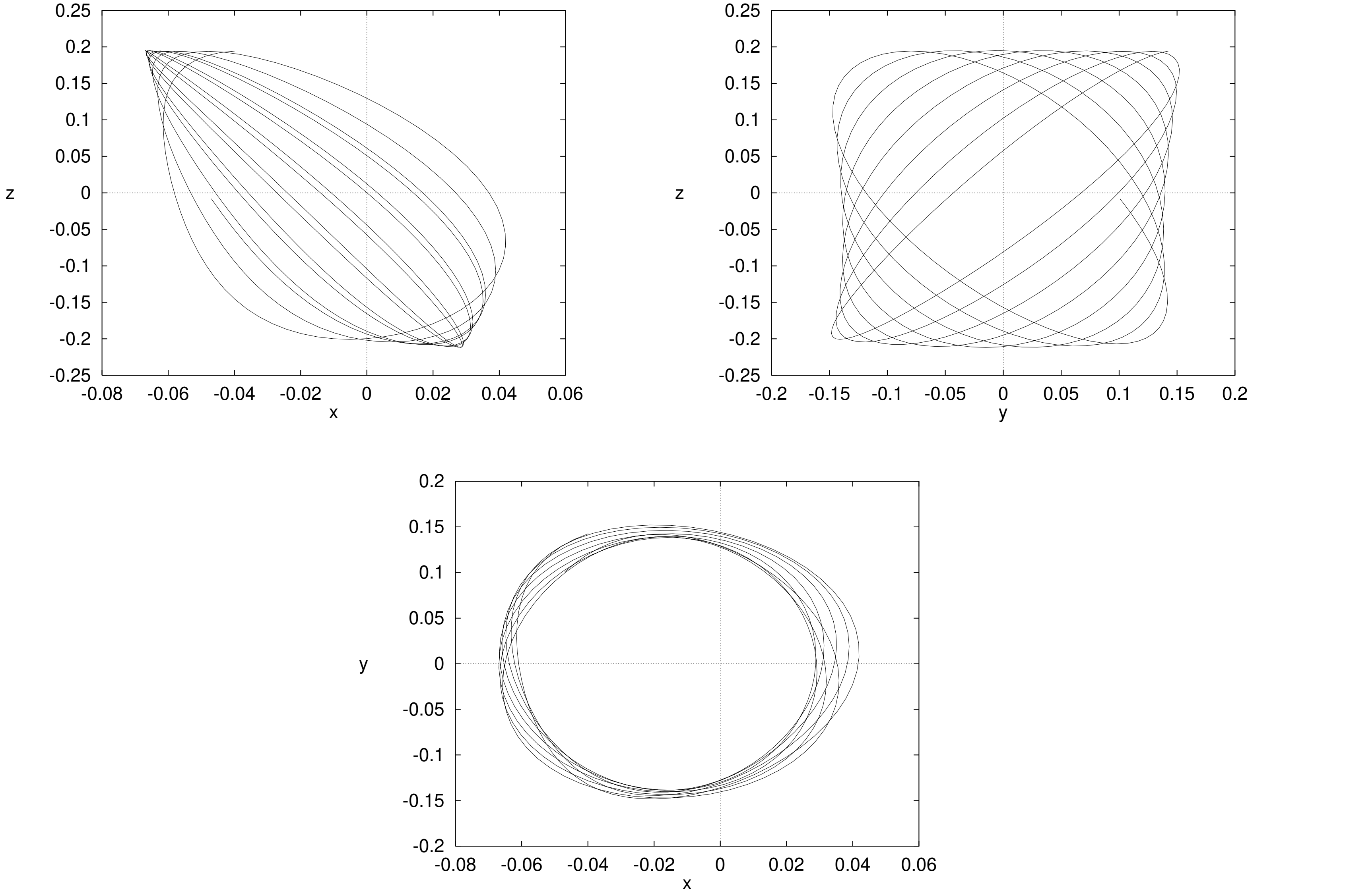

Figure 3.9: Lissajous orbit around L_2 using normalized coordinates. $A = 0.05$, $B = 0.2$, $t_0 = 0$, $t_f = 4T$, $\varphi_1 = 0.8$ and $\varphi_2 = 1.57$.

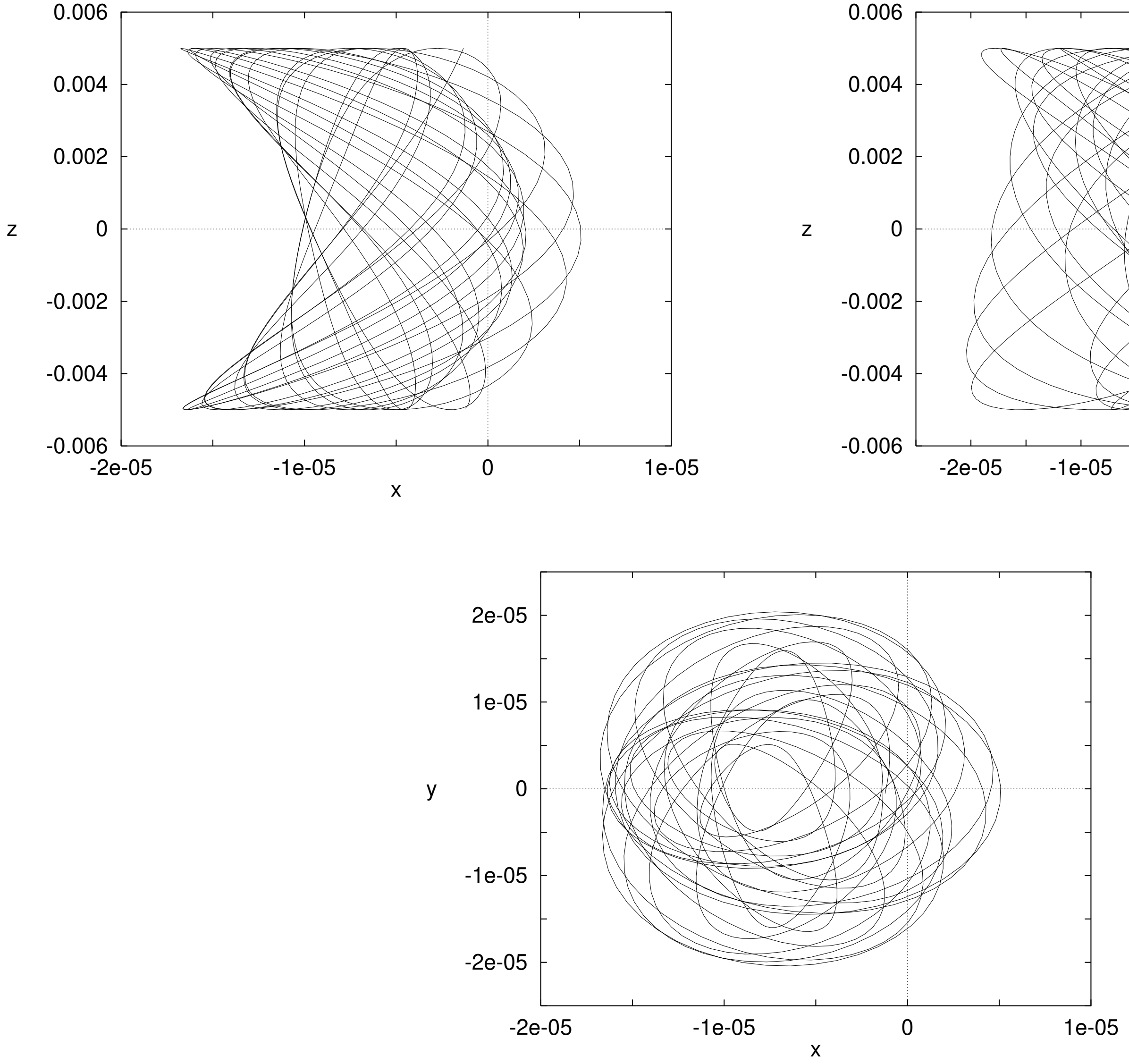

Figure 3.10: Lissajous orbit around L_2 using normalized coordinates. $A = 0.$, $B = 0.005$, $t_0 = 0$, $t_f = 8T$, $\varphi_1 = 0.$ and $\varphi_2 = 0.$

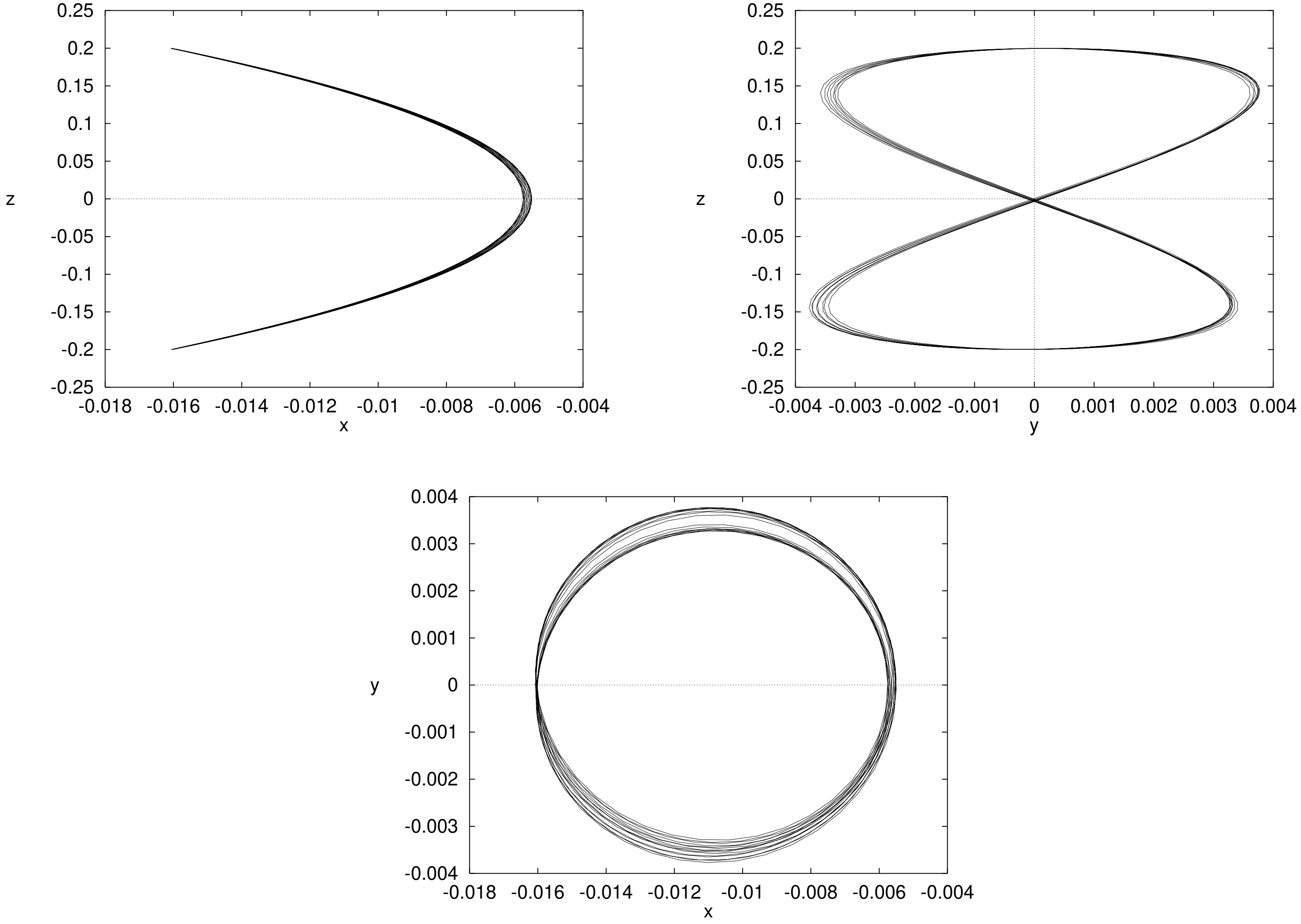

Figure 3.11: Lissajous orbit around L_2 using normalized coordinates. $A = 0.$, $B = 0.2$, $t_0 = 0$, $t_f = 4T$, $\varphi_1 = 0.$ and $\varphi_2 = 0$.

3.5 Quasi-periodic Halo orbits

In this section, we are going to modify the method used to compute the Lissajous orbits, with the purpose of getting the quasi-periodic Halo orbits. We should notice that this method is not going to allow us to get good results in our case. In spite of that, we think that is convenient to explain it.

We can look at the Halo orbits as a particular case of the Lissajous orbits, where the frequency in the plane, $\lambda_1\omega_1$, is equal to the vertical frequency, $\lambda_2\omega_2$. To compute these type of orbits it is suitable to modify the equation (3.5) in the following way:

$$\begin{aligned} \ddot{z} + \lambda z &= z\sum_{n=2}^{\infty} c_{n+1}R_{n-1} + \Delta\cdot z + \\ &+\alpha_{10}\ddot{z} + \alpha_{11}\dot{z} + \alpha_{19}z + \\ &+\alpha_{16}z\sum_{n=2}^{\infty} c_{n+1}R_{n-1} + \alpha_{20}\sum_{n=2}^{\infty}\frac{\partial G_n}{\partial z} , \end{aligned} \tag{3.21}$$

where Δ depends on the amplitudes and should be equal to $\Delta_0 = \lambda - c_2$.

Then, we look for a formal solution of the differential equations (3.3), (3.4) and (3.21) of the form

$$\begin{aligned} x &= \sum x_{ijk_1k_2m}A^iB^j\gamma_1^{k_1}\gamma_2^{k_2}\epsilon^m , \\ y &= \sqrt{-1}\sum y_{ijk_1k_2m}A^iB^j\gamma_1^{k_1}\gamma_2^{k_2}\epsilon^m , \\ z &= \sum z_{ijk_1k_2m}A^iB^j\gamma_1^{k_1}\gamma_2^{k_2}\epsilon^m , \end{aligned} \tag{3.22}$$

where $x_{ijk_1k_2m}$, $y_{ijk_1k_2m}$, $z_{ijk_1k_2m} \in \mathbb{R}$, i, j, k_1, k_2, $m \in \mathbb{Z}$, $i, m \geq 0$, and

$$\begin{aligned} \gamma_1 &= \exp(\sqrt{-1}(\lambda\omega t + \varphi)) , \\ \gamma_2 &= \exp(\sqrt{-1}\omega_s t) , \end{aligned}$$

with ω depending on the amplitudes as follows:

$$\omega = 1 + \sum d_{ijm}A^iB^j\epsilon^m .$$

Simultaneously, the series

$$\Delta = \sum f_{ijm}A^iB^j\epsilon^m$$

is also determined. The condition $\Delta = \Delta_0$ gives a relation between the two basic amplitudes A and B.

In the same way as for Lyapunov and Lissajous orbits, a formal solution of the equations can be computed recursively up to a certain order (n_{ij}, n_e). This means all the terms with $0 \leq i+j \leq n_{ij}$ and $0 \leq m \leq n_e$. The first terms of the recurrence are obtained from the solution of the linearized system, restricted to the central manifold:

$$\begin{aligned} x &= -A\cos(\lambda t + \varphi) &&= -\frac{1}{2}A(\gamma_1 + \gamma_1^{-1}) , \\ y &= KA\sin(\lambda t + \varphi) &&= -\sqrt{-1}\frac{K}{2}A(\gamma_1 - \gamma_1^{-1}) , \\ z &= B\cos(\lambda t + \varphi) &&= \frac{1}{2}B(\gamma_1 + \gamma_1^{-1}) . \end{aligned}$$

Hence, the coefficients of the terms of order (0,0) and (1,0) are

$$x_{00000} = y_{00000} = z_{00000} = 0 \ ,$$

$$x_{10100} = -\frac{1}{2} \ , \qquad y_{10100} = -\frac{K}{2} \ , \qquad z_{01100} = \frac{1}{2} \ ,$$

$$d_{000} = 1 \ , \qquad f_{000} = 0 \ .$$

In the computation of the terms of a certain order, it is necessary to solve some 3×3 linear systems. They can be of one of the following types:

- if $(k_1, k_2) \neq (1, 0)$ we have

$$\begin{aligned} -(W^2 + 1 + 2c_2)\, x_I + 2W\, y_I &= M_I \ , \\ 2W\, x_I + (-W^2 + c_2 - 1)\, y_I &= N_I \ , \\ (-W^2 + \lambda^2)\, z_I &= P_I \ , \end{aligned} \tag{3.23}$$

  where $W = k_1\lambda + k_2\omega_s$ and I means the multiindex $(i\, j\, k_1\, k_2\, m)$. We note that the terms of the right hand side can be computed from the terms of lower order of x, y, z, ω and Δ.

- if $(k_1, k_2) = (1, 0)$ the two first equations of (3.23) have determinant equal to zero. Likewise, the coefficient of z_I vanishes. Then, we set $x_{ij10m} = z_{ij10m} = 0$ and take advantage of this to determine y_I and the corresponding terms of d and f, by solving the system

$$\begin{aligned} 2\lambda\, y_{ij10m} + (\lambda^2 - \lambda K)\, d_{i-1,j,m} &= M_{ij10m} \ , \\ (-\lambda^2 + c_2 - 1)\, y_{ij10m} + (\lambda^2 K - \lambda)\, d_{i-1,j,m} &= N_{ij10m} \ , \\ -\lambda^2\, d_{i,j-1,m} &= P_{ij10m} + \frac{1}{2} f_{i,j-1,m} \ . \end{aligned}$$

  As in the preceding case, the right hand side terms can be computed from terms of lower order.

The coefficients of the analytical solution computed in this way, satisfy the relationships:

(a) $i, j, m \geq 0$, $|k_1| \leq i + j$, for all the series.

(b) $x_{ik_1k_2m} = x_{i,-k_1,-k_2,m}$, $y_{ik_1k_2m} = -y_{i,-k_1,-k_2,m}$ and $z_{ik_1k_2m} = z_{i,-k_1,-k_2,m}$.

(c) For x and y we only have terms with $j \equiv 0 \pmod 2$ and $i - k_1 \equiv 0 \pmod 2$. For z there are only terms with $j \equiv 1 \pmod 2$ and $i - k_1 \equiv 1 \pmod 2$.

(d) $x_{ij10m} = 0$, $\forall (i, j, m) \neq (1, 0, 0)$ and $z_{ij10m} = 0$, $\forall (i, j, m) \neq (0, 1, 0)$.

(e) If i or j are odd then $d_{ijm} = f_{ijm} = 0$.

Of course, after having the solution of the form (3.22), we add all the terms with different powers of the parameter ϵ and we obtain a solution of the form

$$\begin{aligned} x &= \sum \overline{x}_{ijk_1k_2} A^i B^j \gamma_1^{k_1} \gamma_2^{k_2} \ , \\ y &= \sqrt{-1} \sum \overline{y}_{ijk_1k_2} A^i B^j \gamma_1^{k_1} \gamma_2^{k_2} \ , \\ z &= \sum \overline{z}_{ijk_1k_2} A^i B^j \gamma_1^{k_1} \gamma_2^{k_2} \ , \end{aligned} \tag{3.24}$$

and

$$\begin{aligned} \omega &= \sum \overline{d}_{ij} A^i B^j \ , \\ \Delta &= \sum \overline{f}_{ij} A^i B^j \ . \end{aligned}$$

To have a quasi-periodic Halo orbit, it is necessary to give a value of the vertical amplitude B and determine the corresponding horizontal amplitude A through the equation

$$\Delta(A, B) = \Delta_0 \ . \tag{3.25}$$

3.5.1 Difficulties

In the spatial RTBP, the family of planar Lyapunov periodic orbits bifurcates at a certain point, starting the two families of Halo periodic orbits. That bifurcation occurs for an amplitude $A = 0.1051$ in the L_1 case, and for $A = 0.1845$ in the L_2 case.

Now, we want to note that if we put $B = 0$, the computed series of x and y for the Halo case coincide with the series calculated in the Lyapunov case. Therefore, it easy to understand that the method used for the determination of the Halo quasi-periodic orbits will give analytical orbits with poor accuracy. In section 3.3, we saw that we had good agreement between analytical and numerical orbits for $A \leq 0.056$ and $A \leq 0.073$, for L_1 and L_2 respectively. In any case, the Halo quasi-periodic orbits should have bigger amplitude.

In the L_1 case, if one value of B is given, for instance, $B = 0.1$, then the corresponding amplitude A can be found solving the equation (3.25). In order to check the accuracy of the analytical approximation of that orbit, a test was done similar to the one done for the Lissajous orbits in section 3.4.1. The difference between the analytical and the numerical orbit, after a time interval of π, was found to be greater than 10^{-2} in some components. This means that the analytical approximation has poor accuracy.

The L_2 case is specially disappointing, because the relation (3.25) has no solution for all the checked values of B. So, in this case, the Lindstedt-Poincaré method gives no analytical approximation of the Halo orbits. We are going to explain why the results are so bad in the L_2 case. In the spatial RTBP, the period of planar Lyapunov orbits increases when the amplitude rises. For the amplitude $A \simeq 0.136$, we find a resonant orbit. The period of this orbit is $T/2$. Corresponding to this orbit, we have the T-periodic orbits 22, 23, 24 and 25 in the QBCP (see section 2.3). If we continue following the Lyapunov family in the RTBP, we arrive at an amplitude $A \simeq 0.1845$ where the Halo are born. Now, following the Halo family we realize that the period is slightly decreasing with respect to the B amplitude and another resonant orbit is found. Its period is also $T/2$ and it generates the orbits 2A and 2C of the QBCP (see section 2.3). Their amplitudes are $A \simeq 0.203$ and $B \simeq 0.244$. These orbits are the main obstruction to get good analytical approximation for all the family of quasi-periodic Halo orbits in the QBCP, using the method described above. Figure 3.12 shows the orbits 24 and 2A using normalized coordinates. The bifurcating Lyapunov orbit of the RTBP is also drawn, for reference, with dashed lines.

3.6 Analytical refinement

In this section, we are going to present another approach to compute quasi-periodic orbits. We call this method *analytical refinement*. It has been used for computing Halo orbits around L_1 and L_2, but it also would be useful in the computation of another families of quasi-periodic orbits as planar and vertical Lyapunov orbits.

The goal is to obtain an orbit of the form

$$\begin{aligned} x &= \sum_{k\in\mathbb{Z}^2} x_k \gamma_1^{k_1}\gamma_2^{k_2} , \\ y &= \sqrt{-1}\sum_{k\in\mathbb{Z}^2} y_k \gamma_1^{k_1}\gamma_2^{k_2} , \\ z &= \sum_{k\in\mathbb{Z}^2} z_k \gamma_1^{k_1}\gamma_2^{k_2} , \end{aligned} \tag{3.26}$$

where x_k, y_k, $z_k \in \mathbb{R}$, k denotes the multiindex (k_1, k_2) and

$$\begin{aligned} \gamma_1 &= \exp(\sqrt{-1}(\omega_0 t + \varphi_0)) , \\ \gamma_2 &= \exp(\sqrt{-1}\omega_s t) , \end{aligned}$$

where ω_0 is a prefixed frequency and ω_s is the frequency of the Sun (see (3.11) to know the value taken). The phase φ_0 is arbitrary. Moreover, the coefficients of the series satisfy the symmetry conditions $x_k = x_{-k}$, $y_k = -y_{-k}$ and $z_k = z_{-k}$.

Now, consider the space of real Fourier series with two basic frequencies ω_0 and ω_s, which is denoted by $\mathcal{F}$. Let $\mathcal{F}_0$ and $\mathcal{F}_1$ be the subspaces of $\mathcal{F}$ of the even and odd functions, respectively. We define $\mathcal{G}$ as the following Cartesian product:

$$\mathcal{G} = \mathcal{F}_0 \times \mathcal{F}_1 \times \mathcal{F}_0 .$$

We are going to define a function, $F : \mathcal{G} \longrightarrow \mathcal{G}$. For this purpose, from (3.3), (3.4) and (3.5), we write

$$F_1(x, y, z) = -\ddot{x} + 2\dot{y} + (1 + 2c_2)x + \sum_{n=2}^{\infty} c_{n+1}(n+1)\, T_n +$$

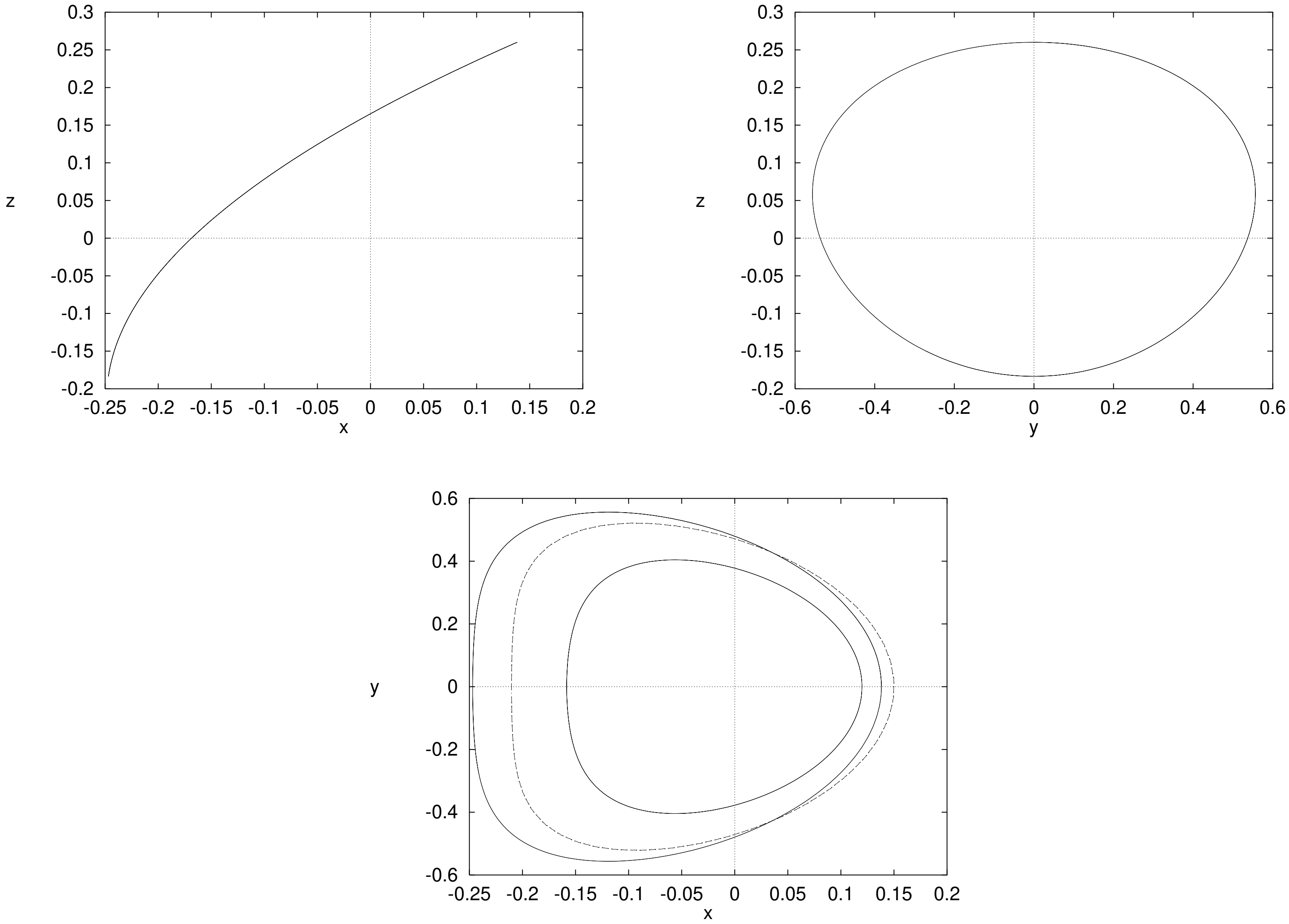

Figure 3.12: Resonant orbits labelled as 24 (planar) and 2A around L_2 in the QBCP. In the RTBP, the Halo orbits bifurcates from the Lyapunov orbit drawn with dashed lines.

$$
\begin{aligned}
& +\alpha_{10}\ddot{x} + \alpha_{11}\dot{x} + \alpha_{12}\dot{y} + \alpha_{13}x + \alpha_{14}y + \alpha_{15} + \\
& +\alpha_{16}\sum_{n=2}^{\infty} c_{n+1}(n+1)\,T_n + \alpha_{20}\sum_{n=2}^{\infty}\frac{\partial G_n}{\partial x}\ , \\
F_2(x,y,z) \ = \ & -\ddot{y} - 2\dot{x} - (c_2-1)y + y\sum_{n=2}^{\infty} c_{n+1}R_{n-1} + \\
& +\alpha_{10}\ddot{y} - \alpha_{12}\dot{x} + \alpha_{11}\dot{y} - \alpha_{14}x + \alpha_{17}y + \alpha_{18} + \\
& +\alpha_{16}y\sum_{n=2}^{\infty} c_{n+1}R_{n-1} + \alpha_{20}\sum_{n=2}^{\infty}\frac{\partial G_n}{\partial y}\ , \\
F_3(x,y,z) \ = \ & -\ddot{z} - c_2 z + z\sum_{n=2}^{\infty} c_{n+1}R_{n-1} + \\
& +\alpha_{10}\ddot{z} + \alpha_{11}\dot{z} + \alpha_{19}z + \\
& +\alpha_{16}z\sum_{n=2}^{\infty} c_{n+1}R_{n-1} + \alpha_{20}\sum_{n=2}^{\infty}\frac{\partial G_n}{\partial z}\ .
\end{aligned}
$$

Then, $F = (F_1, F_2, F_3)^T$ can be considered as a function from the space $\mathcal{G}$ to itself. For any set of Fourier coefficients of x, y and z, it is possible to evaluate F_1, F_2 and F_3, obtaining the coefficients of three series of the same type than x, y and z, respectively. Therefore, our objective can be summarized as finding a zero of the function F.

Let X be an infinite dimensional vector containing the Fourier coefficients of x, y and z. The point is to solve the equation $F(X) = 0$. For this purpose, we use Newton's method. Beginning with an initial approximation $X^{(0)}$, the iterative process is

$$X^{(i+1)} = X^{(i)} - DF^{-1}(X^{(i)})F(X^{(i)})\ ,$$

for $i \geq 0$. If it converges, it does with few iterations because the convergence is quadratic. We also want to remark that, of course, it is not necessary to compute the inverse of the Jacobian matrix. As usual, we find the next iteration solving the linear system of equations:

$$DF(X^{(i)})(X^{(i)} - X^{(i+1)}) = F(X^{(i)})\ .$$

However, there is a difficulty: the system is an infinite dimensional one. In order to reduce the problem to finite dimension, one can select a certain number of frequencies and solve the linear system with respect to these frequencies. In each step of Newton's method, the selected frequencies can be different. The way of choosing the frequencies involved in each iteration is the key of the success of Newton's method.

After doing several test, the implemented algorithm to select the frequencies was the following one. Let $M_i = \|F(X^{(i)})\|_\infty$ and $\kappa \in \mathbb{R}$, $0 < \kappa \ll 1$, for instance $\kappa = 10^{-5}$. The selected frequencies are the ones that their coefficients in $F(X^{(i)})$ are larger than κM_i. This means that, in each iteration of Newton's method, we are solving the linear system of equations taking into account only the largest coefficients of $F(X^{(i)})$. The coefficients less than κM_i are neglected. The iterative process finishes when $\|X^{(i+1)} - X^{(i)}\|_\infty < \delta$ or $\|F(X^{(i)})\|_\infty < \delta$, for a certain threshold δ.

It is important to point out that the fact of selecting the frequencies with a relative threshold is fundamental. The method fails if one tries to use a fixed threshold δ_s to select the frequencies for all the iterations. That means if one chooses the coefficients of $F(X^{(i)})$ greater than a fixed δ_s for each iteration. The reason of the failure is that δ_s should be much smaller than δ, the threshold of Newton's process. But, if δ_s is very small then one should solve a very large linear system in the first iteration of Newton's method, when $X^{(0)}$ is still far from the solution.

3.6.1 Jacobian matrix

In each iteration of Newton's method, the computation of the Jacobian matrix is the task which requires more effort. In this section, we are going to derive some expressions useful to compute the matrix in an efficient way.

Firstly, we notice that the derivatives with respect to the coefficients can be calculated using the chain rule. So,

$$\frac{\partial F}{\partial x_k} = \frac{\partial F}{\partial x}\frac{\partial x}{\partial x_k} + \frac{\partial F}{\partial \dot{x}}\frac{\partial \dot{x}}{\partial x_k} + \frac{\partial F}{\partial \ddot{x}}\frac{\partial \ddot{x}}{\partial x_k} ,$$

and similar expressions hold for y_k and z_k. Therefore, it is convenient to compute and store $\frac{\partial F}{\partial x}$, $\frac{\partial F}{\partial y}$ and $\frac{\partial F}{\partial z}$. After that, multiplying by the corresponding derivative with respect to each coefficient, we obtain the different columns of the Jacobian matrix.

When computing the derivatives of F, some derivatives of the polynomials T_n and R_n appear, as well as second derivatives of the functions G_n. We recall that

$$\frac{\partial T_n}{\partial x} = n\,T_{n-1} \, , \qquad \frac{\partial T_n}{\partial y} = y\,R_{n-2} \, , \qquad \frac{\partial T_n}{\partial z} = z\,R_{n-2} \, , \;\; \forall n \geq 2 \, .$$

Now, it is convenient to introduce a new set of polynomials. We define

$$S_n(x,y,z) = y^{-1}\frac{\partial R_{n+2}}{\partial y} = z^{-1}\frac{\partial R_{n+2}}{\partial z} \, , \;\; \forall n \geq 0 \, .$$

They are homogeneous polynomials of degree n and satisfy the following recurrence:

$$S_n = \frac{2n+7}{n+4}\,xS_{n-1} - \frac{4n+12}{n+4}\,R_n - \frac{n+3}{n+4}\,\rho^2 S_{n-2} \, ,$$

with the initial terms $S_0 = 3$, $S_1 = 15x$. Then, we have

$$\frac{\partial R_n}{\partial x} = (n+2)\,R_{n-1} \, , \qquad \frac{\partial R_n}{\partial y} = y\,S_{n-2} \, , \qquad \frac{\partial R_n}{\partial z} = z\,S_{n-2} \, , \;\; \forall n \geq 2 \, .$$

So, all the terms involving derivatives of T_n or R_n can be computed by recurrence.

On the other hand, the second derivatives of the G_n functions can also be computed recursively. The recurrences come from the ones which were given in section 3.2.2. They are

$$\begin{aligned}
\frac{\partial^2 G_n}{\partial x^2} &= -\frac{2n-1}{n}\gamma\epsilon\left(2\alpha_{22}\frac{\partial G_{n-1}}{\partial x} + ((x-c_1)\alpha_{22}+y\alpha_{23})\,\frac{\partial^2 G_{n-1}}{\partial x^2}\right) - \\
&\quad -\frac{n-1}{n}\gamma^2\epsilon^2\alpha_{21}\left(2G_{n-2} + 4(x-c_1)\frac{\partial G_{n-2}}{\partial x} + \hat{\rho}^2\,\frac{\partial^2 G_{n-2}}{\partial x^2}\right)\,, \\
\frac{\partial^2 G_n}{\partial x\,\partial y} &= -\frac{2n-1}{n}\gamma\epsilon\left(\alpha_{22}\frac{\partial G_{n-1}}{\partial y} + \alpha_{23}\frac{\partial G_{n-1}}{\partial x} + ((x-c_1)\alpha_{22}+y\alpha_{23})\,\frac{\partial^2 G_{n-1}}{\partial x\,\partial y}\right) - \\
&\quad -\frac{n-1}{n}\gamma^2\epsilon^2\alpha_{21}\left(2(x-c_1)\frac{\partial G_{n-2}}{\partial y} + 2y\frac{\partial G_{n-2}}{\partial x} + \hat{\rho}^2\,\frac{\partial^2 G_{n-2}}{\partial x\,\partial y}\right)\,, \\
\frac{\partial^2 G_n}{\partial x\,\partial z} &= -\frac{2n-1}{n}\gamma\epsilon\left(\alpha_{22}\frac{\partial G_{n-1}}{\partial z} + ((x-c_1)\alpha_{22}+y\alpha_{23})\,\frac{\partial^2 G_{n-1}}{\partial x\,\partial z}\right) - \\
&\quad -\frac{n-1}{n}\gamma^2\epsilon^2\alpha_{21}\left(2(x-c_1)\frac{\partial G_{n-2}}{\partial z} + 2z\frac{\partial G_{n-2}}{\partial x} + \hat{\rho}^2\,\frac{\partial^2 G_{n-2}}{\partial x\,\partial z}\right)\,, \\
\frac{\partial^2 G_n}{\partial y^2} &= -\frac{2n-1}{n}\gamma\epsilon\left(2\alpha_{23}\frac{\partial G_{n-1}}{\partial y} + ((x-c_1)\alpha_{22}+y\alpha_{23})\,\frac{\partial^2 G_{n-1}}{\partial y^2}\right) - \\
&\quad -\frac{n-1}{n}\gamma^2\epsilon^2\alpha_{21}\left(2G_{n-2} + 4y\frac{\partial G_{n-2}}{\partial y} + \hat{\rho}^2\,\frac{\partial^2 G_{n-2}}{\partial y^2}\right)\,, \\
\frac{\partial^2 G_n}{\partial y\,\partial z} &= -\frac{2n-1}{n}\gamma\epsilon\left(\alpha_{23}\frac{\partial G_{n-1}}{\partial z} + ((x-c_1)\alpha_{22}+y\alpha_{23})\,\frac{\partial^2 G_{n-1}}{\partial y\,\partial z}\right) - \\
&\quad -\frac{n-1}{n}\gamma^2\epsilon^2\alpha_{21}\left(2y\frac{\partial G_{n-2}}{\partial z} + 2z\frac{\partial G_{n-2}}{\partial y} + \hat{\rho}^2\,\frac{\partial^2 G_{n-2}}{\partial y\,\partial z}\right)\,, \\
\frac{\partial^2 G_n}{\partial z^2} &= -\frac{2n-1}{n}\gamma\epsilon((x-c_1)\alpha_{22}+y\alpha_{23})\,\frac{\partial^2 G_{n-1}}{\partial z^2} - \\
&\quad -\frac{n-1}{n}\gamma^2\epsilon^2\alpha_{21}\left(2G_{n-2} + 4z\frac{\partial G_{n-2}}{\partial z} + \hat{\rho}^2\,\frac{\partial^2 G_{n-2}}{\partial z^2}\right)\,,
\end{aligned}$$

where

$$\hat{\rho}^2 = (x-c_1)^2 + y^2 + z^2\,.$$

Moreover, we note that all the second derivatives of G_0 and G_1 are null.

3.6.2 Halo orbits around L_1

In section 3.5, we found a rough analytical approximation of the Halo family around L_1 using the Lindstedt-Poincaré method. The obtained solution was of the form of (3.24). Taking a certain value of B, one can solve the equation $\Delta(A,B)=\Delta_0$ and obtain the corresponding value of A. Then, the coefficients of (3.26) are

$$x_k = \sum_{i,j} x_{ijk_1k_2} A^i B^j \ , \qquad y_k = \sum_{i,j} y_{ijk_1k_2} A^i B^j \ , \qquad z_k = \sum_{i,j} z_{ijk_1k_2} A^i B^j \ ,$$

and the frequency is $\omega_0 = \omega(A, B)$. So, we have a quasi-periodic Halo orbit with two basic frequencies: ω_0 and ω_s.

The orbits with amplitude $B = 0.04\,j$, $j = 1, \dots, 10$ have been considered. These orbits can be refined with the method explained above. This means that the orbits computed with the Lindstedt-Poincaré method are used as first approximation in Newton's method. The threshold used in Newton's method has been $\delta = 10^{-8}$. In the selection of the frequencies involved in each step of Newton's method, the value $\kappa = 10^{-5}$ was used in all the cases, except for the last one, $B = 0.4$, where it was necessary to use a smaller value $\kappa = 5 \cdot 10^{-6}$.

In table 3.5, we summarize some data about the computation of those orbits. We denote by β the z-amplitude of a orbit, which is defined as $2|z_{1,0}|$. The z-amplitude of the refined orbits is very similar to the one of the initial orbits. The computed orbits are labelled with three digits. The first one makes reference to the point $\mathrm{L_i}$, and so, is equal to 1 or 2. The other two digits are related with the amplitude of the orbit. Table 3.5 also shows the number of iterations of Newton's method, the maximum number of frequencies selected (maximum dimension of the linear system) and the CPU time spent with the computer HP9000/819. In order to know the accuracy of the orbits, a test similar to the one described in section 3.4.1 was done. We compare the analytical and the numerical solution, after a time span of π time units. The last two columns of table 3.5 show the maximum error found in the position and velocity, respectively. We want to recall that, with the units used, 10^{-5} is about 3.8 km in the position and 10 mm/s in the velocity. Moreover, after π time units, the initial error in the orbit is roughly multiplied by 1000. The results prove that the analytical approximation of those orbits are very accurate.

Figure 3.13 shows the relationship between the frequency ω_0 and the z-amplitude of the quasi-periodic Halo orbits around L_1.

Each Halo orbit depends on two basic frequencies, ω_0 and ω_s, and so, it lives in a 2D torus. If we cut the torus by an hyperplane, we expect to see one (or several) $\mathbb{S}^1$. We have implemented an algorithm to look for the section by the hyperplane $y = 0$. For the time $t = 0$ and phase $\varphi_0 = 0$, the analytical expression (3.26) gives a point in $y = 0$. From this point (t_0, φ_0), we can compute a sequence of points (t_j, φ_j) in that plane. Each point is obtained from the previous one. Imagine that (t_j, φ_j) gives a point in the plane $y = 0$. Increasing a little the phase, we have another value φ_{j+1}. The pair (t_j, φ_{j+1}) gives a point which is not in the plane, but is close to it. Then, we can look for the adequate value of the time, t_{j+1}, in such a way that (t_{j+1}, φ_{j+1}) gives another point in the plane. The process finishes when we arrive at a point near the initial point, obtaining a closed curve.

With the previous algorithm, we have computed the section of the torus labelled as 112 with the hyperplane $y = 0$. Figures 3.14a-b show the projection of the curve in the planes x-z and x-$\dot{x}$, respectively. Because of the symmetries, the x-z

projection is a segment, a degenerate case. In the x-$\dot{x}$ projection, we see a curve making two turns.

Once we have the section of the torus, it is possible to define a map from the $\mathbb{S}^1$ to itself. The image of each point is defined by the flux of the Hamiltonian system. The map defined in such a way, is close to a rotation. The rotation number of the map is the quotient of the frequencies ω_s/ω_0 ($\simeq$ 0.40365, in the case of the torus 112).

Figures 3.15, 3.16 and 3.17 show three different Halo orbits. The corresponding tables 3.6, 3.7 and 3.8 show the largest coefficients of each orbit.

Label	β	n.it.	max.dim.	CPU time	error pos.	error vel.
104	0.04000051	2	724	4:46	1.3e−07	4.0e−07
108	0.08000028	2	778	5:08	9.2e−08	2.6e−07
112	0.12000018	3	762	7:08	1.8e−06	5.0e−06
116	0.16000009	3	798	7:31	9.6e−07	3.0e−06
120	0.20000004	4	662	10:04	3.4e−06	1.0e−05
124	0.24000015	4	754	13:56	6.6e−07	2.0e−06
128	0.28000070	5	850	17:50	1.8e−06	5.1e−06
132	0.32000201	4	952	21:45	1.1e−06	3.4e−06
136	0.36000411	5	1252	39:32	2.9e−07	8.4e−07
140	0.40000544	6	1855	2:13:11	1.2e−07	3.3e−07

Table 3.5: Summary of the computations of the Halo orbits around L_1. The columns show, respectively, label, z-amplitude, number of iterations, maximum dimension, CPU time in hours:minutes:seconds with HP 9000/819, results of the test in position and velocity.

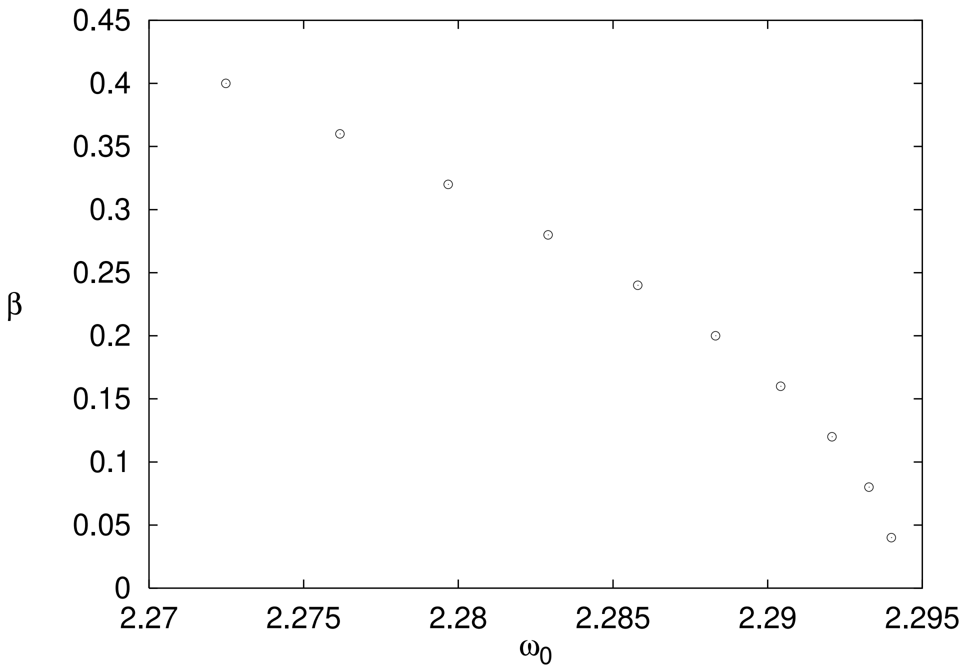

Figure 3.13: Frequency ω_0 and z-amplitude of the Halo orbits around L_1.

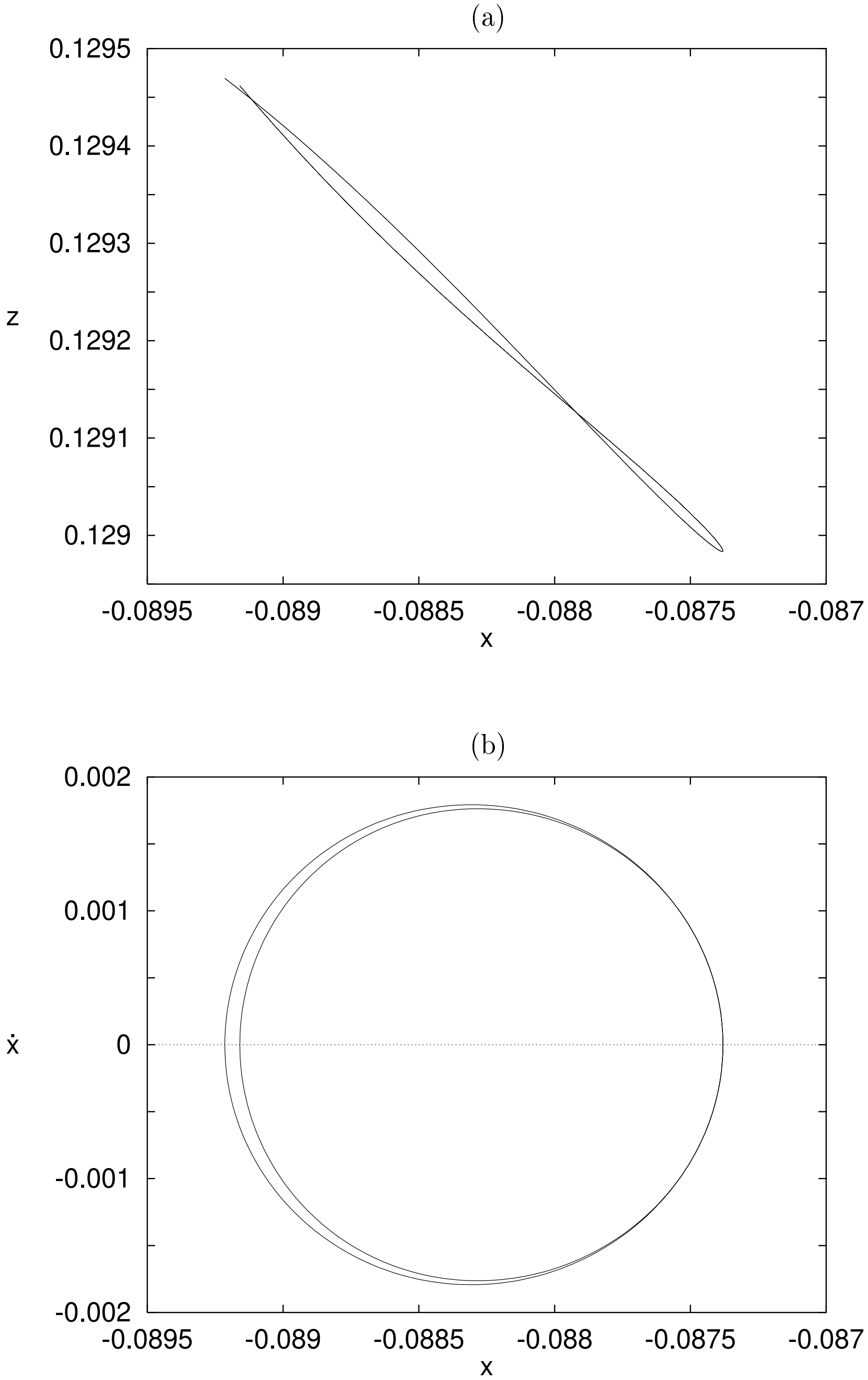

Figure 3.14: Section $y = 0$ of the 2D torus corresponding to the orbit 112. (a) and (b) show the projections on the x-z and the x-$\dot{x}$ planes, respectively.

k_1	k_2	x	k_1	k_2	y	k_1	k_2	z
0	0	3.0121273e−02	0	2	2.4415732e−05	0	0	1.2794346e−02
0	1	1.0131491e−06	0	3	−6.0312726e−06	0	1	1.8757933e−06
0	3	−2.2971044e−06	1	−5	−1.6109325e−06	0	2	9.4083820e−05
1	−4	7.2764471e−07	1	−4	−4.9086485e−06	0	4	6.7311005e−07
1	−3	6.0481444e−07	1	−3	−3.0623766e−06	1	−5	−1.3026177e−06
1	−2	2.4954802e−04	1	−2	1.6194200e−03	1	−3	8.6915052e−07
1	−1	2.4602610e−05	1	−1	1.0167080e−04	1	−2	−4.5797040e−04
1	0	−5.4770179e−02	1	0	−1.9315904e−01	1	−1	−3.1493808e−05
1	1	−3.6085546e−05	1	1	−1.1574133e−04	1	0	6.0000091e−02
1	2	−7.1989227e−04	1	2	−1.8215181e−03	1	1	3.4861975e−05
1	4	−7.2339183e−06	1	4	−1.5846152e−05	1	2	5.0320089e−04
2	−4	−1.2577854e−06	2	−3	−8.7394218e−07	1	4	4.0520824e−06
2	−3	−6.2046247e−07	2	−2	−3.6494741e−05	2	−2	1.6569183e−05
2	−2	9.9906796e−05	2	−1	−2.8239764e−06	2	−1	1.8918460e−06
2	−1	5.2781112e−06	2	0	3.1011277e−03	2	0	−2.0659655e−03
2	0	−4.8501450e−03	2	1	3.6537184e−06	2	1	−2.4444373e−06
2	1	−5.6724807e−06	2	2	5.6374745e−05	2	2	−3.6700293e−05
2	2	−8.3966999e−05	2	4	7.2632964e−07	3	−5	−2.4431714e−06
2	4	−1.0603549e−06	3	−5	−2.2978605e−06	3	−2	−6.7425581e−06
3	−5	−6.3633972e−07	3	−2	1.8901047e−05	3	0	3.1074587e−04
3	−2	−1.0802922e−05	3	−1	1.1173405e−06	3	1	5.4513924e−07
3	−1	−7.5597810e−07	3	0	−7.1216597e−04	3	2	8.2987749e−06
3	0	5.0412406e−04	3	1	−1.2446390e−06	4	−2	1.0775119e−06
3	1	8.9931866e−07	3	2	−1.9084545e−05	4	0	−4.0118984e−05
3	2	1.4375282e−05	4	−2	−2.6596103e−06	4	2	−1.4963397e−06
4	−2	2.8263461e−06	4	0	8.9095617e−05	5	0	6.6660325e−06
4	0	−8.9930186e−05	4	2	3.3756552e−06	6	0	−1.1184072e−06
4	2	−3.3946423e−06	5	−2	6.0479264e−07			
5	−2	−5.3226999e−07	5	0	−1.5809467e−05			
5	0	1.4226335e−05	5	2	−7.5356793e−07			
5	2	6.9079325e−07	6	0	2.6832814e−06			
6	0	−2.5673218e−06						

Table 3.6: Fourier coefficients greater than $5 \cdot 10^{-7}$ of the orbit 112 around L_1. $\omega_0 = 2.29207836122596$.

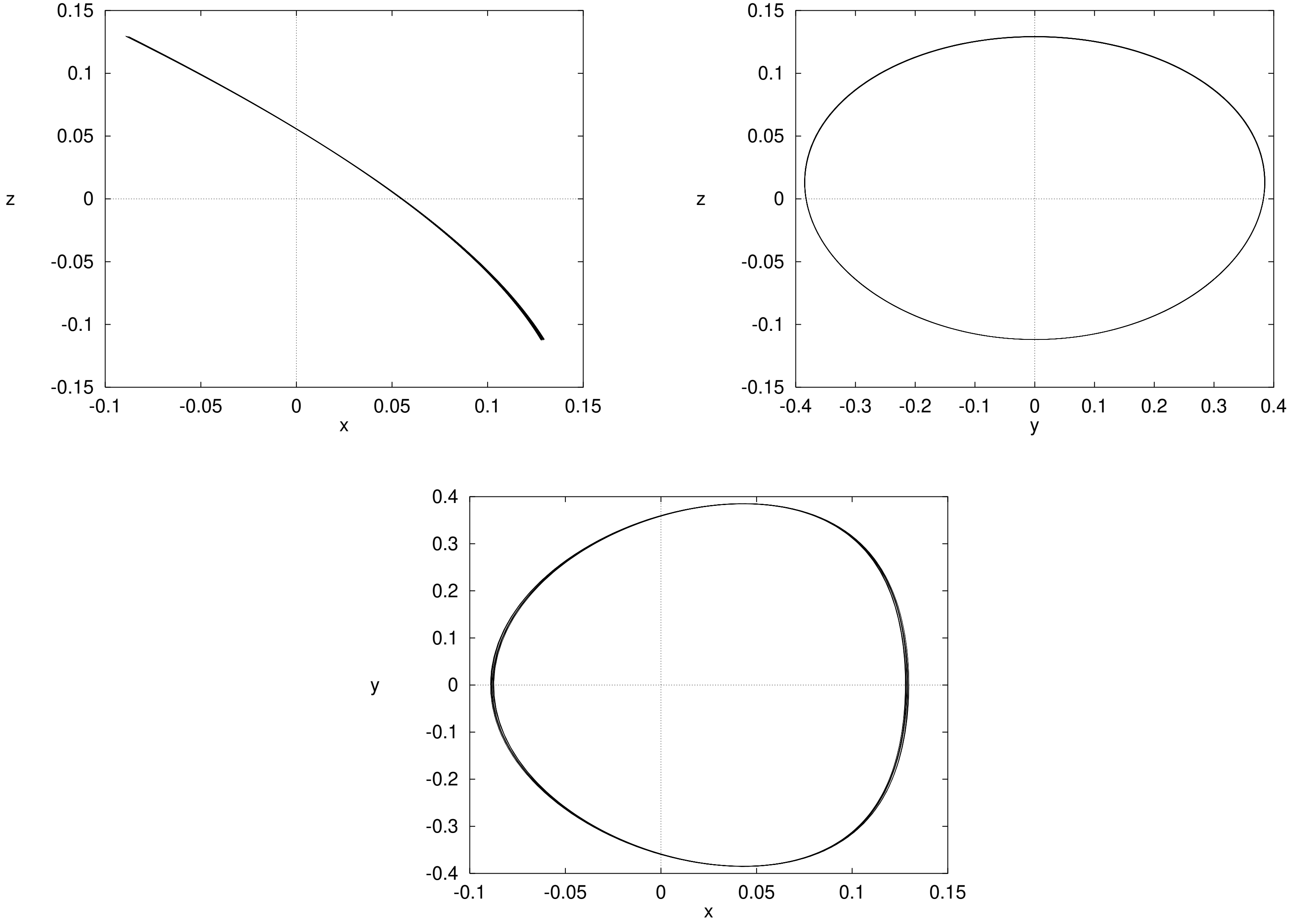

Figure 3.15: Quasi-periodic Halo orbit 112 around L_1 using normalized coordinates. $t_0 = 0$, $t_f = 5T$, $\varphi_0 = 0$.

k_1	k_2	x	k_1	k_2	y	k_1	k_2	z
0	0	4.8570625e−02	0	1	−1.0647667e−06	0	0	3.0082243e−02
0	1	1.9262408e−06	0	2	3.5622845e−05	0	1	4.4652542e−06
0	2	3.3339233e−06	0	3	−5.5935042e−06	0	2	2.3127615e−04
0	3	−2.1370119e−06	1	−4	−6.0473459e−06	0	4	1.6590479e−06
0	4	5.3664346e−07	1	−3	−3.6328102e−06	1	−4	7.3904394e−07
1	−4	9.4302855e−07	1	−2	1.8655052e−03	1	−3	1.7520873e−06
1	−3	6.9382148e−07	1	−1	1.1621573e−04	1	−2	−9.1582657e−04
1	−2	2.9093930e−04	1	0	−2.2130440e−01	1	−1	−6.2811405e−05
1	−1	2.8533505e−05	1	1	−1.3223416e−04	1	0	1.2000008e−01
1	0	−6.3859842e−02	1	2	−2.0828693e−03	1	1	6.9550857e−05
1	1	−4.2052447e−05	1	4	−1.8077815e−05	1	2	1.0053964e−03
1	2	−8.3104587e−04	2	−3	−9.1965690e−07	1	4	8.0791956e−06
1	4	−8.3240378e−06	2	−2	−4.2760757e−05	2	−2	3.8165468e−05
2	−4	−1.5759345e−06	2	−1	−4.6423025e−06	2	−1	4.3925827e−06
2	−3	−7.2579115e−07	2	0	5.1808448e−03	2	0	−4.8357261e−03
2	−2	1.0927603e−04	2	1	6.0830972e−06	2	1	−5.7038219e−06
2	−1	5.0790370e−06	2	2	9.3969411e−05	2	2	−8.5997340e−05
2	0	−4.5484234e−03	2	4	1.2069894e−06	2	4	−1.0932424e−06
2	1	−5.3190590e−06	3	−4	−5.0367090e−07	3	−2	−1.4967308e−05
2	2	−8.0210539e−05	3	−2	2.4018029e−05	3	−1	−1.0806948e−06
2	4	−1.0272658e−06	3	−1	1.5129481e−06	3	0	7.2892356e−04
3	−2	−1.2582090e−05	3	0	−9.9040551e−04	3	1	1.2816612e−06
3	−1	−8.6231936e−07	3	1	−1.7363771e−06	3	2	1.9813661e−05
3	0	5.7443604e−04	3	2	−2.7105620e−05	4	−2	2.6679809e−06
3	1	1.0246181e−06	4	−2	−3.9121237e−06	4	0	−1.0402639e−04
3	2	1.6745988e−05	4	0	1.4065145e−04	4	2	−3.9422410e−06
4	−2	3.2685420e−06	4	2	5.4040512e−06	5	−2	−6.0475525e−07
4	0	−1.0588648e−04	5	−2	9.1076558e−07	5	0	1.8107092e−05
4	2	−4.1256426e−06	5	0	−2.5505861e−05	5	2	8.7361291e−07
5	−2	−6.7469124e−07	5	2	−1.2437764e−06	6	0	−3.2681169e−06
5	0	1.8460170e−05	6	0	4.6673607e−06	7	0	6.2528153e−07
5	2	9.2188088e−07	7	0	−9.0699399e−07			
6	0	−3.5242218e−06						
7	0	6.8447617e−07						

Table 3.7: Fourier coefficients greater than $5 \cdot 10^{-7}$ of the orbit 124 around L_1. $\omega_0 = 2.28580041051318$.

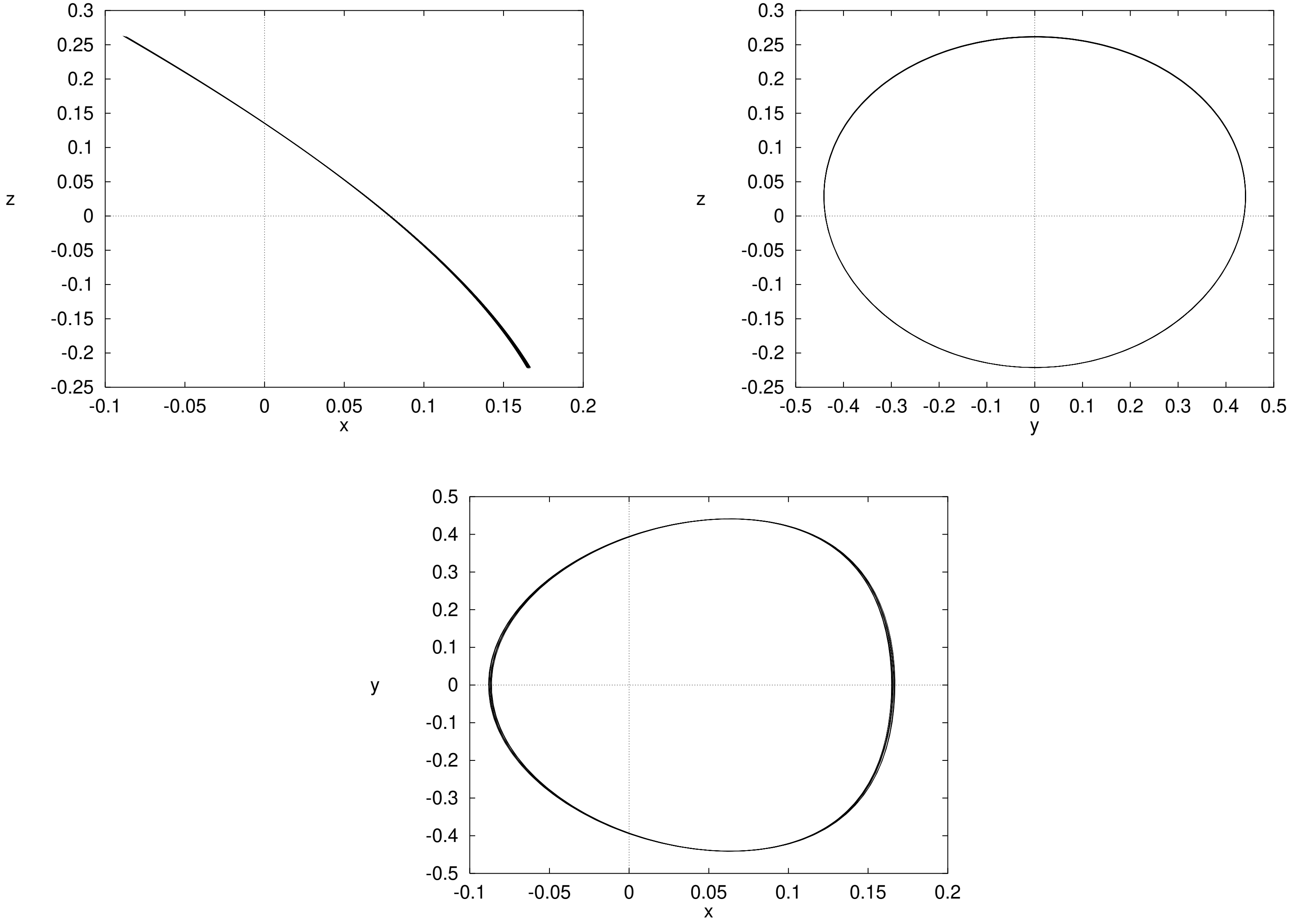

Figure 3.16: Quasi-periodic Halo orbit 124 around L_1 using normalized coordinates. $t_0 = 0$, $t_f = 5T$, $\varphi_0 = 0$.

k_1	k_2	x	k_1	k_2	y	k_1	k_2	z
0	0	8.0164789e−02	0	1	−2.5657062e−06	0	0	5.5825789e−02
0	1	3.4502035e−06	0	2	9.6400004e−05	0	1	8.4575438e−06
0	2	1.7685017e−05	0	3	−4.9514339e−06	0	2	4.7923885e−04
0	3	−1.8805395e−06	0	4	8.3321851e−07	0	3	7.5975409e−07
0	4	1.0321791e−06	1	−4	−8.1636962e−06	0	4	3.4503677e−06
1	−4	1.3865136e−06	1	−3	−4.5462236e−06	1	−4	1.4361647e−06
1	−3	8.2157628e−07	1	−2	2.2310724e−03	1	−3	2.7268431e−06
1	−2	3.5544539e−04	1	−1	1.3704411e−04	1	−2	−1.3739702e−03
1	−1	3.4505557e−05	1	0	−2.6168353e−01	1	−1	−9.3861354e−05
1	0	−7.7866881e−02	1	1	−1.5572125e−04	1	0	1.8000205e−01
1	1	−5.1274890e−05	1	2	−2.4551383e−03	1	1	1.0394002e−04
1	2	−9.8959043e−04	1	4	−2.1211560e−05	1	2	1.5064405e−03
1	4	−9.8291457e−06	2	−4	−6.5426089e−07	1	4	1.2055416e−05
2	−4	−2.1779838e−06	2	−3	−9.7861966e−07	2	−2	7.0086351e−05
2	−3	−9.1652881e−07	2	−2	−5.5480367e−05	2	−1	7.9799300e−06
2	−2	1.2591134e−04	2	−1	−7.7953041e−06	2	0	−8.8997355e−03
2	−1	4.7002227e−06	2	0	8.8604789e−03	2	1	−1.0446069e−05
2	0	−3.9542553e−03	2	1	1.0348781e−05	2	2	−1.5939673e−04
2	1	−4.6075817e−06	2	2	1.6167434e−04	2	4	−2.0296151e−06
2	2	−7.3590046e−05	2	4	2.0802045e−06	3	−2	−2.6775070e−05
2	4	−9.8234095e−07	3	−4	−7.3311727e−07	3	−1	−2.0129215e−06
3	−2	−1.5586122e−05	3	−2	3.3750363e−05	3	0	1.3936080e−03
3	−1	−1.0060420e−06	3	−1	2.2922204e−06	3	1	2.4535081e−06
3	0	6.6549308e−04	3	0	−1.5546909e−03	3	2	3.8916209e−05
3	1	1.1846829e−06	3	1	−2.7300967e−06	3	4	6.9303245e−07
3	2	2.0439681e−05	3	2	−4.3828156e−05	4	−2	5.4804904e−06
4	−2	4.0991056e−06	3	4	−7.8651052e−07	4	0	−2.2613685e−04
4	0	−1.3355171e−04	4	−2	−6.5407101e−06	4	1	−5.3169684e−07
4	2	−5.5139908e−06	4	0	2.5455065e−04	4	2	−8.8147167e−06
5	−2	−9.5173365e−07	4	1	5.9801071e−07	5	−2	−1.3391124e−06
5	0	2.6529842e−05	4	2	1.0047640e−05	5	0	4.2815764e−05
5	2	1.3971964e−06	5	−2	1.6224478e−06	5	2	2.1396276e−06
6	0	−5.5794022e−06	5	0	−4.9371230e−05	6	0	−8.5557779e−06
7	0	1.2036096e−06	5	2	−2.4943086e−06	6	2	−5.2391396e−07
			6	0	9.9904355e−06	7	0	1.7965804e−06
			6	2	6.1816860e−07			
			7	0	−2.1207539e−06			

Table 3.8: Fourier coefficients greater than $5 \cdot 10^{-7}$ of the orbit 136 around L_1. $\omega_0 = 2.27617247465384$.

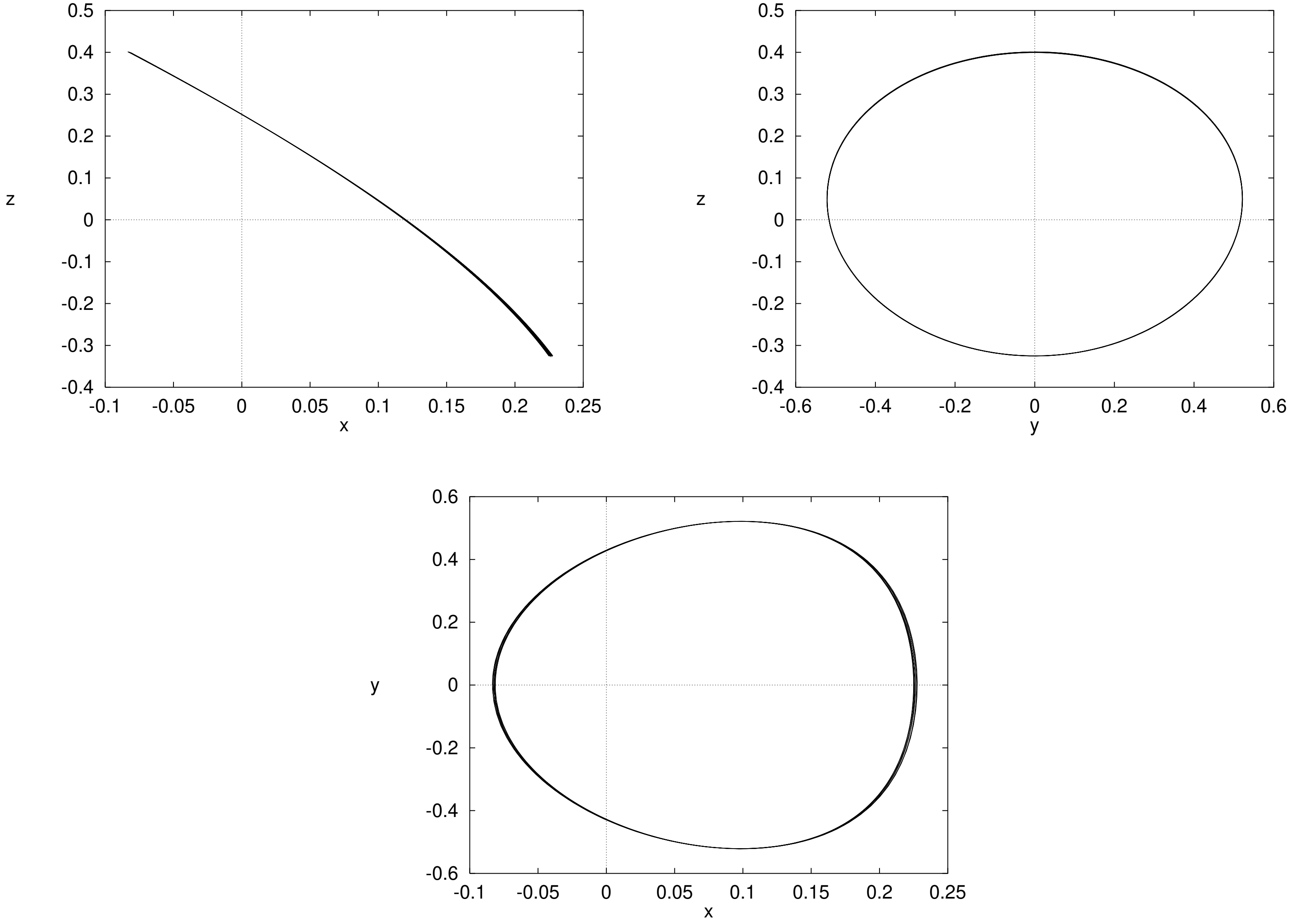

Figure 3.17: Quasi-periodic Halo orbit 136 around L_1 using normalized coordinates. $t_0 = 0$, $t_f = 5T$, $\varphi_0 = 0$.

3.6.3 Halo orbits around L_2

In section 3.5.1, we saw that the Lindstedt-Poincaré method gives no analytical approximation of the Halo orbits in the QBCP, at least up to the order computed. However, in the RTBP the method gives good results (see [8]). Then, we can try to refine Halo orbits of the QBCP from the corresponding ones of the RTBP. In general, it is not possible to do this in one step, but it can be done using a continuation method.

In the equations of the motion (3.3), (3.4) and (3.5), the functions α_k ($k = 10, \dots, 23$) and G_n ($\forall n \geq 0$) depend on the parameter $\epsilon = 1/a_s$. Now, we introduce a new normalized parameter $\bar{\epsilon}$ as

$$\bar{\epsilon} = \epsilon\, a_s \ ,$$

in such a way that for $\bar{\epsilon} = 0$ we have the equations of the RTBP and for $\bar{\epsilon} = 1$ we get the equations of the QBCP. This is a natural parameter to use a continuation method.

Our problem can be formulated in the following terms. We have an equation which depends on one parameter

$$F(X, \bar{\epsilon}) = 0 \ ,$$

and we have a solution X_0 for $\bar{\epsilon} = 0$ which is the Fourier coefficients of the coordinates (x, y, z) of a Halo orbit of the RTBP. Beginning with X_0, we can try to refine an orbit for another value of the parameter $\bar{\epsilon}_1$. If we succeed, we call X_1 the solution obtained. Once we have two solutions for two values of the parameter, we predict for $\bar{\epsilon}_2$ another solution using linear interpolation. The predicted solution must be refined in order to find X_2, and so on. The step in $\bar{\epsilon}$ can be controlled depending on the number of iterations of Newton's method for the refinement. Let n_{it} be the number of iterations of Newton's method to achieve the threshold $\delta = 10^{-8}$. We have used

- if $n_{it} < 4$ then $\Delta\bar{\epsilon}_{new} = 1.5\Delta\bar{\epsilon}_{old}$.
- if $n_{it} = 4$ then $\Delta\bar{\epsilon}_{new} = \Delta\bar{\epsilon}_{old}$.
- if $n_{it} > 4$ then $\Delta\bar{\epsilon}_{new} = 0.5\Delta\bar{\epsilon}_{old}$.

If $n_{it} > 5$ we consider that Newton's method does not converge, and then we also divide the step by two, but we have to come back to the last point in the solution curve. It is also convenient to fix a maximum dimension for the linear system (for example, 2500), as well as a maximum and minimum steps in the continuation method. To select the frequencies involved in Newton's method we used the factor $\kappa = 10^{-5}$ in most cases, but sometimes $\kappa = 5 \cdot 10^{-6}$ was also used. If the number of frequencies selected overflows then we proceed as in the case of no convergence.

We have applied the previous continuation method to the Halo orbits of the RTBP with z-amplitudes $B = 0.1 + 0.02 * j$, for $j = 1, \dots, 15$. The case $B = 0.12$

Label	B	β	n_ϵ	max.dim.	CPU time	error pos.	error vel.
214	0.14	0.08585094	7	2269	4:35:58	1.8e−07	4.5e−07
216	0.16	0.11608493	10	2165	5:00:52	1.3e−07	3.0e−07
218	0.18	0.14245010	8	2190	4:58:50	9.2e−07	2.2e−06
220	0.20	0.16522156	6	2311	5:34:01	3.8e−08	7.3e−08
228	0.28	0.25541482	6	2342	9:53:22*	1.8e−07	4.2e−07
230	0.30	0.28113813	3	2186	2:08:53	1.7e−07	4.4e−07
232	0.32	0.30331018	3	1969	1:28:16	1.5e−08	3.5e−08
234	0.34	0.32491790	2	1366	43:30	7.1e−07	1.7e−06
236	0.36	0.34629701	2	1626	46:03	5.3e−10	1.2e−09
238	0.38	0.36753087	2	1578	46:14	8.4e−09	2.2e−08
240	0.40	0.38865533	3	2069	1:17:09	4.6e−10	9.4e−10

Table 3.9: Summary of results of some Halo orbits around L_2. The columns show, respectively, label, initial (B) and final (β) z-amplitudes, number of step in the continuation method, maximum dimension, CPU time in hours:minutes:seconds with HP 9000/819 (with HP 9000/D250 the case marked with *) and results of the test in position and velocity.

bring some problems because the orbit becomes very flat. The orbits from $B = 0.22, 0.24, 0.26$ also present difficulties, but, in this case, the reason is the proximity of the resonant orbit. In some of these cases, we have observed an increase of the number of the frequencies involved overflowing the maximum chosen and becoming small the step of the continuation method. The summary of the computation of the other orbits can be found in table 3.9. The label of each orbit depends on B the amplitude of the orbit of the RTBP. We realize that β the z-amplitude of the final orbit is smaller than B the amplitude of the initial orbit. The difference increases as the z-amplitude decreases. The number of steps in the continuation method is denoted by n_ϵ. Finally, the numerical test summarized in the last two columns guarantees that the analytical approximation of the Halo orbits is very accurate.

Figure 3.18 (resp. 3.19) shows the relationship between the frequency ω_0 and the x-amplitude (resp. z) of the quasi-periodic Halo orbits around L_2. We also have drawn a horizontal (resp. vertical) dashed line corresponding to the frequency $\omega_0 = 2\omega_s$. As we have said before, there are some difficulties to find Halo orbits in the vicinity of the resonance. Note, also, that the effect of the resonance seems to be stronger on the x component than in the z one. This is quite natural, the resonance acting, mainly, in the horizontal plane.

With the method explained in section 3.6.2, we computed the section of the torus labelled as 216 with the hyperplane $y = 0$. Figures 3.20a-b show the projection of that section in the planes x-z and x-$\dot{x}$, respectively. Figure 3.21 shows the evolution of the section $y = 0$ on the plane x-$\dot{x}$ along the Halo family. With respect to the map defined by the flux from $\mathbb{S}^1$ to itself, we want to point out that the rotation number is a little bit bigger than $1/2$ for the torus with smaller z-amplitude than the resonant orbit. On the contrary, for the torus with bigger z-amplitude than the resonant orbit, the maps have a rotation number a little bit smaller than $1/2$.

Figures 3.22, 3.23, 3.24 and 3.25 show four different Halo orbits. Two of them have z-amplitudes lower than the resonant orbit. The other two orbits have z-amplitudes larger than the resonant orbit. In all the cases, at every turn around the L_2 the orbit follows a path close to the previous turn. This is easy to understand if one looks at the picture 3.20b and reminds of the rotation number of the map is close to $1/2$. With the purpose that the figures look nicer, we have drawn each orbit for several short intervals of time. If we would have drawn only one long interval of time, we would have obtained something similar to a thick periodic orbit. Tables 3.10, 3.11, 3.12 and 3.13 show the largest coefficients of each plotted orbit.

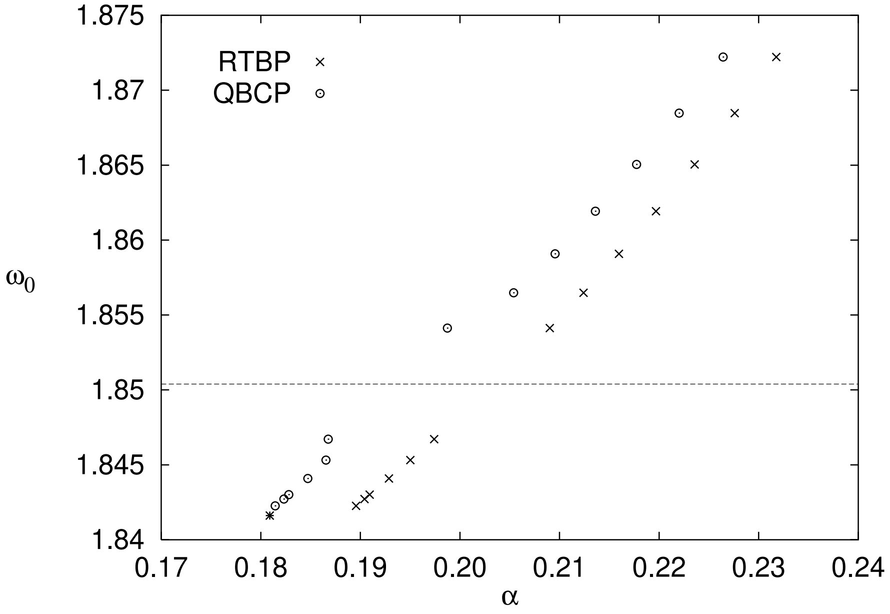

Figure 3.18: Frequency ω_0 and x-amplitude (α) of the Halo orbits around L_2. The horizontal dashed line corresponds to the frequency $\omega_0 = 2\omega_s$. The star corresponds to the bifurcating orbit (computed later on, in section 3.7).

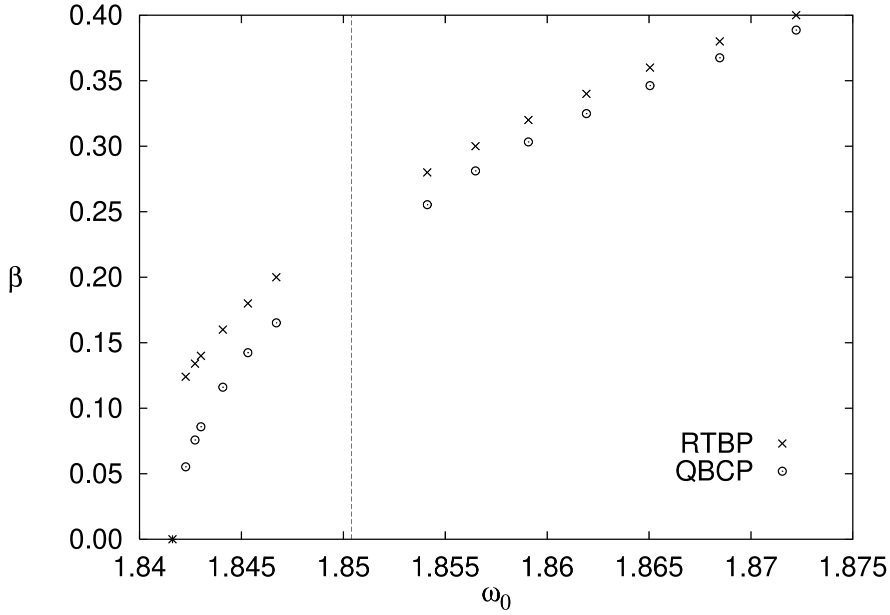

Figure 3.19: Frequency ω_0 and z-amplitude (β) of the Halo orbits around L_2. The vertical dashed line corresponds to the frequency $\omega_0 = 2\omega_s$. The star in the ω_0 axis corresponds to the frequency of the bifurcating orbit (computed later on, in section 3.7).

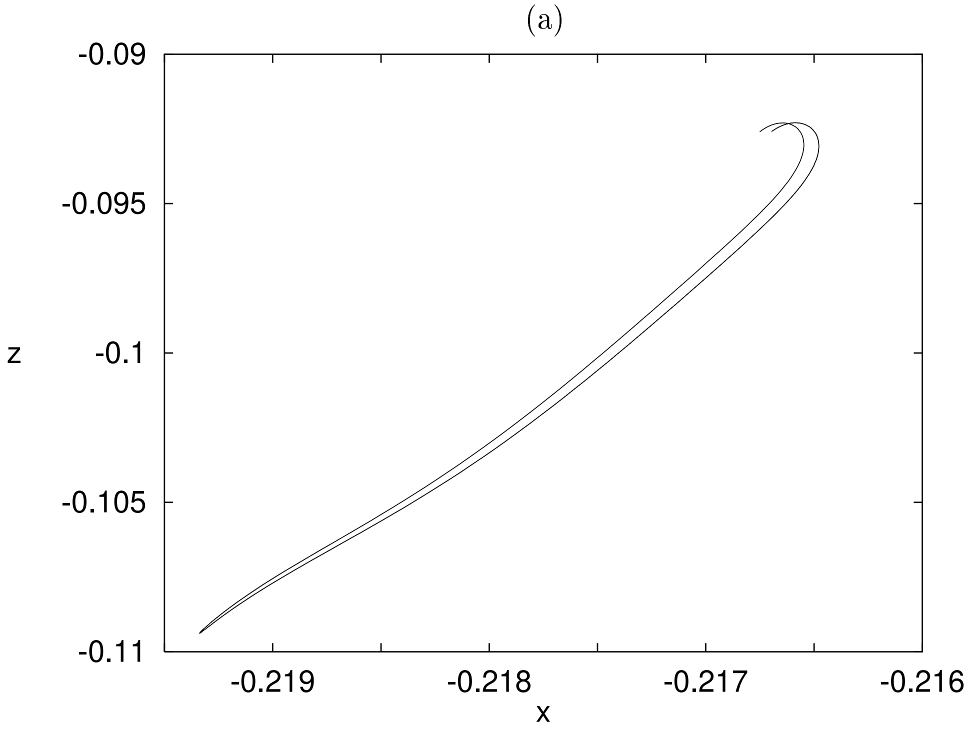

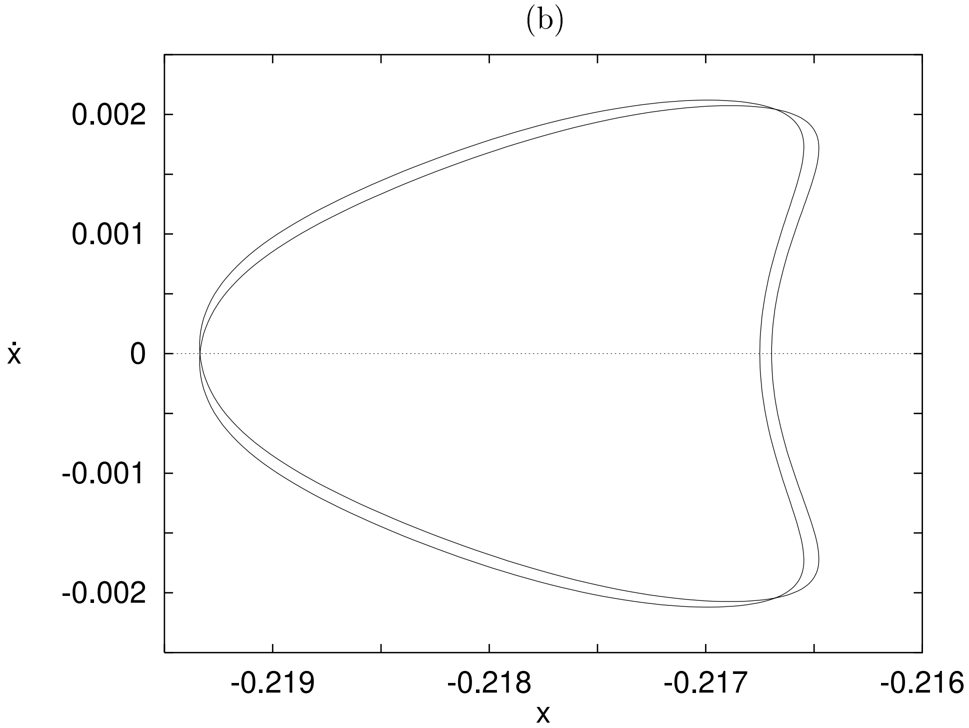

Figure 3.20: Section $y = 0$ of the 2D torus corresponding to the orbit 216. (a) and (b) show the projections on the x-z and the x-$\dot{x}$ planes, respectively.

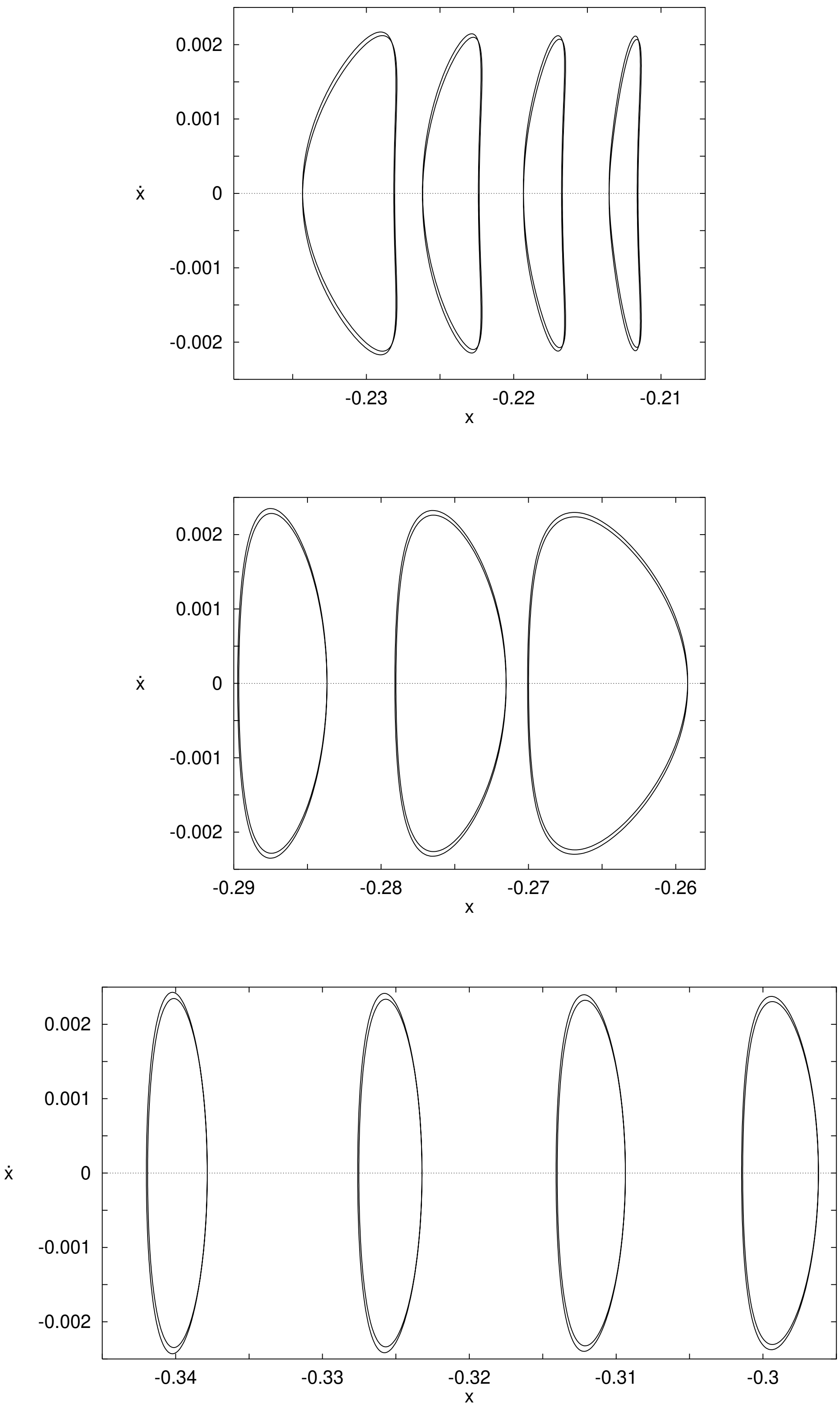

Figure 3.21: Evolution of the section $y = 0$ along the Halo family. Projection on the x-$\dot{x}$ plane. Notice that we have kept the same scale in the three figures.

k_1	k_2	x	k_1	k_2	y	k_1	k_2	z
0	0	−6.2580036e−02	0	2	1.2395454e−02	0	0	2.7923570e−02
0	2	4.4811317e−03	0	3	1.1758432e−05	0	2	4.7899816e−03
0	4	2.2991144e−04	0	4	−3.3667317e−05	0	4	−8.2111621e−05
1	−4	−6.2756753e−04	1	−6	1.2757892e−05	1	−4	−9.2765728e−04
1	−2	1.1534643e−03	1	−4	1.7765420e−03	1	−2	−9.1716120e−04
1	−1	3.1712798e−05	1	−3	−1.1189147e−05	1	−1	2.4116916e−05
1	0	−9.2360329e−02	1	−2	2.2962313e−03	1	0	−5.8042465e−02
1	1	−5.1492802e−05	1	−1	1.1280658e−04	1	1	−2.8057383e−05
1	2	−2.2178014e−03	1	0	−2.6322091e−01	1	2	1.3982244e−04
1	4	2.1449600e−05	1	1	−1.3416915e−04	1	4	−2.4680668e−05
2	−6	−1.7831899e−05	1	2	−1.4722381e−03	2	−6	−4.0617435e−05
2	−4	−1.3028714e−04	1	4	−6.1311922e−05	2	−4	2.9540461e−04
2	−2	−4.0142012e−03	2	−6	5.1408050e−05	2	−2	4.2155520e−04
2	−1	−1.3383637e−05	2	−4	9.3329035e−05	2	0	−4.3450584e−03
2	0	1.2410016e−02	2	−2	−1.0486306e−02	2	2	6.6924476e−05
2	1	1.2496327e−05	2	0	−8.0362401e−03	3	−6	4.2137860e−05
2	2	−7.2663684e−05	2	2	1.5688006e−04	3	−4	−2.9835765e−04
2	4	1.2865014e−05	2	4	−1.2058312e−05	3	−2	−1.3304353e−04
3	−6	−1.1818015e−05	3	−4	1.0370835e−03	3	0	−7.5811857e−04
3	−4	3.3523641e−04	3	−2	−5.1858614e−04	3	2	1.6262831e−05
3	−2	1.0542324e−03	3	0	−1.9859162e−03	4	−6	−1.1060000e−04
3	0	1.9078313e−03	3	2	3.2109462e−05	4	−2	−5.3662798e−05
3	2	−3.3511516e−05	4	−6	1.6234872e−04	4	0	−1.5420667e−04
4	−6	5.9347204e−05	4	−4	4.6140132e−05	5	−12	−2.3131734e−05
4	−4	−9.5422830e−05	4	−2	−2.2679261e−04	5	−2	−1.7009232e−05
4	−2	2.2743591e−04	4	0	−4.2487238e−04	5	0	−3.5694046e−05
4	0	4.4204595e−04	5	−12	2.9289135e−05	6	−12	1.3776391e−05
5	−12	−1.0085272e−05	5	−4	1.5221900e−05	7	−12	−3.8554176e−05
5	−6	−2.3657245e−05	5	−2	−6.5106744e−05			
5	−4	−1.6611065e−05	5	0	−1.0397838e−04			
5	−2	7.0870940e−05	6	−2	−2.0243576e−05			
5	0	1.0504931e−04	6	0	−2.6411556e−05			
6	−2	2.1026344e−05	7	−12	4.9717063e−05			
6	0	2.6601530e−05	8	−14	−1.1487558e−05			
7	−12	1.7737792e−05						

Table 3.10: Fourier coefficients greater than 10^{-5} of the orbit 216 around L_2. $\omega_0 = 1.84408685560270$.

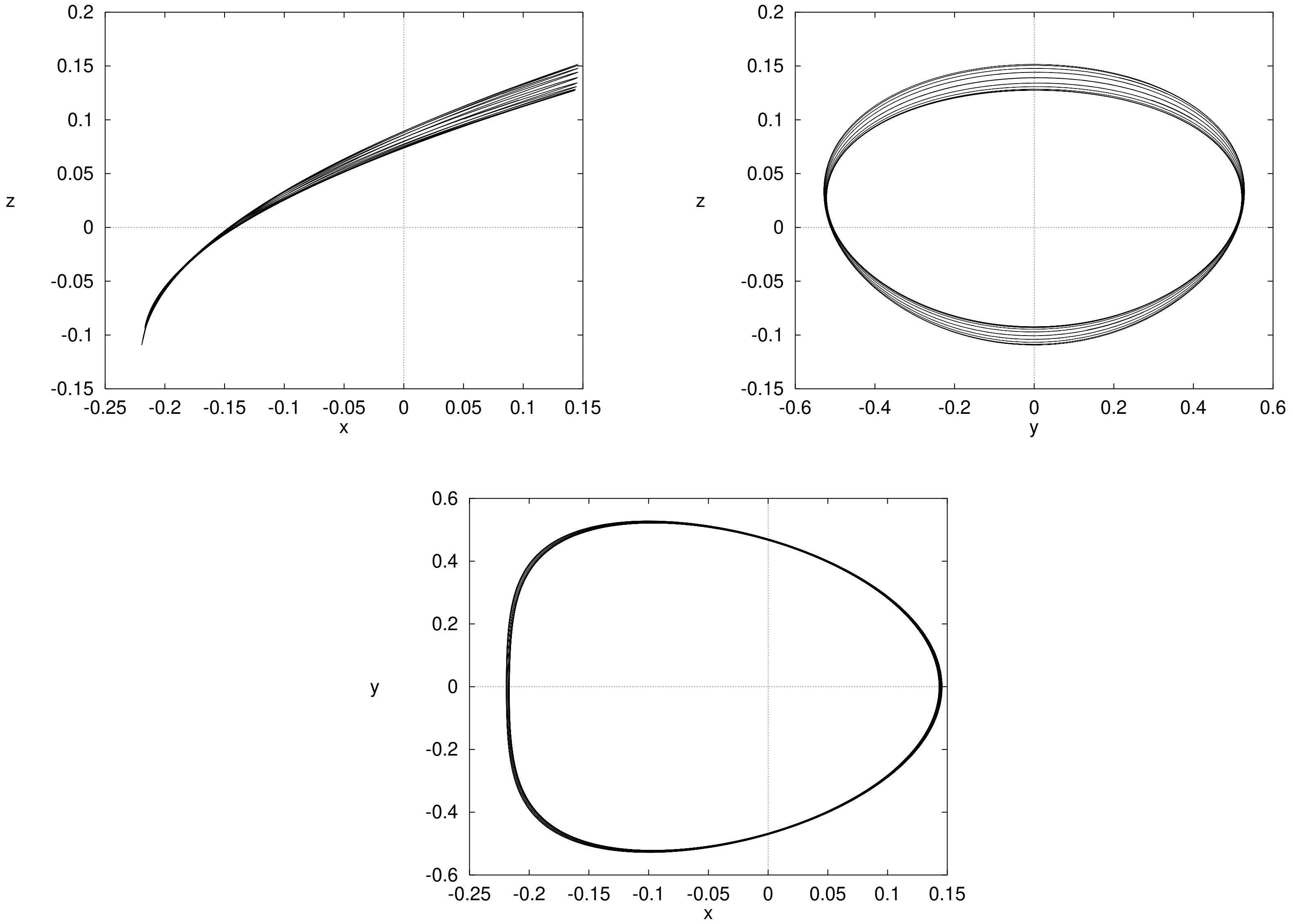

Figure 3.22: Quasi-periodic Halo orbit 216 around L_2 using normalized coordinates. $\varphi_0 = 0$. Time intervals plotted: $[50k, 50k{+}7]$, $k = 0, \ldots, 10$.

k_1	k_2	x	k_1	k_2	y	k_1	k_2	z
0	0	−7.0452119e−02	0	2	3.5330971e−02	0	0	4.1562399e−02
0	2	1.2540647e−02	0	3	2.3567755e−05	0	2	1.3612848e−02
0	4	7.7816844e−04	0	4	−2.3427413e−04	0	4	−3.4620893e−04
1	−6	−7.3177074e−05	0	6	3.1116620e−05	1	−6	2.4262219e−05
1	−4	−1.8331181e−03	1	−4	5.2037619e−03	1	−4	−2.3713436e−03
1	−2	1.7652601e−03	1	−2	2.2941709e−03	1	−2	−1.3343064e−03
1	−1	3.1830822e−05	1	−1	1.1425226e−04	1	−1	3.4346599e−05
1	0	−9.3387293e−02	1	0	−2.6611620e−01	1	0	−8.2610780e−02
1	1	−5.0399100e−05	1	1	−1.3674952e−04	1	1	−4.0675801e−05
1	2	−4.1189676e−03	1	2	9.5615284e−05	1	2	1.2459797e−03
1	4	1.4220635e−04	1	4	−2.1496802e−04	1	4	−1.1617549e−04
2	−4	−1.4447239e−04	2	−6	4.3408291e−05	2	−6	−2.7140478e−05
2	−2	−1.1899528e−02	2	−4	2.9112994e−04	2	−4	3.4094085e−04
2	0	1.1382093e−02	2	−2	−3.2981560e−02	2	−2	−6.9256222e−03
2	2	−5.2188230e−04	2	0	−8.8327458e−03	2	0	−6.1693099e−03
2	4	5.9306334e−05	2	2	6.6101258e−04	2	2	3.5569774e−04
3	−6	−4.8834720e−05	2	4	−6.2166305e−05	2	4	−3.4704053e−05
3	−4	7.6711100e−05	3	−4	4.6235263e−04	3	−6	8.1360630e−05
3	−2	3.0684304e−03	3	−2	−2.0322100e−03	3	−4	9.6670188e−05
3	0	1.7377800e−03	3	0	−1.9263886e−03	3	−2	−1.2944189e−03
3	2	−1.6316593e−04	3	2	1.7025975e−04	3	0	−1.0177329e−03
4	−6	2.2303895e−04	3	4	−2.1181783e−05	3	2	9.0494207e−05
4	−4	1.5314475e−04	4	−6	6.4909311e−04	4	−6	−2.4871846e−05
4	−2	6.9592901e−04	4	−4	−7.6576019e−05	4	−4	−4.4605978e−05
4	0	3.7126740e−04	4	−2	−7.5545794e−04	4	−2	−3.5939421e−04
4	2	−4.5247674e−05	4	0	−3.8371919e−04	4	0	−1.9236940e−04
5	−8	2.9406915e−05	4	2	4.8830520e−05	4	2	2.4425506e−05
5	−6	−7.3207652e−05	5	−8	7.8579667e−05	5	−4	−3.4555808e−05
5	−4	7.7636403e−05	5	−6	4.1280664e−05	5	−2	−9.8871229e−05
5	−2	2.1086334e−04	5	−4	−8.2884980e−05	5	0	−3.9886775e−05
5	0	7.9620841e−05	5	−2	−2.1244902e−04	6	−2	−2.8256520e−05
6	−4	3.8160683e−05	5	0	−8.3631483e−05			
6	−2	6.0801496e−05	6	−4	−3.7492212e−05			
			6	−2	−6.2975924e−05			

Table 3.11: Fourier coefficients greater than $2 \cdot 10^{-5}$ of the orbit 220 around L_2. $\omega_0 = 1.84671600740340$.

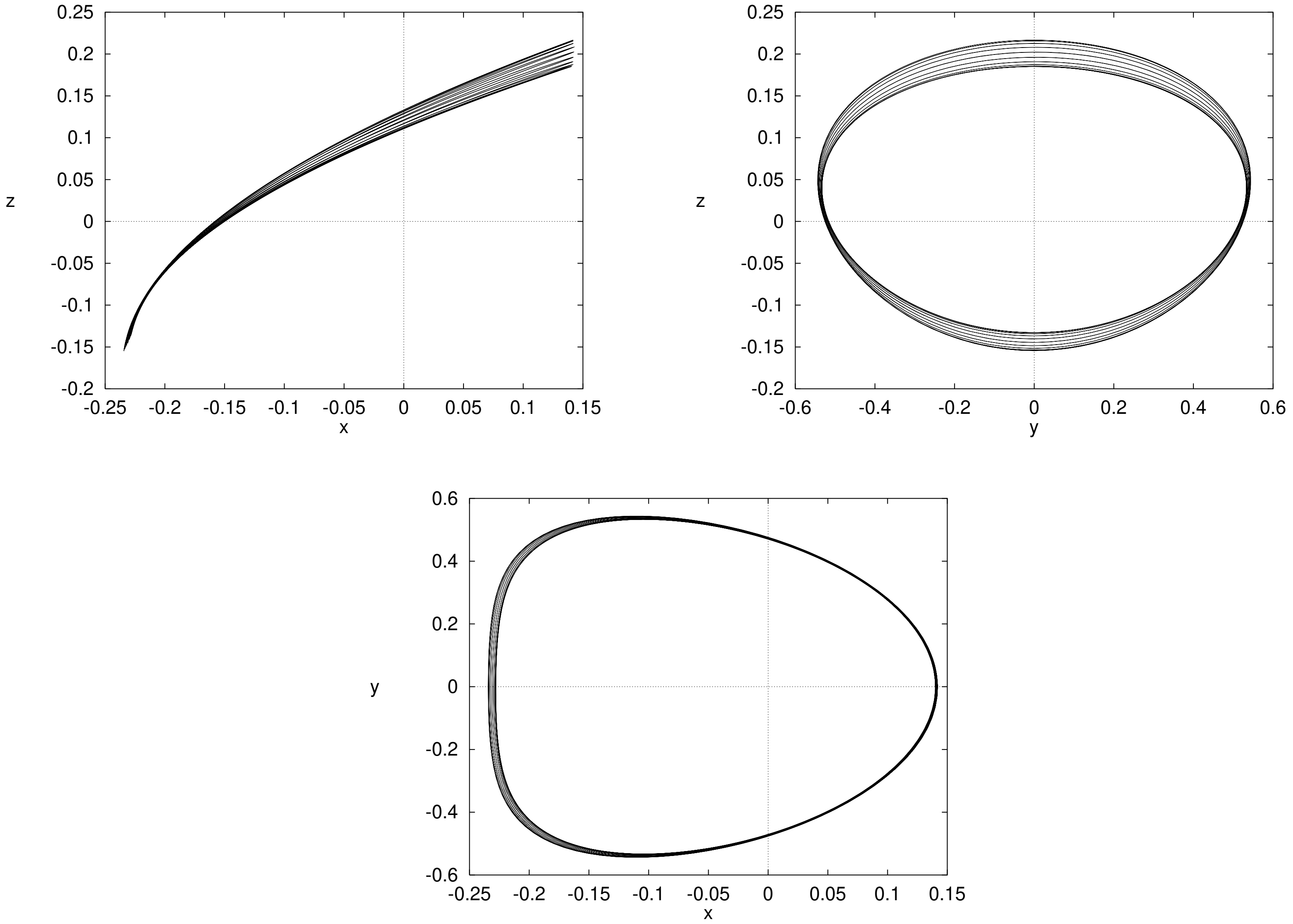

Figure 3.23: Quasi-periodic Halo orbit 220 around L_2 using normalized coordinates. $\varphi_0 = 0$. Time intervals plotted: $[85k, 85k{+}7]$, $k = 0, \ldots, 10$.

k_1	k_2	x	k_1	k_2	y	k_1	k_2	z
0	0	−9.1764139e−02	0	2	3.6486902e−02	0	0	6.9980536e−02
0	2	1.2968674e−02	0	3	2.3893577e−05	0	2	1.4034817e−02
0	4	8.0378552e−04	0	4	−2.4289020e−04	0	4	−3.5843698e−04
0	6	−2.0993653e−05	0	6	3.2992436e−05	1	−6	2.2392515e−05
1	−6	−7.6158156e−05	1	−4	4.9929094e−03	1	−4	−1.5741440e−03
1	−4	−1.7529931e−03	1	−2	2.4504878e−03	1	−2	2.6361285e−03
1	−2	−9.0084305e−04	1	−1	1.2225018e−04	1	−1	5.4085309e−05
1	−1	3.4205469e−05	1	0	−2.8258746e−01	1	0	−1.2770741e−01
1	0	−9.9369479e−02	1	1	−1.4555905e−04	1	1	−6.2745956e−05
1	1	−5.3975566e−05	1	2	3.9932480e−04	1	2	1.5178748e−03
1	2	−4.2025217e−03	1	4	−2.3709163e−04	1	4	−1.4363742e−04
1	4	1.5236469e−04	2	−6	4.4327402e−05	2	−4	−1.3375370e−04
2	−4	2.8347419e−04	2	−4	3.4164228e−04	2	−2	−1.9228192e−02
2	−2	−1.3873455e−02	2	−2	−3.8401846e−02	2	0	−1.0332394e−02
2	0	1.0658166e−02	2	0	−1.1665824e−02	2	2	5.0578084e−04
2	2	−5.7467445e−04	2	2	7.7088241e−04	2	4	−4.7880422e−05
2	4	6.4809198e−05	2	4	−7.4024434e−05	3	−6	−7.0555643e−05
3	−6	5.7757869e−05	3	−4	3.3296878e−04	3	−4	2.2285301e−04
3	−4	2.2082047e−05	3	−2	−3.2422691e−03	3	−2	−3.0142836e−03
3	−2	2.8908352e−03	3	0	−2.3925110e−03	3	0	−1.7500159e−03
3	0	1.8008234e−03	3	2	2.1302513e−04	3	2	1.4088263e−04
3	2	−1.8137565e−04	3	4	−2.6295005e−05	4	−6	4.8548405e−04
3	4	2.2137642e−05	4	−6	8.2531281e−04	4	−4	−1.8225487e−04
4	−6	2.8553739e−04	4	−4	−1.8172046e−04	4	−2	−7.8479490e−04
4	−4	1.6336838e−04	4	−2	−1.0447096e−03	4	0	−3.4430221e−04
4	−2	7.6157117e−04	4	0	−4.9301389e−04	4	2	4.0491880e−05
4	0	3.9995914e−04	4	2	6.3147822e−05	5	−8	6.6436141e−05
4	2	−5.2442786e−05	5	−8	1.0916459e−04	5	−6	7.6741957e−05
5	−8	4.0645202e−05	5	−6	8.1457461e−05	5	−4	−1.0447483e−04
5	−6	−6.1354649e−05	5	−4	−1.3494726e−04	5	−2	−2.1645305e−04
5	−4	9.4769556e−05	5	−2	−3.0349016e−04	5	0	−7.3691186e−05
5	−2	2.4213788e−04	5	0	−1.0974458e−04	6	−4	−4.4923488e−05
5	0	8.9317546e−05	6	−8	2.0214280e−05	6	−2	−6.2540882e−05
6	−4	4.8104585e−05	6	−4	−6.1511496e−05			
6	−2	7.3649493e−05	6	−2	−9.1713005e−05			
6	0	2.0115049e−05	6	0	−2.4573052e−05			
7	−4	2.0359983e−05	7	−4	−2.5736696e−05			
7	−2	2.2349089e−05	7	−2	−2.7563585e−05			

Table 3.12: Fourier coefficients greater than $2 \cdot 10^{-5}$ of the orbit 228 around L_2. $\omega_0 = 1.85412362200710$.

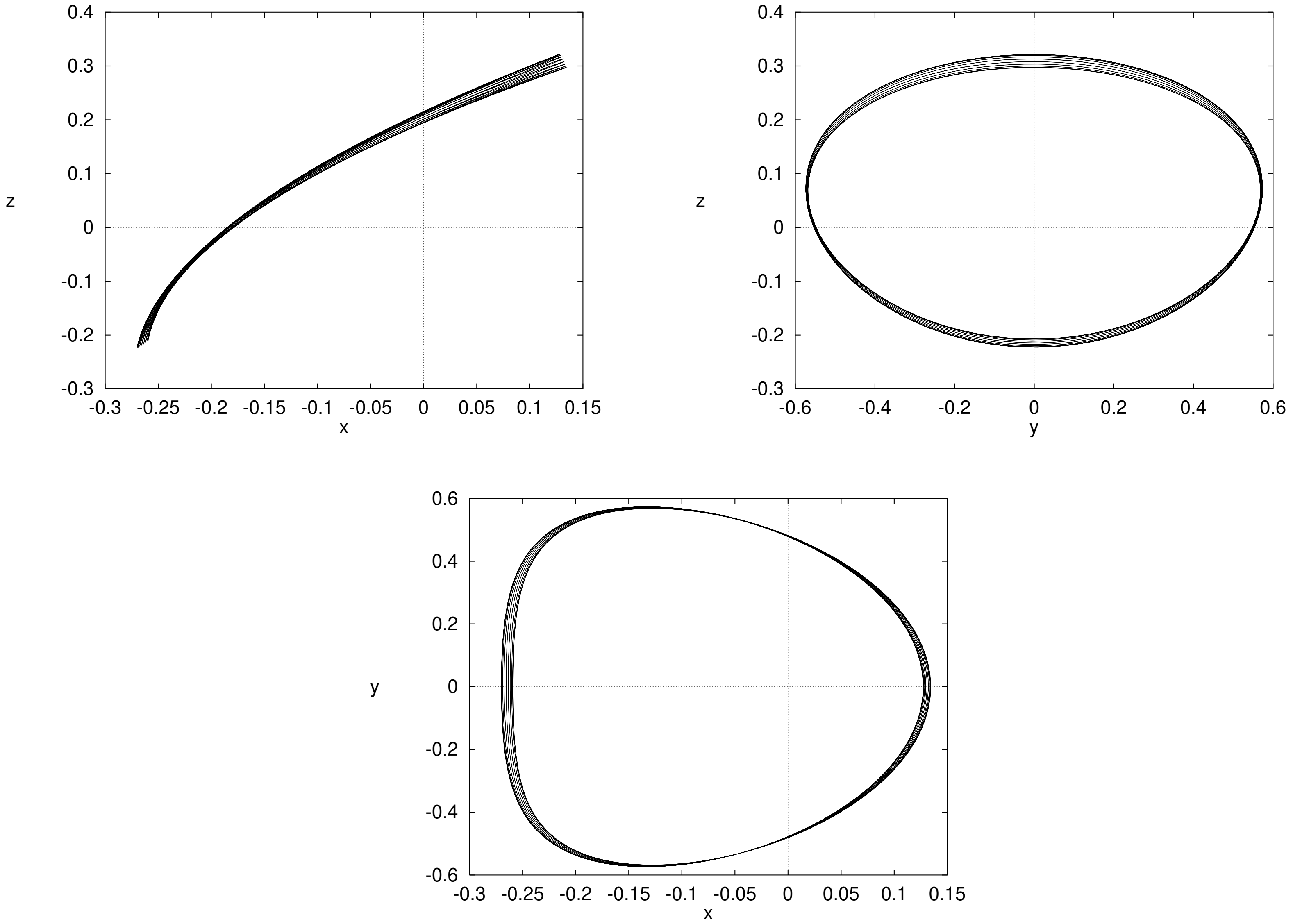

Figure 3.24: Quasi-periodic Halo orbit 228 around L_2 using normalized coordinates. $\varphi_0 = 0$. Time intervals plotted: $[85k, 85k{+}7]$, $k = 0, \ldots, 10$.

k_1	k_2	x	k_1	k_2	y	k_1	k_2	z
0	0	−1.2131983e−01	0	2	3.5060482e−03	0	0	1.0350553e−01
0	2	1.4201624e−03	0	3	6.4153717e−06	0	1	1.6510498e−05
0	4	5.7145453e−05	0	4	6.0999094e−06	0	2	1.1616546e−03
1	−4	−1.2204383e−04	1	−4	3.4158422e−04	0	4	−1.0965195e−05
1	−2	1.7224654e−04	1	−3	−1.2629927e−05	1	−4	−1.6995229e−05
1	−1	3.8897719e−05	1	−2	2.7353282e−03	1	−2	1.6354993e−03
1	0	−1.0886828e−01	1	−1	1.3456181e−04	1	−1	7.3357639e−05
1	1	−6.2159734e−05	1	0	−3.0834215e−01	1	0	−1.7314851e−01
1	2	−1.6354330e−03	1	1	−1.5713669e−04	1	1	−8.3308112e−05
1	4	−6.9224393e−06	1	2	−2.3773446e−03	1	2	−1.0136923e−03
2	−4	1.0093824e−04	1	4	−3.0253290e−05	1	4	−1.4028638e−05
2	−2	−1.4668722e−03	2	−4	3.0140647e−05	2	−4	−9.2725058e−05
2	−1	−1.1288482e−05	2	−2	−3.0272794e−03	2	−2	−1.8727475e−03
2	0	1.0580781e−02	2	−1	9.2694545e−06	2	−1	9.9642973e−06
2	1	1.0623168e−05	2	0	−1.6333816e−02	2	0	−1.6005879e−02
2	2	7.8642689e−05	2	1	−1.5988271e−05	2	1	−1.5726818e−05
3	−4	1.3163879e−04	2	2	−1.3675304e−04	2	2	−1.5571524e−04
3	−2	1.4449343e−04	3	−4	3.9122192e−04	3	−4	2.9393021e−04
3	0	2.1626055e−03	3	−2	−2.7523399e−04	3	−2	−3.0066100e−04
3	2	2.5877429e−05	3	0	−3.5819802e−03	3	0	−3.0640738e−03
4	−4	−2.0714726e−05	3	1	−5.3448451e−06	3	2	−4.4541156e−05
4	−2	4.5997468e−05	3	2	−4.8539488e−05	4	−6	6.5971110e−06
4	0	5.7218490e−04	4	−6	8.9400316e−06	4	−4	4.8123719e−05
4	2	1.0144915e−05	4	−4	4.7524879e−05	4	−2	−8.2113017e−05
5	−4	−7.3100004e−06	4	−2	−8.9264881e−05	4	0	−7.1003192e−04
5	−2	1.7022930e−05	4	0	−8.6346695e−04	4	2	−1.3933154e−05
5	0	1.5750140e−04	4	2	−1.6051329e−05	5	−4	1.2611806e−05
6	−2	5.9503756e−06	5	−4	1.3863064e−05	5	−2	−2.4581032e−05
6	0	4.5513942e−05	5	−2	−2.8170426e−05	5	0	−1.8497252e−04
7	0	1.3592375e−05	5	0	−2.3240218e−04	6	−2	−7.8459519e−06
			5	2	−5.5749582e−06	6	0	−5.1471511e−05
			6	−2	−9.3937290e−06	7	0	−1.4988512e−05
			6	0	−6.6080324e−05			
			7	0	−1.9552319e−05			
			8	0	−5.9545517e−06			

Table 3.13: Fourier coefficients greater than $5 \cdot 10^{-6}$ of the orbit 236 around L_2. $\omega_0 = 1.86504774703280$.

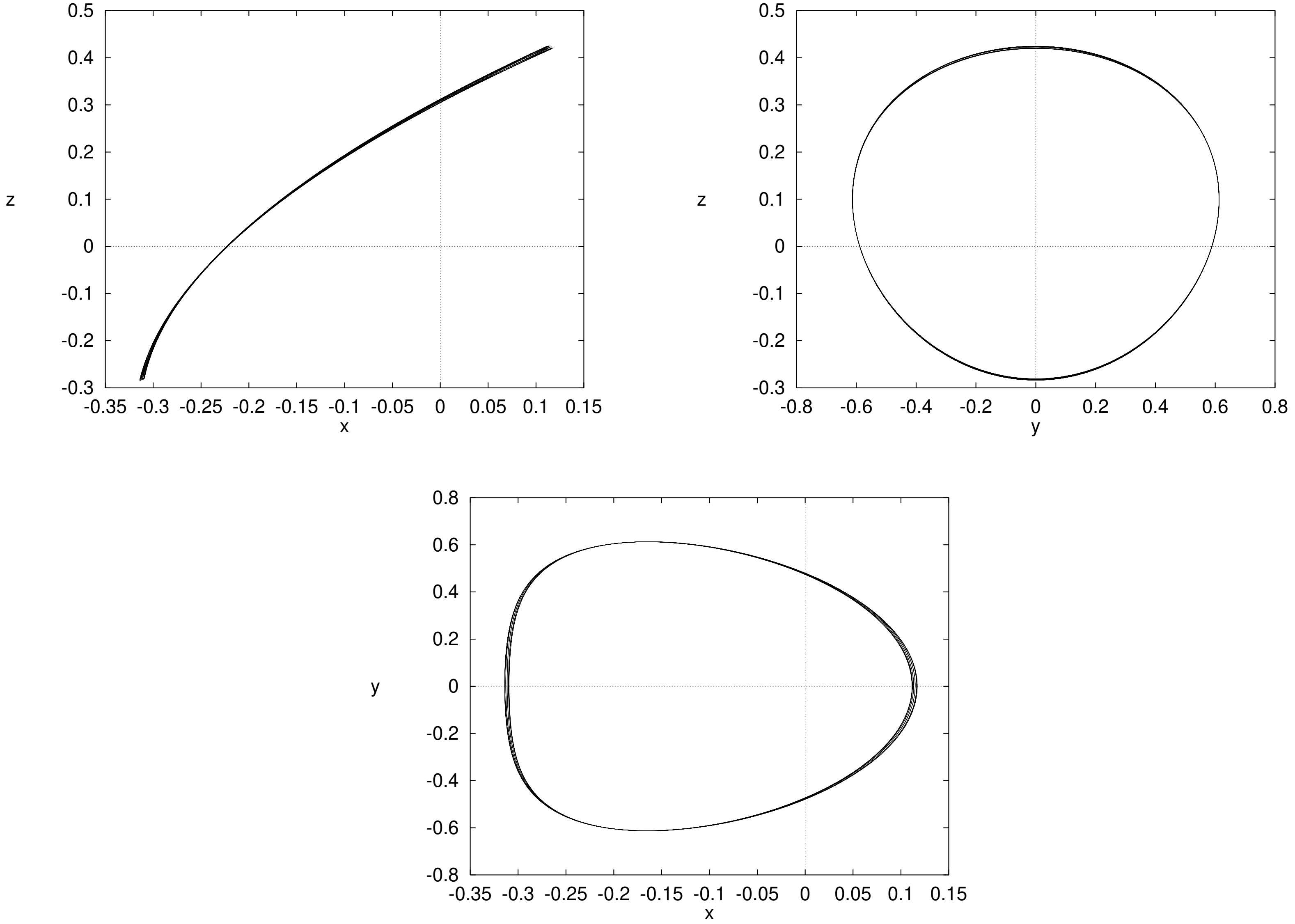

Figure 3.25: Quasi-periodic Halo orbit 236 around L_2 using normalized coordinates. $\varphi_0 = 0$. Time intervals plotted: $[42k, 42k{+}7]$, $k = 0, \ldots, 5$.

3.7 Stability of the Lyapunov family in the QBCP

It is well known that, in the RTBP, the planar Lyapunov family of periodic orbits is stable in the z direction up to the bifurcation of the Halo orbits. Beyond this bifurcation the Lyapunov orbits become unstable in the z direction. In the QBCP, something similar happens, but we are going to see that the present case is much more rich. Here, the Lyapunov family is of 2D tori. Each torus has two basic frequencies, the frequency of the Sun and its proper frequency which decreases slowly when increasing the amplitude of the tori.

To study the stability of the tori, the Lyapunov exponents are used. Here, we present the Lyapunov exponents in a general setting. Consider a system of differential equations of the form

$$\dot{x} = f(t, x) \ ,$$

with $x \in \mathbb{R}^n$. Let $x_0(t)$ be an orbit of that system. The variational equations associated to that orbit are

$$\dot{A} = D_x f(t, x_0(t))\, A \ , \qquad A(0) = I \ ,$$

where A is a $n \times n$ matrix and I denotes the identity matrix. Let $\mu_j(t)$ be the (eventually complex) eigenvalues of $A(t)$ for $j = 1, \ldots, n$. The Lyapunov exponents are defined as

$$\lambda_j = \lim_{t \longrightarrow \infty} \frac{\log |\mu_j|}{t} \ , \tag{3.27}$$

provided that the limit exists. A Lyapunov exponent equal to zero is related with linear stability and a positive Lyapunov exponent is associated with unstable directions.

In a similar way, we define the normal frequencies as

$$\omega_j = \lim_{t \longrightarrow \infty} \frac{\arg(\mu_j)}{t} \ , \tag{3.28}$$

where the argument must be taken on the lift (without taking mod 2π). Normal frequencies give information about the rotating behaviour of the flow nearby $x_0(t)$, in the stable case as well as in the unstable one.

The variational equations of the QBCP were given in section 2.2.2. Now, we are interested in the case of planar orbits on $z = 0$. Furthermore, we only want to study the stability in the z direction. Then, it is only necessary to integrate the variational equations

$$\dot{A}_z = \begin{pmatrix} \alpha_2(t) & \alpha_1(t) \\ b_6(t, x_0(t)) & -\alpha_2(t) \end{pmatrix} A_z \ , \qquad A_z(0) = I \ , \tag{3.29}$$

where A_z is a 2×2 matrix; α_1 and α_2 are T-periodic functions given in section 1.5.1; the function b_6 was given in section 2.2.2. In this case, if the limits (3.27) exist, there are only two Lyapunov exponents, λ_1 and λ_2. Moreover, due to the fact that QBCP is a Hamiltonian system, we have $\lambda_1 = -\lambda_2$. For the same reason, in this case, there is only one normal frequency which is denoted by ω_z.

To study the stability of the planar Lyapunov tori of the QBCP, we follow the next steps:

1. For a given x-amplitude, we compute an analytical approximation of the Lyapunov periodic orbit of the RTBP. For this purpose, we use the series given by the Lindstedt-Poincaré method. In section 3.3, we explained how this series can be obtained for the QBCP. The case of the RTBP is simpler and it can be considered as a particular case of the other one. In the RTBP case, there is no difficulty in obtaining a high order analytical approximation of the Lyapunov orbits.

2. Computation of an analytical approximation of a Lyapunov torus in the QBCP. This is done using the analytical refinement method used in section 3.6 for the computation of the Halo orbits. That method looks for the Fourier coefficients of a solution of the differential equations of the QBCP using a Newton's process. As first approximation, the orbit of the RTBP of the previous point is used. Usually three steps of a continuation method are also required.

3. Computation of the Lyapunov exponents. Let $x_0(t)$ be the quasi-periodic orbit of the previous point, expressed as a Fourier series with two basic frequencies. To obtain accurate results in the computation of the Lyapunov exponent, we have checked that, in our case, it is sufficient to use the coefficients of $x_0(t)$ larger than 10^{-9}. This means that, for the orbits considered here, we have used about 160 terms in each of the two components of the planar orbit $x_0(t)$. We integrate numerically the variational equations (3.29) along the orbit $x_0(t)$. To compute the limits (3.27) and (3.28), the quotients are evaluated, typically, for equally spaced on time values $t = T_p(10^5 + 10^4\,k)$, $k = 0, 1, 2, \ldots$, where $T_p = 2\pi/\omega_p$, being ω_p the proper frequency of the Lyapunov orbit. The process is stopped when three consecutive quotients differ by less than some threshold (typically, we have used 10^{-7} for the Lyapunov exponent and 10^{-9} for the normal frequency). It is possible to avoid the numerical integration of the variational equations for a long time span, using a very fast method described in [4]. Later on, we will summarize that method.

We have computed 401 Lyapunov orbits of the RTBP with amplitudes equally spaced on the interval $[0.17, 0.18]$. For these orbits, the proper frequency decreases from 1.84319829 to 1.84074873. The corresponding 401 Lyapunov orbits of the QBCP have been computed. Their amplitudes are in the interval [0.17456011, 0.18426829]. Figure 3.26 shows the positive Lyapunov exponent of those orbits. The instability tongues labelled as (k), $k = 0, \ldots, 5$, correspond to the resonances $2\omega_z = k(2\omega_s - \omega_p)$. Of course, there are infinitely many resonances, but the instability tongues associated to them are very small. Resonances for $k = 4, 5$ also have been pointed even though they are hardly visible using that scale. In the interval studied, the most relevant resonances correspond to $k = 0, 1, 2, 3$. When the branch of (0) starts, the families of Halo orbits are born. This occurs for an approximate amplitude $\alpha = 0.18089485$ and proper frequency $\omega_p = 1.84161851$.

Figure 3.27 shows the normal frequency modulus ω_p. There is a step corresponding to each tongue of positive Lyapunov exponent. Due to the fact that there are infinitely many resonances, there are also infinitely many steps. The curve displayed in figure 3.27 is an example of "devil's staircase" (see [17]). We also want to note that, near the end points of the long steps, the curve shows the typical behaviour of the square root function (see [4]).

3.7.1 Interpolation method for computing Lyapunov exponents of tori

Consider a $n \times n$ matrix differential equations of the form

$$\dot{A} = B(\theta_p, \theta_s)\, A\ , \qquad A(0) = I\ , \tag{3.30}$$

where B is 2π-periodic in θ_p and θ_s. These angles are $\theta_p = \theta_{p,0} + \omega_p t$ and $\theta_s = \theta_{s,0} + \omega_s t$, and let $T_p = 2\pi/\omega_p$. That is linear differential equation with quasi-periodic coefficients. The system (3.29) is of this form.

Now, we fix the phase $\theta_{p,0} = 0$ and consider the map time the period T_p by the flow, Φ, of (3.30):

$$\theta_{s,0} \in [0, 2\pi] \ \longrightarrow\ P(\theta_{s,0}) = \Phi(\theta_{p,0} = 0, \theta_{s,0}, I)\ .$$

From this map, we define the following sequence

$$\begin{pmatrix} M_k \\ \theta_s^{(k)} \end{pmatrix} = \begin{pmatrix} P(\theta_s^{(k-1)})\ M_{k-1} \\ \theta_s^{(k-1)} + \omega_s T_p \ (\mathrm{mod}\ 2\pi) \end{pmatrix}\ , \tag{3.31}$$

with M_0=I and $\theta_s^{(0)} = 0$. To study the Lyapunov exponents of the system (3.30), it is only necessary to estimate the eigenvalues of the product matrix

$$M_k = P(\theta_s^{(k-1)}) \cdots P(\theta_s^{(1)})\, P(\theta_s^{(0)})\ ,$$

when k tends to infinity. We also want to comment that the normal frequencies can be estimated through the same matrices M_k. In our case, it is only necessary to take an arbitrary initial vector and count the angle of rotation after the successive multiplications by the matrices $P(\theta_s^{(k)})$.

The key of the method is the way to compute the matrices $P(\theta_s^{(k)})$. Since P is 2π-periodic in $\theta_{s,0}$, we compute these matrices in a grid in $[0, 2\pi]$, integrating the differential equations (3.30). After that, if we want to know P for any other value of the interval, we use interpolation. In our case, we have used 1000 equally spaced points for the grid and interpolating polynomials of degree 7 computed by

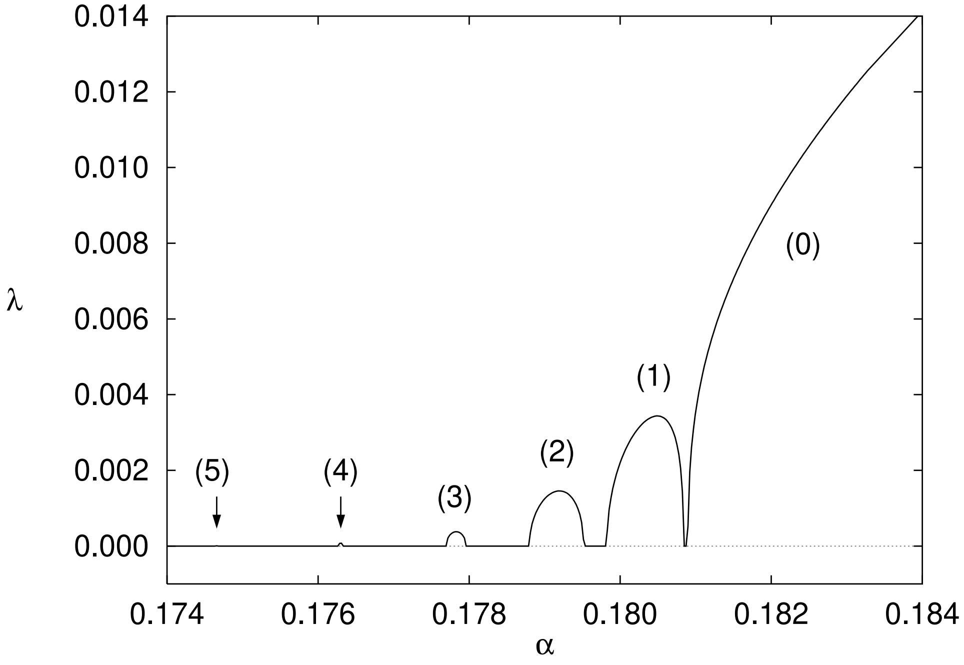

Figure 3.26: Lyapunov exponents of planar Lyapunov 2D tori. λ is the positive Lyapunov exponent. α is the x-amplitude of the tori.

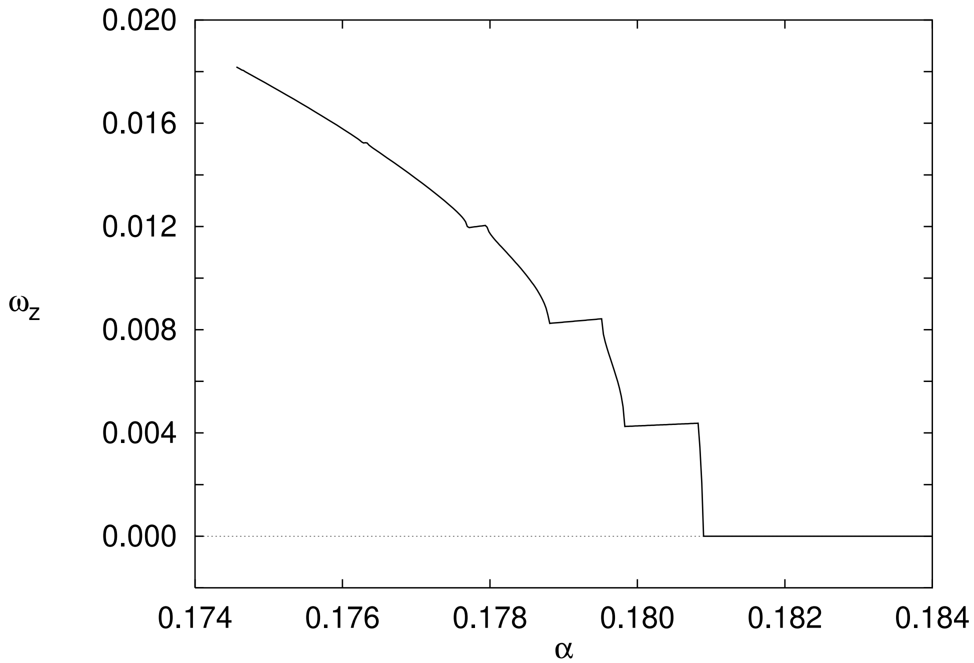

Figure 3.27: Normal frequency of planar Lyapunov 2D tori. ω_z is the normal frequency. α is the x-amplitude of the tori.

Lagrange method. This is a very fast method to compute the matrices M_k. A Pentium computer (233 MHz) spends about 85 sec. for the computation of the 1000 initial P matrices. After that, it only needs 9 sec. to compute 10^6 iterations of the sequence (3.31), given estimations of the Lyapunov exponent and the normal frequency every 10^4 iterations. It is clear that the interpolation method allows to achieve very accurate estimates of the limits (3.27) and (3.28) in a very short time.

Chapter 4

The vicinity of L_2 in the QBCP

4.1 Introduction

In the previous chapters, we have computed periodic orbits around L_2, quasi-periodic orbits like Lyapunov orbits or Halo orbits (2D tori) and small Lissajous orbits (3D tori) around L_2. In each case, these objects have been computed using different techniques. Now, we want to have a full description of the orbits in a big neighbourhood around the L_2 geometrically defined libration point of the Earth-Moon system in the QBCP. That is accomplished by means of the reduction of the Hamiltonian to the central manifold. This chapter is devoted to that purpose. The main reference for the reduction to the central manifold is [11]. We have followed precisely the method explained there.

We have to thank Dr. J.Masdemont for providing us a lot of code which helped us to implement the reduction to the central manifold of the Hamiltonian of the QBCP. We also are in debt with J.M. Mondelo for his help, comments and suggestions about the Fourier analysis of the orbits. He also provided us code to perform Fourier analysis with an efficient algorithm based on the methods described in [11], appendix B.

4.2 Lie transformation method

We are interested in the computation of the Hamiltonian reduced to the central manifold in the vicinity of the point L_2. The same could be done around the other Lagrange points.

As we saw in section 1.5.1, the Hamiltonian of the QBCP is

$$\begin{aligned} H &= \frac{1}{2}\alpha_1(p_x^2+p_y^2+p_z^2)+\alpha_2(p_x x+p_y y+p_z z)+\alpha_3(p_x y-p_y x)+ \\ &\quad +\alpha_4 x+\alpha_5 y-\alpha_6\left(\frac{1-\mu}{q_{pe}}+\frac{\mu}{q_{pm}}+\frac{m_s}{q_{ps}}\right)\ , \end{aligned} \tag{4.1}$$

where

$$\begin{aligned} q_{pe}^2 &= (x-\mu)^2 + y^2 + z^2 \ , \\ q_{pm}^2 &= (x-\mu+1)^2 + y^2 + z^2 \ , \\ q_{ps}^2 &= (x-\alpha_7)^2 + (y-\alpha_8)^2 + z^2 \ . \end{aligned}$$

The α_k functions are of the form

$$\begin{aligned} \alpha_k(\theta) &= \alpha_{k0} + \sum_{j\geq 1} \alpha_{kj}\cos(j\theta) \ , \qquad && \text{for } k = 1,3,4,6,7, \\ \alpha_k(\theta) &= \sum_{j\geq 1} \alpha_{kj}\sin(j\theta) \ , && \text{for } k = 2,5,8, \end{aligned}$$

with $\theta = \omega_s t$ and the coefficients α_{kj} were given in table 1.5. We also want to recall that the potential can be expanded using Legendre polynomials. That was done in section 3.2.2. The only difference is that, there the unit of length was the distance between the Moon and $\mathrm{L_i}$ (i=1,2) and here, we take the unit of length as the distance between the Earth and the Moon. So, the Hamiltonian might be expressed in the form

$$H = \sum_{|k|\geq 1} (\sum_j h_{kj} e^{\sqrt{-1}\, j\theta}) x^{k_1} y^{k_2} z^{k_3} p_x^{k_4} p_y^{k_5} p_z^{k_6} \ ,$$

where $h_{kj} \in \mathbb{C}$, k is the multiindex $(k_1, k_2, k_3, k_4, k_5, k_6)$ and $|k| = \sum_i k_i$. In fact, for practical reasons, the expansion of the Hamiltonian is not computed now. It will be expanded after the computation of the Floquet change of variables.

The Hamiltonian of the QBCP has three and a half degrees of freedom, but we can consider as four degrees of freedom introducing a new momentum y_θ, associated with the variable θ. This allows to manage time as another variable, through the angle θ. We also rename the position as $x = (x_1, x_2, x_3)$ and the momentum $y = (y_1, y_2, y_3)$. The new Hamiltonian, denoted again as H, is

$$H(x, y, \theta, y_\theta) = \omega_s y_\theta + \sum_{|k|\geq 1} H_{|k|}(x, y, \theta) \ , \tag{4.2}$$

where $H_{|k|}$ means terms of degree $|k|$ in x and y.

To perform canonical changes of variables, we use Lie's method. Given a generating function G, the new Hamiltonian is obtained by means of

$$\tilde{H} = H + \{H, G\} + \frac{1}{2!}\{\{H, G\}, G\} + \frac{1}{3!}\{\{\{H, G\}, G\}, G\} + \dots \ ,$$

where $\{\cdot, \cdot\}$ is the Poisson bracket. For two functions, f and g, depending on (x, y, θ, y_θ), the Poisson bracket is defined as

$$\{f, g\} = \sum_{i=1}^{3} \frac{\partial f}{\partial x_i}\frac{\partial g}{\partial y_i} - \frac{\partial f}{\partial y_i}\frac{\partial g}{\partial x_i} + \frac{\partial f}{\partial \theta}\frac{\partial g}{\partial y_\theta} - \frac{\partial f}{\partial y_\theta}\frac{\partial g}{\partial \theta} \ .$$

In the particular case of a Hamiltonian of the form of (4.2) and a generating function G not depending on y_θ then

$$\{H,G\} = \sum_{i=1}^{3} \frac{\partial H}{\partial x_i}\frac{\partial G}{\partial y_i} - \frac{\partial H}{\partial y_i}\frac{\partial G}{\partial x_i} - \omega_s \frac{\partial G}{\partial \theta} \,.$$

The change of variables associated to the generating function G is obtained from

$$u = \tilde{u} + \{\tilde{u},G\} + \frac{1}{2!}\{\{\tilde{u},G\},G\} + \frac{1}{3!}\{\{\{\tilde{u},G\},G\},G\} + \dots \,,$$

where u represents any of the variables and $\tilde{u}$ the corresponding new one.

4.3 Cancelling terms of degree one

The first step of the reduction to the central manifold is to cancel the terms of the Hamiltonian with degree one in x and y. That is accomplished with the translation to the periodic orbit of the QBCP which substitutes the equilibrium point L_2 of the RTBP. We notice that the translation depends on time. In this way, the origin of coordinates becomes a fixed point.

That periodic orbit was computed numerically in section 2.3. It also was computed analytically in section 3.3.1, using the Lindstedt-Poincaré method. Here, we are going to use the Fourier series of the orbit. These series also can be obtained integrating the orbit with constant step and performing Fourier analysis to determine the amplitudes.

For the translation to the periodic orbit, the generating function, G_1, is of the form

$$G_1 = g_{11}(\theta)x_1 + g_{12}(\theta)y_1 + g_{13}(\theta)x_2 + g_{14}(\theta)y_2 \,,$$

where $g_{11}(\theta)$, $g_{12}(\theta)$, $g_{13}(\theta)$ and $g_{14}(\theta)$ are trigonometric polynomials in θ. The associated change of variables is

$$\begin{aligned}
x_1 &= \tilde{x}_1 + g_{12}(\theta) \,, \\
y_1 &= \tilde{y}_1 - g_{11}(\theta) \,, \\
x_2 &= \tilde{x}_2 + g_{14}(\theta) \,, \\
y_2 &= \tilde{y}_2 - g_{13}(\theta) \,, \\
y_\theta &= \tilde{y}_\theta - \frac{\partial G_1}{\partial \theta} - \frac{1}{2}\left(g'_{11}(\theta)g_{12}(\theta) - g'_{12}(\theta)g_{11}(\theta) + \right. \\
&\qquad \left. + g'_{13}(\theta)g_{14}(\theta) - g'_{14}(\theta)g_{13}(\theta)\right) \,,
\end{aligned}$$

where $'$ denotes the derivative. The other variables, x_3, y_3 and θ, remain unchanged. We remind that the involved periodic orbit is planar, being $x_3 = y_3 = 0$. The variable θ does not change because the function G_1 was chosen not depending on y_θ. The fact that θ remains unchanged means that the time also does not vary.

4.4 Normal form of order two

The purpose of this section is to explain how to perform a change of variables in such a way that the terms of second degree of the Hamiltonian, $H_2(x, y, \theta)$, become of the form

$$\nu_1 x_1 y_1 + \nu_2 x_2 y_2 + \nu_3 x_3 y_3 \ ,$$

where ν_1, ν_2 and ν_3 are constant complex numbers. This can be carried out with the use of the symplectic Floquet's theorem reducing, directly, to a diagonal form. The theorems which appear below, their proofs and the algorithm for the diagonalization of the terms of second degree of the Hamiltonian, can be found in [11]. Note that, for the application to the studied problem, the values of ν_1, ν_2 and ν_3 are $\sqrt{-1}\,\omega_1$, ω_2 and $\sqrt{-1}\,\omega_3$, respectively, where the ω_j will be introduced later.

Firstly, we are going to remind the most known Floquet's theorem.

Floquet's theorem: *Consider an homogeneous system of linear differential equations*

$$\dot{z} = A(t) z \ , \tag{4.3}$$

where $A(t)$ is a T-periodic integrable $n \times n$ matrix.

Any fundamental matrix solution $Z(t)$ of (4.3) *with T-periodic coefficients can be expressed in the form*

$$Z(t) = P(t) e^{Bt} \ ,$$

where $P(t)$ and B are $n \times n$ matrices, $P(t)$ is T-periodic, nonsingular for all t, and B is constant. The T-periodic change of variables $z = P(t)u$ transforms the initial system into

$$\dot{u} = Bu \ ,$$

which is a system with constant coefficients.

Moreover, a linear change $u = Rv$ can be applied and then the system is reduced to

$$\dot{v} = R^{-1} B R v \ .$$

The matrix R can be chosen in such a way that $R^{-1}BR$ was as simple as possible, for instance, the Jordan form of the matrix B.

We also want to remark that P satisfies the matrix differential equation

$$\dot{P} = AP - PB \ . \tag{4.4}$$

This equality is easily obtained derivating $Z(t)$ and substituting into (4.3). The differential equation (4.4) will be used later on to compute $P(t)$.

For the Hamiltonian case, we have the corresponding version of the Floquet's theorem.

Symplectic Floquet's theorem: *Let the Hamiltonian be*

$$H(X, Y, \Theta, Y_\Theta) = \omega Y_\Theta + X^T Q_1 X + X^T Q_2 Y + Y^T Q_3 Y \ , \tag{4.5}$$

where $Q_i = Q_i(\Theta)$ *are* $n \times n$ 2π*-periodic matrices in the variable* $\Theta = \omega t$ *(say* T*-periodic with respect to the time* t*,* $T = 2\pi/\omega$*), and assume* Q_1 *and* Q_3 *are symmetric.*

We consider the Hamiltonian equations associated with the angular variables X *and their respective momenta* Y*:*

$$\begin{array}{rcrcrr} \dot{X} & = & D_Y H & = & Q_2^T X & +2Q_3 Y \ , \\ \dot{Y} & = & -D_X H & = & -2Q_1 X & -Q_2 Y \ . \end{array}$$

We note this system of equations by $\dot{Z} = Q(t)Z$ *where* $Z = (X^T, Y^T)^T$*.* Q *is a* $2n \times 2n$ T*-periodic matrix with respect* t *and the dots denote the derivative with respect* t*.*

Using the Floquet theorem, there exists a $2n \times 2n$ T*-periodic matrix* $P(t)$ *such that the change of variables*

$$\begin{pmatrix} X \\ Y \end{pmatrix} = \begin{pmatrix} P_{11} & P_{12} \\ P_{21} & P_{22} \end{pmatrix} \begin{pmatrix} x \\ y \end{pmatrix} ,$$

which we note $Z = Pz$*, where* $z = (x^T, y^T)^T$*, transforms* $\dot{Z} = QZ$ *into* $\dot{z} = Bz$*, where* B *is a* $2n \times 2n$ *constant matrix which we split in four* $n \times n$ *matrices* B_{11}*,* B_{12}*,* B_{21}*,* B_{22}*, in the same way we do for* P*.*

Consider the complete change of variables:

$$\begin{array}{rcl} X & = & P_{11}x + P_{12}y \ , \\ Y & = & P_{21}x + P_{22}y \ , \\ \Theta & = & \theta \ , \\ Y_\Theta & = & y_\theta + x^T F_{11}^T x + y^T F_{12}^T x + x^T F_{21}^T y + y^T F_{22}^T y \ , \end{array}$$

being F_{11}*,* F_{12}*,* F_{21} *and* F_{22} *the following* $n \times n$ T*-periodic matrices:*

$$\begin{array}{rcl} F_{11}^T & = & \dfrac{-1}{2\omega} B_{21} - \dfrac{1}{\omega}(P_{11}^T Q_1 P_{11} + P_{11}^T Q_2 P_{21} + P_{21}^T Q_3 P_{21}) \ , \\ F_{12}^T & = & \dfrac{1}{2\omega} B_{11} - \dfrac{1}{\omega}(P_{12}^T Q_1 P_{11} + P_{12}^T Q_2 P_{21} + P_{22}^T Q_3 P_{21}) \ , \\ F_{21}^T & = & \dfrac{-1}{2\omega} B_{22} - \dfrac{1}{\omega}(P_{11}^T Q_1 P_{12} + P_{11}^T Q_2 P_{22} + P_{21}^T Q_3 P_{22}) \ , \\ F_{22}^T & = & \dfrac{1}{2\omega} B_{12} - \dfrac{1}{\omega}(P_{12}^T Q_1 P_{12} + P_{12}^T Q_2 P_{22} + P_{22}^T Q_3 P_{22}) \ . \end{array}$$

Then we have:

i) The matrix B *can be chosen such that it satisfies,* $B^T J B = J$ *(it is symplectic),* $B_{22} = -B_{11}^T$*,* $B_{21} = B_{21}^T$ *and* $B_{12} = B_{12}^T$*, where* J *is the symplectic matrix*

$$J = \begin{pmatrix} 0 & I \\ -I & 0 \end{pmatrix} ,$$

and I *is the* $n \times n$ *identity matrix.*

ii) The complete change of variables is symplectic.

iii) The complete change of variables transforms the initial Hamiltonian $H(X, Y, \Theta, Y_\Theta)$ into

$$\tilde{H}(x, y, \theta, y_\theta) = \omega y_\theta - \frac{1}{2} x^T B_{21} x - x^T B_{22} y + \frac{1}{2} y^T B_{12} y \ .$$

4.4.1 The algorithm

We are going to explain the algorithm followed for the computation of the symplectic change of coordinates diagonalizing the part of second degree of the Hamiltonian of the QBCP. We notice that this change of coordinates is computed managing the initial Hamiltonian without expanding it. The expansion is performed later on.

The matrix $P(t)$ involved in the Floquet's theorem can be taken in such a way that $P(0) = I$ and so $P(T) = I$. The linearized differential equations are the variational equations. Then, integrating numerically those equations along the periodic orbit, the monodromy matrix $M = e^{BT}$ is obtained. Therefore, the matrix B is a logarithm of the matrix M divided by the period.

To get the matrix B, the next step is to compute the eigenvalues of the matrix M. Since M is a 6×6 symplectic matrix, the eigenvalues are three pairs of complex numbers λ_1, λ_1^{-1}, λ_2, λ_2^{-1}, λ_3 and λ_3^{-1}. There is a complex symplectic matrix of change of basis, S, such that $M = SD_MS^{-1}$, where D_M is the diagonal matrix

$$D_M = \left(\begin{array}{ccc|ccc} \lambda_1 & 0 & 0 & 0 & 0 & 0 \\ 0 & \lambda_2 & 0 & 0 & 0 & 0 \\ 0 & 0 & \lambda_3 & 0 & 0 & 0 \\ \hline 0 & 0 & 0 & \lambda_1^{-1} & 0 & 0 \\ 0 & 0 & 0 & 0 & \lambda_2^{-1} & 0 \\ 0 & 0 & 0 & 0 & 0 & \lambda_3^{-1} \end{array} \right) .$$

Now, the matrix B can be calculated as $B = SD_BS^{-1}$, where

$$D_B = \frac{1}{T} \log(D_M) \ .$$

It is important to remark that the complex logarithms of the elements of the diagonal of D_M are determined except by multiples of $2\pi\sqrt{-1}$. This means that we have certain freedom in choosing D_B, adding some multiple of $\omega_s\sqrt{-1}$ to any element of the diagonal of D_B and subtracting the same quantity to the conjugated element.

Although the matrices S and D_B are complex, B must be real. Then, it is also possible to express $B = RJ_BR^{-1}$, where R is a real symplectic matrix and J_B is the real Jordan form of B. The matrix R is easily obtained from S storing by columns the real and the imaginary parts of each complex eigenvector and its conjugated. In the case of the point L_2 of the QBCP, the Jordan matrix is of the form

$$J_B = \left(\begin{array}{ccc|ccc} 0 & 0 & 0 & \omega_1 & 0 & 0 \\ 0 & \omega_2 & 0 & 0 & 0 & 0 \\ 0 & 0 & 0 & 0 & 0 & \omega_3 \\ \hline -\omega_1 & 0 & 0 & 0 & 0 & 0 \\ 0 & 0 & 0 & 0 & -\omega_2 & 0 \\ 0 & 0 & -\omega_3 & 0 & 0 & 0 \end{array}\right),$$

where we have used the values

$$\begin{aligned} \omega_1 &= 1.34709425\text{e}{-02}\,, \\ \omega_2 &= 2.16306748\text{e}{+00}\,, \\ \omega_3 &= -6.02217885\text{e}{-02}\,. \end{aligned} \tag{4.6}$$

As a consequence of the multiple determination of the complex logarithm, it would be possible to use another values of ω_1 and ω_3, adding a multiple of ω_s (we remind that $\omega_s \simeq 0.925196$). For example, we also might use

$$\begin{aligned} \bar{\omega}_1 &= \omega_1 + 2\omega_s = 1.86386291\,, \\ \bar{\omega}_3 &= \omega_3 + 2\omega_s = 1.79017018\,. \end{aligned} \tag{4.7}$$

In such case, these values coincide with the normal frequencies associated to the small periodic orbit around L_2. Moreover, they are very similar to the frequencies of the equilibrium point L_2 in the RTBP. In the next section, we will see the advantage of taking the values 4.6 respect to other ones.

Once the matrix B is known, it is possible to compute the matrix $P(t)$ of the Floquet's theorem by means of the matrix differential equation (4.4), with the initial condition $P(0) = I$. In fact, we are interested in computing $\tilde{P}(t) = P(t)R$, with the purpose that the final form of the Hamiltonian involves J_B instead of B. Then, the differential equation (4.4) is integrated over a period and the values of $\tilde{P}$ are stored equally spaced on time in a prefixed number of points. After, these points are used to perform an FFT obtaining a Fourier series for each component of the matrix $\tilde{P}$.

Apart from the Floquet's change of variables, the matrices F_{11}, F_{12}, F_{21} and F_{22} should also be computed. So, at the same time that $\tilde{P}$ is computed and stored, the matrices

$$\begin{aligned} F_{11}^T &= \frac{-1}{2\omega_s} J_{B21} - \frac{1}{\omega_s}\left(\tilde{P}_{11}^T Q_1 \tilde{P}_{11} + \tilde{P}_{11}^T Q_2 \tilde{P}_{21} + \tilde{P}_{21}^T Q_3 \tilde{P}_{21}\right), \\ F_{12}^T &= \frac{1}{2\omega_s} J_{B11} - \frac{1}{\omega_s}\left(\tilde{P}_{12}^T Q_1 \tilde{P}_{11} + \tilde{P}_{12}^T Q_2 \tilde{P}_{21} + \tilde{P}_{22}^T Q_3 \tilde{P}_{21}\right), \\ F_{21}^T &= \frac{-1}{2\omega_s} J_{B22} - \frac{1}{\omega_s}\left(\tilde{P}_{11}^T Q_1 \tilde{P}_{12} + \tilde{P}_{11}^T Q_2 \tilde{P}_{22} + \tilde{P}_{21}^T Q_3 \tilde{P}_{22}\right), \\ F_{22}^T &= \frac{1}{2\omega_s} J_{B12} - \frac{1}{\omega_s}\left(\tilde{P}_{12}^T Q_1 \tilde{P}_{12} + \tilde{P}_{12}^T Q_2 \tilde{P}_{22} + \tilde{P}_{22}^T Q_3 \tilde{P}_{22}\right), \end{aligned}$$

are also computed and stored.

Then performing the symplectic change

$$\begin{aligned} X &= \tilde{P}_{11}x + \tilde{P}_{12}y \ , \\ Y &= \tilde{P}_{21}x + \tilde{P}_{22}y \ , \\ \Theta &= \theta \ , \\ Y_\Theta &= y_\theta + x^T F_{11}^T x + y^T F_{12}^T x + x^T F_{21}^T y + y^T F_{22}^T y, \end{aligned}$$

a Hamiltonian of the form (4.5) is transformed into

$$\begin{aligned} H(x,y,\theta,y_\theta) &= \omega_s y_\theta - \frac{1}{2}x^T J_{B21} x - x^T J_{B22} y + \frac{1}{2} y^T J_{B12} y = \\ &= \omega_s y_\theta + \frac{1}{2}\omega_1 (x_1^2 + y_1^2) + \omega_2 x_2 y_2 + \frac{1}{2}\omega_3 (x_3^2 + y_3^2) \ . \end{aligned}$$

Now, we introduce the canonical change of variables given by the complexification

$$x_j = \frac{\tilde{x}_j + \sqrt{-1}\,\tilde{y}_j}{\sqrt{2}} \ , \qquad y_j = \frac{\sqrt{-1}\,\tilde{x}_j + \tilde{y}_j}{\sqrt{2}} \ ,$$

for $j = 1, 3$, the non hyperbolic part of the Hamiltonian. In this way, the new Hamiltonian is of the form

$$H(x,y,\theta,y_\theta) = \omega_s y_\theta + \omega_1 \sqrt{-1}\, x_1 y_1 + \omega_2 x_2 y_2 + \omega_3 \sqrt{-1}\, x_3 y_3 \ ,$$

where we have used the same name for the new complex variables than before for the real old ones. In the next section, we will see that the complexification is necessary to apply an efficient algorithm to put in partial normal form terms of the Hamiltonian of order greater than two. This partial normal form allows to reduce the Hamiltonian to the center manifold and to obtain a “simplified” expression for the reduced Hamiltonian.

4.4.2 Expanding the Hamiltonian

We want to insist that, till now, it was not necessary to expand the Hamiltonian. The translation to the periodic orbit and the Floquet's change of variables are computed using the initial Hamiltonian. The composition of the three changes of variables (translation + Floquet + complexification) gives us another one of the form

$$\begin{aligned} z &= P(\theta)\tilde{z} + V(\theta) \ , \\ \theta &= \tilde{\theta} \ , \\ y_\theta &= \tilde{y}_\theta + \sum_{j=0}^{2} p_j(z,\theta) \ , \end{aligned} \tag{4.8}$$

where $z = (x_1, x_2, x_3, y_1, y_2, y_3)^T$. $P(\theta)$ is a 6×6 matrix including the Floquet's change and the complexification. Its elements are trigonometric polynomials in θ. $V(\theta)$ is the vector

$$(g_{12}, g_{14}, 0, -g_{11}, -g_{13}, 0)^T \ .$$

$p_j(z,\theta)$ are homogeneous polynomials of degree j in z and trigonometric polynomials in θ. In particular, p_0 does not depend on z and it is written as

$$p_0 = -\frac{1}{2}\left(g'_{11}(\theta)g_{12}(\theta) - g'_{12}(\theta)g_{11}(\theta) + g'_{13}(\theta)g_{14}(\theta) - g'_{14}(\theta)g_{13}(\theta)\right) .$$

Now, we insert the change (4.8) into the Hamiltonian of the QBCP. The potentials of the Earth, Moon and Sun are expanded using the recurrences involving the Legendre polynomials, but substituting the old variables by the expressions (4.8). We notice that this is the best way to perform the expansion. If we would have expanded the Hamiltonian at the very beginning and after we would have made the change of variables, the computational effort would be tremendous.

So, after the expansion, we get a Hamiltonian of the form

$$H(x,y,\theta,y_\theta) = \omega_s y_\theta + \omega_1\sqrt{-1}\,x_1y_1 + \omega_2x_2y_2 + \omega_3\sqrt{-1}\,x_3y_3 + \sum_{|k|\geq 3} H_{|k|}(x,y,\theta) ,$$

where $H_{|k|}(x,y,\theta)$ are homogeneous polynomials of degree $|k|$ in the complex variables x_1, x_2, x_3, y_1, y_2 and y_3, whose coefficients are trigonometric polynomials in θ.

4.5 Cancelling terms of order higher than two

At this point, we suppose that our Hamiltonian has the second order terms in diagonal form

$$H_2(x,y) = \omega_1x_1y_1 + \omega_2x_2y_2 + \omega_3x_3y_3 ,$$

where $\omega_i \in \mathbb{C}$, for $i = 1,2,3$. So, the complete Hamiltonian is

$$H(x,y,\theta,y_\theta) = \omega_s y_\theta + H_2(x,y) + \sum_{r\geq 3} H_r(x,y,\theta) , \tag{4.9}$$

with

$$H_r(x,y,\theta) = \sum_{|k|=r} h_r^k(\theta)\, x_1^{k_1}y_1^{k_2}x_2^{k_3}y_2^{k_4}x_3^{k_5}y_3^{k_6} ,$$

where $k = (k^1,k^2)$, with $k^1 = (k_1,k_3,k_5)$ and $k^2 = (k_2,k_4,k_6)$.

We are going to show how is possible to cancel some terms of order r of the Hamiltonian. The proposition below gives us explicitly the suitable generating function of the change of variables.

Proposition 4.1 *Consider the Hamiltonian*

$$H = \omega_s y_\theta + H_2(x,y) + \sum_{i=3}^{r-1} H_i(x,y,\theta) + H_r(x,y,\theta) + H_{r+1}(x,y,\theta) + \cdots ,$$

where $r > 2$, $H_2(x,y) = \sum \omega_i x_i y_i$ $(\omega_i \in \mathbb{C}\ )$, $H_i(x,y,\theta) = \sum_{|k|=i} h_i^k(\theta) x^{k^1} y^{k^2}$, *and* $h_i^k(\theta) = \sum_j h_{i,j}^k \exp(j\theta\sqrt{-1})$. *Let* $G_r(x,y,\theta) = \sum_{|k|=r} g_r^k(\theta) x^{k^1} y^{k^2}$ *be a generating function with*

$$g_r^k(\theta) = \sum_{j \notin J_k} \frac{h_{r,j}^k - \tilde{h}_{r,j}^k}{j\omega_s\sqrt{-1} - < \omega, k^2 - k^1 >} \exp(j\theta\sqrt{-1}) \ ,$$

where $J_k = \left\{ j \in \mathbb{Z} : j\omega_s\sqrt{-1} - < \omega, k^2 - k^1 >= 0 \right\}$ *and* $\omega = (\omega_1, \omega_2, \omega_3)$. *The coefficients* $\tilde{h}_{r,j}$ *are arbitrary, except for* $j \in J_k$ *for which* $\tilde{h}_{r,j} = h_{r,j}$. *Then, the new Hamiltonian* $\tilde{H}$ *obtained from* H *by means of the change of variables given by the generating function* G_r,

$$\tilde{H} = H + \{H, G_r\} + \frac{1}{2}\{\{H, G_r\}, G_r\} + \cdots \ ,$$

satisfies that

$$\tilde{H} = \omega_s y_\theta + H_2(x,y) + \sum_{i=3}^{r-1} H_i(x,y,\theta) + \tilde{H}_r(x,y,\theta) + \tilde{H}_{r+1}(x,y,\theta) + \cdots \ ,$$

where $\tilde{H}_r(x,y,\theta) = \sum_{|k|=r} \tilde{h}_r^k(\theta) x^{k^1} y^{k^2}$ *and* $\tilde{h}_r^k(\theta) = \sum_j \tilde{h}_{r,j}^k \exp(j\theta\sqrt{-1})$.

Remarks: We notice that the terms with $j \in J_k$ are resonant terms. At this point, they can not be modified. In order to get a Hamiltonian as simple as possible, the coefficients $\tilde{h}_{r,j}^k$ (for $j \notin J_k$) are usually taken equal to zero. Nevertheless, when $j\omega_s\sqrt{-1} - < \omega, k^2 - k^1 >$ is small, it is also advisable not to cancel the corresponding term. In such case, we also set $\tilde{h}_{r,j} = h_{r,j}$.

Proof: The terms of order r of the new Hamiltonian come from

$$\tilde{H}_r = H_r + \{\omega_s y_\theta, G_r\} + \{H_2, G_r\} \ .$$

By straightforward calculation we get the Poisson brackets,

$$\begin{aligned} \{\omega_s y_\theta, G_r\} &= -\omega_s \frac{\partial G_r}{\partial \theta} \ , \\ \{H_2, G_r\} &= \sum_{|k|=r} < \omega, k^2 - k^1 > g_r^k(\theta) x^{k^1} y^{k^2} \ . \end{aligned}$$

Then,

$$\tilde{H}_r = H_r - \omega_s \frac{\partial G_r}{\partial \theta} + \sum_{|k|=r} < \omega, k^2 - k^1 > g_r^k(\theta) x^{k^1} y^{k^2} \ .$$

Imposing that $\tilde{H}_r = \sum_{|k|=r} \tilde{h}_r^k(\theta) x^{k^1} y^{k^2}$, we arrive at a linear differential equation for the functions $g_r^k(\theta)$. That is

$$\omega_s \frac{dg_r^k}{d\theta} - < \omega, k^2 - k^1 > g_r^k(\theta) = h_r^k(\theta) - \tilde{h}_r^k(\theta) \; .$$

A solution of this equation is

$$g_r^k(\theta) = \sum_{j \notin J_k} \frac{h_{r,j}^k - \tilde{h}_{r,j}^k}{j\omega_s\sqrt{-1} - < \omega, k^2 - k^1 >} \exp\left(j\theta\sqrt{-1}\right) \; .$$

We notice that if $j \in J_k$ then $\tilde{h}_{r,j}^k$ must be equal to $h_{r,j}^k$ in order to avoid secular terms. ■

At that point, we stress that the simplicity in obtaining the generating function from the terms to be cancelled in H_r relies on the fact that we use the complexification introduced at the end of subsection 4.4.1. Then, in the Fourier space, the systems to be solved are diagonal.

4.6 Reduction to the central manifold

In this section, suppose that we have a Hamiltonian of the form (4.9), where the hyperbolic part corresponds to the variables x_2 and y_2. We recall that their exponents in the expansion have been called k_3 and k_4, respectively. To obtain the Hamiltonian reduced to the central manifold it is only necessary to cancel all the terms with $k_3 + k_4 = 1$. That is, $k_3 = 1$ and $k_4 = 0$, or $k_3 = 0$ and $k_4 = 1$. Moreover, in order to get a final Hamiltonian with the terms not depending on x_2 and y_2 as simple as possible, it would be desirable to cancel all those terms which depend on time. We also decided to cancel all the terms not depending on time, x_2 and y_2, as long as the divisor involved in the generating function was larger than 0.05. Other strategies may be used. For example, it would be possible to cancel also terms with a small divisor if the corresponding coefficient $h_{r,j}^k$ is small enough.

We notice that there is no difficulty in cancelling the terms of degree 1 in the couple x_2 and y_2. The divisor in the generating function to cancel those terms is

$$j\omega_s\sqrt{-1} \pm \omega_2 \; ,$$

which is always different from zero, and even more, it is never small (see the present value of ω_2 in 4.6).

Concerning the terms not depending on x_2 and y_2, we discuss separately two different cases:

- Terms not depending on time: in this case, there are resonant terms which can not be cancelled. They are the ones which have $k^1 = k^2$. Apart from those terms, there are some others which can introduce small divisors in the change of variables, leading to convergence problems. For this reason, we choose the threshold $\varepsilon = 0.05$ and we kept all the terms with $< \omega, k^2 - k^1 > < \varepsilon$.

- Terms depending on time: it is very important to point out that it is possible to remove the dependency on time without introducing small divisors at low order. This is due to the fact that we choose the values of ω_1 and ω_3 as small as possible (see 4.6). If we would have selected some other values like $\bar{\omega}_1$ and $\bar{\omega}_3$, then small divisors would have appeared at low order, for instance, $\bar{\omega}_1 - 2\omega_s$, and so, the Hamiltonian reduced to the central manifold would depend on time. However, using the smallest values of ω_1 and ω_3, the first divisor smaller than 0.05 is $\omega_s + 15\,\omega_3$. In this way, the final Hamiltonian is autonomous up to high order.

Using the proposition 4.1, we can find generating functions G_3, G_4, ..., G_n to put the Hamiltonian in partial normal form up to order n. We want to point out that each change of variables G_r modifies the terms of order higher than r of the Hamiltonian. This means that before computing the next change G_{r+1}, it is necessary to transform the Hamiltonian by G_r.

Once we have the Hamiltonian in partial normal form, the central manifold is simply $x_2 = y_2 = 0$. So, the Hamiltonian reduced to the central manifold is the Hamiltonian restricted to $x_2 = y_2 = 0$. That is the terms not depending on x_2 and y_2.

In order to get the Hamiltonian in real coordinates, another change of variables must be applied. We call it *realification* and it is the inverse of the complexification done before. It is

$$\begin{aligned} x_i &= \frac{\tilde{x}_i - \sqrt{-1}\,\tilde{y}_i}{\sqrt{2}} , \\ y_i &= \frac{-\sqrt{-1}\,\tilde{x}_i + \tilde{y}_i}{\sqrt{2}} , \end{aligned}$$

for $i = 1, 3$. As usual, the variables with tilde are the new ones, but, in the following, we denote the new variables with the same name that the old ones. If all the computations done are correct, the final Hamiltonian must be real. In other words, the imaginary part of the Hamiltonian must be zero.

Using all these changes of variables, the Hamiltonian reduced to the central manifold around L_2 up to order 16 was computed. It is of the form

$$H_{CM} = \frac{1}{2}\omega_1(x_1^2 + y_1^2) + \frac{1}{2}\omega_3(x_3^2 + y_3^2) + \sum_k h_k\, x_1^{k_1} y_1^{k_2} x_3^{k_5} y_3^{k_6} , \qquad (4.10)$$

with $h_k \in \mathbb{R}$. Although there were some few terms of order 15 and 16 leading to small divisors, they were also cancelled because they were not important (that is, their coefficients were small enough). So, with the reduction to the central manifold, we obtain an autonomous Hamiltonian. Table 4.1 shows the coefficients of the Hamiltonian reduced to the central manifold up to order 6 around L_2.

We want to comment that the Hamiltonian H_{CM} presents a symmetry

$$\tilde{S}_1 : (x_1, y_1, x_3, y_3) \quad \longleftrightarrow \quad (x_1, y_1, -x_3, -y_3) .$$

We also computed the composition of all the changes of variables performed. We recall that they are the translation to the periodic orbit, the Floquet's change, the complexification, the changes generated by G_3, G_4, ..., G_{16} and the realification. The result is a change of variables of the form

$$\begin{aligned} x_j &= p_j(\tilde{x}, \tilde{y}, \theta) , \\ y_j &= q_j(\tilde{x}, \tilde{y}, \theta) , \qquad\qquad j = 1, 2, 3, \\ \theta &= \tilde{\theta} , \\ y_\theta &= \tilde{y}_\theta + r(\tilde{x}, \tilde{y}, \theta) , \end{aligned}$$

where p_j, q_j and r are polynomials of degree 15 in x_1, x_2, x_3, y_1, y_2 and y_3, whose coefficients are trigonometric polynomials in θ. It is a change of variables T-periodic with respect to the time.

4.7 Description of the neighbourhood of L_2

We would like to study the Hamiltonian restricted to the central manifold H_{CM}. In fact, we are only able to study some polynomial approximation of it. Typically, we take the approximation of order 16. When required we make comments on the approximation of other degrees. For shortness, we shall keep the name H_{CM} for the order 16 approximation. All the objects studied (say fixed points, periodic orbits, invariant manifolds, ...), should be interpreted in terms of the initial coordinates of the QBCP. From now on, the coordinates of the central manifold are called central coordinates.

The origin of the central coordinates is a fixed point that, by construction, corresponds to the small periodic orbit around L_2 (see figure 2.3). However, we have found four additional fixed points in the plane $x_3 = 0$. Their coordinates and energy levels are shown in table 4.2. They have been labelled with the same label that their corresponding periodic orbits 22, 23, 24 and 25 (see figure 2.10). Those periodic orbits are the ones coming from the planar Lyapunov periodic orbit of the RTBP with period $T/2$. This means that the frequency of these orbits is resonant with $2\omega_s$.

We want to comment that the fixed points 22-25 have the same stability character that their corresponding orbits. The points 22 and 24 are center×center. The other ones, 23 and 25, are saddle×center. All this, of course, inside the central manifold.

Besides the fixed points on the plane $x_3 = 0$, there are another four fixed points outside of the plane. They should correspond to the resonant Halo orbits of the QBCP, labelled as 2A and 2C (and the symmetric ones) in chapter 2 (see figure 2.12). But, the location of these fixed points changes a lot when considering the Hamiltonian H_{CM} up to order 12, 14 and 16. This suggests that those Halo orbits are too big and there the Hamiltonian H_{CM} does not give a good approximation of the central manifold. Later on, we will talk about the accuracy of the reduction to the central manifold. The table 4.3 shows the coordinates of one of the fixed points at different orders.

2	0	0	0	6.7354712316966e−03	3	0	0	2	−5.8044675423270e−02
0	2	0	0	6.7354712316966e−03	2	1	0	2	−5.7658029096397e−02
0	0	2	0	−3.0110894235045e−02	1	2	0	2	−5.7658028261671e−02
0	0	0	2	−3.0110894235045e−02	0	3	0	2	−5.8044675028007e−02
3	0	0	0	5.8425430477497e−04	1	0	2	2	6.3460508607054e−02
2	1	0	0	5.8032148799055e−04	0	1	2	2	6.3460508653628e−02
1	2	0	0	5.8032140416523e−04	1	0	0	4	3.1730254303527e−02
0	3	0	0	5.8425438804155e−04	0	1	0	4	3.1730254326814e−02
1	0	2	0	2.7356827092887e−04	6	0	0	0	−2.7367839948456e+00
0	1	2	0	2.7356835588679e−04	5	1	0	0	4.1869541110887e−02
1	0	0	2	2.7356827092887e−04	4	2	0	0	−8.2103519833796e+00
0	1	0	2	2.7356835588679e−04	3	3	0	0	8.3739082221775e−02
4	0	0	0	−4.8649689279931e−01	2	4	0	0	−8.2103519822224e+00
3	1	0	0	4.9428142536864e−03	1	5	0	0	4.1869541110887e−02
2	2	0	0	−9.7299378564824e−01	0	6	0	0	−2.7367839936884e+00
1	3	0	0	4.9428142536864e−03	4	0	2	0	3.5467715078410e+01
0	4	0	0	−4.8649689284892e−01	3	1	2	0	−4.1328221157921e−01
2	0	2	0	7.8868569642648e−01	2	2	2	0	7.0935430151485e+01
1	1	2	0	−4.5823783204011e−03	1	3	2	0	−4.1328221157921e−01
0	2	2	0	7.8868569627411e−01	0	4	2	0	3.5467715073075e+01
0	0	4	0	−3.2236673891427e−01	2	0	4	0	−3.2360676287824e+01
2	0	0	2	7.8868569642648e−01	1	1	4	0	2.0156264504323e−01
1	1	0	2	−4.5823783204011e−03	0	2	4	0	−3.2360676286492e+01
0	2	0	2	7.8868569627411e−01	0	0	6	0	−1.7154534331248e+00
0	0	2	2	−6.4473347782855e−01	4	0	0	2	3.5467715078410e+01
0	0	0	4	−3.2236673891427e−01	3	1	0	2	−4.1328221157921e−01
5	0	0	0	1.4507302003533e−03	2	2	0	2	7.0935430151485e+01
4	1	0	0	1.4413422556020e−03	1	3	0	2	−4.1328221157921e−01
3	2	0	0	2.8920739745417e−03	0	4	0	2	3.5467715073075e+01
2	3	0	0	2.8920725106237e−03	2	0	2	2	−6.4721352575647e+01
1	4	0	0	1.4413437741884e−03	1	1	2	2	4.0312529008646e−01
0	5	0	0	1.4507302550217e−03	0	2	2	2	−6.4721352572985e+01
3	0	2	0	−5.8044675423270e−02	0	0	4	2	−5.1463602993744e+00
2	1	2	0	−5.7658029096397e−02	2	0	0	4	−3.2360676287824e+01
1	2	2	0	−5.7658028261671e−02	1	1	0	4	2.0156264504323e−01
0	3	2	0	−5.8044675028007e−02	0	2	0	4	−3.2360676286492e+01
1	0	4	0	3.1730254303527e−02	0	0	2	4	−5.1463602993744e+00
0	1	4	0	3.1730254326814e−02	0	0	0	6	−1.7154534331248e+00

Table 4.1: Hamiltonian reduced to the central manifold up to order 6 around L_2.

Label	x_1	y_1	h
22	5.7778288e−02	5.7778292e−02	2.30211298e−05
23	−6.6225712e−02	−4.5813575e−02	2.21256116e−05
24	−5.6944434e−02	−5.6943907e−02	2.21256717e−05
25	−4.5813275e−02	−6.6225920e−02	2.21256116e−05

Table 4.2: Fixed points of H_{CM} on the plane $x_3 = 0$. The fourth column shows the energy level $h = H_{CM}(x_1, y_1, 0, 0)$.

Order	$x_1 \simeq y_1$	$x_3 \simeq y_3$
12	9.4359e−02	2.9656e−02
14	9.1658e−02	2.5544e−02
16	8.9707e−02	2.2546e−02

Table 4.3: A fixed point outside the plane $x_3 = 0$ when H_{CM} is taken up to orders 12, 14 and 16.

The Hamiltonian H_{CM} has two degrees of freedom, so the phase space has dimension four. For each level of energy, we can define the Poincaré map through the surface of section $\{x_3 = 0,\ \dot{x}_3 > 0\}$. This is a map defined from a two dimensional space to itself. In the following pages, there are several figures showing some hundreds of iterations of the Poincaré map for different levels of energy.

We observe that the surface $x_3 = y_3 = 0$ is invariant for the change of variables relating the initial coordinates with the central ones. This means that the orbits living on the plane $x_3 = 0$ also stand on the plane when coming back to the initial coordinates of the QBCP. For those orbits, the Poincaré map is not defined. Later on, we will talk about the boundary of the region where the Poincaré map is defined and we will see that sometimes it is a planar orbit on $x_3 = 0$, but in other cases it is an orbit outside this plane (see figure 4.7 and related text).

Figure 4.1a shows the Poincaré map for the level of energy $h = 2.25{\cdot}10^{-5}$, which is smaller than h_{22}, the highest possible level of energy. In that figure, an island is seen. In the middle of the island there is a fixed point of the Poincaré map. That is a *vertical* periodic orbit of the Hamiltonian H_{CM}. Here, vertical means locally orthogonal to the plane $x_3 = 0$. Going back to the initial coordinates of the QBCP, we see that it corresponds to a 2D torus. That torus is close to the periodic orbit labelled as 22. In fact, we will see later that there is a family of $2D$ tori starting at the orbit 22. That is a resonant family of tori which is characterized by the fact that the main *horizontal* frequency is equal to $2\omega_s$. Here, horizontal means on the (x, y)-plane.

For the level h_{22} there is only one admissible point on the Poincaré section. It corresponds, of course, to orbit of label 22 and it is located very close to center of the innermost invariant curve shown in figure 4.1a.

The boundary of the region where the Poincaré map of figure 4.1a is defined is a planar orbit. It is a periodic orbit on the plane $x_1 y_1$. That is a planar 2D torus in the coordinates of the QBCP. Figure 4.3 shows a section of that torus. That section was obtained integrating numerically the equations of H_{CM}, taking a point of the boundary as initial condition for $t = 0$. Then, all the points with $t = 0 \pmod{T/8}$ were stored. After that, they were transformed into the initial coordinates of the QBCP. Since the main frequency of the torus is $2\omega_s$, we have four points per revolution around L_2. Those points describe four curves. Each one is homeomorphic to an $\mathbb{S}^1$. As it is natural, any slice of a 2D torus is expected to be an $\mathbb{S}^1$ (except degenerated cases).

Figure 4.1b corresponds to the level $h = 2.212562 \cdot 10^{-5}$. It is between h_{24} and $h_{23} = h_{25}$. In the left lower part of the figure, we see a narrow island associated with the elliptic fixed point 24. The same comments made for the island of figure 4.1a hold for the islands of figure 4.1b.

Figure 4.1c shows the case of $h = h_{23} = h_{25}$. Fixed points 23 and 25 have the same energy. In the figure, the invariant manifolds of that points have also been displayed. These manifolds are planar because they are the boundary of the region where the Poincaré map is defined for this level of energy. There is a double heteroclinic connection between the points 23 and 25. That is, the unstable manifolds of one of them coincide with the stable manifolds of the other one. They are algebraic curves satisfying

$$H_{CM}(x_1, y_1, 0, 0) = h_{23} = h_{25} \ .$$

We recall that here H_{CM} denotes the present approximation of the Hamiltonian reduced to the center manifold, that is, a polynomial of degree 16. A "true" center manifold is, probably, only C^∞ and the same happens for the reduced Hamiltonian. Furthermore, because of the invariance of the $x_3 = y_3 = 0$ plane, $H_{CM}(x_1, y_1, 0, 0)$ is a Hamiltonian of one degree of freedom. This explains why an "exact" connection appears. It is difficult to appreciate the heteroclinic connection of the left lower part of figure 4.1c. The manifolds are very close and so, in the figure, it is not possible to see neither the difference between the manifolds nor the island inside.

Now, we are interested in knowing how the previous manifolds look like in the initial coordinates of the QBCP. For this purpose, we take points in the stable/unstable manifolds for $t = 0 \pmod{T}$. Those points are transformed by means of the change of variables, coming back to the initial coordinates. Figure 4.4 shows the resulting points. These points describe curves tending to the points of the orbits for $t = 0$. For example, in the stable manifold of the periodic orbit 25, there are orbits rotating around L_2 in a way similar to the periodic orbit. But, the orbit in the stable manifold has a certain precession. That means that it rotates a little bit faster (or slower, depending on the branch of the stable manifold) than the periodic orbit. Therefore, looking at the orbits for instants of time spaced by the period T, the periodic orbit gives a fixed point. The orbit in the stable manifold gives a set of points tending to that fixed point.

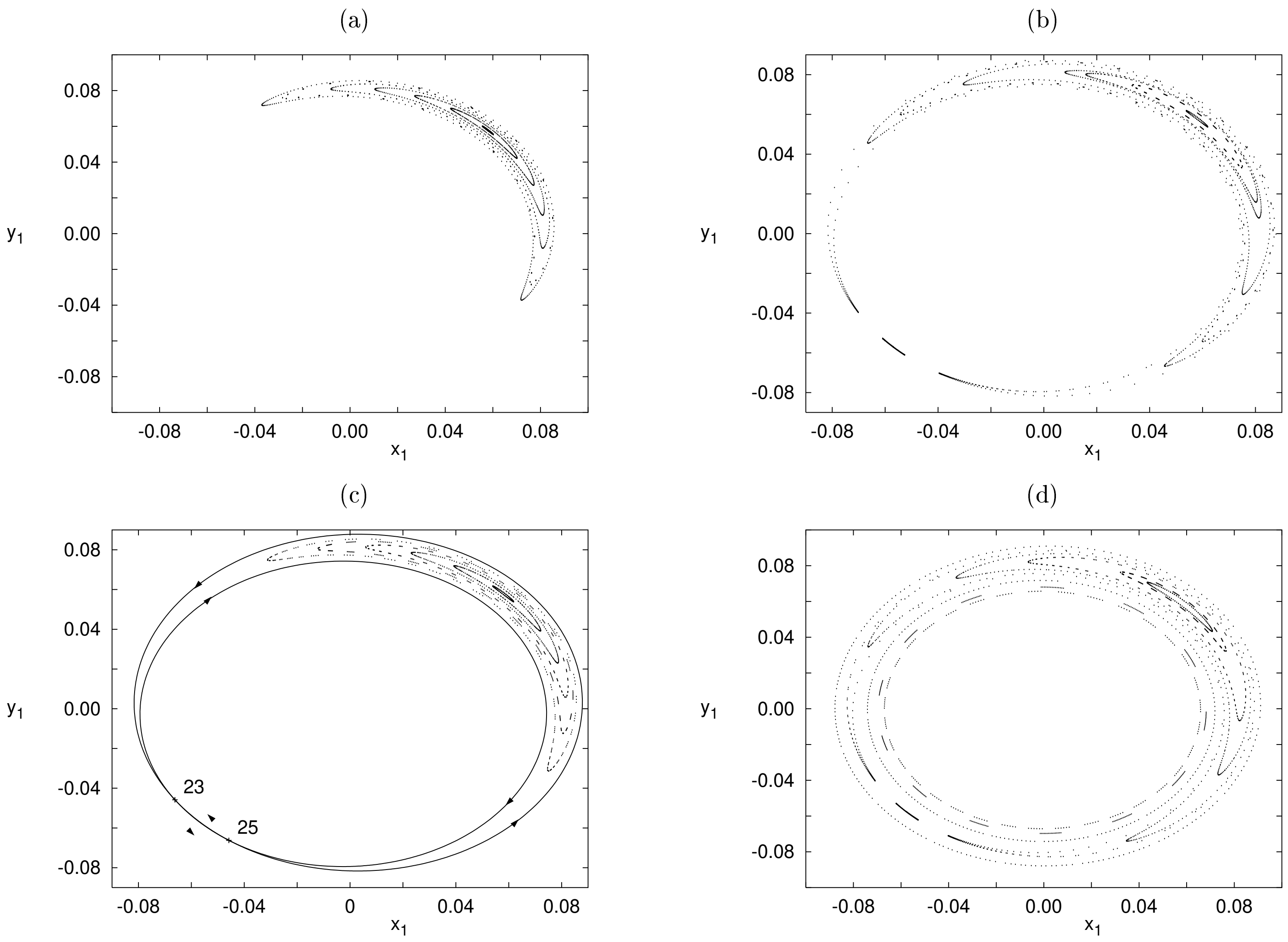

Figure 4.1: Poincaré map for several energy levels: (a) $h = 2.25 \cdot 10^{-5}$, (b) $h = 2.212562 \cdot 10^{-5}$, (c) $h = 2.21256116 \cdot 10^{-5}$, (d) $h = 2 \cdot 10^{-5}$.

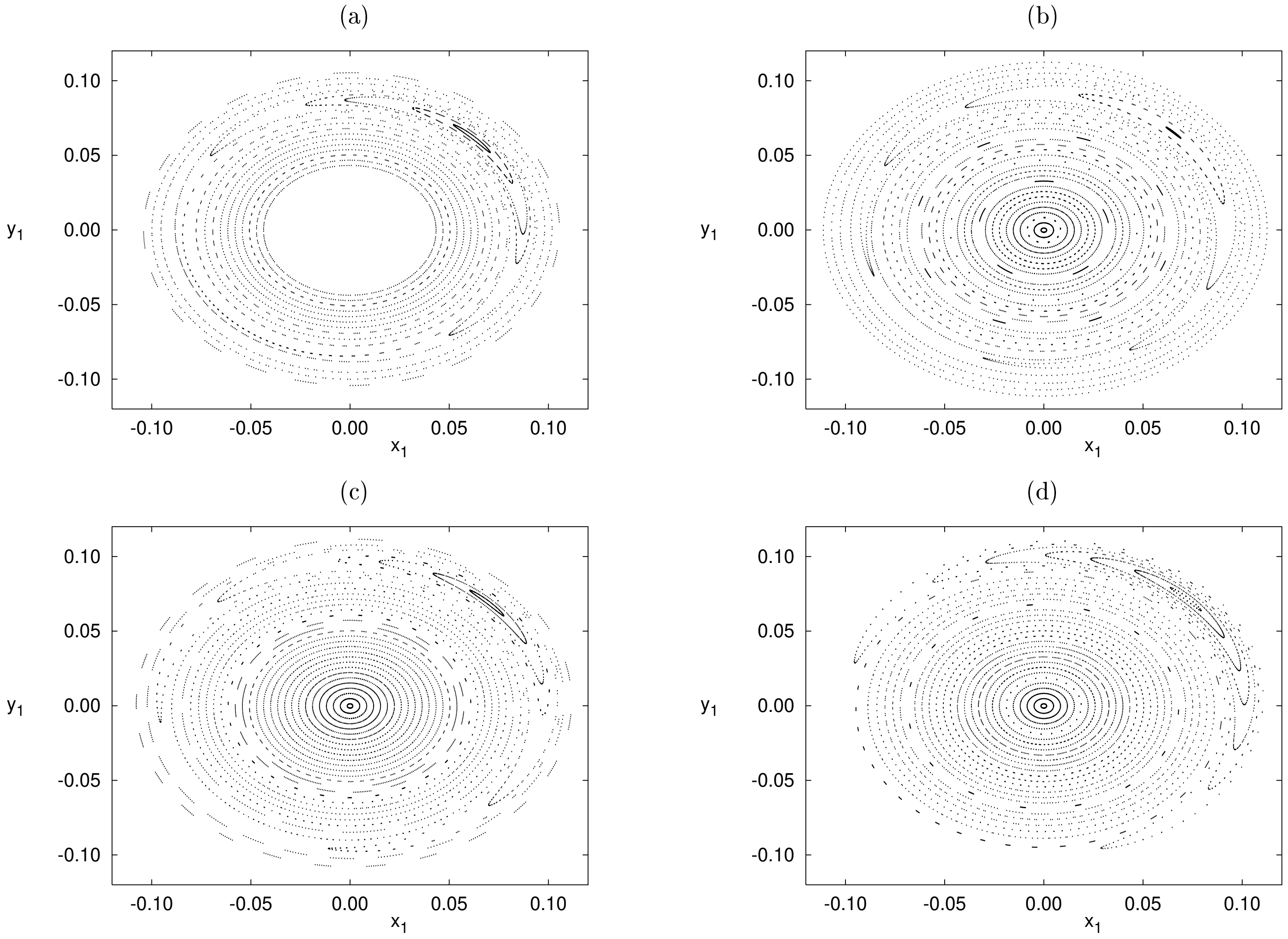

Figure 4.2: Poincaré map for several energy levels: (a) $h = 10^{-5}$, (b) $h = 0$, (c) $h = -10^{-5}$, (d) $h = -1.60122 \cdot 10^{-5}$.

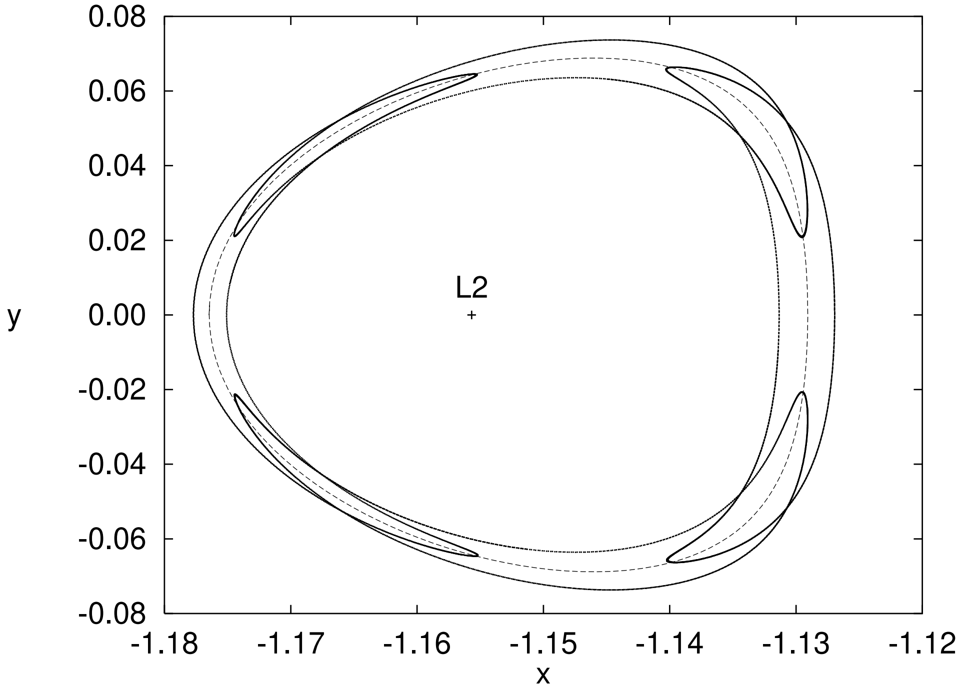

Figure 4.3: Section $t = 0 \pmod{T/8}$ of the boundary torus of figure 4.1a (QBCP coordinates). The dashed line is the periodic orbit 22. It has been plotted only for reference.

We remark that, in the Hamiltonian H_{CM}, the invariant manifolds of the point 23 coincide with the ones of the point 25. However, in the QBCP, probably, there is an splitting of the stable (resp. unstable) manifold of the periodic orbit 23 and the unstable (resp. stable) one of the orbit 25. The source of this splitting relies on the lack of convergence of the reduction to the center manifold and the "autonomization" of the Hamiltonian by cancelling the dependence with respect to θ.

Figure 4.1d shows the Poincaré map for the level $h = 2{\cdot}10^{-5}$. The region where the Poincaré map is defined is an annulus. The boundaries of this annulus are planar quasi-periodic Lyapunov orbits of the QBCP. Note that two of such orbits (the inner one and the outer one) sit in the same level of energy of H_{CM}. They have been drawn in figure 4.5. In that level of energy, we observe that there are four fixed points of the Poincaré map. One in the right upper part of the figure and the other three in the left lower part. Two of them are elliptic and the other two hyperbolic. We denote by $p_2(h)$, $p_3(h)$, $p_4(h)$ and $p_5(h)$ the fixed points of the Poincaré map at energy level h, related to the fixed points of H_{CM} labelled as 22, 23, 24 and 25, respectively. All of these fixed points are *vertical* periodic orbits of the Hamiltonian H_{CM}. Coming back to the coordinates of the QBCP, they become 2D tori. Each of these tori belongs to a family of 2D tori which starts at one of the planar Lyapunov resonant periodic orbits (labelled also as 22, 23, 24 and 25). Of course, these families are not continuous. They are supposed to be Cantor sets of 2D tori, but there is not any proof of it.

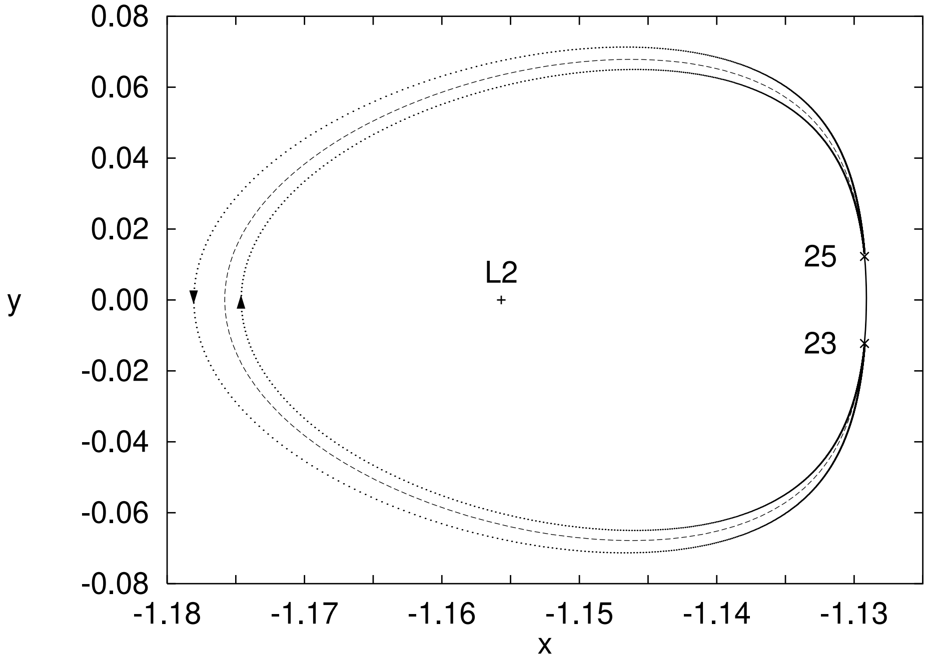

Figure 4.4: Invariant manifolds of the periodic orbits 23 and 25, for $t = 0 \pmod{T}$. (QBCP coordinates). The periodic orbit 23 (dashed line) has been drawn for reference.

Figure 4.2a, corresponding to the energy level 10^{-5}, is similar to 4.1d, but there are two differences. One of them is evident: the "hole" of the annulus is smaller than in the previous case. We see that decreasing the value of the energy, the size of the hole is also decreasing. The other difference is that there are only two fixed points of the Poincaré map. One of them, p_2, in the upper right part of figure 4.2a and the other one, p_4, in the lower left part. Notice that, by decreasing the energy, the fixed points p_3, p_4 and p_5 have joined at a pitchfork bifurcation. This happens for the level of energy $h_b = 1.707 \cdot 10^{-5}$ (see figure 4.6). For $h > h_b$, p_4 is elliptic and for $h < h_b$, p_4 becomes hyperbolic. This means that the three families of 2D tori of the QBCP coming from periodic orbits 23, 24 and 25 join at a bifurcation and after this, only one family subsists.

Figure 4.2b is for the value of the energy $h = 0$. This is the energy of the origin of coordinates. That point is a fixed point of the Hamiltonian H_{CM} of the type center $\times$ center. That fixed point corresponds to the small periodic orbit around L_2 (see figure 2.3). From the origin, two families of 2D Lyapunov tori start. The planar one and the vertical one. We have already mentioned the planar one and we are going to talk later on about the other one.

In the RTBP, two Lyapunov families of periodic orbits emanate from the equilibrium point L_2. The results of [14], about the persistence of lower dimensional tori under quasi-periodic perturbations, suggest that, in the QBCP, two Lyapunov families are Cantor sets of 2D tori, as in the BCP.

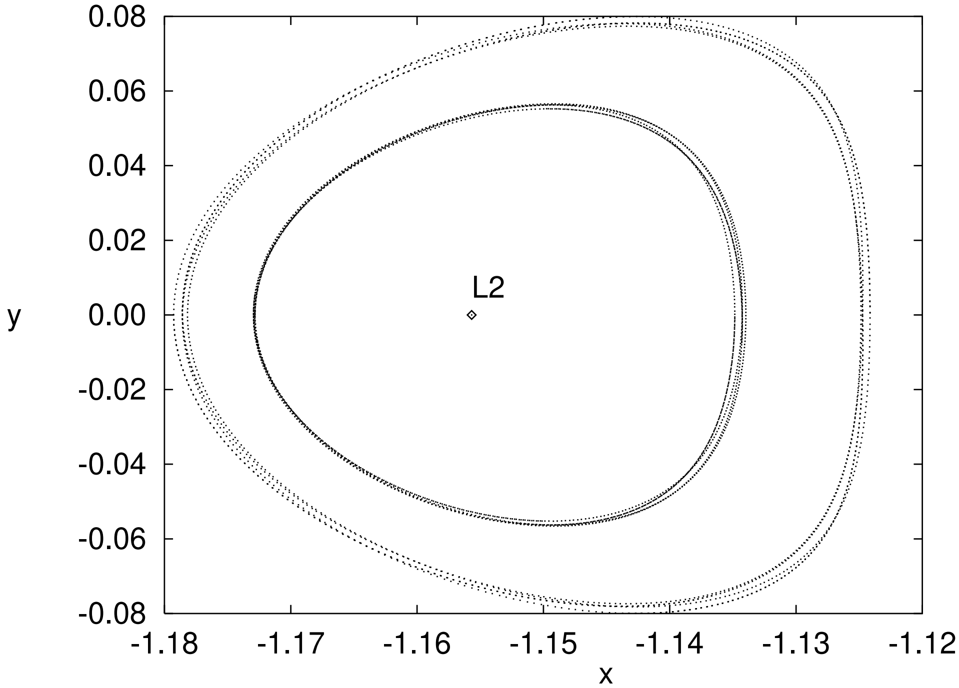

Figure 4.5: Planar quasi-periodic Lyapunov orbits of the boundary of the Poincaré map for $h = 2 \cdot 10^{-5}$. We have drawn the points for the time $t = kT/8$, $k = 0, \ldots, 2048$.

Now, we want to comment something more about the boundary of the domain of the Poincaré map. For higher levels of energy, that boundary is a planar orbit. It corresponds to a quasi-periodic orbit of the QBCP. To study the boundary of the Poincaré map, firstly, we consider orbits with initial conditions on the line $x_1 = y_1$ on the plane $x_3 = 0$. For levels of energy $h \geq h_c = 2.5304405 \cdot 10^{-6}$, the boundary is a planar orbit. For $h < h_c$, this is not true. Figures 4.7a-d show the value of y_3 along a piece of the line $x_1 = y_1$ on the plane $x_3 = 0$, for energy levels $h = 10^{-5}, h_c, 0, -5 10^{-6}$. We note that h_c is the critical value for the change of behaviour. For energy $h < h_c$, there is a narrow zone in the right hand side of figures 4.7c-d where there are two positive possible values of y_3 for each x_1. However, this can not be seen in figure 4.2b because it affects to a very small zone. It also can not be seen in figures 4.2c-d because that zone is too far. Now, for a given angle φ, consider orbits with initial conditions on the straight line in the direction of the vector $(\cos\varphi, \sin\varphi)$ on the (x_1, y_1)-plane. Decreasing the level of energy, there is a value $h_c(\varphi)$ where the boundary starts to be an orbit outside this plane. Figure 4.7e shows the critical value h_c as function of φ.

Figure 4.2c corresponds to the level of energy $h = -10^{-5}$. It is similar to the previous one. In the top right part, as usual, there is an elliptic fixed point corresponding to a 2D torus. Several projections of that torus are shown in figure 4.8. In the Poincaré section, around that fixed point, there are invariant curves. Coming back to the QBCP coordinates, these curves become 3D tori around the

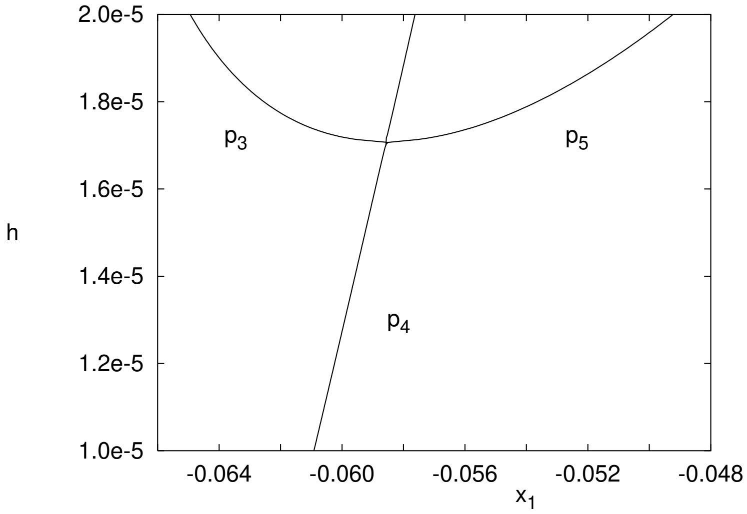

Figure 4.6: Bifurcation of 2D tori of the QBCP. Decreasing the energy, families of fixed points of the Poincaré maps p_3, p_4 and p_5 join at $h = 1.707 \cdot 10^{-5}$. After that, only the branch of p_4 subsists. These fixed points correspond to the families of 2D tori related to periodic orbits 23, 24 and 25.

previous 2D torus. In figure 4.9, we have plotted the points for the time $t = kT/8$, $k = 0, \ldots, 8192$. Since the main frequency in the xy-plane of this torus is $2\omega_s$, those points are describing four nice 2D tori. As it is natural, the section of a 3D torus looks like a 2D torus. Figure 4.10 shows a magnification of one of those tori. In that figure, we also have included the corresponding section of the 2D torus which is the core of the family of 3D tori.

We have said before that, in the QBCP, a family of *vertical* quasi-periodic Lyapunov orbits starts from the orbit substituting the point L_2. In the Poincaré map, for negative values of the energy, that family of 2D tori is the origin of coordinates. That point is a fixed point of the Poincaré map. For $h = 0$, it is also a fixed point of H_{CM}. However, for negative values of the energy, it is a periodic orbit of H_{CM}. That periodic orbit becomes a 2D torus when applying the change of variables to come back to the coordinates of the QBCP. That family of 2D tori is called the *eight-shaped* family. The reason of that name is clear when looking at one of this torus. Figure 4.11 shows several projections of the torus corresponding to the level $h = -10^{-5}$. Note the small relative size of the scale in the y variable.

In the Poincaré map, around the origin, there are invariant curves. Generically, these curves are 3D torus of the QBCP. They are tori of the Lissajous type. Figure 4.12 shows one of these tori for the level of energy $h = -10^{-5}$. We have talked before about the invariant curves around fixed point p_2 of the Poincaré map. They are 3D tori of the QBCP. These tori and the Lissajous tori are effectively separated by the stable and unstable manifolds of the 2D tori associated with the hyperbolic fixed points of the Poincaré map. We recall that p_3 and p_5 are hyperbolic for $h > h_b$ and p_2 is hyperbolic for $h < h_b$. We note that, probably, there is an splitting between

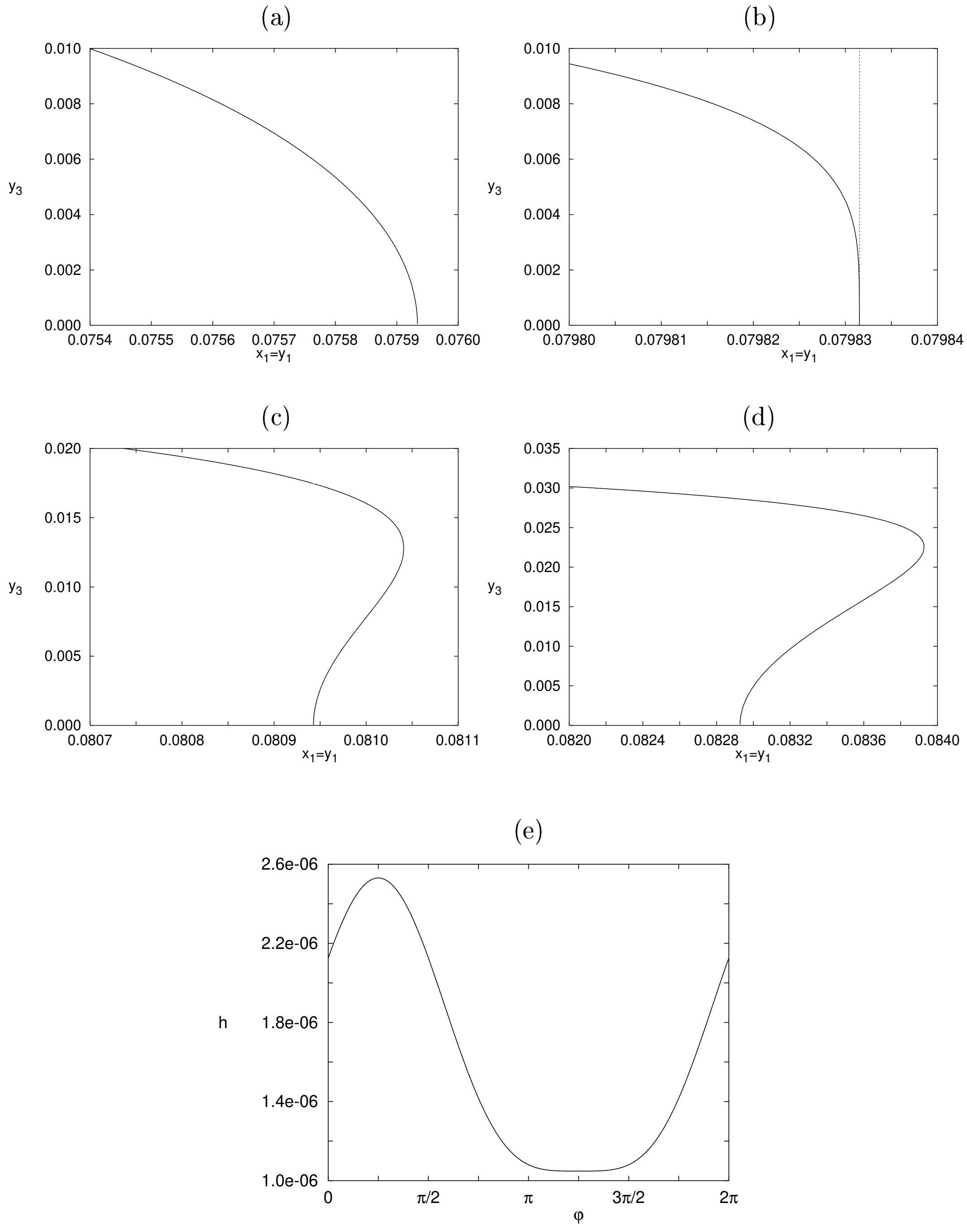

Figure 4.7: Boundary of the domain of the Poincaré map. Positive value of y_3 along $x_1 = y_1$, $x_3 = 0$, for the levels of energy $h = 10^{-5}, h_{c,\pi/4}, 0, -5\cdot 10^{-6}$ (a, b, c and d, respectively), where $h_{c,\pi/4} = 2.5304405\cdot 10^{-6}$. Figure (e) shows the critical value h_c along straight lines in the direction of $(\cos\varphi, \sin\varphi)$ on the (x_1, y_1)-plane.

the stable and the unstable manifolds, but a particle crossing the separatrix zone would spend a very long time.

The last Poincaré section shown is at figure 4.2d. It is similar to the previous one. The only reason to include this figure is to notice that the island in the top right part of the figure is going farther when decreasing the energy.

4.7.1 Accuracy of the central manifold

In order to check all the computations done for the reduction to the central manifold, several tests have been implemented for different parts of the process. Here, we are going to talk only about a check involving the final Hamiltonian, H_{CM}, and the initial one, H_{QBCP}.

We take an initial point in the central manifold, say $x_{cm}^{(0)}$. The Hamiltonian equations of H_{CM} are integrated with that initial condition, for a time interval of $T/2$, for instance. Let $x_{cm}^{(1)}$ be the point obtained. Both points, $x_{cm}^{(0)}$ and $x_{cm}^{(1)}$, can be transformed by the change of variables obtaining $x_{qbcp}^{(0)}$ and $x_{qbcp}^{(1)}$, in the coordinates of the QBCP. Integrating the Hamiltonian equations of H_{QBCP} for a time span of $T/2$ with initial condition $x_{qbcp}^{(0)}$, it is expected to get a point close to $x_{qbcp}^{(1)}$. Let d be the distance between $x_{qbcp}^{(1)}$ and the resulting point of the integration. That distance can be considered as a function of $x_{cm}^{(0)}$.

We remind that the orbits around L_2 in the QBCP are highly unstable. If the initial conditions have some error, after the integration for a time interval of $T/2$, that error is amplified by a factor about 1000.

The distance d has been computed for several points in the central manifold along the line $x_1 = y_1$, $x_3 = 0$, for some levels of energy. Figure 4.13 shows the results for $h = 10^{-5}, 0, -10^{-5}$, respectively. The tests have been done using the Hamiltonian reduced to the central manifold up to order 8, 12 and 16. We notice that, for large orbits, the results do not improve when increasing the order. That is related to the fact that the expansions are not convergent in any open set. However, the reduction to the central manifold up to order 16 gives a good approximation of the dynamics in a neighbourhood of L_2 up to a distance of about 10000 km.

4.7.2 Frequency analysis

We are interested in knowing where the Halo orbits are located inside the central manifold. Unfortunately, in the Poincaré maps shown before, it is not possible to see easily them. The main key to detect where these orbits are located has been the Fourier analysis to estimate the frequencies and the amplitudes of several orbits of the central manifold. For this purpose, we have used a very accurate method developed in [11] and [21]. The method combines a classical FFT with an iterative improvement of the frequencies and amplitudes (see [21] for details).

The Halo orbits are characterized by the fact that the main horizontal frequency is equal to the main vertical one. In the RTBP, Halo orbits are a one parameter

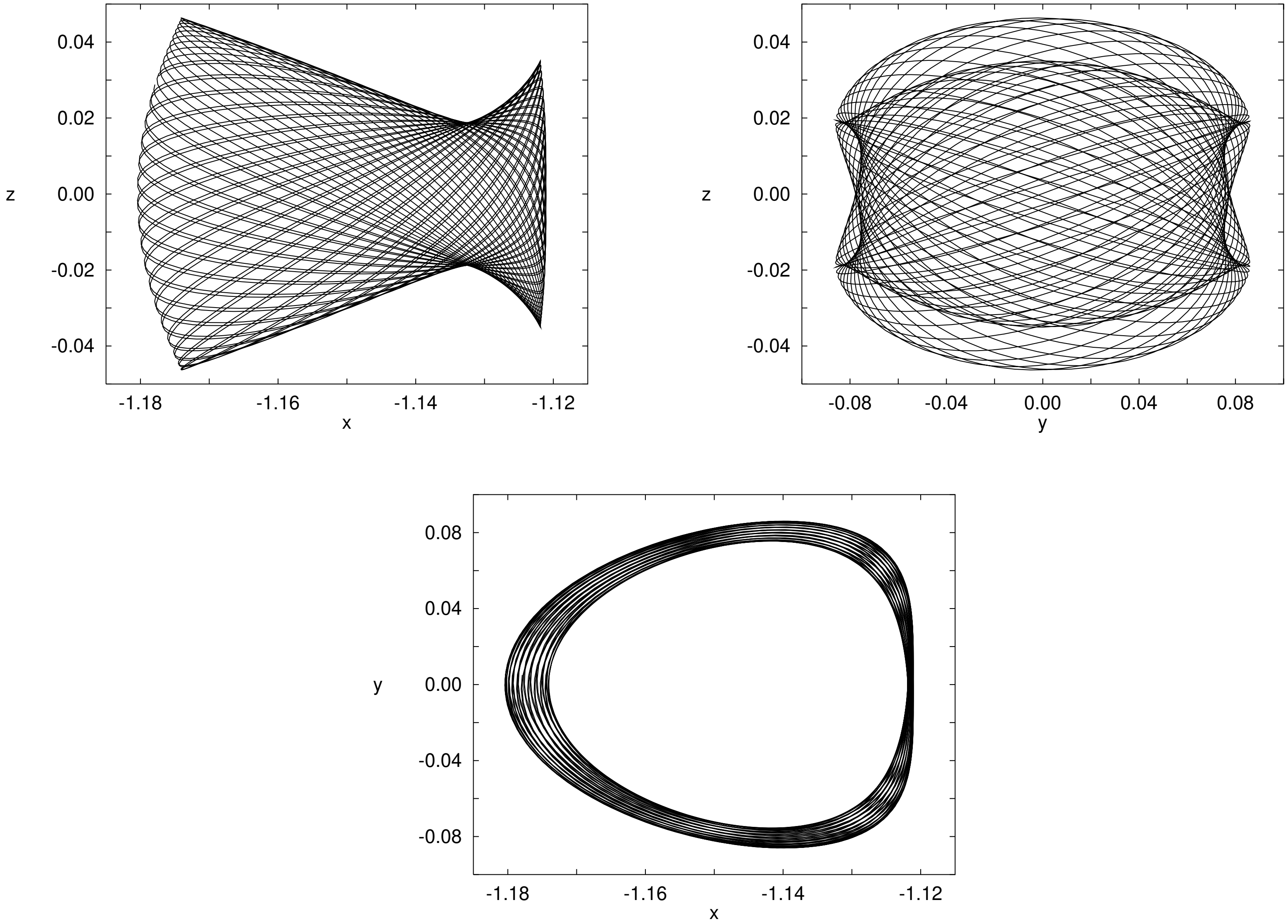

Figure 4.8: 2D torus corresponding to a fixed point of the Poincaré map for $h = -10^{-5}$. The orbit has been drawn for a time span of $22\,T$.

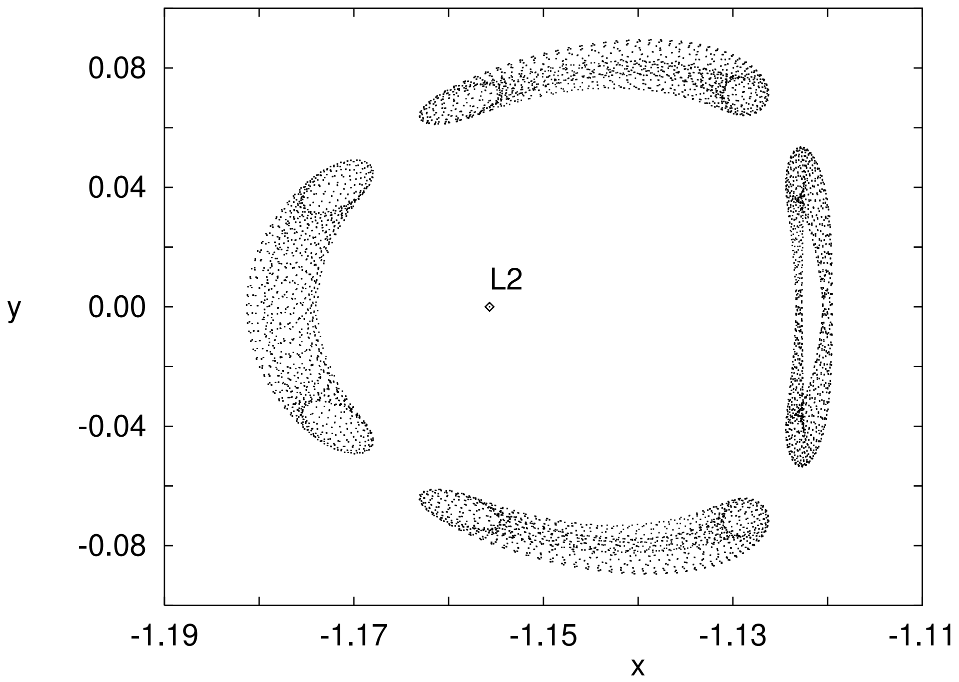

Figure 4.9: Section of a 3D torus around the 2D torus of figure 4.8. We have plotted the points for time $t = kT/8$, $k = 0, \ldots, 8192$.

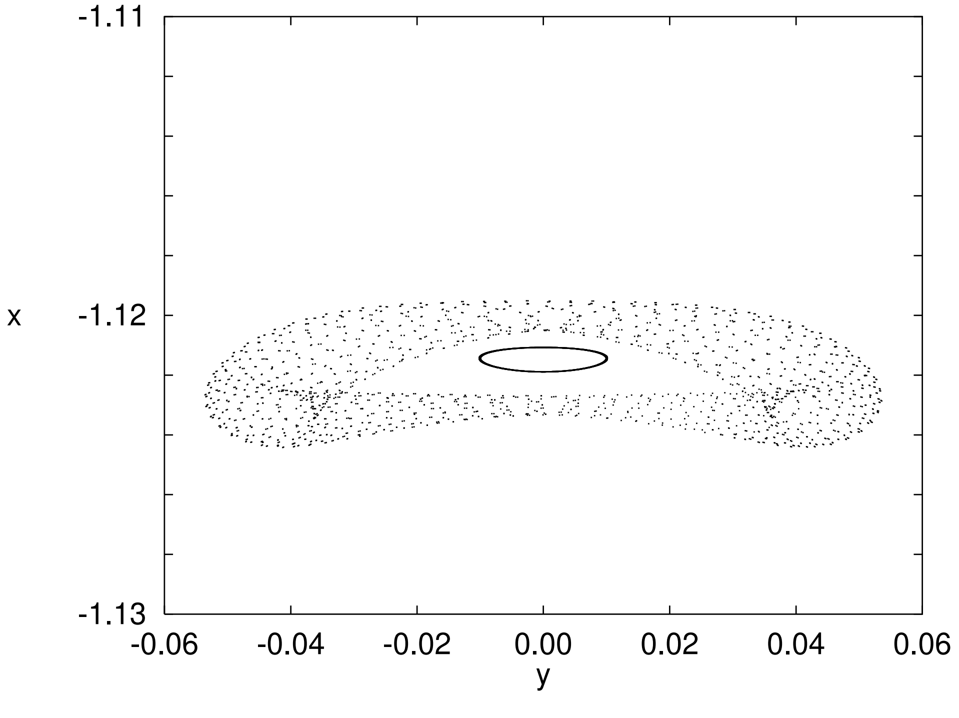

Figure 4.10: Magnification of the torus on the right part of figure 4.9. Here, a section of the torus of figure 4.8 has also been displayed.

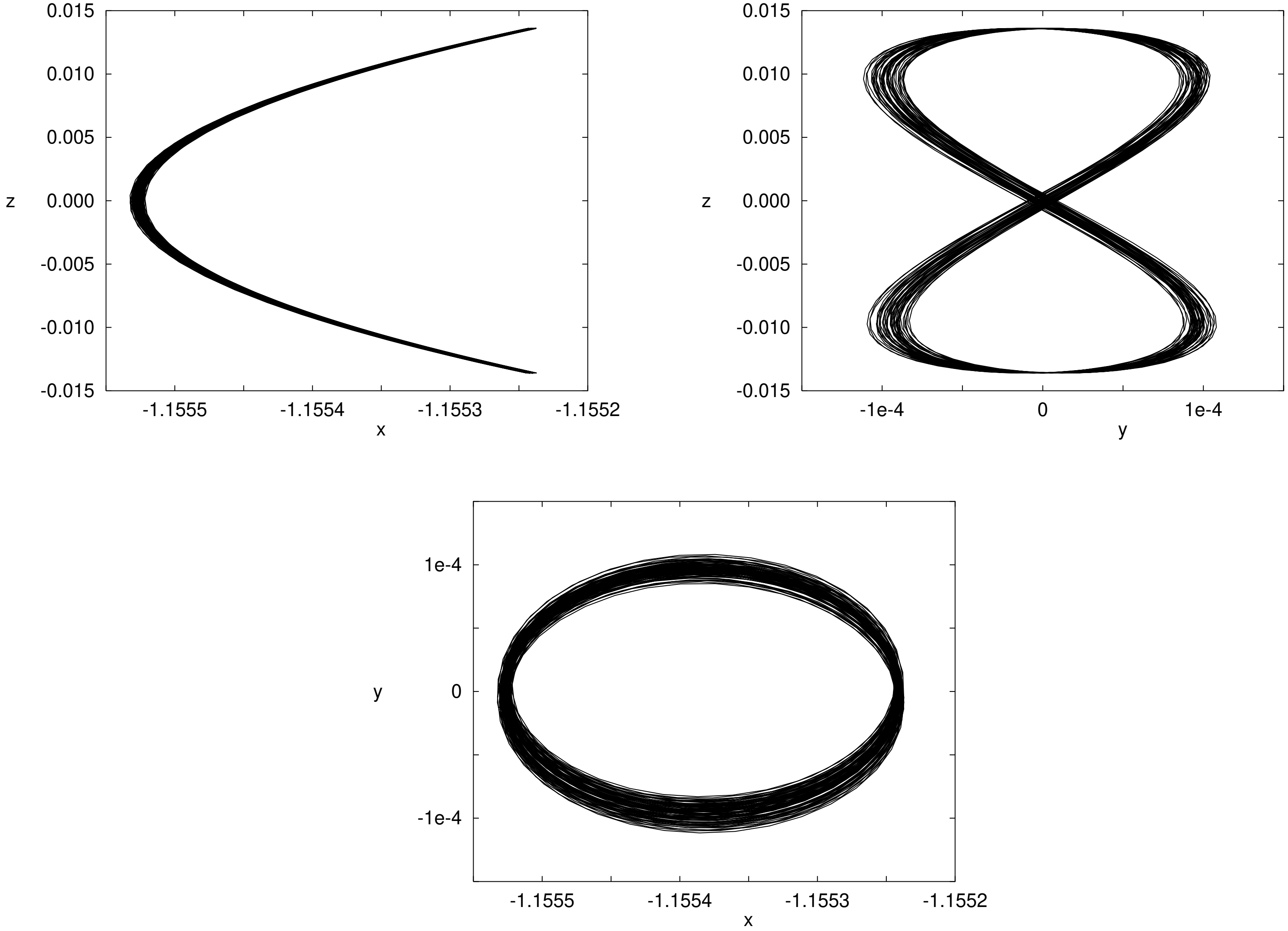

Figure 4.11: Eight-shaped 2D torus corresponding to the origin of coordinates of the Poincaré map for $h = -10^{-5}$. The orbit has been plotted for a time interval of $22T$.

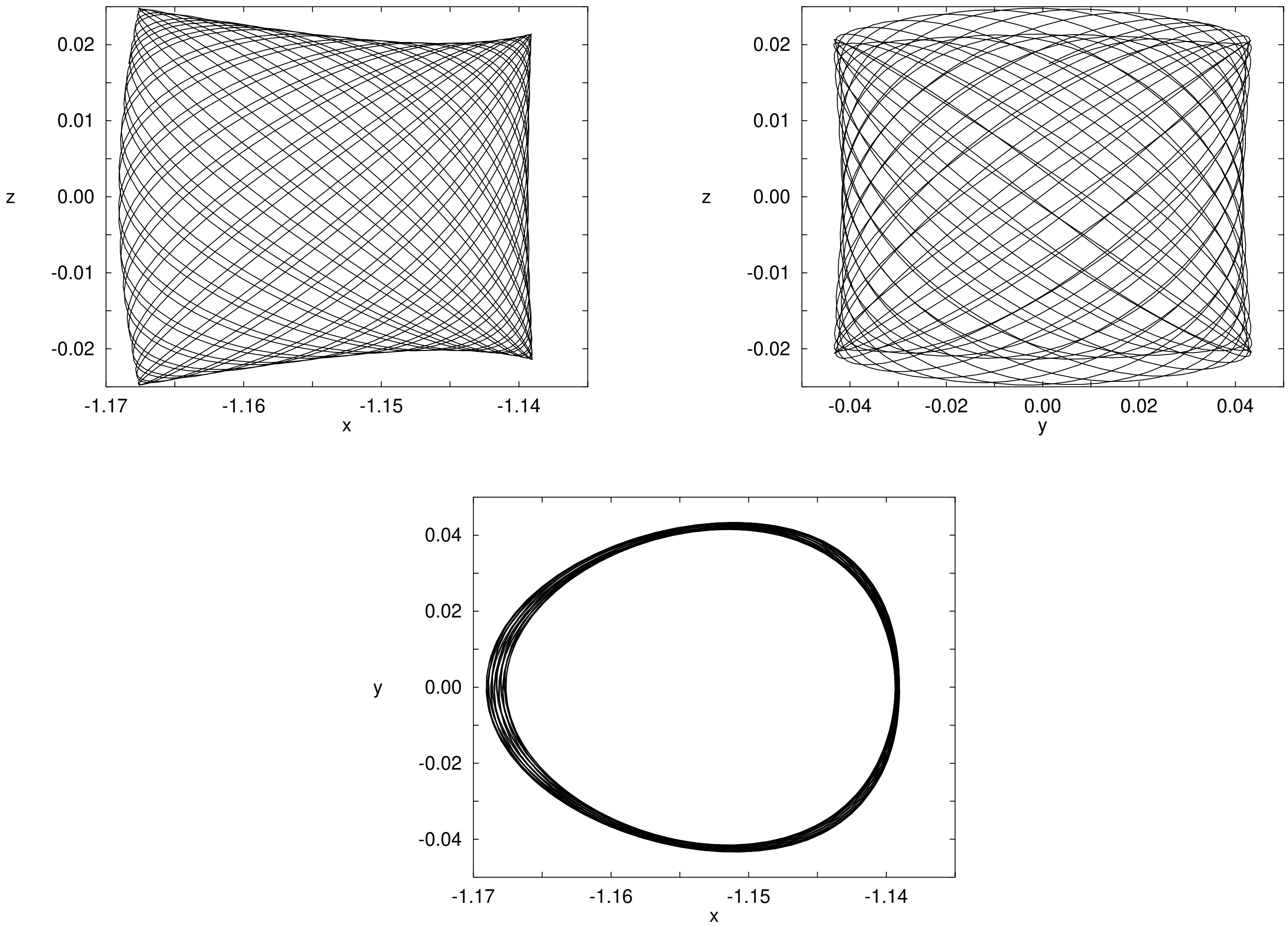

Figure 4.12: A 3D torus of the Lissajous type. Level of energy $h = -10^{-5}$. The orbit has been drawn for a time interval of $14\,T$.

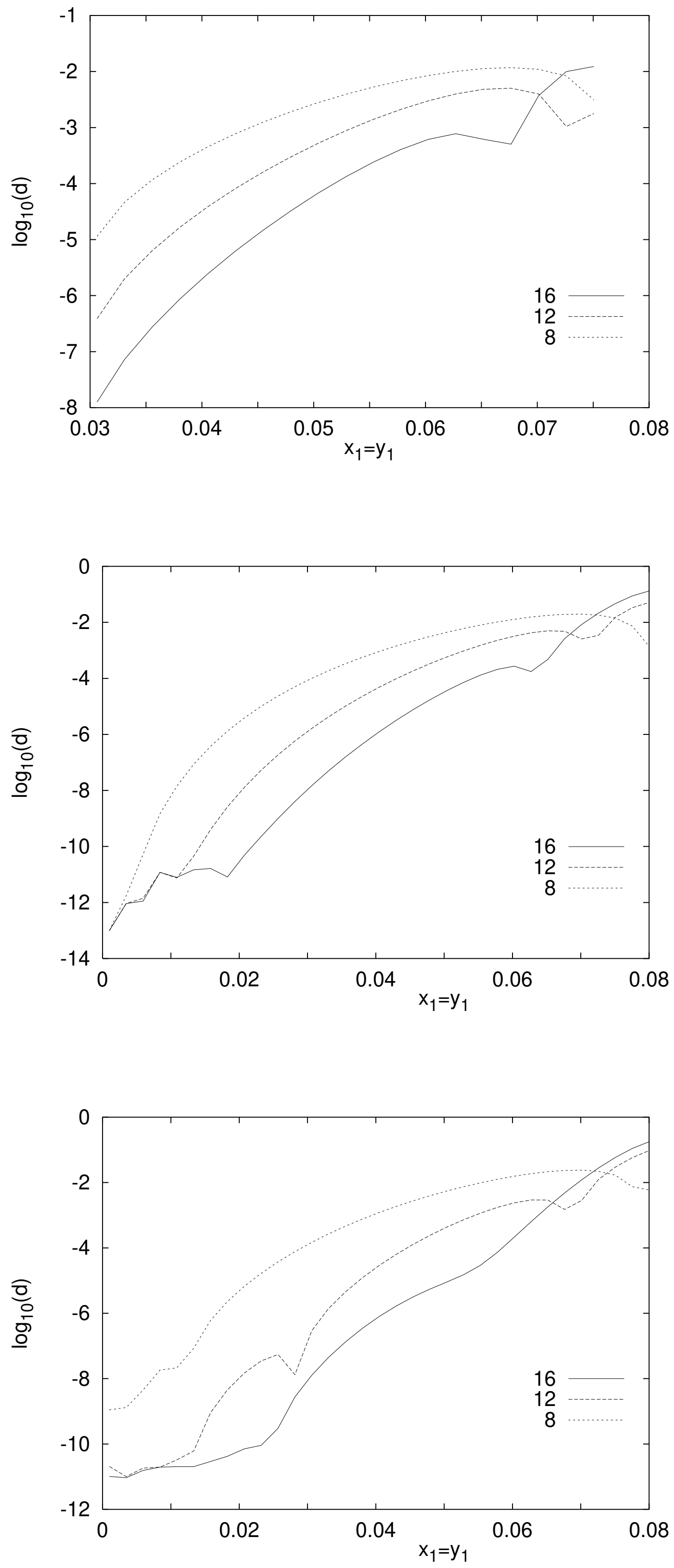

Figure 4.13: Results of a test of accuracy for $h = 10^{-5}, 0, -10^{-5}$, respectively.

family of periodic orbits. In the QBCP, they have another basic frequency. That is the frequency of the Sun, ω_s. Here, we can comment the same that we have said before for the Lyapunov families of tori. The results of [14] suggest that, in the QBCP, Halo families are Cantor sets of 2D tori.

For a fixed level of energy, we take initial conditions on the line $x_1 = y_1$, $x_3 = 0$. Then, the Hamiltonian H_{CM} is numerically integrated for a time interval of $1024\,T$, storing all the points at values of time multiples of $T/8$. That means that we get 8192 points equally spaced on time. Before the frequency analysis, all those points must be transformed into the initial system of reference of the QBCP. This task is the most expensive from the point of view of the CPU time. A more efficient procedure is as follows. Assume that the initial points scanned are labelled as P_k, $k = 1, \ldots, N$, and let P_{kj} be $\phi(t = jT/8, P_k)$ the image under the flow at time $jT/8$. One can compute P_{kj} for all k and successive values $j = 1, \ldots, 8192$. After computing $\{P_{kj}\}_{k=1,N}$ for a given j, one does the transformation to the initial system. In this way, all the time dependence of the change of variables is computed only once for every j. Noting that we use times which are multiples of $T/8$, it would be also possible to compute a priori the eight changes of coordinates for $j = 0, \ldots, 7$. Then, we will reduce the transformation, for all j, to use the corresponding change with index $j(\mathrm{mod}\ 8)$. These changes only depend on the coordinates.

It is required to use a long time interval to be able to detect small frequencies. We have seen that, in the analysis of orbits close to a resonance, there are small frequencies playing an important role. For instance, if one of the basic frequencies of an orbit is $\omega_0 \simeq 2\omega_s$, then it is important to estimate also the amplitude of the frequency $\omega_0 - 2\omega_s$.

Figure 4.14 shows the main frequencies (i.e., those having the largest amplitudes) of the orbits with initial conditions at the bisectrix of the first quadrant of the plane $x_1\,y_1$. The line (1) corresponds to the frequency, $\omega^{(1)}$ on that plane with the largest amplitude. The line (2) is for the main vertical frequency, $\omega^{(2)}$. On the right part of the figure, the line (3) also has been plotted. It corresponds to another vertical frequency, $\omega^{(3)}$, which is comparatively important for those orbits such that $\omega^{(2)} + \omega^{(3)} = 2\omega^{(1)}$. The dashed lines are for reference. The horizontal one is at the frequency $2\omega_s$. The vertical ones are the boundaries of the island (see figure 4.2a).

The frequency analysis corroborates what we have said before for the Poincaré maps for several levels of energy. The orbits around the origin are generically in 3D tori. They have three basic frequencies. For $h = 10^{-5}$, they are the frequencies $\omega^{(1)}$ and $\omega^{(2)}$ of figure 4.14, and the frequency of the Sun ω_s. We also confirm that the fixed point in the right top part of the Poincaré section corresponds to a resonant orbit with horizontal frequency equal to $2\omega_s$. Furthermore, the fact that there is no intersection between the lines (1) and (2) indicates that there are not Halo orbits for this level of energy.

Decreasing the level of energy, the outer boundary of the domain of the Poincaré map is going farther. We recall that, at this level of energy, the boundary is still a planar quasi-periodic Lyapunov orbit of the QBCP. For a value of the energy close to $7.5{\cdot}10^{-6}$, the families of Halo orbits start at a bifurcation of the Lyapunov orbits.

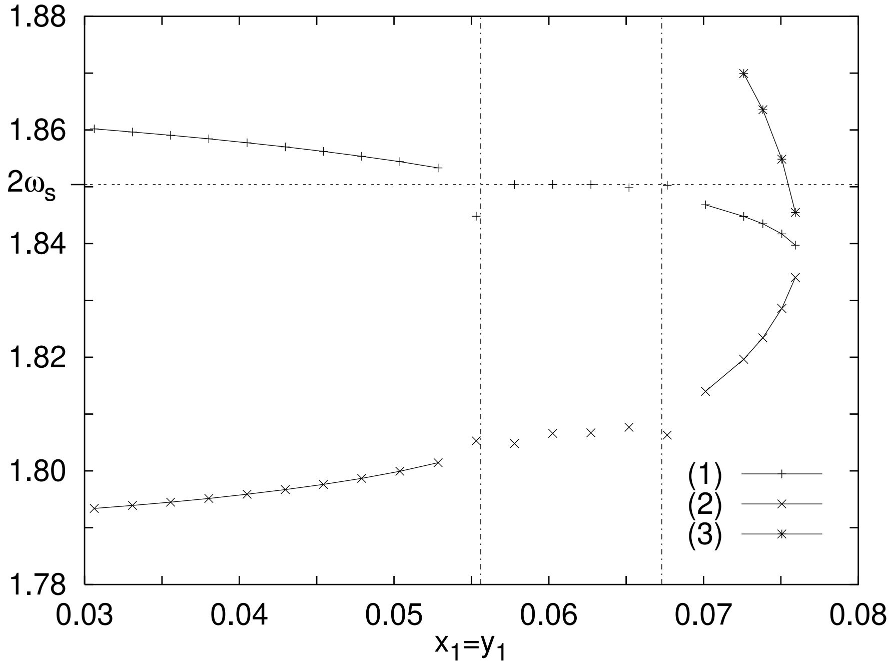

Figure 4.14: Main frequencies at the energy level $h = 10^{-5}$.

Drawing a figure like 4.14 for the bifurcating value of the energy, we would obtain a similar picture, with the difference that the right end of the lines (1) and (2) would be in contact.

For levels of energy lower than the bifurcating level, the lines (1) and (2) intersect at a point. That point corresponds to a Halo orbit. Figure 4.15 shows the main frequencies of the orbits for the energy $h = 0$. Figure 4.16 is a magnification of the previous one. There, it is possible to "see" that the third curve, corresponding to another vertical frequency, also intersects with the lines (1) and (2) at the same point. Unfortunately, the Halo orbits are too large to be computed in this way. In the zone where Halo orbits exist, the Hamiltonian H_{CM} agrees with H_{QBCP} with poor accuracy. However, all this helps to understand the kind of orbits that it is possible to find around L_2. We also want to comment that, using H_{CM}, the determination of the bifurcation where Halo orbits start has poor accuracy. For this goal, it is much better the method used in section 3.7.

Of course, in all the previous analysis it has been assumed, implicitly, that the Cantor sets of 3D tori (and of 2D tori corresponding to Halo orbits) are "thick" enough to be considered as continuous sets. Furthermore, one requires probably a quite long time to discover that an orbit suspected to be in a torus is, in fact, on a hole of the family of tori.

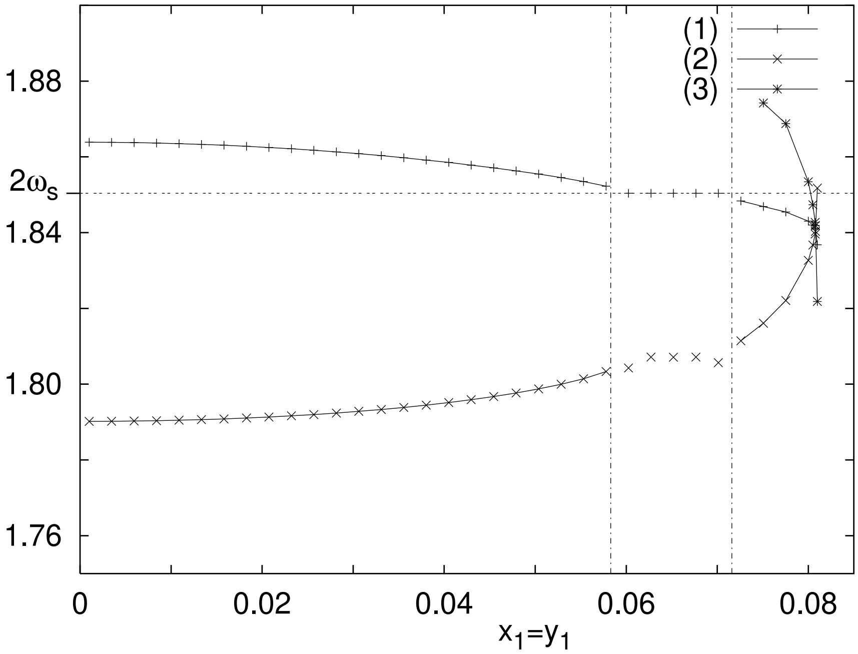

Figure 4.15: Main frequencies at the energy level $h = 0$.

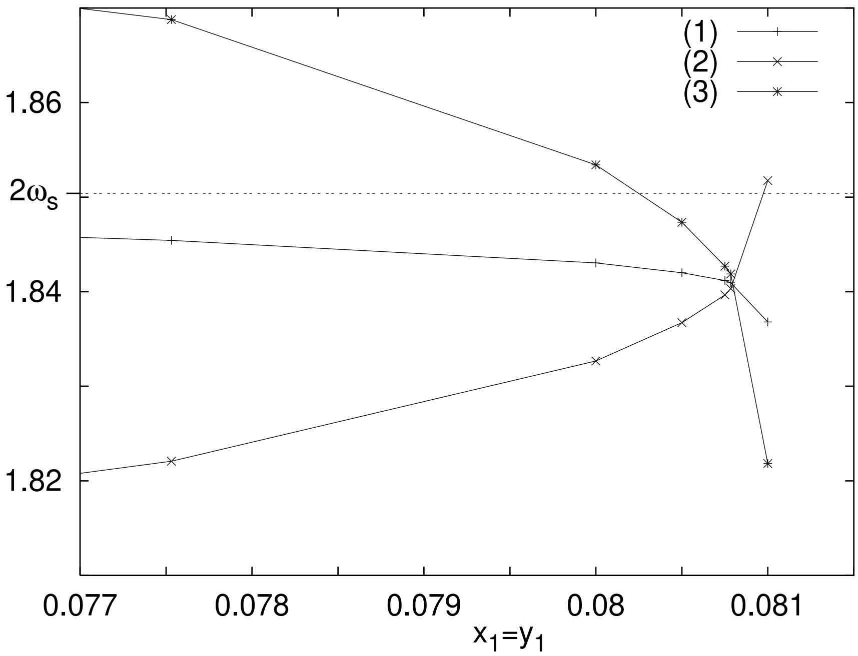

Figure 4.16: Magnification figure 4.15.

4.7.3 A family of 2D resonant tori

We have talked before about the 2D family of tori characterized by having the main horizontal frequency equal to $2\omega_s$. This family starts at the planar Lyapunov periodic orbit related to the $T/2$-periodic orbit of the RTBP. In fact, there are four families of this kind, one for each resonant periodic orbit. We have followed one of these families which corresponds to the fixed point p_2 of the Poincaré maps.

For each level of energy, the fixed point of the Poincaré map is computed. Then, the Hamiltonian equations of H_{CM} are numerically integrated, storing the points at time $t = k\,T/64$, $k = 0, \ldots, 16383$. Those points are transformed into the initial coordinates of the QBCP. After that, the Fourier analysis provides us the main frequencies and amplitudes of each torus.

Figure 4.17 shows the x-amplitude α and the z-amplitude β. The Moon-L_2 distance has been taken as unit of length. The family of 2D resonant tori is continued for the Hamiltonian up to degree 8, 12 and 16. The last piece of these curves are not reliable. We conjecture that the family follows, more or less, a curve similar to the dotted line labelled as C. That means that we think that the family of 2D resonant tori is “connected” with the resonant Halo periodic orbit. Unfortunately, this can not be shown with the reduction to the central manifold. The resonant Halo orbits are too large. The family of 2D tori might be continued using the numerical Simó's method for the computation of invariant tori (see [26], [27]).

Figure 4.17 also shows the 2D Halo tori computed in section 3.6.3. They have been drawn using small circles. Finally, the star on the α axis corresponds to the bifurcation where the Halo family starts. It corresponds to the change of stability computed in section 3.7.

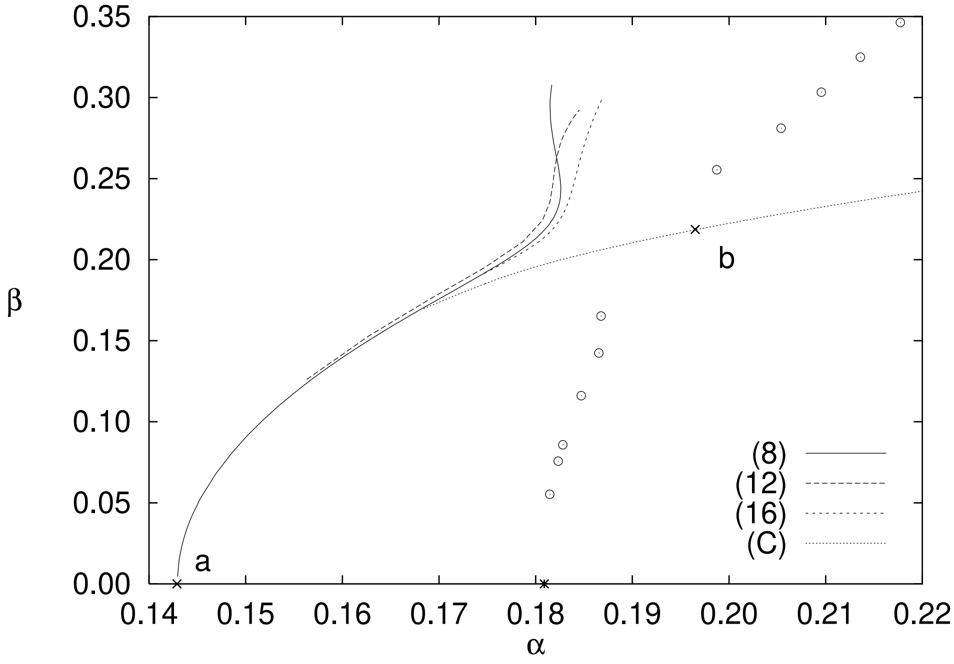

Figure 4.17: A family of 2D resonant tori starting from the planar Lyapunov resonant periodic orbit 22 (cross labelled as a). α and β are the x and z amplitudes, respectively. The unit of length is the Moon-L_2 distance. The family of 2D tori has been followed using the H_{CM} up to degrees 8, 12 and 16. The dotted line labelled as C is a conjecture about the behaviour of that family. The cross labelled as b corresponds to the resonant Halo orbit 2A computed in section 2.3. The 2D Halo tori computed in section 3.6.3 have been displayed using small circles. The star on the α axis corresponds to the bifurcation where the Halo families start (value computed in section 3.7).

Chapter 5

Translunar Halo orbits in the Solar System

5.1 Introduction

The main motivation for introducing the QBCP was the desire of obtaining translunar Halo orbits in the Solar System for a long time interval. Several people have been working in this topic before. In [7], Farquhar and Kamel computed analytical quasi-periodic Halo orbits for a simplified model of the Solar System. In [8] G.Gómez *et al.* obtained numerical Halo orbits of the Solar System using a parallel shooting method and taking as initial guess Halo orbits of the RTBP and quasi-periodic orbits, computed semianalytically, of some intermediate simplified model. However, it was difficult to compute this kind of orbits for a time interval longer than 2-3 years. We recall that, typically, a Halo orbit in a vicinity of the L_2 (translunar) libration point of the Earth-Moon system has a proper period close to two weeks. Many "revolutions" are required for long time intervals.

The QBCP seems to fit better the real problem than the RTBP does. Evidence for that believe will be given at the end of this chapter. For this reason, it has been possible to obtain Halo orbits of the Solar System from the quasi-periodic Halo orbits of the QBCP. Some of these orbits have been computed for a time interval about 22 years. An orbit for 45 years also has been obtained.

To integrate the equations of the motion of a particle in the Solar System, the JPL ephemeris (DE403 file) has been used. For this purpose, we have used the software developed by the authors of the reports [8], [9] and [10]. We have to thank all of them for providing us their software.

5.2 Parallel shooting method

One of the difficulties to get Halo orbits in the Solar System is that they are highly unstable. To have an approximate idea of their instability, we note that the errors in a Halo orbit are amplified by a factor 10^6 for each revolution of the Moon around the Earth. Therefore, to compute numerically Halo orbits it is convenient to use a parallel shooting method. There are several references for it, for example [28].

We are interested in looking for an orbit in the full Solar System. That is, a solution of a differential equation of the form

$$\dot{x} = g(t, x) , \tag{5.1}$$

where $x \in \mathbb{R}^6$ (position and velocity) and the vector field g can be computed from the JPL ephemeris. On the other hand, we have several points

$$(t_0, \bar{x}_0), (t_1, \bar{x}_1), \ldots, (t_n, \bar{x}_n) ,$$

which are taken as a first approximation of the wanted orbit. Those points can be taken on a quasi-periodic Halo orbit of the QBCP. The objective is to refine iteratively the initial points, in order that the different orbits which go through them match together and give (approximately) an unique orbit of (5.1). In this respect, we note that a strong (partial) hyperbolicity is helpful, like in the proof of the existence of true orbits in the shadowing lemma (see [2]).

Let $\phi(t, t', x)$ be the flow of the equation (5.1) going from time t to t' with initial condition x. We consider a set of fixed times $\{t_k\}$, for $k = 0, \ldots, n$, and we want to compute the corresponding states $\{x_k\}$, for $k = 0, \ldots, n$, satisfying the matching equations:

$$\phi(t_k, t_{k+1}, x_k) = x_{k+1} , \qquad k = 0, \ldots, n-1 .$$

To apply Newton's method to solve these equations, we linearize the system getting

$$\begin{pmatrix} A_1 & -I & & & & \\ & A_2 & -I & & & \\ & & A_3 & -I & & \\ & & & \ddots & \ddots & \\ & & & & A_n & -I \end{pmatrix} \begin{pmatrix} \Delta x_0 \\ \Delta x_1 \\ \Delta x_2 \\ \vdots \\ \vdots \\ \Delta x_n \end{pmatrix} = \begin{pmatrix} b_1 \\ b_2 \\ b_3 \\ \vdots \\ b_n \end{pmatrix} , \tag{5.2}$$

where A_k are 6×6 matrices coming from the integration of the variational equations of (5.1); the independent term is formed by the vectors $b_k = x_k - \phi(t_{k-1}, t_k, x_{k-1})$ and the quantities Δx_k are the corrections to the states x_k. We notice that the linear system is infradetermined. It has $6n$ equations and $6n + 6$ unknowns. If we would be looking for a periodic orbit (assuming it exists, which is not the case in the present problem) then we would have 6 extra conditions of periodicity.

System (5.2) can be solved, for instance, adding some minimizing condition for the corrections Δx_k. In a system of the form $A \Delta x = b$, requiring to minimize

$$\sum_{k=0}^{n} (\Delta x_k)^2 ,$$

leads to

$$\Delta x = A^T (A\, A^T)^{-1} b , \tag{5.3}$$

which can be derived by using Lagrange multipliers.

For very large linear systems, it is also possible to require to be minimum only

$$\sum_{j=0}^{p} (\Delta x_{jm})^2 , \tag{5.4}$$

where $p = n/m$ and m is some integer dividing n. Then, the linear system (5.2) is reduced to another one of the form

$$\begin{pmatrix} B_1 & -I & & & \\ & B_2 & -I & & \\ & & \ddots & \ddots & \\ & & & B_p & -I \end{pmatrix} \begin{pmatrix} \Delta x_0 \\ \Delta x_m \\ \Delta x_{2m} \\ \vdots \\ \Delta x_{pm} \end{pmatrix} = \begin{pmatrix} c_1 \\ c_2 \\ \vdots \\ c_p \end{pmatrix} , \tag{5.5}$$

with

$$\begin{aligned} B_j &= A_{i+m} A_{i+m-1} \cdots A_{i+1} , \\ c_j &= A_{i+m}(\cdots(A_{i+3}(A_{i+2}\, b_{i+1} + b_{i+2}) \cdots) + b_{i+m} , \end{aligned}$$

for $j = 1, \ldots, p$ and being $i = (j-1)m$. Then, we obtain Δx_0, Δx_m, …, Δx_{pm}, solving the equations (5.3) for the system (5.5). After this, the other corrections, Δ_k, for $k \neq 0 \pmod{m}$, can be computed from (5.2).

We want to stress that (5.5) looks like a parallel shooting method using only the set of times $\{t_{jm},\ j = 0, \ldots, p\}$. The main difference is that, to compute the matrices B_j we do not integrate the variational equations of (5.1) from t_{jm} to $t_{(j+1)m}$, but we take the composition of the A_{jm+k} matrices using arcs which, hopefully, are closer to the correct solution.

5.3 Some Halo orbits of the Solar System

First of all, we have to define what a Halo orbit of the Solar System is. A simple definition could be: a Halo orbit is an orbit revolving, in the configuration space, around a collinear libration point (defined geometrically, of course) never passing through a neighbourhood of the axis joining the two primaries (Earth-Moon, in our case). But, this is a too rough definition. A neighbourhood of the libration point, excluding a neighbourhood of the primaries axis will be denoted as *Halo domain*. We note that the (y, z)-projection of a Halo domain is inside an annulus (using the usual synodical coordinates).

In the RTBP, Halo periodic orbits are well known. Around each Halo orbit there is a (Cantor) set of quasi-periodic orbits living in 2D tori (denoted as quasi-halo orbits in [12]). They have two basic frequencies: the proper frequency of the Halo orbit and a frequency close to the normal frequency to the Halo orbit. In fact, the second frequency depends on the amplitude of the quasi-halo orbit respect to its core Halo orbit and, of course, on the amplitude of the core Halo orbit. Quasi-halo orbits also keep an exclusion zone around the axis of the two primaries. Therefore, they would be considered as Halo orbits with the rough definition.

Assuming that the Solar System is quasi-periodic (this is not true, but it is a good approximation for practical purposes during a moderate time span) then Halo orbits are also quasi-periodic, having all the frequencies of the Solar System. Most of them, probably with an amplitude rather small. As we said before, in the RTBP there are Halo periodic orbits and quasi-halo orbits. This suggests the definitions we shall use here. A *Halo orbit of the Earth-Moon system under the full action of the Solar System* is an orbit lying forever in the Halo domain and having, as basic frequencies, the ones of the Solar System and one single proper frequency. In a similar way, *quasi-halo orbits of the Earth-Moon system under the full action of the Solar System* have two proper frequencies, beyond the external ones. One of them plays the role of normal frequency. At present, we do not have any theoretical result ensuring the existence of these orbits, but there is numerical evidence of their presence. Furthermore, Halo orbits should depend on two parameters: amplitude and initial epoch, while quasi-halo ones depend on two amplitudes and the initial epoch. We usually are going to call Halo orbits both kind of solutions and we will be more precise when it is required.

Now, we are going to show some translunar Halo orbits of the Solar System computed for time intervals longer than $18\frac{2}{3}$ years. This is the so called Saros period. During this time interval, all the orbital elements of the Moon have covered, at least, one revolution. Halo orbits of the Solar System have been obtained from the quasi-periodic Halo orbits of the QBCP computed in chapter 3. The parallel shooting method has been used. In our case, there is an extra condition that we can require: if the first point of the orbit, $\bar{x}_0$, is on the plane $y = 0$ then the y component of Δx_0 can be set to zero. This condition is related to the fact that the Halo orbits of the QBCP have a phase free.

Due to the fact that the orbits are highly unstable, it is necessary to take about 4 points per day. Taking into account that each revolution around L_2 spends about 15 days, it means that about 60 points per revolution are taken. For example, if we are interested in an orbit for a time span of 8000 days, we have to compute 32000 points and the linear system has dimension 192000. There is no problem in solving such a system because the matrix is symmetric and block tridiagonal, being 6×6 the size of each block. However, there are difficulties in the convergence of Newton's method. It is better to use the minimizing condition (5.4). After some trials, the orbits of this section were computed using $m = 30$. The dimension of the normal equations is then $6n/m = 6400$. In this case, we have seen that Newton's method is convergent for longer orbits than using $m = 1$. Figure 5.1 shows the CPU time (with a Pentium 233 MHz computer) per iteration of Newton's method. The CPU time depends, roughly, lineary on the dimension of the system. We note that most of the time is spent in filling the matrix, not in solving the linear system. In fact, the CPU time to solve the system is negligible. In the computed examples, typically, Newton's method needs 8-9 iterations to achieve an orbit with an error,

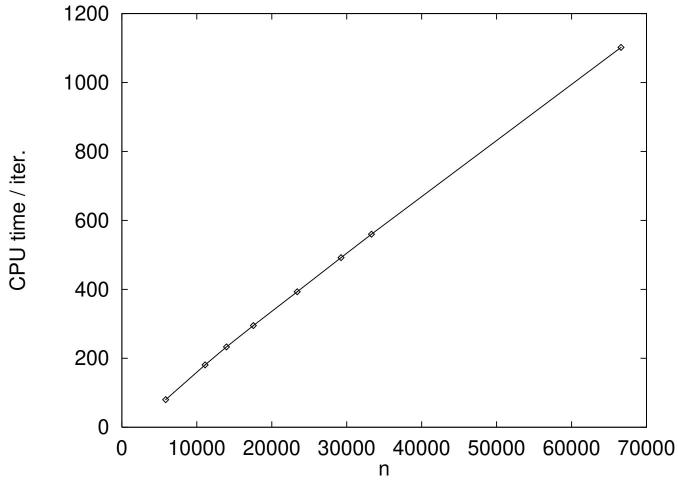

Figure 5.1: CPU time (in seconds) per iteration of the Newton's method depending on the number of points, n, used in the parallel shooting method.

at each matching point, less than one millimeter in position and of the order of a few millimeters per hour in velocity.

Another thing that we want to comment is that if one is interested in computing orbits of the Solar System for a long time interval, we recommend to take pieces of about 5-7 years of an orbit of the QBCP. Then, they can be refined, put all them together, one after the other, and proceed to refine again to obtain the complete orbit. Figures 5.2-5.5 show the (y, z) and the (time,z) projections of several Halo orbits in the Solar System for a time interval of about 22 years. Halo orbits shown in those figures were computed in that way. Concretely, for each orbit, we have used 3 pieces of a Halo orbit of the QBCP of 11101 points, except for the orbit shown in figure 5.3 that we have used 4 pieces of 8311 points. We recall that 60 points per revolution around L_2 are taken. We want to note that taking different number of points of the initial orbit, the final orbit can be quite different. Later on, we will return to this question. The initial points used for the computation of the orbits of figures 5.2-5.5 were taken on the orbits labelled as 216, 220, 228 and 236 in chapter 3. The unit of length is the distance between the Moon and L_2 (about 60000 km). Time is measured in days starting at January 1 of the year 2000.

Looking at the profile of the (time,z)-projection of the Halo orbits, it seems to be formed by two main superposed waves. A long period wave and a short period one. The long period one is related to the difference $\omega_p - 2\omega_s$, where ω_p is the proper frequency of the Halo orbit and ω_s is the frequency of the Sun. A similar wave can be also observed in the case of the QBCP. In the (time,z)-projections shown in the figures of this chapter we have included in grey the corresponding initial orbit of the QBCP. Concerning the short period wave, we will see that it is related to the normal frequency to the Halo orbit.

We have said before that the final orbit obtained can be quite different depending on the number of points taken in the initial orbit. This is specially true for the amplitude of the short period wave observed in the profile of the (time,z)-projection of the orbits. Figure 5.6 shows this projection for a Halo orbit of the Solar System for 12 years. The orbit was obtained refining with the parallel shooting method three pieces of 5851 points of the orbit 216 of the QBCP. After that, the three pieces were stored consecutively and refined again all together. We notice the strong difference between the orbits of figures 5.6 and 5.2.

To check the interpretation of the long and short period waves in the z amplitude, it is necessary to perform a Fourier analysis of the orbits. However, the frequencies ω_p and $2\omega_s$ are very close for these orbits. To separate both frequencies with Fourier analysis, an orbit for a longer time interval is needed. For this reason, we computed an orbit for a time interval of 45 years which is shown in figure 5.7. This orbit was obtained from four consecutive pieces of orbits similar to the orbit of figure 5.6. The final orbit for 45 years has 66601 matching points. We have done a Fourier analysis of the z coordinate taking 2^{16} points of the orbit of figure 5.7. Figure 5.8a shows the result of the FFT using Hanning filter of order 2. Figure 5.8b shows the estimated frequencies and amplitudes in the same interval. To obtain them, we have used Laskar's method to detect relative maxima of the Fourier Transform (see [15]). In the interval of frequencies shown in these figures, we notice that there are a lot of frequencies which have comparatively important amplitudes. In order to have a better estimation of the frequencies involved, it would be convenient to get an orbit for a time span much more longer. Table 5.1 shows the values obtained for the constant term and the 34 frequencies with the largest amplitudes. B_j and A_j are the amplitudes in sine and cosine terms, respectively. The total amplitude is $C_j = \sqrt{A_j^2 + B_j^2}$.

In the RTBP, we know that the normal frequency to the Halo orbits has a value about $\omega_p/27$ (see [12]). Then, it is expected that the normal frequency of the Halo orbits of the Solar System has a similar value. With this hypothesis, we try to fit the frequencies of table 5.1 as linear combination of $\omega_p = \omega_1$, $\tilde{\omega}_s = \omega_2/2 \simeq \omega_s$ and the normal frequency, ω_n. If a torus with the frequencies ω_p, $\tilde{\omega}_s$ and ω_n really exists, then it is expected that these frequencies satisfy a Diophantine condition

$$|k_1\omega_p + k_2\tilde{\omega}_s + k_3\omega_n| \geq \frac{c}{|k|_1^\tau} ,$$

where c is a positive constant, $\tau > 2$, k denotes the multiindex (k_1, k_2, k_3) and $|k|_1 = |k_1| + |k_2| + |k_3|$. Then, for a given integer N and a positive threshold δ, we define the function

$$\Psi_{N,\delta}(\omega_n) = \sum_{j=1}^{34} C_j \min\{|(k,\omega)| \cdot |k|^2 \ : \ |k| \leq N, \ |(k,\omega)| < \delta\} ,$$

where C_j are the amplitudes of table 5.1, ω denotes $(\omega_p, \tilde{\omega}_s, \omega_n)$ and (k,ω) is the scalar product. Figure 5.9 shows this function for $N = 100$ and $\delta = 5 \cdot 10^{-4}$. The function Ψ can be used to estimate the goodness of the fit of the frequencies given by the Fourier analysis as linear combination of the selected basic frequencies. A

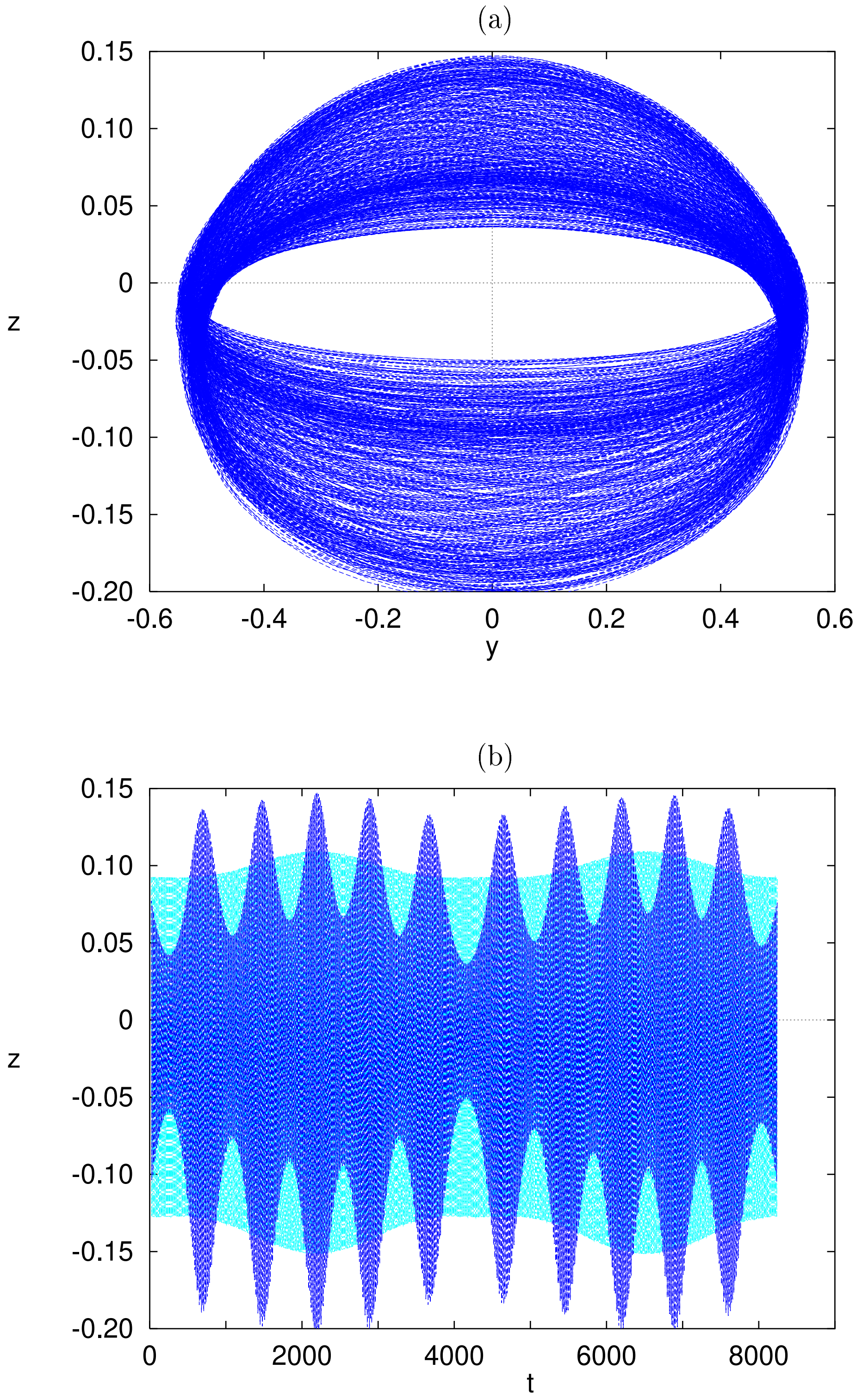

Figure 5.2: A Halo orbit of the Solar System for 22 years computed from orbit 216 of the QBCP. Normalized units are used. Time is measured in days. (a) (y, z)-projection. (b) (time,z)-projection (black) and (time,z) projection of the QBCP orbit taken as initial guess (grey). The same black-grey convention will be used in subsequent figures.

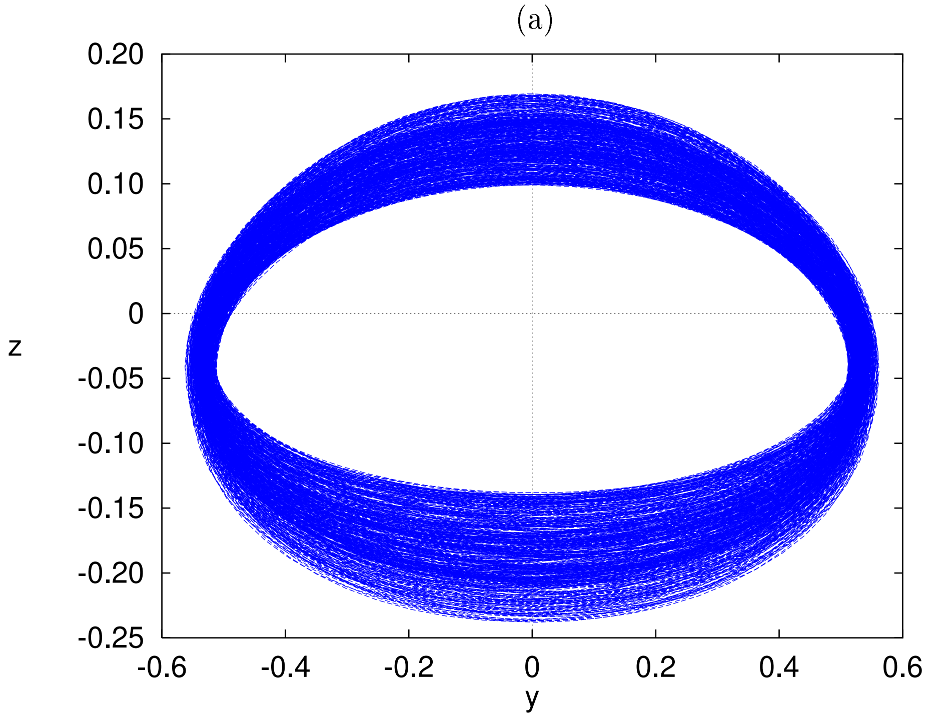

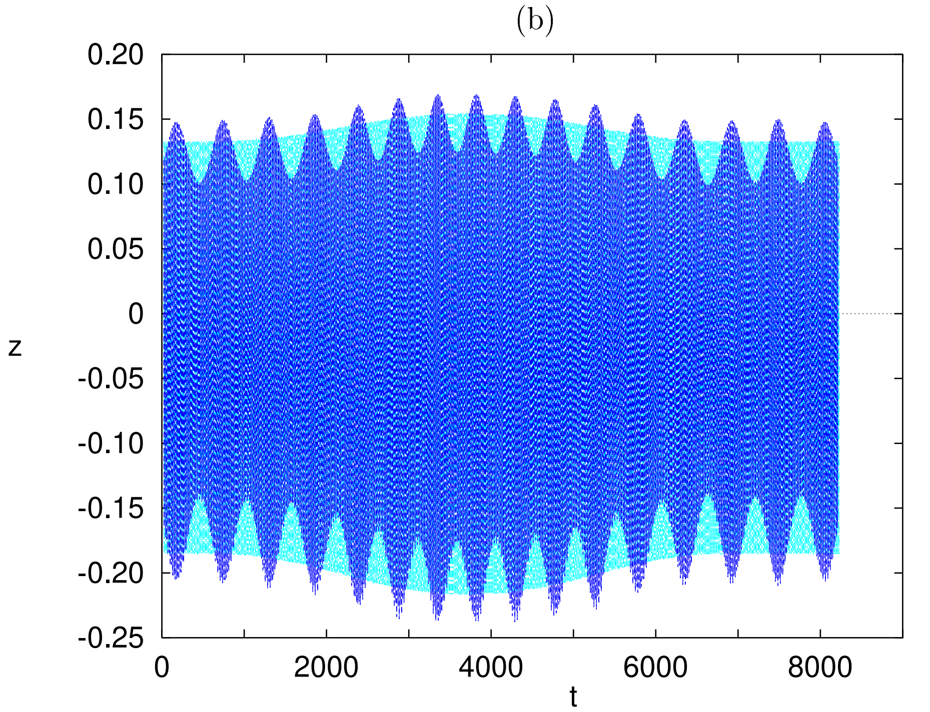

Figure 5.3: A Halo orbit of the Solar System for 22 years computed from orbit 220 of the QBCP. Normalized units are used. Time is measured in days. (a) (y, z)-projection. (b) (time,z)-projection.

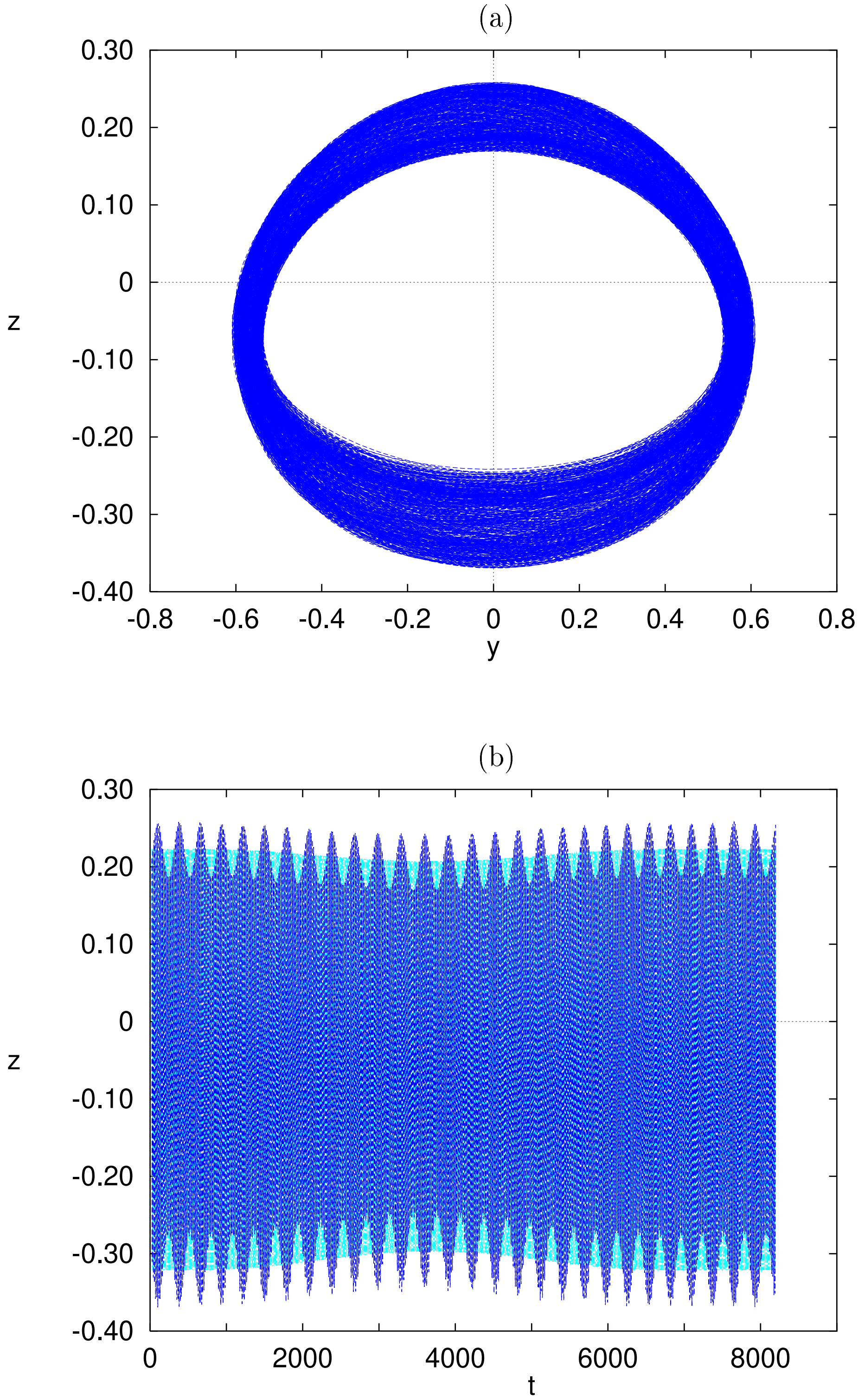

Figure 5.4: A Halo orbit of the Solar System for 22 years computed from orbit 228 of the QBCP. Normalized units are used. Time is measured in days. (a) (y, z)-projection. (b) (time,z)-projection.

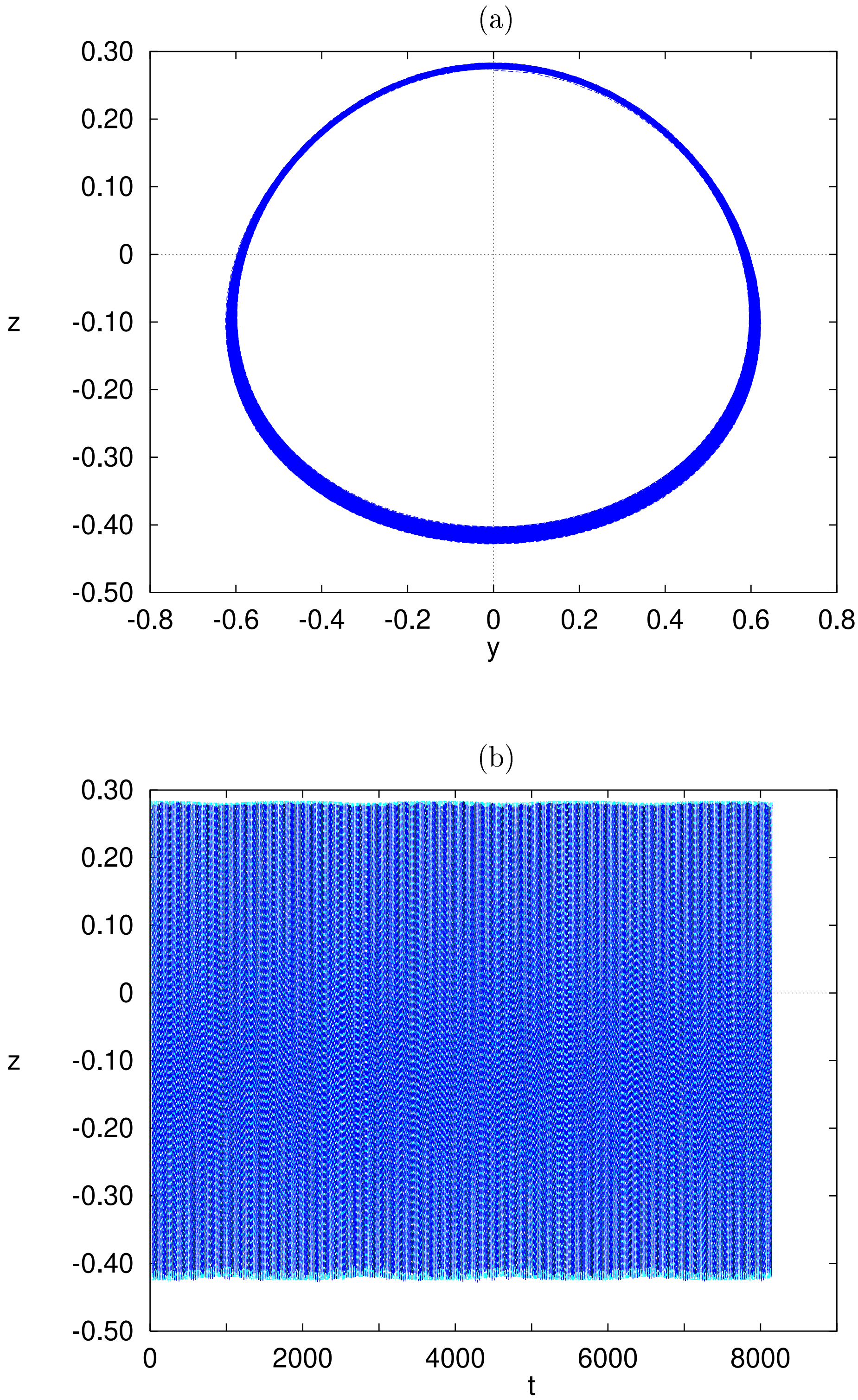

Figure 5.5: A Halo orbit of the Solar System for 22 years computed from orbit 236 of the QBCP. Normalized units are used. Time is measured in days. (a) (y, z)-projection. (b) (time,z)-projection.

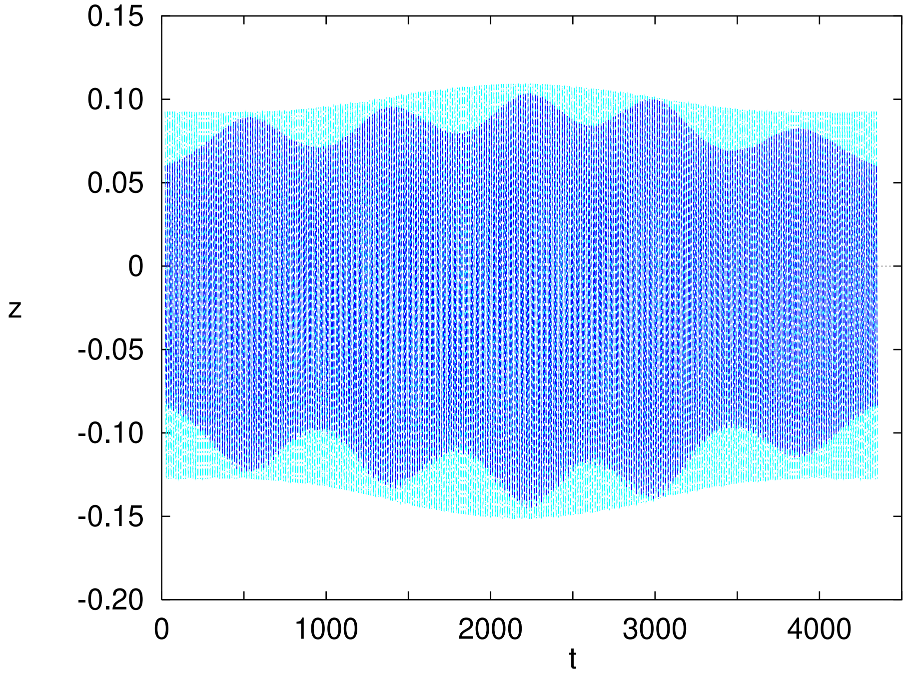

Figure 5.6: A Halo orbit of the Solar System for 12 years computed from orbit 216 of the QBCP. (time,z)-projection is shown. Normalized units are used. Time is measured in days.

good value of the normal frequency must be in a minimum (at least, local) of the function Ψ. We have chosen the value $\omega_n = 0.06635729$, which is marked in figure 5.9 with a dashed line. It is true that Ψ depends on the values of N and δ. However, we have seen that changing the values of N and δ, slight variations on the location of the local minima are observed. Table 5.2 shows a possible identification of the frequencies. Selecting another value of ω_n corresponding to another local minimum of the function Ψ, some of the coefficients (k_1, k_2, k_3) can be different. But, it is important to point out that, in any case, the set of frequencies of table 5.2 is divided into two subsets: the frequencies involving the normal frequency ($k_3 \neq 0$) and the ones independent of it ($k_3 = 0$). These two subsets seem to be invariant with respect to the selected ω_n for the range shown in figure 5.9. Notice that, in fact, the minima of the function Ψ displayed in the figure are in a very narrow interval.

Figure 5.10a shows the graphic of the trigonometric polynomial of table 5.1. The profile shown there is very similar to the one of figure 5.7. Analogously figure 5.10b, but in this case we only have considered the terms of table 5.1 without normal frequency (that is, with $k_3 = 0$).

It seems clear that, due to the "neutral" character of the central mode (associated to the normal frequency) the parallel shooting method detects a quasi-halo orbit of the Solar System close (in some norm) to the initial guess. There is no reason at all to assume the orbit obtained has only one proper frequency. This quasi-halo orbit can be seen as a 2D torus "dancing" also quasi-periodically at the rhythm of the external frequencies. This suggests the following question: how can we compute a "pure" Halo orbit of the Solar System? Here, "pure" means without component in the normal frequency direction. It is necessary to develop an algorithm to produce such kind of orbits. Furthermore, suitable parameters to "label" the orbit can be the initial epoch and the proper frequency.

(a)

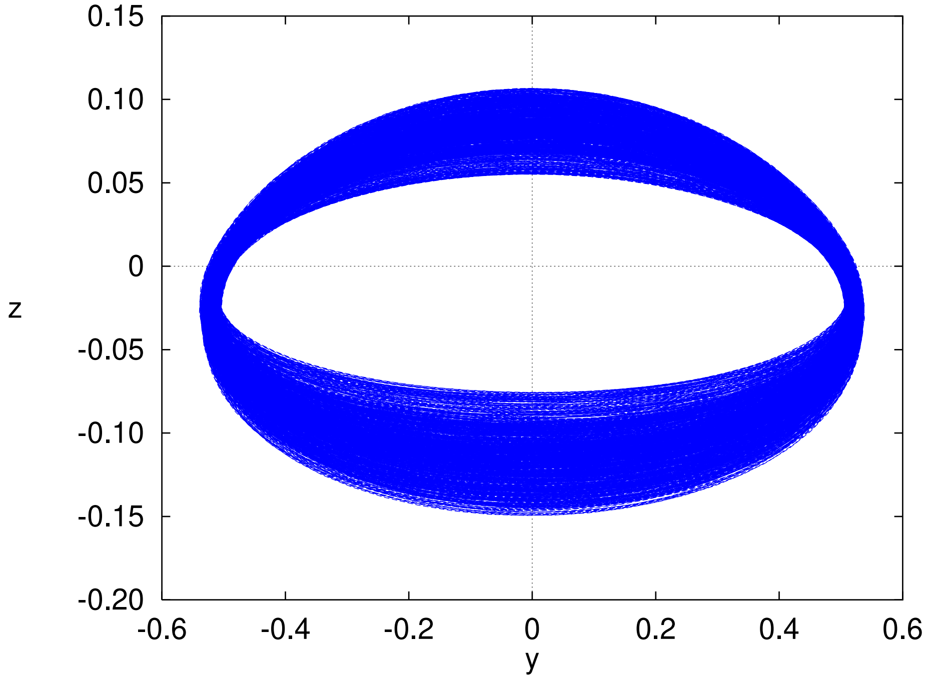

(b)

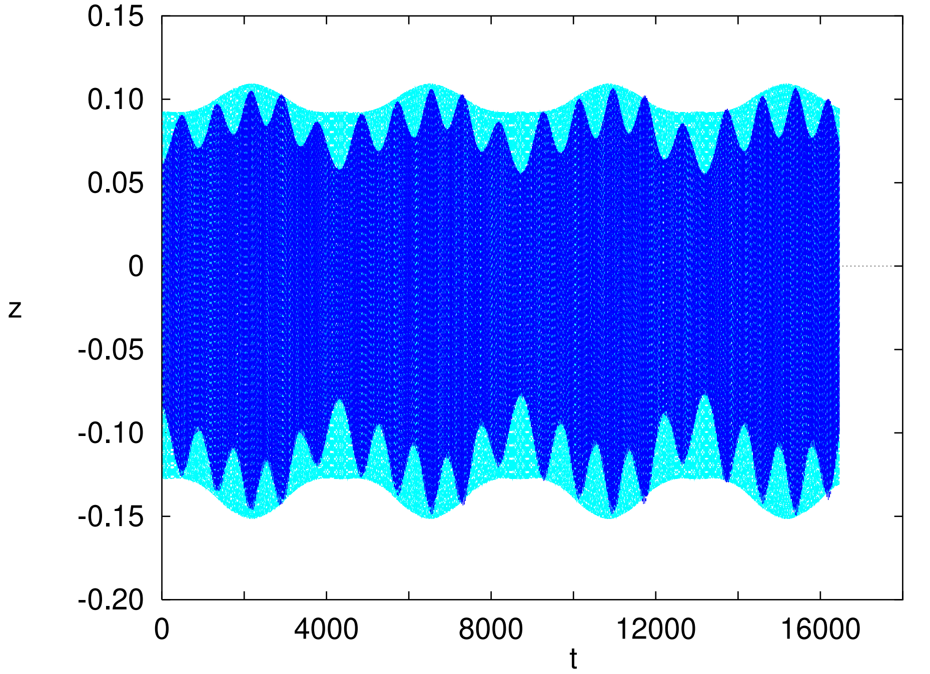

Figure 5.7: A Halo orbit of the Solar System for 45 years computed from orbit 216 of the QBCP. Normalized units are used. Time is measured in days. (a) (y, z)-projection. (b) (time,z)-projection.

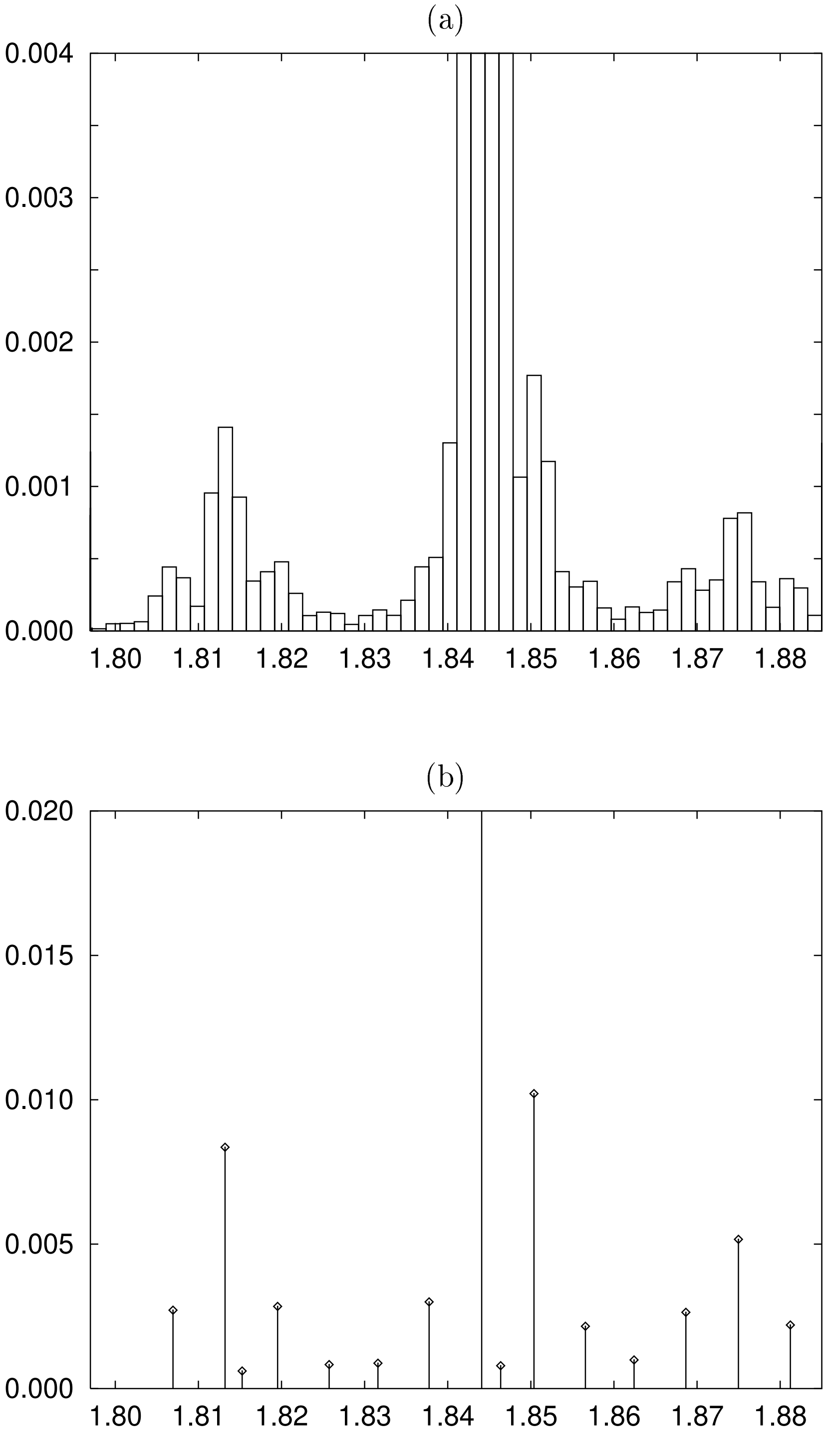

Figure 5.8: (a) FFT of a Halo orbit of the Solar System for 45 years. In the interval of frequencies (around the proper frequency) shown in the figure, there are a lot of frequencies with amplitudes comparatively important. (b) Estimated frequencies and amplitudes in the same interval of (a) (see more in table 5.1). In both plots the vertical window has been selected to display terms with small amplitude.

j	ω_j	A_j	B_j	C_j
0		−2.29133395e−02		2.29133395e−02
1	1.84408415	9.57643588e−02	−2.30900883e−03	9.57921914e−02
2	1.85037689	−1.02134330e−02	8.30912613e−05	1.02137710e−02
3	2.83562895	−5.66657889e−03	6.16251852e−03	8.37178302e−03
4	1.81319487	−4.86888483e−03	−6.79277343e−03	8.35750025e−03
5	0.85253866	5.30487707e−03	5.16938037e−03	7.40703814e−03
6	3.68816706	6.93982907e−03	−4.00970605e−04	6.95140309e−03
7	1.87497599	−2.20273945e−03	4.67266587e−03	5.16583656e−03
8	0.03089029	1.61433739e−03	−2.65536446e−03	3.10757874e−03
9	1.83775483	−2.98814556e−03	2.97724045e−04	3.00294080e−03
10	1.81952035	−1.13777847e−03	−2.60541546e−03	2.84301417e−03
11	0.00630041	2.71872531e−03	5.89982341e−05	2.71936538e−03
12	1.80694087	1.17413632e−03	2.44635988e−03	2.71353511e−03
13	1.86865179	−7.23319682e−04	2.54096706e−03	2.64191312e−03
14	1.88122056	7.81696076e−04	−2.05681794e−03	2.20035197e−03
15	1.85655523	−4.43501870e−04	2.11343476e−03	2.15946762e−03
16	2.70292363	−1.24804991e−03	−1.31041887e−03	1.80964808e−03
17	0.98522791	9.50510093e−04	−1.18423397e−03	1.51851228e−03
18	0.02456681	4.50676802e−04	−1.28439365e−03	1.36116738e−03
19	4.67971171	−8.13262736e−04	9.45097992e−04	1.24683860e−03
20	5.53225154	1.16355777e−03	−1.03389440e−04	1.16814214e−03
21	0.99155733	7.87632498e−04	−7.83907205e−04	1.11124950e−03
22	0.03713564	−3.73769599e−04	1.02811938e−03	1.09395300e−03
23	1.86240946	−7.21669007e−04	6.77431422e−04	9.89807803e−04
24	2.84191611	6.34655129e−04	−6.89691068e−04	9.37262450e−04
25	2.69661750	6.66892364e−04	6.15463907e−04	9.07491733e−04
26	1.83159954	−2.35871667e−04	−8.44874104e−04	8.77181678e−04
27	1.82572677	−4.25570959e−04	−7.13630685e−04	8.30890724e−04
28	1.84636963	−6.70235898e−04	4.21473718e−04	7.91742542e−04
29	2.80473846	7.04468134e−04	1.22441740e−04	7.15029602e−04
30	0.01247864	1.67551505e−04	−6.56117735e−04	6.77173530e−04
31	3.82717376	−3.61073643e−05	−6.36941879e−04	6.37964497e−04
32	0.82164839	1.21622489e−04	−6.19443796e−04	6.31270660e−04
33	1.81525479	−6.09696376e−04	−1.01061343e−05	6.09780129e−04
34	0.85882562	−4.16621425e−04	−4.26959184e−04	5.96546357e−04

Table 5.1: Fourier analysis of z coordinate of the Halo orbit of the Solar System shown in figure 5.7. Here, we have used adimensional units for the time.

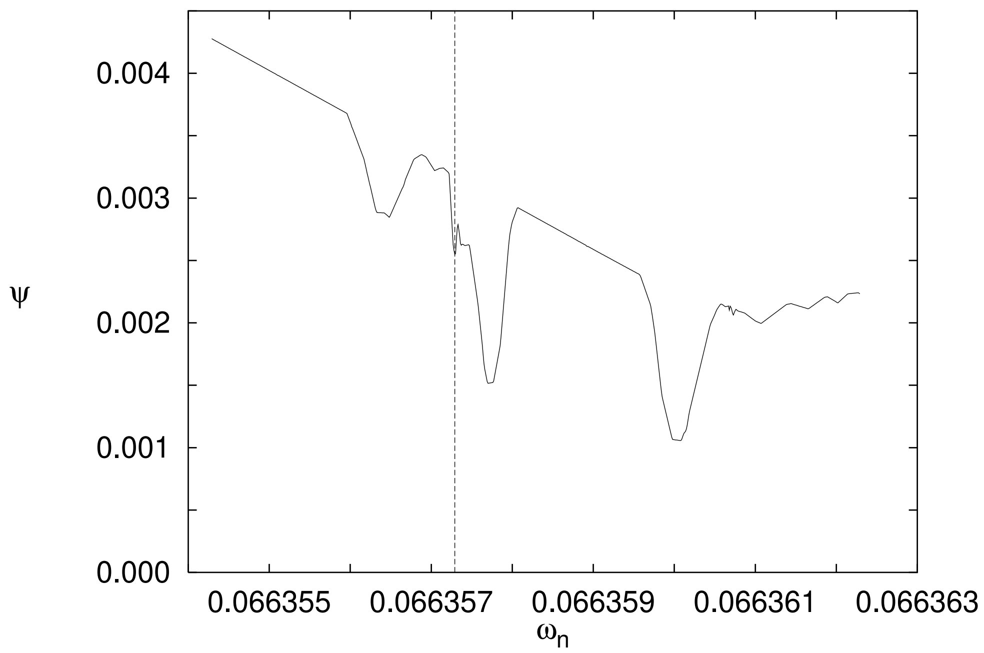

Figure 5.9: Function $\Psi_{100,0.0005}(\omega_n)$ for the estimation of the normal frequency. We have chosen for ω_n the value marked with a dashed line.

5.4 Comparison of the Halo orbits computed for several models

In this section, we compare some Halo orbits of RTBP, QBCP and Solar System (JPL-DE403 ephemeris). The conclusion will be that, in the vicinity of L_2, the dynamics of the QBCP is closer to the real problem than the RTBP.

We recall that, in chapter 3, for a given frequency ω_p, we computed a periodic Halo orbit of RTBP. From this, using the analytical refinement method, we obtained a quasi-periodic Halo orbit of QBCP, with the same proper frequency. In the previous section, we have refined some Halo orbits of the QBCP to the Solar System using a parallel shooting method and JPL ephemeris. We are interested in comparing the proper frequency and the x and z amplitudes of the Halo orbits of the three different models. Table 5.3 shows those magnitudes for four Halo orbits of those models. Due to the numerical refinement, small variations are produced in the frequency when going from the QBCP to the JPL model. Note that the larger variations are produced for orbits with labels 220 and 228, the ones closer to the resonance $w_p = 2\omega_s$. The x-amplitude α is $\sqrt{\alpha_c^2+\alpha_s^2}$, where α_c and α_s are the coefficients of $\cos(\omega_p t)$ and $\sin(\omega_p t)$ in the x variable, respectively. Analogously, the z-amplitude, β, is computed using the z variable. In the QBCP, for the orbits that we have considered, the coefficient of $\sin(\omega_p t)$ is zero. So, in this case, the values of α and β are the coefficients of $\cos(\omega_p t)$ in the x and z variables, respectively. For

j	ω_j	k_1	k_2	k_3	d
1	1.84408415	1	0	0	0.000e+00
2	1.85037689	0	2	0	−1.000e−10
3	2.83562895	1	1	1	−9.330e−07
4	1.81319487	1	2	−83	8.331e−07
5	0.85253866	1	−1	−1	2.465e−07
6	3.68816706	2	0	0	−1.228e−06
7	1.87497599	3	2	−83	1.740e−06
8	0.03089029	2	2	−83	1.824e−07
9	1.83775483	2	−2	0	−3.658e−05
10	1.81952035	2	0	−83	3.357e−05
11	0.00630041	1	−2	0	7.670e−06
12	1.80694087	0	4	−83	3.957e−05
13	1.86865179	4	0	−83	−2.973e−05
14	1.88122056	2	4	−83	−4.643e−05
15	1.85655523	1	−4	0	−1.144e−04
16	2.70292363	1	1	−1	8.333e−06
17	0.98522791	1	−1	1	−2.509e−05
18	0.02456681	3	0	−83	−3.056e−05
19	4.67971171	2	1	1	−2.318e−06
20	5.53225154	3	0	0	−8.950e−07
21	0.99155733	0	1	1	1.160e−05
22	0.03713564	1	4	−83	−4.721e−05
23	1.86240946	5	−2	−83	2.069e−05
24	2.84191611	0	3	1	−6.508e−06
25	2.69661750	2	−1	−1	−5.061e−06
26	1.83159954	3	−4	0	1.009e−04
27	1.82572677	3	−2	−83	−5.275e−05
28	1.84636963	3	−14	84	−3.785e−06
29	2.80473846	1	1	−84	−1.312e−06
30	0.01247864	2	−4	0	−1.068e−04
31	3.82717376	1	2	2	−1.855e−06
32	0.82164839	1	3	−82	8.405e−08
33	1.81525479	5	−12	1	−2.285e−04
34	0.85882562	0	1	−1	−5.534e−06

Table 5.2: Identification of frequencies of table 5.1. They can be expressed approximately as linear combination of $\omega_p = 1.8440841458$, $\tilde{\omega}_s = 0.9251884437$ and $\omega_n = 0.06635729$. Last column shows the difference $d = \omega_j - |k_1\omega_p + k_2\tilde{\omega}_s + k_3\omega_n|$.

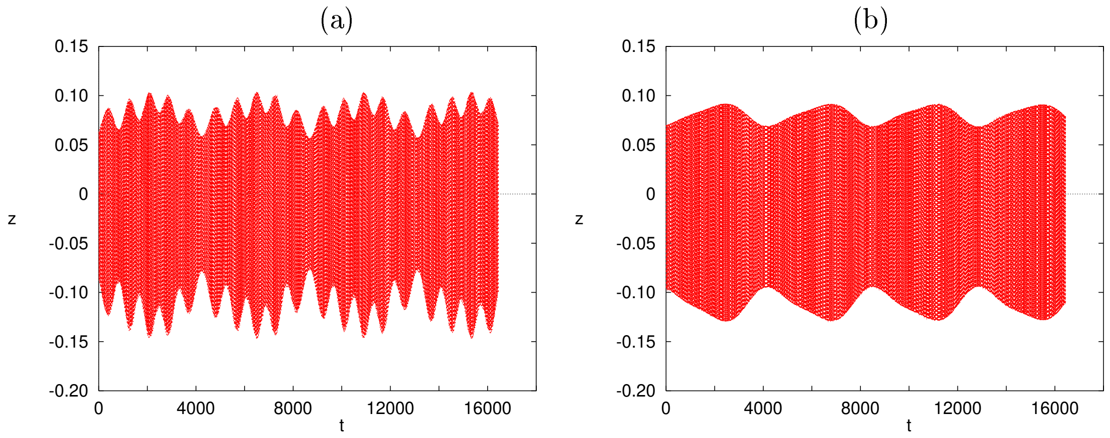

Figure 5.10: Trigonometric polynomials of table 5.1. (a) All the terms. (b) Only terms with $k_3 = 0$ are considered.

the JPL results, the value of ω_p was determined by Fourier methods. Then, when ω_p is known, α and β are determined again by Fourier analysis. Figure 5.11 shows the amplitudes of several Halo orbits for RTBP, QBCP and JPL model. Just for reference, points on figure 5.11 corresponding to, roughly, the same proper frequency (in the JPL case, we take as proper here the one along the "pure" Halo orbit) are joined with dotted lines. We see two main things:

1. The resonant effect due to $\omega_p \simeq 2\omega_s$. It is seen both in the QBCP and JPL models.

2. The Halo orbits in the QBCP model are much closer to the corresponding JPL ones than the related Halo orbits of the RTBP. This gives strong numerical evidence of the convenience to use the QBCP as reference model, at least for this region of the phase space.

Orbit	Model	ω_p	α	β
	RTBP	1.84409	0.1929	0.1600
label 216	QBCP	1.84409	0.1847	0.1161
figure 5.7	JPL	1.84408	0.1819	0.0967
	RTBP	1.84672	0.1974	0.2000
label 220	QBCP	1.84672	0.1868	0.1652
figure 5.3	JPL	1.84651	0.1839	0.1510
	RTBP	1.85412	0.2090	0.2800
label 228	QBCP	1.85412	0.1987	0.2554
figure 5.4	JPL	1.85423	0.1932	0.2502
	RTBP	1.86505	0.2236	0.3600
label 236	QBCP	1.86505	0.2177	0.3463
figure5.5	JPL	1.86506	0.2150	0.3388

Table 5.3: Comparison of Halo orbits of several models. ω_p is the proper frequency of the Halo orbit; α and β are x and z amplitudes, respectively.

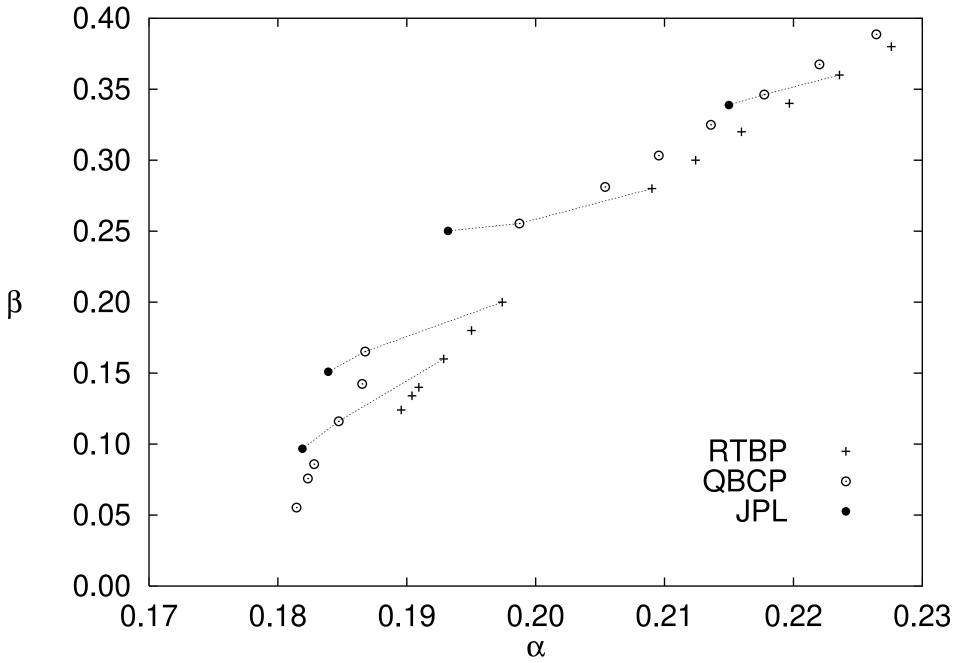

Figure 5.11: Amplitudes of Halo orbits of RTBP, QBCP and JPL model. The points displayed of the QBCP correspond to the orbits computed in chapter 3. The ones of JPL model correspond to the orbits of the table 5.3. The dotted lines relate orbits of the three models with roughly equal proper frequency.

Conclusions and outlook

This thesis is just only the beginning of a new line of research in the Celestial Mechanics world: the Quasi-bicircular Problem and its application to a better understanding of some real problems. This model has been very useful to start to understand the real dynamics around L_2 in the Earth-Moon case. It allowed to compute quasi-periodic Halo orbits which were refined to similar orbits in the Solar System. It is expected that the QBCP will be useful for the design of future spacecraft missions in the vicinity of the Earth-Moon system.

In the immediate future, our research will continue with the following topics, not necessarily in the order in which they are presented:

1. Design of a new algorithm to produce "pure" Halo orbits of the Solar System.

2. Since the reduction to the central manifold is not accurate in the neighbourhood of the resonant Halo orbits, we are planning to perform the following numerical computations.

    - Continuation of the family of 2D resonant tori of section 4.7.3, in order to check our conjecture.
    - Numerical computation of the stable/unstable invariant manifolds of the periodic orbit 2C. That will give us the zone around that periodic orbit where quasi-periodic Halo orbits do not exist. The unstable manifold has dimension two, being one of the associated eigenvalues of the order of 10^6 and the other one very close to 1. The main difficulty is that we are specially interested in the computation of the manifold in the direction of the eigenvalue nearby 1.

3. Careful study of bifurcations of families of 2D tori. From the planar Lyapunov family, the bifurcation where the four families of tori with horizontal frequency $2\omega_s$ are born. Three of these families join at a bifurcation for a certain z-amplitude. From the Lyapunov orbits also, the bifurcation where the Halo families start.

4. In chapter 4, we computed the reduction to the central manifold around L_2. Now, with a reasonable effort, we can compute in the same way the reduction around L_1 and L_5.

5. In a 3D neighbourhood of L_5, it is possible to perform simulations to detect global stable regions. The results will be compared with the ones obtained for the BCP and for the Solar System in [11]. We expect that the stable regions of the QBCP will fit better the real problem than the BCP does.

6. Computation of the invariant objects surrounding the stable zones of the previous item. The reduction of the Hamiltonian to the central manifold mentioned above can help to identify those objects. However, we think that it will be necessary to use numerical technics to determine them.

7. Computation of stable/unstable invariant manifolds of 2D tori:

   - In the case of translunar Halo orbits, if the stable manifold passes nearby the Earth at some epoch, it might be useful to perform a transfer from an orbit around the Earth to a Halo orbit.
   - In the case of L_1, we will compute the invariant manifolds of the planar quasi-periodic Lyapunov orbits. It will be interesting to see if there are orbits passing consecutively nearby the Earth, L_1 and the Moon. If such orbits exists they will provide an efficient way to go from the Earth to the Moon.
   - The points L_1^s and L_2^s of the system Sun-(Earth+Moon) also can be considered. The study of the invariant manifolds associated to them can help to find orbits going from the Earth to the Moon passing nearby L_1^s and L_2. It is known that such orbits exists in the Solar System.

Bibliography

[1] Abramowitz, M., Stegun, I.: Handbook of Mathematical Functions, Dover, New York (1972).

[2] Bowen, R.: On Axiom A diffeomorphisms, Conference Board Math. Sci. 33, A.M.S. (1977).

[3] Breakwell, J.V., Brown, J.V.: The 'halo' family of 3-dimensional periodic orbits in the Earth-Moon restricted 3-body problem, Celestial Mechanics 20, 389-404 (1979).

[4] Broer, H., Simó, C.,: Hill's equation with quasi-periodic forcing: resonance tongues, instability pockets and global phenomena, Bulletin of Brazilian Mathematical Society (in press).

[5] Broucke, R.A.: Periodic Orbits in the Restricted Three Body Problem with Earth-Moon masses, JPL Technical Report 32-1168 (1968).

[6] Farquhar, R.W.: The Control and Use of Libration-Point Satellites, NASA TR R346 (1970).

[7] Farquhar, R.W, Kamel, A.A.: Quasi-periodic orbits about the translunar libration point, Celestial Mechanics 7, pp. 458-473 (1973).

[8] Gómez G., Llibre J., Martínez R. and Simó C.: Station keeping of libration point orbits, ESOC contract 5648/83/D/JS(SC), Final Report (1985).

[9] Gómez G., Llibre J., Martínez R. and Simó C.: Study on orbits near the triangular libration points in the perturbed restricted three body problem, ESOC contract 6139/84/D/JS(SC), Final Report (1987).

[10] Gómez G., Jorba A., Masdemont J. and Simó C.: Study refinement of semianalytical halo orbit theory, ESOC contract 8625/89/D/MD(SC), Final Report (1991).

[11] Gómez G., Jorba A., Masdemont J. and Simó C.: Study of Poincaré maps for orbits near Lagrangian points, ESOC contract 9711/91/D/IM(SC), Final Report (1993).

[12] Gómez G., Masdemont J. and Simó C.: Quasihalo orbits associated with libration points, Journal of the Astronautical Sciences (to appear).

[13] Howell, K.C.: Three-dimensional, periodic, 'halo' orbits, Celestial Mechanics 32, 53-71 (1984).

[14] Jorba, À., Villanueva, J.: On the persistence of lower dimensional invariant tori under quasi-periodic perturbations, Journal of Nonlinear Science, Vol. 7, pp. 427-473 (1997).

[15] Laskar, J., Froeschlé, C., Celletti, A.: The measure of chaos by the numerical analysis of the fundamental frequencies. Application to the standard mapping, Physica D, 56, 253-269 (1992).

[16] Kolenkiewicz, R., Carpenter, L.: Stable periodic orbits about the Sun perturbed Earth-Moon triangular points, AIAA 6, 1301-1304 (1968).

[17] Mandelbrot, B.: Fractals, W.F. Freeman, San Francisco (1977).

[18] Marchal, C.: The Three-Body Problem, Elsevier (1990).

[19] Meyer, K.R., Hall, G.R.: Introduction to Hamiltonian Dynamical Systems and the N-Body Problem, AMS 90, Springer-Verlag (1992).

[20] Mohn, L., Kevorkian, J.: Some limiting case of the restricted four body problem, Astron. Jour. 72, 959-963 (1967);

[21] Mondelo, J.M.: Numerical Fourier analysis of a quasi-periodic function, Catalan Days of Applied Mathematics, Tarragona (1998).

[22] Richardson, D.L.: A note on a Lagragian formulation for motion about the collinear points, Celestial Mechanics 22, pp. 231–236 (1980).

[23] Richardson, D.L.: Analytic construction of periodic orbits about the collinear points, Celestial Mechanics 22, pp. 241–253 (1980).

[24] Scheeres, D.J., Vinh, N.X.: The Restricted Hill Four-Body Problem, 43$^{\text{rd}}$ Congress of the International Astronautical Federation, Washington (1992).

[25] Simó, C.: Analytical and numerical computation of invariant manifolds. In D. Benest et C. Froeschlé, editors, *Modern methods in celestial mechanics*, pag. 285-330, Editions Frontières, 1990.

[26] Simó, C.: Effective Computations in Hamiltonian Dynamics, in *Cent ans après les Méthodes Nouvelles de H. Poincaré*, Société Mathématique de France, 1–23, 1996.

[27] Simó, C.: Effective Computations in Celestial Mechanics and Astrodynamics, CISM Course on "Modern Methods of Analytical Mechanics and their applications", Udine, June 16 to 20, 1997.

[28] Stoer, J., Bulirsch, R.: Introduction to numerical analysis, Springer-Verlag (1980).

[29] Wiesel, W.: The restricted Earth-Sun-Moon problem I: Dynamics and libration point orbits, Dept. Aeron. and Astron., Air Force Institute of Technology Wright-Patterson AFB, Ohio (1984).

[30] Yakubovich, V.A., Starzhinskii, V.M.: Linear differential equations with periodic coefficients, John Wiley & Sons, New York (1975).